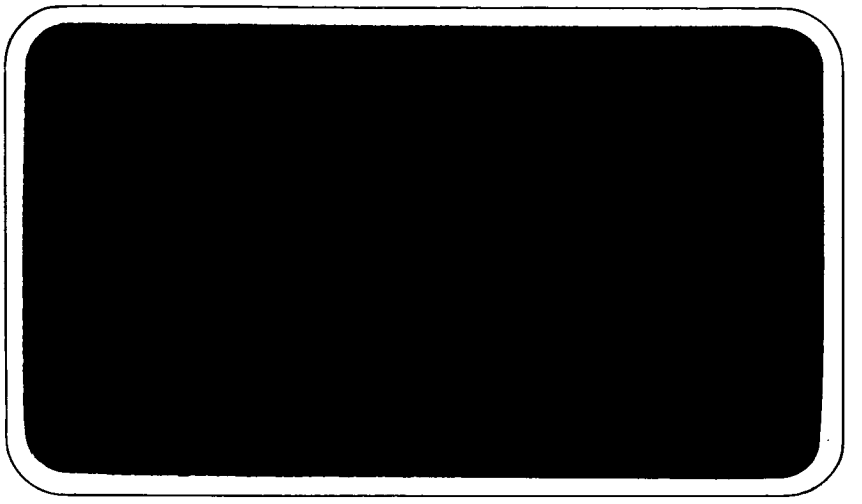





# Westinghouse

ELECTRIC CORPORATION

1750D

# VOLUME IV - PARTS I AND II
# EARTH ORBITAL RENDEZVOUS

Compilation Report
for
ADVANCED SPACEBORNE DETECTION,
TRACKING, AND NAVIGATION SYSTEMS
STUDY AND ANALYSIS

NAS 8 - 11205

July 1964

Prepared for

GEORGE C. MARSHALL SPACE FLIGHT CENTER
Huntsville, Alabama

By

WESTINGHOUSE DEFENSE AND SPACE CENTER
Aerospace Division
Baltimore, Maryland

N65 - 19859
N65 - 19861
N65 - 19858
N65 - 19860
N65 - 10111

## ABSTRACT

19860

This is Volume IV of a five-volume report compiled for the Marshall Space Flight Center by the Aerospace Division, Westinghouse Defense and Space Center, Baltimore under contract NAS 8-11205. Material for this set of volumes has been obtained from independent studies performed to determine sensor requirements for space missions.

Although the studies are applicable to space missions in general, it is desired to place primary emphasis on the manned lunar mission. The main volumes of this report, therefore, deal with the various phases of the mission. Earth rendezvous - the procedure by which two vehicles are brought into close proximity while in orbit about the earth - is not postulated as a segment of the manned lunar mission. Consequently, the work pertaining to earth rendezvous is compiled within this volume to present it as an independent part of the overall report.

These studies have been organized along guidelines furnished by MIL-D-8684A, paragraphs 3.4.3.1 and 3.4.3.2. The study method utilized is objective in nature and is separated in this Volume IV into two parts: Section 1, Part I, the Problem Definition, which defines the basic problem with respect to (a) the goals to be realized, (b) the constraints imposed by physical laws and natural phenomena, and (c) possible mathematical solutions to the problem; Section 2, Part II, the Analytical Solution, which then uses the groundwork of Section 1 to determine somewhat ideal nominal solutions as well as parametric studies of variations about nominal values. This type of approach, rather than determining the manner in which given subsystems operate together, defines basic specifications for the system and its subsequent mechanization.

Although this report is concerned with sensor requirements, overall systems, including the guidance and control sections, are defined to provide a method for evaluation. Local (onboard) navigation, guidance, and control is assumed. Error criteria to be used as a basis for evaluation are then established and the results specify sensor requirements for rendezvous.

In the analyses, extensive use is made of various computer programs to simulate the rendezvous procedure. These programs are discussed in the appendixes which are a part of this volume.

AUTHOR →

TABLE OF CONTENTS

TABLE OF CONTENTS (Continued)



LIST OF APPENDICES



LIST OF ILLUSTRATIONS

LIST OF ILLUSTRATIONS (Continued)

## LIST OF ILLUSTRATIONS (Continued)



## LIST OF TABLES

LIST OF TABLES (Continued)

# SUMMARY

This document, which examines the earth orbital rendezvous procedure, is a compilation of independent parallel studies performed by the Missile and Space Division of Raytheon Company under contract NASW-469 and by the Aerospace Division of the Westinghouse Defense and Space Center, Baltimore under contract NASW-460 and is organized according to guidlines furnished by MIL-D-8684A(Aer) paragraphs 3.4.3.1 and 3.4.3.2. In accordance with this specification, this document contains a Section 1 (Problem Definition), which examines the problem to be solved and which delineates the considerations and assumptions forming the groundwork for analysis, and a Section 2 (Analytical Solution), which solves the problem as defined in Section 1 and contains the analyses performed and the results obtained.

In Section 1, the entire rendezvous procedure is separated into four sequential segments: injection, midcourse, active rendezvous, and docking. Visual observation and control is postulated for the docking phase, which is not examined further in this report. The area of detailed investigation extends from injection of the chaser into the transfer orbit through termination of active rendezvous which occurs when the chaser achieves a present standoff range and range rate with respect to the target. A nominal mission profile and guidance and control system are established to serve as a model for the analyses.

In Section 2, this model is incorporated into computer programs, and these computer programs are then utilized to determine parametrically the effects of sensor errors on allowable injection errors and active rendezvous maneuver errors. The allowable magnitude of sensor erros is then determined with respect to deviations in the desired terminal conditions and with respect to fuel consumption.

Three active phase guidance and control systems are utilized for the analyses of the rendezvous procedure. The first system is an automatically controlled, variable thrust level system based on proportional navigation and referred to as modified proportional navigation (MPN). Paragraph 2.2.1 contains the analysis and results utilizing this system. A second system comprises an automatically controlled constant thrust level, on-off technique. The analysis using this system is contained in paragraph 2.2.2. The third system is similar to the second in principle of operation but includes a pilot in the control loop. Paragraph 2.2.3 presents the analysis and results using this system.

Injection is considered to be an impulsive maneuver; i. e., a velocity impulse is imparted instantaneously by the chaser vehicle to achieve the transfer orbit. Consequently no simulation of guidance and control techniques is employed for this maneuver.

Paragraph 2. 2. 4 discusses a midcourse measurement procedure for reducing the uncertainties in estimating the state variables (position and velocity) of the chaser.

Using the models and criteria assumed, it appears that present state-of-the art sensor capabilities are sufficiently adequate for rendezvous procedures. It is noted, however, that as sensor accuracies are increased, fuel consumption is reduced - an important consideration in space missions. Dynamic errors (i. e., mechanization and control errors) also have an effect in that larger dynamic errors necessitate more stringent sensor requirements.

Including a pilot in the control loop enables sensor requirements to be relaxed somewhat. This appears to be the result of the inherent human ability to filter, or smooth, observed data.

Appendixes A through G discuss the various computer programs used in obtaining the sensor requirements. Appendix H shows the effect of random noise on switching boundaries of a nominal on-off rendezvous guidance and control system.

# 1. PROBLEM DEFINITION

## 1.1 INTRODUCTION

Rendezvous refers to the process of bringing two vehicles into close spacial proximity while in orbit about a prime body. The purpose of the rendezvous maneuver is to transfer men and supplies from one vehicle to another and/or to join two vehicles to form one larger vehicle.

Earth rendezvous procedures will constitute an integral part of future space missions such as the construction and resupply of a space station or large interplanetary vehicle in orbit about the earth. Physical constraints and energy limitations dictate that a facility of appreciable size be launched from earth in sections and assembled in orbit. Thus, as each section is launched, it must rendezvous with the preceding section(s) to be incorporated into the structure.

Once a long duration orbital facility is established it will be necessary to provide logistic support by ferrying men and materials from earth. Consequently, the ferry vehicle must be capable of performing rendezvous with the space station.

For purposes of generality, the vehicle with which rendezvous is to be established is hereinafter referred to as the target vehicle, and the vehicle performing the rendezvous is referred to as the chaser. During rendezvous, it is postulated that the target vehicle assumes a passive role and the chaser assumes an active role by executing the necessary maneuvers to close upon the target in a prescribed manner. Local (onboard) navigation, guidance, and control is assumed.

Rendezvous must, of necessity, be automatic for unmanned vehicles and may be either manual, automatic, or a combination of the two for manned vehicles. If the chaser vehicle is manned, docking, which is the final phase of rendezvous, is expected to be accomplished under manual control using visual observations.

This report presents analyses performed to establish navigational sensor requirements for rendezvous. Navigation with respect to vehicle guidance and control may be said in a general sense to be: (a) the sensing of vehicle position and possibly position time derivatives, (b) prediction of the vehicles state variables based upon sensor information, and (c) comparison of the output of the prediction computation with a nominal set of conditions. Guidance in the same respect may be said to be navigation plus the employment of the

discrepancy between the computed and the nominal set of conditions to compute control commands. Guidance control (including signals for attitude control) may, in general, be said to be the employment of control commands, possibly together with further sensor data through control actuators and vehicle dynamics to influence vehicle position and its time derivatives. Thus, the navigation function constitutes the basis for guidance, and guidance and control together determine the vehicle trajectory in space. The primary emphasis in this study is upon the navigation function and, in particular, upon the sensor accuracy requirements. Therefore, the entire guidance function is considered only to the extent that it affects navigation requirements, and control is not considered except in terms of directional thrust control. To determine navigational sensor requirements, however, guidance and control systems must, in general, be studied, evaluated, selected and assumed as a basis for sensor accuracy requirements, and control accuracies must be allotted. In general, the results of these studies are applicable to either the manned or the unmanned case, the principal assumption being that of local guidance.

The notations used in the analytical methods for determining sensor requirements for earth rendezvous missions are summarized below.

## SUMMARY OF NOTATION

$a_L$ Longitudinal acceleration of chaser

$a_N$ Normal acceleration of chaser

$e$ Orientation of LOS (line of sight) with respect to an inertial reference

$\dot{e}$ Line of sight angular rate with respect to inertial space

$g$ $9.81\ m/sec^2$

$h$ Chaser altitude

$I_{sp}$ Propellant specific impulse

$K$, $K_1$, and $K_2$ Control parameters.

$M_o$ Initial mass of chaser

$M_p$ Propellant consumed by chaser because of thrusting

$R$ Chaser-to-target range

$\dot{R}$ Chaser-to-target range rate

$R_o$ Chaser-to-target range at initiation of active rendezvous

$S$ Control parameter

$t$ Time

$t_F$ Firing time of chaser engines

$t_s$ Data storage time for smoothing process

$t_i$ Time interval between data measurements

$\Delta V$ Velocity increment

$\Delta V_h$ Velocity increment required for nominal Hohmann transfer

$X, Y, Z$ Position components (general)

$\dot{X}, \dot{Y}, \dot{Z}$ Velocity components (general)

$\psi$ Yaw (out-of-plane) attitude angle of chaser

$\gamma$ Pitch (in-plane) attitude angle of chaser

$\phi$ Central angle between chaser and target radius vectors during rendezvous

$\omega_T$ Angular orbital velocity of target

Subscripts:

$f$ Value of quantity at termination of active rendezvous

$i$ Value of quantity at injection

$o$ Value of quantity at start of active rendezvous

### 1.1.1 Profile of Rendezvous Phase

At initiation of the rendezvous maneuver, the target vehicle is in a nominal circular parking orbit about the earth. The chaser then achieves a transfer orbit which intercepts the orbit of the target at the point of rendezvous. Injection of the chaser into the transfer orbit may be made by direct ascent from the earth or from an intermediate parking orbit. Figure 1-1 illustrates each of these procedures.

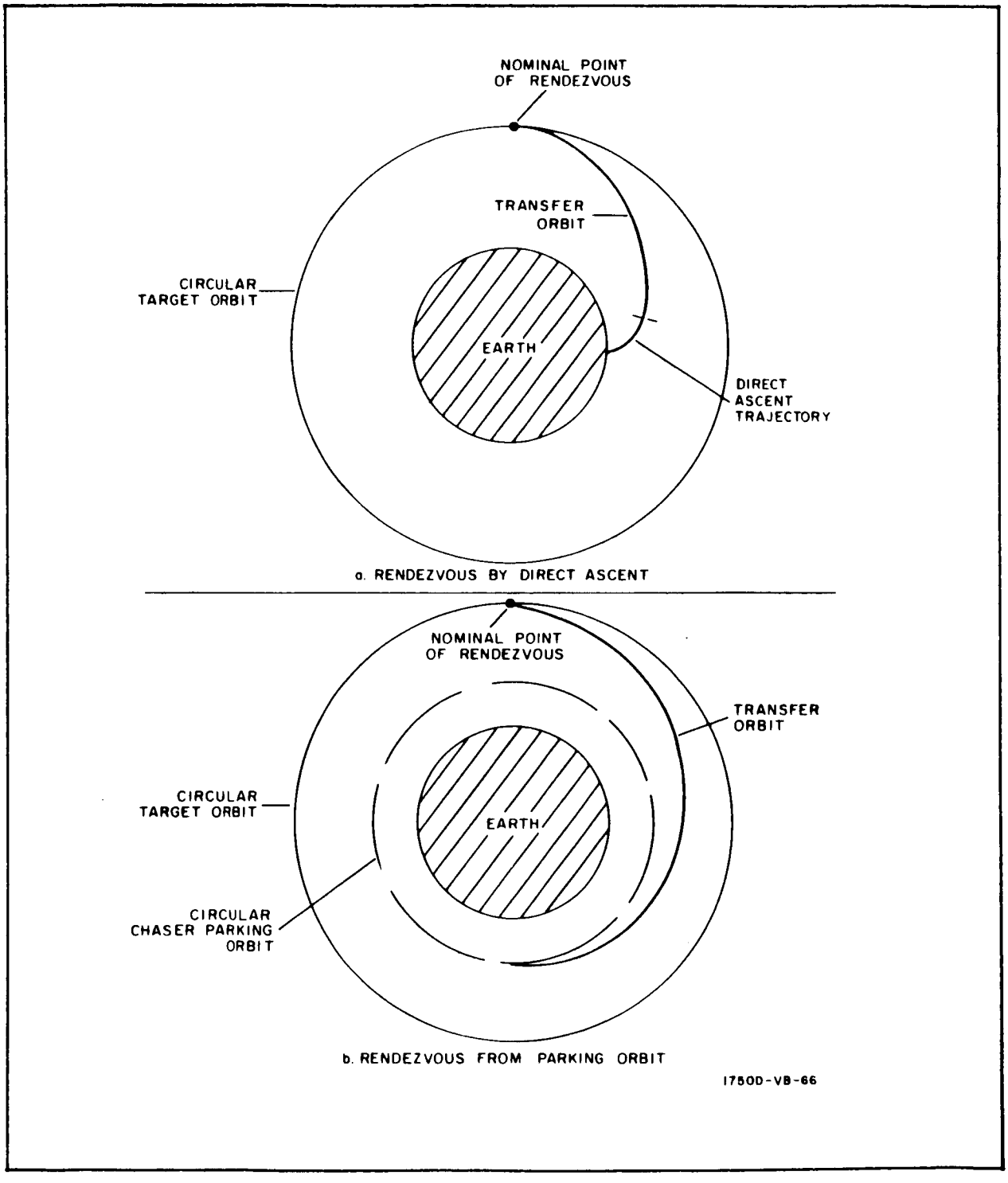


Figure 1-1. Rendezvous Procedures

A complete rendezvous procedure is considered to be composed of four sequential segments:

a. Injection into transfer orbit

b. Midcourse phase

c. Active phase prior to the rendezvous point

d. Docking

Within the scope of this investigation, however, rendezvous is considered complete when the chaser achieves a prescribed range and relative velocity with respect to the target. Docking is not investigated because of the likely dependence on manual control.

Injection occurs when the chaser, on the basis of prior or present measurements, determines that it is properly phased with the target. It then imparts a computed incremental velocity vector, by rocket propulsion, to establish a transfer ellipse which either intersects or is tangential to the target vehicle orbit at the anticipated rendezvous point. Measurement data, from which the incremental velocity is computed, are based on the relative positions and velocities of the target and chaser.

The midcourse portion of this transfer trajectory is covered with the chaser in an inactive or coasting mode. Then, at relatively short range (approximately 20-50 km), the active phase of rendezvous commences. On the basis of rendezvous sensor measurements to the target, the chaser executes a series of maneuvers to close smoothly and safely to within a prescribed range and range rate relative to the target.

It is seen, then, that sensors are required for the proper execution of the injection maneuver and the active rendezvous phase. Also, it may be desirable to make observations during the midcourse phase in order to maintain greater accuracy in the estimation of the state variables (position and velocity) of the chaser. The objective of the analysis contained herein is to establish sensor requirements, both in accuracy and dynamic range, for earth rendezvous procedures, and to present the techniques used in the analyses.

### 1.1.2 Observables

The nature of the rendezvous problem specifies that knowledge of the relative geometry and dynamics between the chaser and target is required to execute the procedure. Consequently, observables measured by the rendezvous sensor system should give this information. Observables examined in this study are:

a. Chaser-to-target range

b. Chaser-to-target range rate

c. LOS (line of sight) azimuth angle

d. LOS azimuth angular rate

e. LOS elevation angle

f. LOS elevation angular rate

## 1.2 FORMULATION OF ANALYTICAL MODEL

In this study, a fundamental rendezvous model is formulated and used as a tool in the determination of required sensor accuracies and dynamic ranges. This model defines the basic geometrical and dynamic relationships of a rendezvous procedure. These basic relationships can then be combined with various navigation, guidance, and control techniques in order to evaluate the effects of sensor performance on the overall system.

### 1.2.1 Geometry

It is postulated that the target is in a circular orbit about the earth at an altitude between 500 and 1000 km. At the start of the rendezvous, the chaser is in a circular parking orbit of approximately 185 km (100 n. mi) which is essentially coplanar with the target orbit. To initiate the rendezvous, the chaser injects into a transfer orbit which intersects the target orbit at the nominal point of rendezvous. The transfer orbit is the nominal Hohmann or 180-degree which is the minimum energy two pulse transfer between orbits. Use of the coplanar, 180-degree transfer is made since a rendezvous requiring a change of plane and/or a non-Hohmann transfer can require substantial energy expenditures, - an important consideration in space missions. Also, use of a parking orbit, rather than direct ascent, is postulated. This reduces the sensitivity in the launch windows and allows greater time for proper phasing of the chaser and target prior to injection because of the inherent difference in their orbital velocities. Consequently, the proposed model is felt to be commensurate with anticipated space procedure.

A spherical nonrotating earth is assumed and the effects of orbital precession and line of apside rotation are ignored because of the relatively short time required for rendezvous. The essentially fixed geometry of this model poses no serious drawbacks since it is the propagation of navigation errors, rather than the rendezvous itself, which is of primary interest and navigation accuracy is relatively insensitive to changes in mission geometry.

### 1.2.2 Injection

Injection is essentially an impulsive maneuver by which an incremental velocity vector is imparted to the chaser to place it on the transfer orbit.

This incremental velocity is computed from knowledge of the relative geometry and dynamics between target and chaser and is imparted by rocket thrust.

Errors in the injection maneuver cause deviations from the desired or reference transfer orbit. These errors may be introduced as position errors, velocity vector errors, and timing errors.

Position errors may be separated into three components:

a. The radial error occurs owing to the lack of precise knowledge of the radius from the center of the earth's gravitational field to the point of injection (nominally, perigee of the Hohmann transfer ellipse).

b. Lateral displacement reflects an out-of-plane condition of the chaser which must be corrected, preferably at the nodal point of the planes of the transfer ellipse and target orbit. Nominally, the parking orbit will be coplanar with the target orbit.

c. In-track displacement errors are equivalent to phasing errors which are discussed subsequently.

Velocity vector errors occur in magnitude and direction as follows:

a. The magnitude of the incremental velocity imparted may be in error because of improper command due to poor orbital information or because of an error in execution such as erroneous velocity cutoff due to an accelerometer error or incorrect termination of the rocket thrust itself.

b. The direction of the velocity maneuver may have an angular error in elevation (in the orbital plane) or azimuth (out of the orbital plane). These directional errors may result from erroneous commands, vehicle attitude errors during firing or thrust misalignment.

Phasing errors develop when the chaser fails to inject into the desired transfer ellipse at the correct time, either because of inaccurate information or because of an error in execution.

Each of the above errors will propagate along the transfer ellipse resulting in final errors in position and velocity at rendezvous should no active corrections be employed. These errors are a combination of measurement errors and control errors (computational errors are assumed to be negligible), and no attempt is made to separate the two sources.

### 1.2.3 Midcourse

Deviations in the state variables of the chaser from the state variables of the reference transfer orbit result from errors in injection. During the midcourse phase, therefore, it may be desirable to perform measurements which can be used to reduce the uncertainties in the estimation of the true state variables. Greater accuracy in the knowledge of the chaser position and velocity can result in more efficient corrective maneuvers prior to or during the active rendezvous phase.

The accuracy with which the state variables may be determined is dependent upon the error inherent in measurement of observables and the computational technique employed to obtain the deviations at the point of rendezvous.

The procedure investigated makes use of the Clohessey-Wiltshire matrix, described in Ref. 1-1., to describe the propagation of the uncertainties in the state variables along the reference trajectory. At some point in the midcourse phase, measurements are performed on the relative dynamics between the chaser and target. These measurements are utilized in a correction matrix which is used to operate on the predicted uncertainties in the state variables at that point. This operation yields a new, reduced set of uncertainties which may then be propagated to a future point on the reference trajectory, either the point of next measurement or the terminal rendezvous point.

The primary objective of the midcourse analysis is to determine the optimum combinations of observables which, when used in the correction matrix, yield the minimum uncertainties in the estimated state variables.

### 1.2.4 Active Rendezvous

When the chaser-to-target range has decreased to approximately 20-50 km, the chaser initiates a procedure of maneuvering to close on the target in a prescribed manner. For analysis of this active phase, it is necessary to specify a guidance technique and thrust program for the chaser. Sensor errors may then be incorporated to determine their effect on the active phase.

#### 1.2.4.1 Basic Guidance Techniques

a. On-Off Guidance - This rendezvous guidance philosophy is representative of many guidance schemes. The basic characteristics are described in the following paragraphs.

Guidance and control is separated into two channels, normal control and longitudinal control. Normal control is exercised so as to maintain the

line-of-sight inertial angular rate at a value near zero so that the chaser maintains a closing course on the target. This is accomplished by firing a rocket thrust normal to the line of sight and in the plane of line-of-sight rotation when the magnitude of the line-of-sight rotation exceeds a given threshold. The thrust direction is such that the magnitude of the angular rate is driven below the threshold value.

For the Hohmann transfer, the line of sight maintains a relatively constant orientation with respect to inertial space during the portion of the trajectory covered by the active phase. Consequently, only minor rotations of the line of sight due to orbital perturbations and injection errors should be encountered.

Longitudinal control is exercised to reduce the range and range rate in a manner which prevents collision of the target and chaser. A graphical illustration of longitudinal control is illustrated in figure 1-2 in which a phase plane (range vs range rate) is shown.

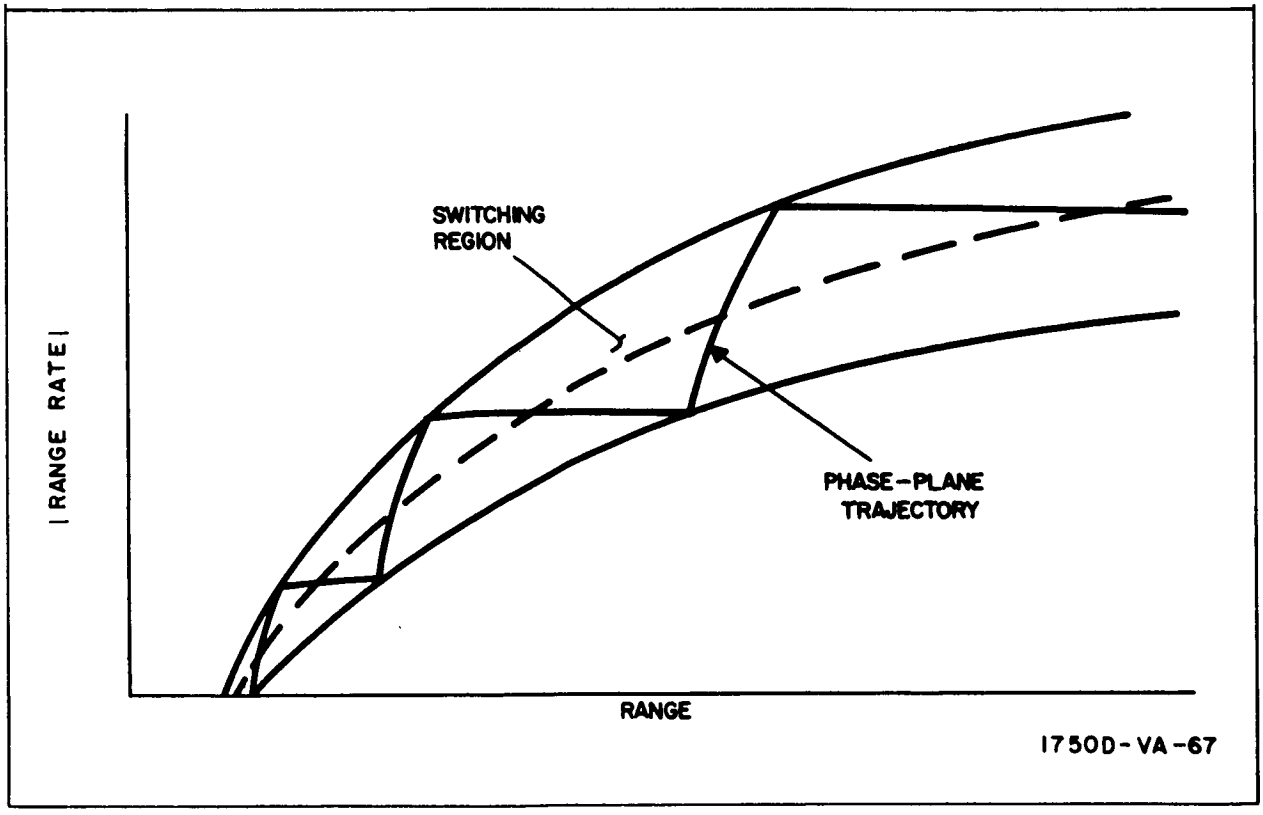


Figure 1-2. Typical Phase Plane Trajectory for Active Rendezvous

The magnitude of range and range rate at a given instant of time may be plotted as a point on the phase plane. Plotting points over successive

intervals of time produces a time history of the relative dynamics (called a phase plane trajectory) between the chaser and target (see figure 1-2).

Ideally, the phase plane trajectory follows the broken line. This type of performance, however, necessitates variable thrust levels along the longitudinal axis of the chaser.

When constant level thrust is employed for discrete intervals of time the longitudinal control system is mechanized so that all points of range versus range rate during the rendezvous maneuver are made to fall within the switching region on the phase plane. This region is defined by two curves which are determined through consideration of the mission geometry and dynamics and the chaser acceleration capabilities. When the points of the phase plane trajectory fall above the upper curve, thrusting is initiated along the longitudinal axis so as to decrease the range rate and cause the trajectory to fall within the switching region. Thrust is applied until the trajectory falls below the lower curve at which time thrusting ceases. The range then decreases at essentially constant value, and the trajectory approaches the upper boundary. The process is repeated until the final values of range and range rate are achieved.

Equations of the switching region boundaries have the general form:

$$\dot{R} = \sqrt{K\, a_L \left| R - R_f \right|} \qquad (1\text{-}1)$$

where

$\dot{R}$ = range rate

$R$ = range

$R_f$ = final or standoff range at termination of the active phase

$a_L$ = longitudinal acceleration of the chaser

$K$ = constant having a different value for each boundary such that $K_1 > K_2$ where $K_1$ applies to the upper boundary and $K_2$ to the lower boundary.

Consideration must be taken of orbital characteristics and vehicle dynamic capabilities in determining the values of the thresholds and constants for the active phase guidance laws.

It is postulated that both the normal and longitudinal rockets have constant thrust levels and that the percentage variation of the chaser mass during active rendezvous is slight, thereby resulting in constant accelerations in both channels.

b. Modified Proportional Navigation - A modified proportional navigation scheme is considered in addition to the on-off system. Control is separated into a longitudinal and a normal channel, but variable acceleration levels are employed. The magnitude of the accelerations are determined by the relative dynamics as defined by the following equations.

$$a_L = \frac{K - 1}{K} \quad \frac{\dot{R}^2 - \dot{R}_f^2}{R - R_f} \tag{1-2}$$

$$a_N = \left(1 + \frac{SK - 1}{K}\right) \dot{R}\, \dot{e} \quad , \tag{1-3}$$

where

$R$ = chaser-to-target range

$\dot{R}$ = chaser-to-target range rate

$R_f$, $\dot{R}_f$ = desired values of range and range rate at termination of the active phase

$\dot{e}$ = LOS angular rate in inertial space

$S, K$ = control parameters

For analysis, this control technique has an inherent advantage over the on-off system in that it lends itself to linearization.

1.2.4.2 Chaser Vehicle Configuration

For purposes of this investigation a basic vehicle configuration is defined to facilitate incorporation of the guidance and control techniques. The extent of this definition is such that the relationship of the thrust rockets to the line of sight is defined.

A cartesian coordinate system is assumed coincident with the center of mass of the chaser. The $X_b$-axis is the longitudinal axis along which the longitudinal engine is aligned and therefore is aligned in the general direction of the line of sight. It also serves as the reference axis from which the line-of-sight azimuth and elevation angles are measured.

The $Y_b$- and $Z_b$-axes, then, are the normal axes. It is postulated that engines aligned along these axes can be fired in either direction to null the line-of-sight rotation with minimum attitude control requirements.

1.2.4.3 Errors in Measurement of Observables

Types of errors which are assumed to occur in the measurement of the observables are typical of the sensor systems considered. In the measurement of range and range rate, two types of error are considered: a bias error and a normally distributed random error. Each of these errors, in turn, comprises two parts: one which is independent of range and one which is a percent of range. Angle and angular rate measurements, however, are assumed to have errors which are independent of the measured quantity; i.e., a bias and/or a normally distributed random error, each independent of the magnitude of the measured observable.

The inertial platform forms the attitude reference to which the line-of-sight angles are measured. Although the platform may have an attitude error, the platform is assumed to be rate stabilized with sufficient accuracy that the angular rate error is essentially negligible.

## 1.3 ANALYSIS

To analyze the effects of sensor errors on the rendezvous procedure, the various guidance schemes are combined with the basic geometry and incorporated in computer programs. Automatic and piloted control of the active rendezvous phase are investigated, resulting in both digital and analog simulations. Use of computer simulations enables the effects of errors to be studied in a parametric manner.

Other than overall mission safety, two considerations are utilized in determining allowable sensor performance. The first and perhaps most significant is propellant consumption. The amount of propellant expended in executing an orbital transfer and rendezvous is of great importance to a space mission because of the equivalent vehicle mass penalty. In this phase of the study, an equivalent incremental velocity $\Delta V/\Delta V_H$, applied during the rendezvous phase is considered as a non-dimensional measure of propellant consumption independent of fuel specific impulses and vehicle mass. The equivalent mass of propellant consumed may be found by the relation

$$M_p = M_o \left[ 1 - \exp\left( - \frac{\Delta V}{g I_{sp}} \right) \right] \qquad (1\text{-}4)$$

where

$M_o$ = initial vehicle mass

$I_{sp}$ = propellant specific impulse

$g = 9.81 \text{ m/sec}^2$

Both injection errors and sensor errors cause incremental velocity requirements which are in excess of that required for a perfect Hohmann transfer ($\Delta V_H$). By postulating a maximum value for the ratio, $\frac{\Delta V}{\Delta V_H}$, resulting from a given error, the maximum value of that error can be determined.

It is postulated that a $3\sigma$ error at injection shall not result in more than a 20-percent increase in $\Delta V$ over the nominal $\Delta V_H$, when no sensor errors are included during the active rendezvous phase. Similarly, a given $3\sigma$ error occurring in a measured observable during active rendezvous shall not result in more than a 50-percent increase in $\Delta V$ over nominal $\Delta V_H$.

A second consideration is to specify the maximum deviation in the specified chaser-to-target range and range rate at termination of the rendezvous, resulting from sensor error. The maximum allowable deviations are arbitrarily set at ±20 percent for both range and range rate.

# 2. ANALYTICAL SOLUTION

This section presents analytical methods for determining sensor requirements for earth rendezvous missions. The basic problem is discussed in Section 1, Problem Definition. Also, the nominal geometric and dynamic relationships of rendezvous are outlined and the ground rules for analysis are presented.

It is to be noted that no specific types of equipment are used in the analysis. Instead, specifications for the operation of the overall system and its subsequent mechanization are defined. Consequently, the results obtained are nominal solutions as well as parametric variations about the nominal.

## 2.1 BACKGROUND

The two vehicles between which the rendezvous is to be established are referred to as the target and chaser. The target is postulated as taking a passive role by remaining in a nominally circular orbit about the earth. All active maneuvering required to establish the rendezvous is performed by the chaser vehicle.

### 2.1.1 Mission Profile

Initially, the chaser may be in a parking orbit which is essentially coplanar with the target orbit. A transfer orbit, which intersects or is tangential to the target orbit at the nominal point of rendezvous is then achieved by the chaser in order to close on the target.

An alternate method is to have the chaser ascend directly from the earth's surface to achieve the transfer orbit. However, because of the increased launch window sensitivity, this method is not considered.

Four sequential phases make up the overall rendezvous procedure. These are injection, midcourse, active rendezvous, and docking.

- Injection. Injection occurs when the chaser, using measurements of the relative geometry and dynamics between the chaser and target, imparts a computed incremental velocity vector thereby achieving the transfer orbit.

- Midcourse. The midcourse phase encompasses the major portion of the time that the chaser is travelling the transfer orbit. During this time, no active maneuvering is performed by the chaser.

- Active Rendezvous. At a chaser-to-target range of 25 to 50 km, the chaser begins a series of active maneuvers to effect closure upon the target in a manner prescribed by the guidance law used. Control of the active rendezvous may be completely automatic or may include a pilot in the control loop. This phase ends when the relative range and range rate between the target and chaser have been reduced to specified values.

- Docking. The docking phase brings the chaser into physical contact with the target. It is envisioned that manual control based upon visual observations by the pilot will be used to effect docking. This phase is considered to be beyond the scope of this report and is not investigated.

### 2.1.2 Observables

Rendezvous is basically a problem involving the relationship of two vehicles and requires information concerning the relative geometry and dynamics between them. This consideration dictates the observables to be utilized:

a. Range

b. Range rate

c. LOS elevation angle

d. LOS elevation angular rate

e. LOS azimuth angle

f. LOS azimuth angular rate

The angles and angular rates may be measured either with respect to the chaser or with respect to inertial space.

### 2.1.3 Rendezvous Model

A basic rendezvous model is formulated which is composed of two basic parts: (a) geometry and (b) guidance and control. These parts, which are discussed in the following subsections, are combined into computer simulations which are utilized in the analysis.

#### 2.1.3.1 Basic Geometry

At initiation of rendezvous the target is assumed to be in a circular orbit at an altitude of 555 to 925 km (300 to 500 n.mi). The chaser is assumed to be in a 185 km (100 n.mi) circular parking orbit which is essentially coplanar with the target orbit. A Hohmann transfer, the minimum energy to pulse transfer between orbits, is chosen as the reference trajectory.

The above geometry is chosen for the rendezvous primarily on the basis of energy considerations. Perturbations such as precession of the orbital planes and rotation of the line of apsides are neglected because of the relatively short time required to perform the rendezvous.

#### 2.1.3.2 Guidance and Control

Injection is considered to be an impulsive maneuver, consequently no simulation of guidance and control techniques is performed. An incremental velocity is assumed to be imparted to the chaser at the injection point.

Active rendezvous is assumed to occur during the last few hundred seconds of the transfer orbit. During this phase, the attitude of the chaser is maintained such that the $X_b$-axis (longitudinal axis) is essentially along the line of sight to the target, and the $Y_b$- and $Z_b$-axes are in the orbital plane and perpendicular to the orbital plane respectively.

Variations of a basic guidance and control scheme for the chaser are utilized in the simulations. This basic scheme is separated into two channels, longitudinal and normal.

Longitudinal control is exercised to cause a definite chaser-to-target range-range-rate relationship to occur. The relationship is best illustrated using a phase plane plot of range vs range rate as shown in figure 2-1. Plotting instantaneous values of range and range rate over successive intervals of time yields a phase plane trajectory.

One guidance and control scheme studied utilizes a method of longitudinal control which calls for continuously applied thrust of variable magnitude along the longitudinal axis, the magnitude being determined by the relative dynamics between the target and chaser. The direction of thrust is such as

to decrease the range rate. In this case, the phase-plane trajectory is made to follow the dashed line of figure 2-1.

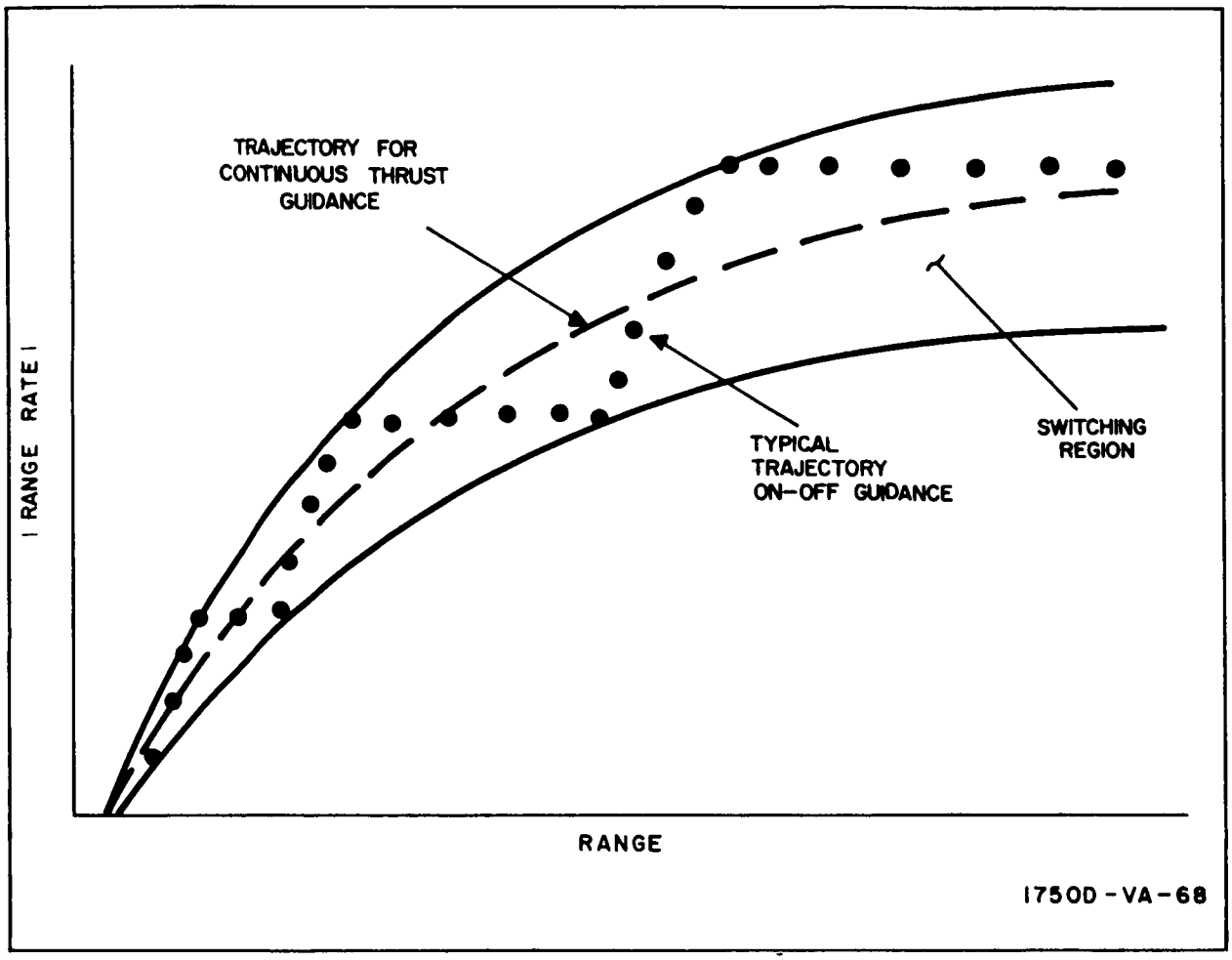


Figure 2-1. Phase Plane Trajectories for Two Variations of the Basic Longitudinal Control

In the case where constant magnitude thrusting during discrete intervals (on-off guidance) is postulated, the phase plane trajectory is made to fall within the switching region bounded by the two solid lines. This is accomplished by firing the longitudinal engines when the trajectory reaches the upper boundary thereby reducing the range rate. When the trajectory reaches the lower boundary, thrust is shut down. A typical phase plane trajectory for on-off guidance is shown by the dotted line of figure 2-1.

Normal control is exercised to keep the magnitude of the line-of-sight rotation rate with respect to inertial space close to zero. This maintains the chaser on a closing course with the target and is accomplished by thrusting with rockets mounted normal to the longitudinal axis of the chaser (and, therefore, essentially normal to the line of sight). It is postulated that thrust may be applied in either direction along the normal axis thereby reducing the attitude control problem.

When variable thrust is used, the magnitude is proportional to the line-of-sight rotation. In the case of the on-off system, upper and lower thresholds are established. Thrust is applied when the magnitude of the line-of-sight rate exceeds the upper threshold and is not used when the magnitude falls below the lower threshold.

In either of the above cases, the normal axis along which the thrust is applied must be kept in the plane of line-of-sight rotation by controlling the roll attitude of the chaser.

More detailed descriptions of the guidance and control philosophies used, including pertinent equations, are included in subsection 2.2.

### 2.1.4 Error Characterization

Errors investigated in this study occur during rendezvous at two points: in the injection manuever and in the measurement of observables during active rendezvous.

#### 2.1.4.1 Injection Errors

Errors occurring during the injection maneuver belong to one of the following categories.

a. Position Error - Errors in the position of the chaser may be separated into in-track errors, radial errors, and lateral or out-of-plane errors.

b. Velocity Errors - The incremental velocity imparted to the chaser may have errors in magnitude and/or direction. Errors in magnitude occur because of errors in determination of the required velocity increment or improper actuation of the thrust rockets. A directional error results from improper control of the vehicle attitude.

c. Timing Errors - A timing error occurs when the chaser imparts the incremental velocity at the incorrect time. This is equivalent to a down range or in-track error in position.

Injection errors may be the result of measurement errors and/or control errors. Since no control philosophy is postulated at injection, no attempt is made to separate the error sources.

2.1.4.2 Errors in Measurement of Observables During Active Rendezvous

The observables, all or combination of which may be measured during active rendezvous, are range, range rate, line-of-sight angle, and line-of-sight angular rate. The form of the errors for each is as follows:

a. Range Measurement Errors. - These errors are assumed to have a bias error or a normally distributed random error or both. Each of these errors comprises a fixed component and a component which is a given percentage of range.

b. Range Rate Measurement Errors. - Errors in measurement of range rate are postulated to have the same form as range measurement errors but are uncorrelated to the range measurement errors.

c. Angle Measurement Errors. - These errors are random in nature and follow a normal distribution about the actual value.

d. Angular Rate Measurement Errors. - These errors are assumed to be similar in nature, but uncorrelated to angle measurement errors.

2.1.5 Analytical Effort

Investigation of both manned and unmanned rendezvous requires a variety of computer programs, digital and analog, to be used in determining the effects of errors on the rendezvous procedure.

Each injection error is studied with respect to the resulting errors in the state variables at rendezvous and the increase in fuel expenditures. Sensitivity coefficients relating injection errors to errors at the nominal point of rendezvous are derived, and the increased velocity requirements to correct for these errors during the active rendezvous phase are determined utilizing the computer programs and analytical methods. No measurement errors are assumed during active rendezvous when analyzing injection errors.

In determining the effect of measurement errors, the active rendezvous is simulated, with a fixed injection error for each run to establish a basis for comparison. Measurement errors are included individually to find their relative effect on the ability of the chaser to achieve the desired terminal condition. Incremental velocity requirements are also determined.

It is stipulated that each individual injection error of $3\sigma$ magnitude shall not result in a velocity increase of more than 20 percent over the velocity requirements for the ideal Hohmann transfer. The velocity requirements are determined by including the active phase guidance and control with no errors included on the measurement of observables.

Two criteria are used in determining the allowable magnitude of measurement errors.

a. An individual $3\sigma$ measurement error shall not require more than a 50-percent incremental velocity increase (for the complete rendezvous) over that of the ideal Hohmann transfer.

b. An individual $3\sigma$ measurement error shall not result in more than a $\pm$20-percent deviation in the desired position and velocity at termination of the active rendezvous phase.

## 2.2 ANALYSIS

It was stated previously that there are three phases of rendezvous which are of concern in this investigation: (a) injection into ascent trajectory, (b) midcourse, and (c) active rendezvous. Sensors are required to obtain the information necessary for execution of maneuvers. In this subsection are set forth those assumptions and procedures used to determine the accuracies and dynamic ranges required of the injection and rendezvous sensors.

Three separate analyses of injection and active rendezvous are performed in this investigation. Each analysis utilizes a separate rendezvous model. Included are discussions of the specific models including the pertinent techniques, equations and constants, the analysis performed, and the results of the analyses.

Each model is built around the basic framework presented previously in which the chaser parking orbit is essentially coplanar with the target orbit and the reference transfer trajectory between the orbits is defined as the Hohmann transfer.

The three models differ primarily in the guidance techniques used. The first guidance technique is automatic and utilizes a modified proportional navigation system which assumes continuous applied thrust of varying magnitude.

The second type of guidance is an on-off system which assumes constant thrust engines. Engine firing is controlled by means of a predetermined program based upon the relative dynamics between chaser and target. This system is also considered to be automatic.

The third technique is similar to the second except that manual control by a pilot is utilized to determine the effect of a human in the overall system loop. Results based on this guidance technique are more qualitative than quantitative.

Results obtained from each investigation are dependent upon the assumption made and the model employed. Since each rendezvous analysis presented is essentially different from and independent of the others it is felt that the model, techniques, and results of each study should be presented as an entity. Consequently, paragraph 2.2.1 contains a discussion of the modified proportional navigation model, the procedures and the assumptions made for its use, and the results obtained. Paragraphs 2.2.2 and 2.2.3 contain equivalent information for the automatic on-off and the manned on-off systems respectively.

In paragraph 2.2.4 is presented an analysis which derives a procedure for reducing the uncertainties in the determination of the state variables of the chaser by utilizing measurements during the midcourse phase. Results of this analysis are presented to demonstrate the effectiveness of the midcourse measurements.

### 2.2.1 Modified Proportional Navigation System

This paragraph contains a discussion of the analysis performed using modified proportional navigation (MPN). The pertinent characteristic of this system is continuously applied, variable level thrust utilized in both the longitudinal and normal channels.

#### 2.2.1.1 Model

In this rendezvous model, the active phase of which is simulated on a digital computer, the target is assumed to be in a 555 km (300 n.mi) circular orbit and the chaser in a 185 km (100 n. mi) circular parking orbit. Injection occurs when the chaser, by means of onboard and/or ground measurements, assumes it is properly phased with the target and, therefore, at perigee of the transfer orbit. At this time the chaser imparts a velocity impulse by means of a rocket thrust thereby assuming the ascent trajectory.

After injection, the chaser travels the transfer orbit in a coasting mode until the chaser-to-target range decreases to 18.5 km (10 n.mi), at which time active rendezvous begins. At this point the onboard sensor acquires the target and the guidance system dictates the proper closure on the target. Observables utilized are the chaser-to-target range and range rate and the angular rate between the line of sight and an inertial reference.

During the active rendezvous phase, longitudinal and lateral accelerations are applied continuously. The instantaneous magnitude and direction of these accelerations are defined by the following equations:

$$a_L = (0.6)^* \frac{\dot{R}^2 - \dot{R}_f^2}{R - R_f} \text{ m/sec}^2 \qquad (2\text{-}1)$$

$$a_N = (2.1)^* \dot{R}\dot{e} \text{ m/sec}^2 \qquad (2\text{-}2)$$

where

$R$, $\dot{R}$ = chaser-to-target range (m) and range rate

$R_f$, $\dot{R}_f$ = desired final chaser-to-target range (km) and range rate

$\dot{e}$ = angular rate between the line of sight and an inertial reference (rad)

The values of $R_f$ and $\dot{R}_f$ which have been selected are 305 m (1,000 ft) and -3.05 m/sec (-10/sec) respectively.

Longitudinal acceleration is applied in one direction only, that direction being such as to decrease the chaser-to-target closing velocity. Normal acceleration may be applied in either of two directions (±) along the axis which is normal to the line of sight and in the plane of line-of-sight rotation. By permitting thrust to be applied in either direction (as determined by the direction of the line-of-sight rotation) a minimum amount of attitude control capability is required to keep the thrust axis in the plane of line-of-sight rotation, thereby permitting a smoother, more accurate active rendezvous phase.

Measurement of the relative dynamics between the target and chaser is done in a rotating cartesian coordinate system centered at the target vehicle. The plane of rotation of this system is the XY-plane with the X-axis along the local horizontal and the Y-axis along the radius vector from the center of the earth's gravitational field. The Z-axis, therefore, is normal to the plane of rotation and defines the axis of rotation (see figure 2-2).

Appendix A (Volume IV) contains a discussion of the computer program. Presented are the equations utilized in the program mechanization. Further discussion of the guidance technique including determination of equations 2-1 and 2-2 is contained in Appendix B (Volume IV).

---

* The values for the coefficients in equations 2-1 and 2-2 result when the control parameters in equations 1-2 and 1-3 are assigned the following values:

K = 2.5

S = 1.5

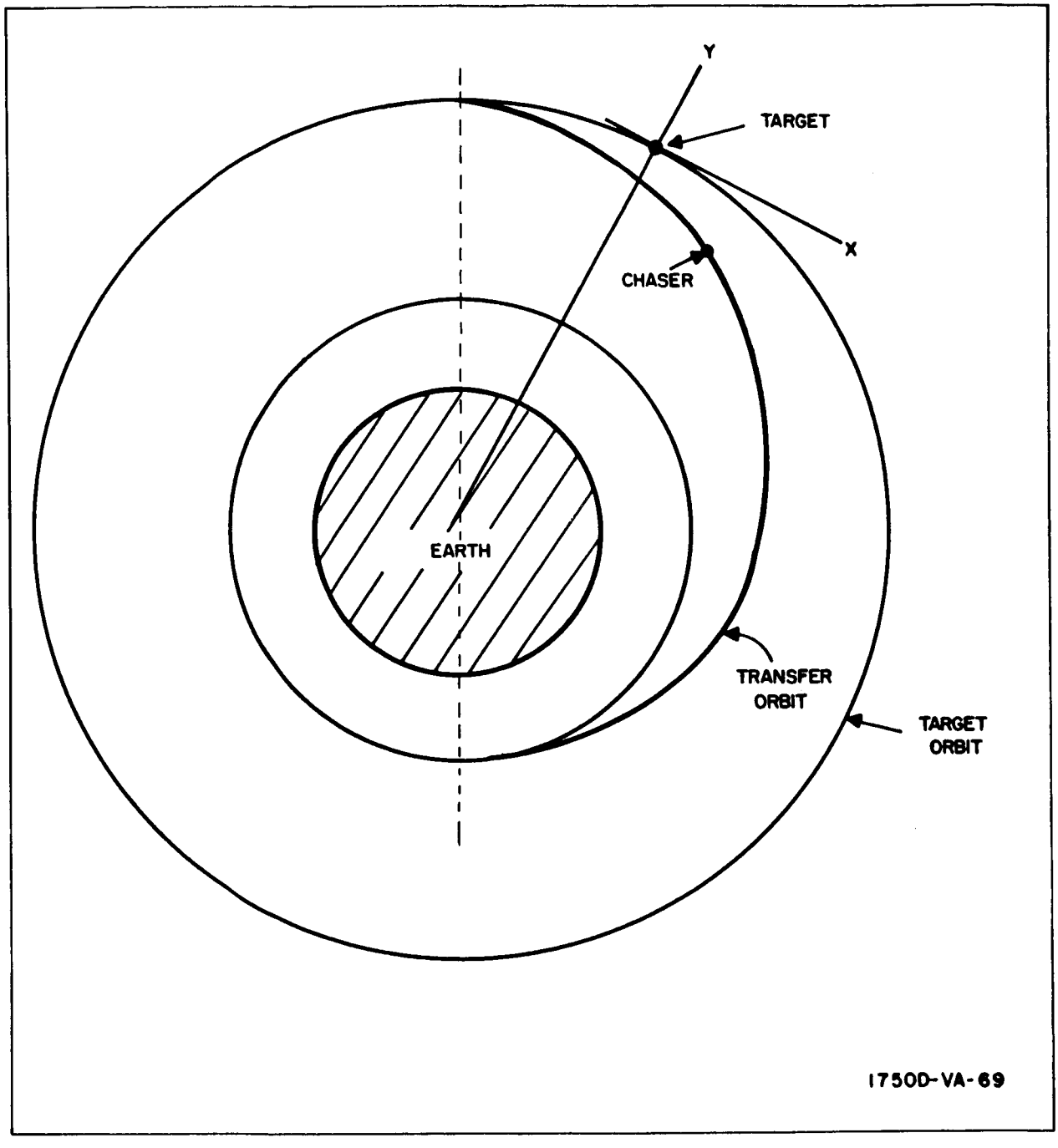


Figure 2-2. Coordinate System for MPN Rendezvous Model

2.2.1.2 Analysis of Injection Maneuver

Errors encountered by the chaser, upon injecting from the parking orbit to the transfer orbit, propagate along the reference trajectory and result in position and/or velocity errors at initiation of the active rendezvous phase. A linear analysis is performed to relate the errors at injection to the deviations from the reference trajectory at the start of active rendezvous. Consideration of the guidance law then determines the incremental velocities which must be imparted during the active rendezvous phase to compensate for these errors.

Injection errors in position and velocity are postulated. These are represented by the column vector

$$\begin{bmatrix} \Delta X_i \\ \Delta Y_i \\ \Delta Z_i \\ \Delta \dot{X}_i \\ \Delta \dot{Y}_i \\ \Delta \dot{Z}_i \end{bmatrix}$$

where the X-, Y-, and Z-components are measured in the rotating coordinate system centered at the target vehicle.

Position and velocity errors at initiation of active rendezvous are also expressed as a column vector.

$$\begin{bmatrix} \Delta X_o \\ \Delta Y_o \\ \Delta Z_o \\ \Delta \dot{X}_o \\ \Delta \dot{Y}_o \\ \Delta \dot{Z}_o \end{bmatrix}$$

These errors are then related to the injection errors by the Clohessey-Wiltshire error propagation matrix, $[A]$. (See Ref. 6.)

This relationship is expressed by the matrix equation

$$\begin{bmatrix} \Delta X_o \\ \Delta Y_o \\ \Delta Z_o \\ \Delta \dot{X}_o \\ \Delta \dot{Y}_o \\ \Delta \dot{Z}_o \end{bmatrix} = [A] \begin{bmatrix} \Delta X_i \\ \Delta Y_i \\ \Delta Z_i \\ \Delta \dot{X}_i \\ \Delta \dot{Y}_i \\ \Delta \dot{Z}_i \end{bmatrix} \tag{2-3}$$

where (2-4)

$$[A] = \begin{bmatrix} 1 & 6(\omega_T t - \sin \omega_T t) & 0 & \frac{4}{\omega_T} \sin \omega_T t - 3t & \frac{2}{\omega_T}(1 - \cos \omega_T t) & 0 \\ 0 & 4 - 3 \cos \omega_T t & 0 & \frac{-2}{\omega_T}(1 - \cos \omega_T t) & \frac{1}{\omega_T} \sin \omega_T t & 0 \\ 0 & 0 & \cos \omega_T t & 0 & 0 & \frac{1}{\omega_T} \sin \omega_T t \\ 0 & 6\omega_T(1 - \cos \omega_T t) & 0 & 4 \cos \omega_T t - 3 & 2 \sin \omega_T t & 0 \\ 0 & 3\omega_T \sin \omega_T t & 0 & -2 \sin \omega_T t & \cos \omega_T t & 0 \\ 0 & 0 & -\omega_T \sin \omega_T t & 0 & 0 & \cos \omega_T t \end{bmatrix}$$

$\omega_T$ = angular orbital velocity of target ($1.096 \times 10^{-3}$ rad/sec)

Velocity increments necessary to effect rendezvous are determined from considerations of the modified-proportional-navigation guidance law and are expressed as:

$$V_L = \left| \dot{R}_o \right| \tag{2-5}$$

$$V_N = \left( \frac{1 + a}{a} \right) \left| R_o \dot{e}_o \right| \quad \text{(in-plane normal velocity increment)} \tag{2-6}$$

$$V'_N = \left( \frac{1 + a}{a} \right) \left| R_o \dot{e}'_o \right| \quad \text{(out-of-plane normal velocity increment)} \tag{2-7}$$

where $a = \frac{SK - 1}{K}$

where $R_o$ = chaser-to-target range at initiation of the active rendezvous

$\dot{e}_o$ = in-plane line-of-sight angular rate at initiation of active rendezvous

$\dot{e}'_o$ = out-of-plane line-of-sight angular rate at initiation of rendezvous

The quantities on the right-hand sides of equations 2-5, 2-6, and 2-7 can be expressed in the target-centered coordinate system as follows:

$$R_o = \sqrt{X_o^2 + Y_o^2} \tag{2-8}$$

$$\dot{R}_o = \frac{X_o \dot{X}_o + Y_o \dot{Y}_o'}{\sqrt{X_o^2 + Y_o^2}} \tag{2-9}$$

$$\dot{e}_o = -\omega_T + \frac{Y_o \dot{X}_o - \dot{Y}_o X_o}{X_o^2 + Y_o^2} \tag{2-10}$$

$$\dot{e}'_o = \frac{Z_o (X_o \dot{X}_o + Y_o \dot{Y}_o)}{\sqrt{(X_o^2 + Y_o^2)^3}} - \frac{\dot{Z}_o}{\sqrt{X_o^2 + Y_o^2}} \tag{2-11}$$

where $\omega_T$ is the angular rate of the coordinate system which is equivalent to the angular orbital velocity of the target. Substituting equations 2-8 through 2-11 in equations 2-5, 2-6, and 2-7 yields:

$$V_L = \left| \frac{X \dot{X}_o + Y \dot{Y}_o}{\sqrt{X_o^2 + Y_o^2}} \right| \tag{2-12}$$

$$V_N = \left[ \frac{1+a}{a} \right] \left| \left[ \sqrt{X_o^2 + Y_o^2} \right] \left[ -\omega_T + \frac{Y_o \dot{X}_o - \dot{Y}_o X_o}{X_o^2 + Y_o^2} \right] \right| \tag{2-13}$$

$$V'_N = \left[ \frac{1+a}{a} \right] \left| \left[ \sqrt{X_o^2 + Y_o^2} \right] \left[ \frac{Z_o X_o \dot{X}_o + Z_o Y_o \dot{Y}_o}{\sqrt{(X_o^2 + Y_o^2)^3}} - \frac{\dot{Z}_o}{\sqrt{X_o^2 + Y_o^2}} \right] \right| \tag{2-14}$$

Consequently, the velocities required for executing the active rendezvous maneuver can be expressed as

$$V_L = f_1(X_o, Y_o, Z_o, \dot{X}_o, \dot{Y}_o, \dot{Z}_o)$$

$$V_N = f_2(a, X_o, Y_o, Z_o, \dot{X}_o, \dot{Y}_o, \dot{Z}_o)$$

$$V'_N = f_3(a, X_o, Y_o, Z_o, \dot{X}_o, \dot{Y}_o, \dot{Z}_o)$$

where the o subscripts indicate the nominal state variables of the reference trajectory at initiation of the active phase.

Deviations from the nominal values of the state variables result in increased velocities to complete rendezvous. These velocity increases are found by taking the differentials of equations 2-12, 2-13, and 2-14.

$$\Delta V_L = \frac{\partial f_1}{\partial X_o} \Delta X_o + \frac{\partial f_1}{\partial Y_o} \Delta Y_o + \frac{\partial f_1}{\partial Z_o} \Delta Z_o + \frac{\partial f_1}{\partial \dot{X}_o} \Delta \dot{X}_o + \frac{\partial f_1}{\partial \dot{Y}_o} \Delta \dot{Y}_o + \frac{\partial f_1}{\partial \dot{Z}_o} \Delta \dot{Z}_o$$

(similarly for $\Delta V_N$ and $\Delta V'_N$)

The partial derivatives $\frac{\partial f}{\partial X_o}, \frac{\partial f}{\partial Y_o}, \frac{\partial f}{\partial Z_o}$ etc, are arranged in a 3 x 6 matrix, $[B]$, and the deviations in the state variables $\Delta X$, $\Delta Y$, etc can be expressed as a column vector resulting in the following equation:

$$\begin{bmatrix} \Delta V_L \\ \Delta V_N \\ \Delta V'_N \end{bmatrix} = \begin{bmatrix} \frac{\partial f_1}{\partial X_o} & \frac{\partial f_1}{\partial Y_o} & \frac{\partial f_1}{\partial Z_o} & \frac{\partial f_1}{\partial \dot{X}_o} & \frac{\partial f_1}{\partial \dot{Y}_o} & \frac{\partial f_1}{\partial \dot{Z}_o} \\ \frac{\partial f_2}{\partial X_o} & \frac{\partial f_2}{\partial Y_o} & \frac{\partial f_2}{\partial Z_o} & \frac{\partial f_2}{\partial \dot{X}_o} & \frac{\partial f_2}{\partial \dot{Y}_o} & \frac{\partial f_2}{\partial \dot{Z}_o} \\ \frac{\partial f_3}{\partial X_o} & \frac{\partial f_3}{\partial Y_o} & \frac{\partial f_3}{\partial Z_o} & \frac{\partial f_3}{\partial \dot{X}_o} & \frac{\partial f_3}{\partial \dot{Y}_o} & \frac{\partial f_3}{\partial \dot{Z}_o} \end{bmatrix} \begin{bmatrix} \Delta X_o \\ \Delta Y_o \\ \Delta Z_o \\ \Delta \dot{X}_o \\ \Delta \dot{Y}_o \\ \Delta \dot{Z}_o \end{bmatrix} \quad (2\text{-}15)$$

or more briefly

$$\left[\Delta V\right] = \left[B\right] \begin{bmatrix} \Delta X_o \\ \Delta Y_o \\ \Delta Z_o \\ \Delta \dot{X}_o \\ \Delta \dot{Y}_o \\ \Delta \dot{Z}_o \end{bmatrix} \tag{2-16}$$

Substituting equation 2-3 into equation 2-16 gives

$$\left[\Delta V\right] = \left[B\right]\left[A\right] \begin{bmatrix} \Delta X_i \\ \Delta Y_i \\ \Delta Z_i \\ \Delta \dot{X}_i \\ \Delta \dot{Y}_i \\ \Delta \dot{Z}_i \end{bmatrix} \tag{2-17}$$

Multiplication of the $\left[A\right]$ matrix by the $\left[B\right]$ matrix yields a third matrix, $\left[C\right]$. The elements, $C_{ij}$, of this matrix are the sensitivity coefficients relating the errors at injection to the velocity penalties incurred by these errors.

a. Results of Injection Analysis for MPN. - Expanding equation 2-17 and evaluating the partial derivatives at a chaser-to-target range of 18.5 km yields the following values relating the total velocity penalties to the respective injection errors:

$$\frac{\partial(\Delta V)}{\partial X_i} = 0 \qquad \frac{\partial(\Delta V)}{\partial \dot{X}_i} = 47$$

$$\frac{\partial(\Delta V)}{\partial Y_i} = 9 \times 10^{-2} \qquad \frac{\partial(\Delta V)}{\partial \dot{Y}_i} = 1$$

$$\frac{\partial(\Delta V)}{\partial Z_i} = 1.25 \times 10^{-2} \qquad \frac{\partial(\Delta V)}{\partial \dot{Z}_i} = 0$$

To determine the allowable level of error in the injection sensor, the criterion is arbitrarily made that a $3\sigma$ error in any one state variable at injection shall not result in more than a 20-percent increase in propellant consumption compared with the perfect Hohmann transfer. For example, the allowable velocity expenditure to correct for an X-position error is stated as:

$$\frac{\partial(\Delta V)}{\partial X_i} \Delta X_{i\,(3\sigma)} \leq 0.2\ \Delta V_h \tag{2-18}$$

$$\Delta X_{i\,(3\sigma)} = \frac{0.2\ \Delta V_H}{\frac{\partial(\Delta V)}{\partial X_i}} \tag{2-19}$$

for the 185- to 555-km transfer

$$\Delta V_H = 211 \text{ m/sec} \tag{2-20}$$

computing the $3\sigma$ values of the errors in the state variables at injection yields the values given in table 2-1.

TABLE 2-1

ALLOWABLE ($3\sigma$) POSITION AND VELOCITY ERRORS AT INJECTION

| | |
|---|---|
| $\Delta X_i$ = ——— | $\Delta \dot{X}_i$ = 0.9 m/sec |
| $\Delta Y_i$ = 0.47 km | $\Delta \dot{Y}_i$ = 42.25 m/sec |
| $\Delta Z_i$ = 3.38 km | $\Delta \dot{Z}_i$ = ——— |

Since $\frac{\partial(\Delta V)}{\partial X_i} = \frac{\partial(\Delta V)}{\partial Z_i} = 0$, the effect of errors in $\Delta X_i$ and/or $\Delta \dot{Z}_i$ is insignificantly small.

It should be noted that the allowable injection errors given in table 2-1 are composed of the errors due to computation, control and execution of the injection maneuver. Consequently, the actual sensor errors that can be tolerated are less than the values indicated. Mechanization accuracies must be determined in order to perform the necessary tradeoff considerations.

b. Variation of Injection Requirements With Active Rendezvous Starting Range. - Varying the starting range of the active rendezvous maneuver results in variations in the sensitivity coefficients. These

variations are determined for starting ranges from 18.5 to 75 km (10 to 40 n. mi.) and presented in figure 2-3. Processing injection errors through the corresponding sensitivity coefficients in the manner outlined above, produces the injection accuracy requirements as a function of the starting range for active rendezvous. These results are presented in figure 2-4.

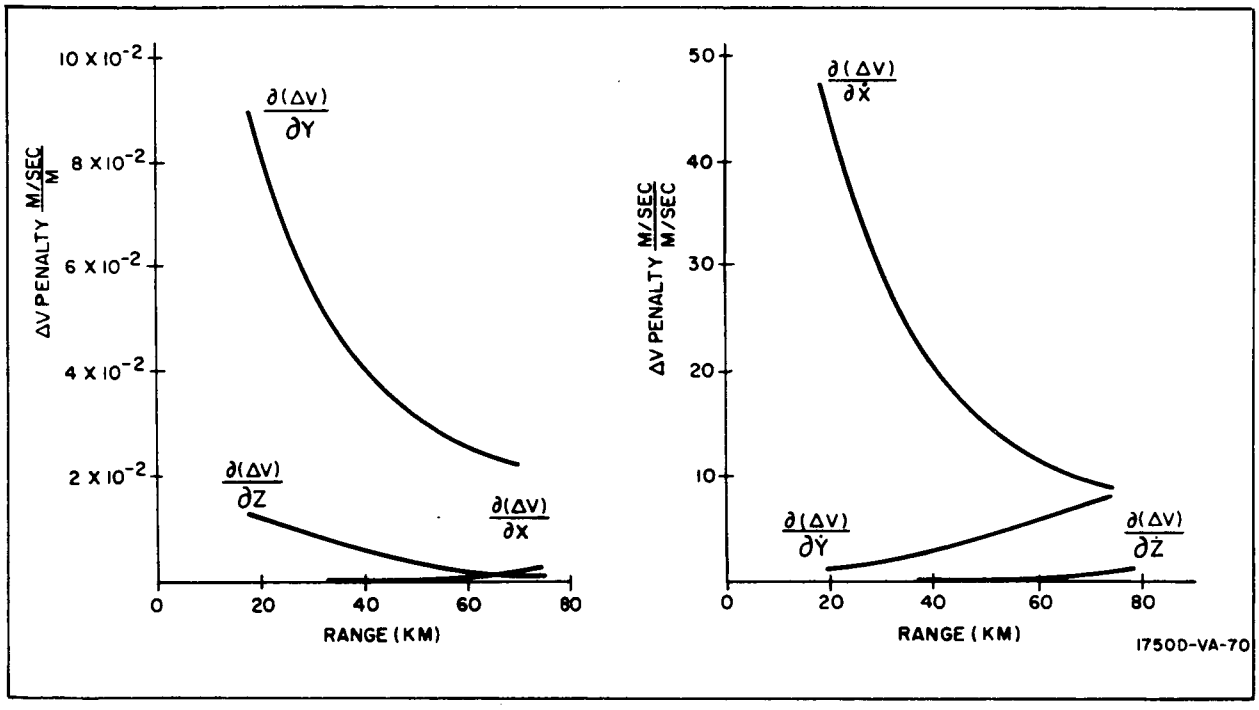


Figure 2-3. Injection Sensitivity Coefficients vs Initial Range of Active Rendezvous (MPN System)

2.2.1.3 Analysis of Active Rendezvous Phase

Two quantities must be specified in stating active rendezvous sensor requirements: The allowable magnitude of errors in the measurements which can be tolerated and the dynamic range required. Determination of these requirements is set forth in this subsection.

To facilitate determination of the allowable noise levels, a special digital program is used. This special program consists of equations adjoint to the linearized equations of Appendix A of Volume IV. The linearized and adjoint equations are given in Appendixes C and D, respectively, and a general discussion of the adjoint techniques is presented in subsection 6.2 of Appendix A (Volume V). Use of the adjoint model yields answers in one run which would otherwise require a Monte-Carlo approach.

a. Determination of Allowable Sensor Errors. - During the active rendezvous, sensors are required to measure the observables utilized by

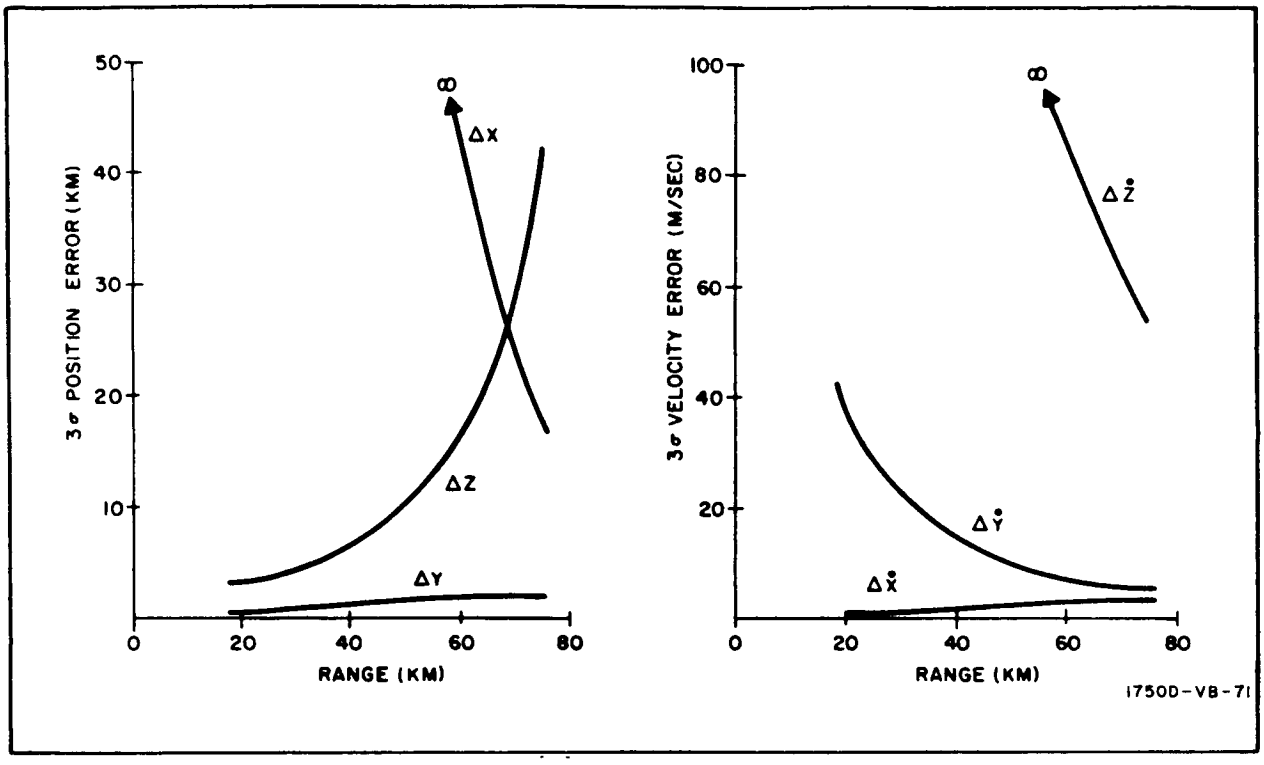


Figure 2-4. Allowable Injection Errors ($3\sigma$) for Various Starting Ranges of Active Rendezvous

the MPN guidance system: chaser-to-target range, range rate, and the line-of-sight angular rate. Errors, inherent in the measurement of these quantities, will cause deviations in range and range rate from the desired values at termination of the rendezvous maneuver.

To determine the maximum level of errors which can be tolerated, the following procedure is used: Errors are included on the sensor measurements, and the adjoint program is run to determine the effect of the errors on the terminal conditions.

Measurement errors are assumed which are typical of rendezvous sensors. Two types of errors are assumed for the range measurement: a bias error and a normally distributed random error. Each of these errors comprises two parts: one which is independent of range and one which is a percent of range. Similar errors are assumed for the range rate measurement.

Measurement of the line-of-sight angular rate is postulated as having errors which are independent of the angular rate itself; i.e., a bias and a normally distributed random part each independent of the magnitude and direction of the angular rate.

From the program results, an error matrix is set up which relates the terminal errors to the magnitude of each type of sensor error. Various levels of sensor errors are then processed through the matrix to find the resulting terminal errors. A maximum deviation from the nominal terminal conditions is postulated, and these deviations must not be exceeded when all errors are included on the measurements. Any combination of sensor errors which produce unacceptable terminal conditions is considered excessive.

Error matrices for three sensor bandwidths are presented in table 2-2. These matrices are obtained from computer runs of the adjoint program. Since the rendezvous model is two-dimensional, the Z and $\dot{Z}$ quantities are omitted. (The X and Y values are measured in the rotating coordinate system centered at the target vehicle.)

Units associated with the elements of the error matrices are given in table 2-3.

Multiplying the $1\sigma$ value of a given sensor error by the proper matrix element produces the $1\sigma$ value of the error in the corresponding terminal condition. For example, the error in X due to a fixed random error in the measurement of range may be expressed as:

$$\Delta X_{\sigma} = 0.06\ \Delta R_{\sigma} \qquad (2\text{-}21)$$

At termination of the rendezvous, the nominal range and range rate are 305 m and -3.05 m/sec. The allowable terminal errors are assumed to be twenty percent of the nominal values; i.e., 61 m in range and 0.61 m/sec in range rate.

Sensor errors considered representative of the 1970 time period are used in the analysis. The ranges of magnitude of these errors are given in table 2-4.

b. Determination of Dynamic Range Requirements. - The dynamic range requirements for the rendezvous sensor must be determined for each observable measured. For the modified proportional navigation system this includes range, range rate, and angular rate.

The dynamic range for chaser-to-target range measurements is determined by the range at which the active rendezvous phase begins (assuming no prior range measurement is desired for midcourse correction or the injection maneuver). For the mission postulated, the active rendezvous phase starts at 18.5 km, and range information is required into essentially zero range.

A time histroy of range rate for three target altitudes is obtained from the program. The relationship of range rate versus chaser-to-target range is plotted in figure 2-5. Assuming that range rate information would not be

TABLE 2-2

RENDEZVOUS ERROR MATRICES

Rendezvous Parameters

Trajectory: Target altitude = 555 km; $R_o$ = 18.5 km
$\dot{R}_o$ = -103 m/sec; $\dot{e}_o$ = 0; $R_F$ = 305 m
$\dot{R}_F$ = -3.05 m/sec

MPN Guidance Law: Control, K = 2.5 and S = 1.5
Thrust bandwidth = 5.0 rad/sec
Sensor damping ratio = 0.7

| Terminal Errors | Sensor Errors | | | | |
|---|---|---|---|---|---|
| | Range (m) | % Range | Range Rate (m/sec) | % Range Rate | LOS Rate (mr/sec) |
| Random Errors (Sensor Bandwidth = 1.0 rad/sec) | | | | | |
| X (m) | 0.133 | 1.07 | 8.5 | 1.77 | 0.48 |
| Y (m) | 0.0052 | 0.112 | 0.443 | 0.212 | 20.0 |
| $\dot{X}$ (m/sec) | 0.0138 | 0.045 | 1.03 | 0.0396 | 0.007 |
| $\dot{Y}$ (m/sec) | $1.87 \times 10^{-4}$ | 0.00253 | 0.0137 | 0.00458 | 0.34 |
| Bias Errors (Sensor Bandwidth = 1.0 rad/sec) | | | | | |
| X (m) | -0.95 | -13.2 | -83.6 | 21.2 | -3.6 |
| Y (m) | 0.023 | -0.67 | -0.045 | 1.46 | -237.0 |
| $\dot{X}$ (m/sec) | $-6.8 \times 10^{-4}$ | 0.13 | 0.089 | -0.246 | 0.0488 |
| $\dot{Y}$ (m/sec) | $-6.7 \times 10^{-5}$ | -0.0024 | -0.084 | 0.048 | 3.26 |

TABLE 2-2 (Continued)

| Terminal Errors | Range (m) | % Range | Range Rate (m/sec) | % Range Rate | LOS Rate (mr/sec) |
|---|---|---|---|---|---|
| Random Errors (Sensor Bandwidth = 5.0 rad/sec) | | | | | |
| X (m) | 0.06 | 0.485 | 3.8 | 0.793 | 0.0216 |
| Y (m) | 0.0023 | 0.05 | 0.198 | 0.0955 | 8.96 |
| $\dot{X}$ (m/sec) | 0.012 | 0.0366 | 0.85 | 0.0284 | 0.00284 |
| $\dot{Y}$ (m/sec) | $0.85 \times 10^{-4}$ | 0.00113 | 0.0063 | 0.002 | 0.152 |
| Bias Errors (Sensor Bandwidth = 5.0 rad/sec) | | | | | |
| X (m) | -0.95 | -13.1 | -83.6 | 21.2 | -3.6 |
| Y (m) | 0.023 | -0.67 | -0.045 | 1.45 | -237.0 |
| $\dot{X}$ (m/sec) | $-6.8 \times 10^{-4}$ | 0.131 | 0.089 | -0.247 | 0.0488 |
| $\dot{Y}$ (m/sec) | $-6.7 \times 10^{-5}$ | -0.0244 | -0.084 | 0.048 | 3.26 |
| Random Errors (Sensor Bandwidth = 10.0 rad/sec) | | | | | |
| X (m) | 0.043 | 0.341 | 2.71 | 0.564 | 0.015 |
| Y (m) | 0.00164 | 0.0357 | 0.141 | 0.0676 | 6.35 |
| $\dot{X}$ (m/sec) | 0.0087 | 0.0027 | 0.65 | 0.0021 | 0.00198 |
| $\dot{Y}$ (m/sec) | $0.61 \times 10^{-4}$ | 0.0008 | 0.0044 | 0.00145 | 0.108 |

TABLE 2-2 (Continued)

| Terminal Errors | Range (m) | % Range | Range Rate (m/sec) | % Range Rate | LOS Rate (mr/sec) |
|---|---|---|---|---|---|
| Bias Errors (Sensor Bandwidth = 10.0 rad/sec) | | | | | |
| X (m) | -0.95 | -13.2 | -83.6 | 21.2 | -3.6 |
| Y (m) | 0.023 | -0.67 | -0.045 | 1.45 | -237.0 |
| $\dot{X}$ (m/sec) | $-6.8 \times 10^{-4}$ | 0.131 | 0.089 | -0.247 | 0.0476 |
| $\dot{Y}$ (m/sec) | $-6.7 \times 10^{-5}$ | -0.0244 | -0.084 | 0.0481 | 3.26 |

TABLE 2-3

UNITS FOR ERROR MATRIX COEFFICIENTS

| Terminal Errors | Sensor Errors | | | | |
|---|---|---|---|---|---|
| | Range (m) | % Range | Range Rate (m/sec) | % Range Rate | LOS Rate (mr/sec) |
| X (m) | - | m | sec | m | $\frac{\text{m sec}}{\text{mr}}$ |
| Y (m) | - | m | sec | m | $\frac{\text{m sec}}{\text{mr}}$ |
| $\dot{X}$ (m/sec) | $\text{sec}^{-1}$ | $\frac{\text{m}}{\text{sec}}$ | - | $\frac{\text{m}}{\text{sec}}$ | $\frac{\text{m}}{\text{mr}}$ |
| $\dot{Y}$ (m/sec) | $\text{sec}^{-1}$ | $\frac{\text{m}}{\text{sec}}$ | - | $\frac{\text{m}}{\text{sec}}$ | $\frac{\text{m}}{\text{mr}}$ |

TABLE 2-4

TYPICAL SENSOR ERROR LEVELS

(1970 Time Period)

| Random (Fluctuation) Error Levels (1σ) | | | | | |
|---|---|---|---|---|---|
| Type / Range | Range (m) | %Range | Range Rate $\left(\frac{m}{sec}\right)$ | %Range Rate | LOS Rate $\left(\frac{mr}{sec}\right)$ |
| Low | 0.61 (2 ft) | 0.2 | 0.03 (0.1 ft/sec) | 0.05 | 0.03 |
| Medium | 1.52 (5 ft) | 0.5 | 0.15 (0.5 ft/sec) | 0.20 | 0.10 |
| High | 3.04 (10 ft) | 1.0 | 0.06 (2.0 ft/sec) | 0.50 | 0.20 |
| BIAS ERROR LEVELS (1σ) | | | | | |
| Type / Range | Range (m) | %Range | Range Rate $\left(\frac{ft}{sec}\right)$ | %Range Rate | LOS Rate $\left(\frac{mr}{sec}\right)$ |
| Low | 0.305 (1 ft) | 0.2 | 0.03 (0.1 ft/sec) | 0.05 | 0.03 |
| Medium | 0.61 (2 ft) | 0.5 | 0.15 (0.5 ft/sec) | 0.20 | 0.10 |
| High | 3.05 (10 ft) | 2.0 | 0.6 (2.0 ft/sec) | 0.50 | 0.20 |

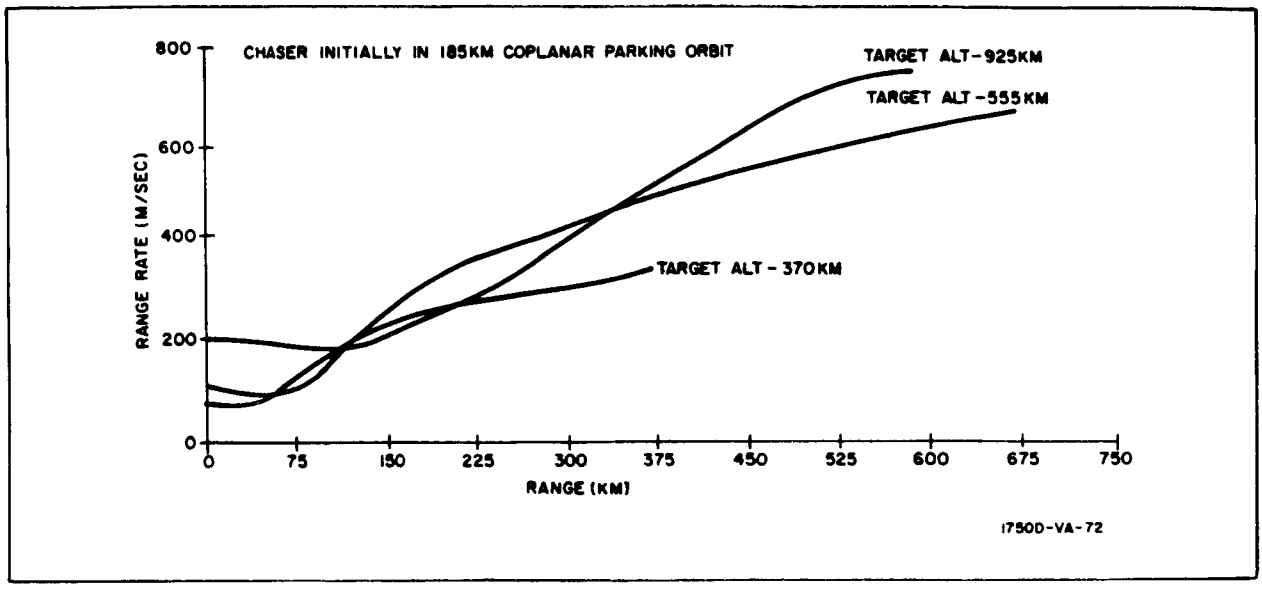


Figure 2-5. Range Rate vs Range for an Ideal Hohmann Transfer

required prior to active rendezvous, the values of range rate occuring at ranges less than the acquisition range is the significant factor. As can be seen from figure 2-5, the values of range rate at ranges less than 20 km extend from zero to approximately 200 m/sec. If the acquisition range is extended to 75 km a closing range rate of 300 m/sec may be encountered.

Angular rate information as a function of range is presented in figure 2-6. This figure indicates that the magnitude of the LOS rate varies from 0 to 0.4 mr/sec at ranges below 75 km for the nominal Hohmann transfer. Higher rates can be expected however, as the true trajectory deviates from the nominal because of errors.

c. Sensor Requirements. - Typical results of the procedure outlined in paragraph a above are shown in figures 2-7 and 2-8, which show the effects of bias and random errors on the final conditions for a sensor bandwidth of 5 rad/sec. Also included are the errors due to the mechanization assumed, i.e., errors due to the gains and time lags of the modified proportional navigation system.

In figure 2-7, the allowable final position error is indicated by the circle about the origin of the X-Y target-centered coordinates. Figure 2-8 shows the allowable final relative velocity error in a similar manner.

The bias errors are processed in a manner such as to give the worst case; i.e., they all add in the same direction. These errors are indicated by the vectors for the low, medium, and high error levels.

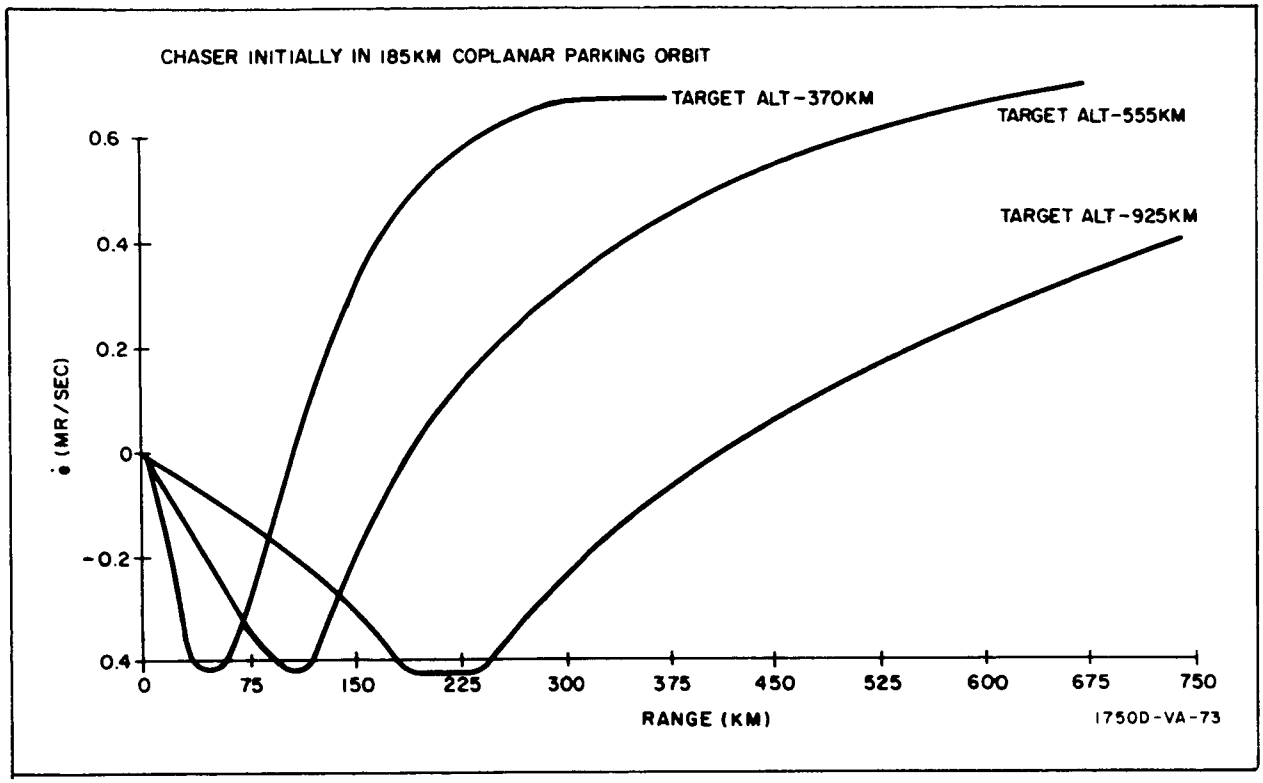


Figure 2-6. Line-of-Sight Rate vs Range for an Ideal Hohmann Transfer

Low, medium, and high random errors are indicated by the ellipses centered at the end of the respective bias errors. The semimajor and semiminor axis of the ellipses are equal in magnitude to the $3\sigma$ values of the respective random errors.

On the basis of the criteria established, it is seen that the high levels of sensor errors is unacceptable while the medium and low levels produce terminal conditions which are acceptable. Consequently the medium level of errors is stated as being the sensor requirements for the active phase of rendezvous.

For acceptable values of sensor errors, it is informative to analyze the individual contributions to each of the four components of terminal error. Table 2-5 gives the breakdown of the total terminal errors in X, Y, $\dot{X}$, $\dot{Y}$, both bias and random, for the five contributing input sensor errors. The predominant contributor to each terminal error is indicated, showing that errors accruing in the X and $\dot{X}$ terminal condition are primarily due to errors in measuring range rate and that errors in the y and $\dot{y}$ terminal conditions are due to errors in the measurement of line-of-sight rate.

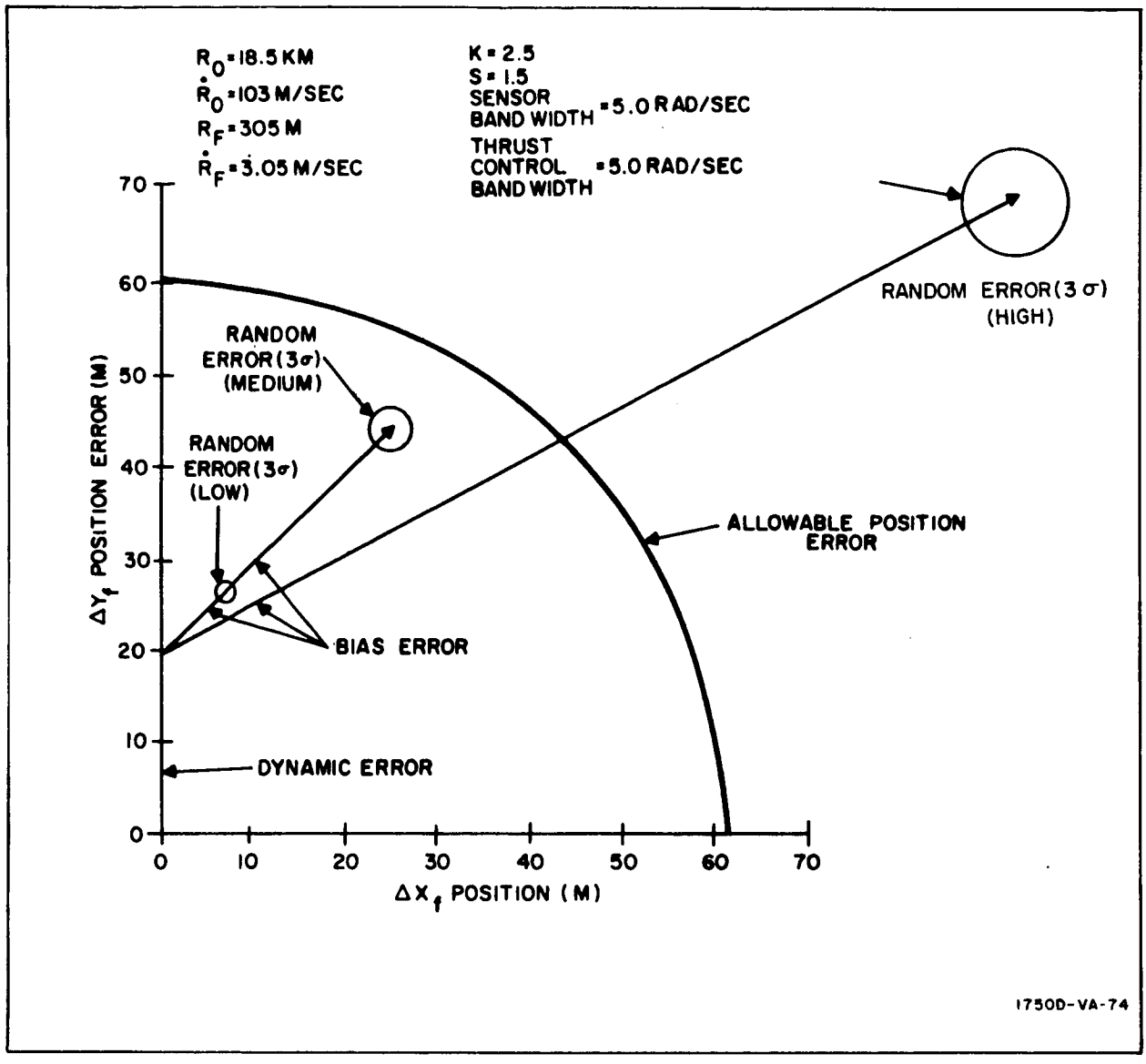


Figure 2-7. Rendezvous Terminal Position Error vs Sensor Error Level for MPN

Using the conditions stated in paragraph b above and allowing for errors and uncertainties, the sensor dynamic range requirements, given in table 2-6, are obtained.

## 2.2.2 On-Off Guidance

On-off guidance utilizes constant level thrusting as opposed to the variable level thrusting for modified proportional navigation. Consequently, thrust is applied for discrete intervals, rather than continuously and multiple

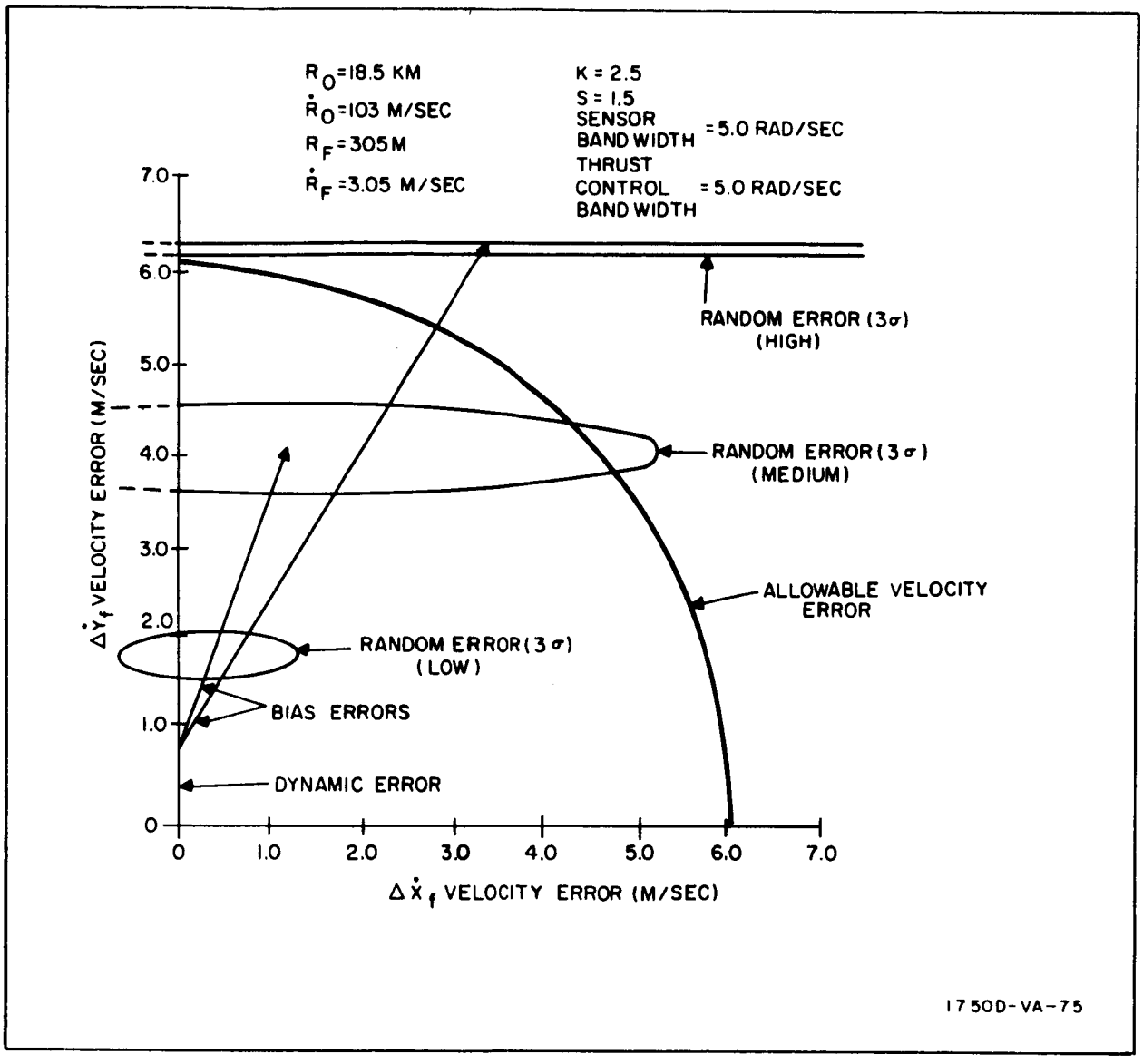


Figure 2-8. Rendezvous Terminal Velocity Error vs Sensor Error Level for MPN

restart capability of the engines is required. This guidance method is a compromise with the various systems that have been proposed for rendezvous using different guidance laws, propulsion sensors, attitude references, and data processing methods. It is combined with the basic rendezvous model and programed for the IBM 7094 digital computer. The program simulates the radar measurements, data processing, computations and maneuvering of a chaser achieving a rendezvous with a nonmaneuvering target.

Inputs to the program are designed so that the effects of a number of different parameters can easily be studied. Among the inputs to the program

TABLE 2-5

TERMINAL ERROR BREAKDOWN

(Sensor Error Level: Medium)

(Sensor Bandwidth = 5 rad/sec)

| Random Errors (1σ) | | | | | | | |
|---|---|---|---|---|---|---|---|
| Error Source / Coordinate | Range | % Range | Range Rate | % Range Rate | LOS Rate | Total | Predominant Contributor |
| X | 0.0914 | 0.8 | 0.579 | 0.52 | 0.07 | 0.656 m | Range rate |
| Y | 0.00975 | 0.08 | 0.0305 | 0.06 | 2.94 | 0.9 m | LOS rate |
| $\dot{X}$ | 0.0183 | 0.06 | 0.1311 | 0.019 | 0.009 | 0.13 $\frac{m}{sec}$ | Range rate |
| $\dot{Y}$ | $12.19 \times 10^{-4}$ | 0.002 | 0.000914 | 0.0014 | 0.05 | 0.016 $\frac{m}{sec}$ | LOS rate |
| **Bias Errors (1σ)** | | | | | | | |
| Error Source / Coordinate | Range | % Range | Range Rate | % Range Rate | LOS Rate | Total | Predominant Contributor |
| X | -0.579 | -21.6 | -12.74 | -13.9 | -1.2 | -24.5 m | Range rate |
| Y | 0.01524 | -1.1 | -0.0061 | -0.96 | -77.8 | -24.3 m | LOS rate |
| $\dot{X}$ | $-0.396 \times 10^{-3}$ | 0.15 | 0.01524 +0.05 | 0.16 | 0.016 | 0.12 m/sec | % Range rate |
| $\dot{Y}$ | $-0.305 \times 10^{-4}$ | -0.04 | -0.01280 | -0.03 | 1.07 | 0.02 m/sec | LOS rate |

TABLE 2-6

SENSOR DYNAMIC RANGE REQUIREMENTS

| Measurement | Min | Max |
|---|---|---|
| Range | 0 km | 25 km (for 18.5-km acquisition range) |
| | 0 km | 80 km (for 75-km acquisition range) |
| Range rate | -350 m/sec (closing) | 100 m/sec (opening) |
| LOS angular rate | -2 mr/sec | +2 mr/sec |

are four quantities which represent errors in the injection of the chaser from parking orbit into the transfer orbit. Other inputs include the specification of standard deviations of noise quantities, the order of smoothing to be used on the simulated radar readings and the number of points to be smoothed.

The main computational problem encountered in this study is a loss of accuracy in the computation of orbital elements from position and velocity vectors which becomes noticeable near the end of the maneuver when the orbit of the chaser begins to approach a circle. The problem is sufficiently reduced by performing all the computations of that particular method in double precision. Appendix G contains the equations used to mechanize this model.

2.2.2.1 Model

The target is assumed to be in a posigrade circular orbit about the earth at an altitude of 500 km. The chaser vehicle is considered to be in a 200-km circular parking orbit coplanar with the orbital plane of the target. When correctly phased, the chaser injects into an ascending transfer orbit - nominally the Hohmann transfer. Near the end of the ascent, at a chaser-to-target range of 25 km, the chaser commences the active phase of rendezvous with the target.

a. Chaser Vehicle Characteristics and Guidance Logic. - It is assumed that the chaser is provided with an inertial platform. When the range between the chaser and target has decreased to 25 km, the inertial reference is aligned to the range vector and the geocentric vertical and is thereafter maintained in this orientation (see figure 2-9). The chaser is attitude

stabilized to this reference for the duration of the rendezvous with the longitudinal axis (X-axis) along the range vector and the normal axis (Y-axis) in the orbit plane perpendicular to the longitudinal axis. Rockets are aligned in both directions (±) along the normal axis eliminating the need for rapid changes in vehicle attitude to orient thrust rockets.

With the nominal trajectory and without injection errors, the curve of range as a function of transit time is shown in figure 2-10. Figure 2-11 illustrates the variation in elevation angle with transit time where the elevation angle is referred to an inertial reference. Of particular interest is the small angle at ranges below 25 km. This indicates a very small line-of-sight angular change up to rendezvous even without corrective control, fitting in nicely with the control scheme actually used.

Because of the discontinuous application of thrust required by this guidance technique, switching regions and thresholds levels must be defined in order to control the thrust in the proper manner to accomplish rendezvous.

(1) Normal Control

Thrusting along the normal axis is applied whenever the magnitude of the line-of-sight rate (with respect to the inertial reference) exceeds a given

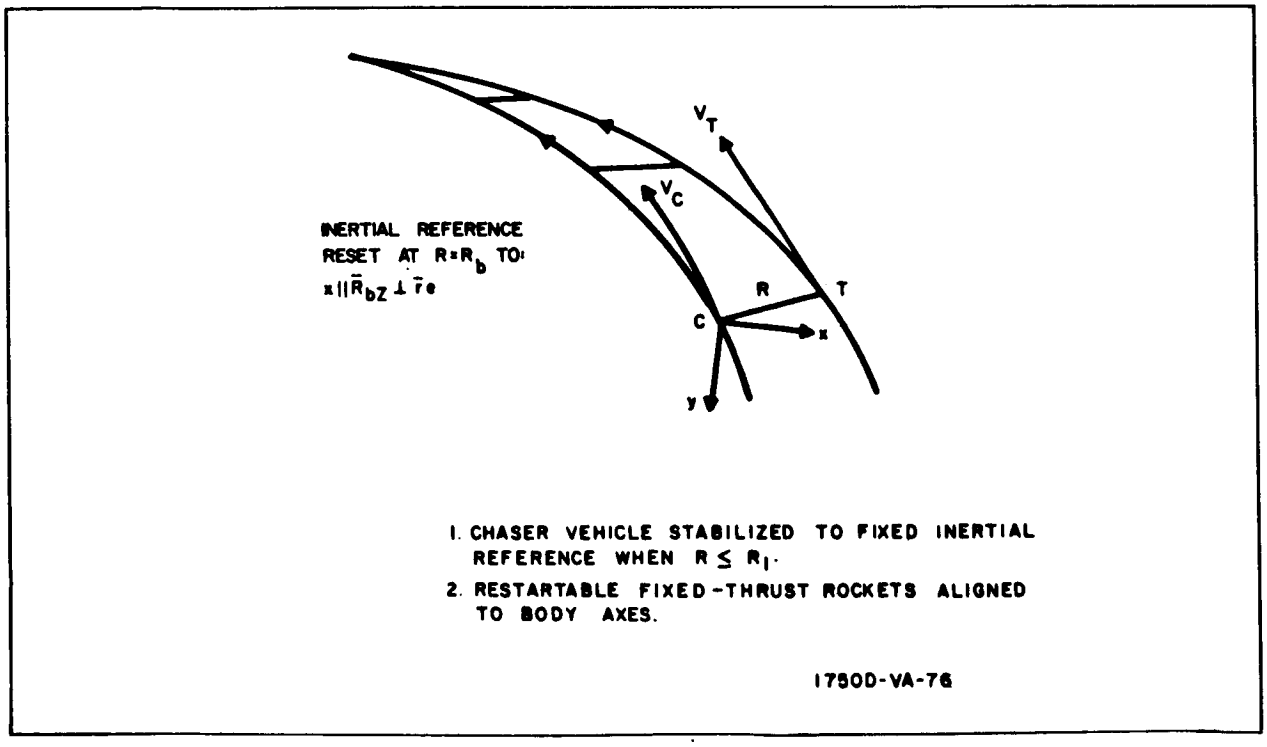


Figure 2-9. Active Rendezvous Geometry

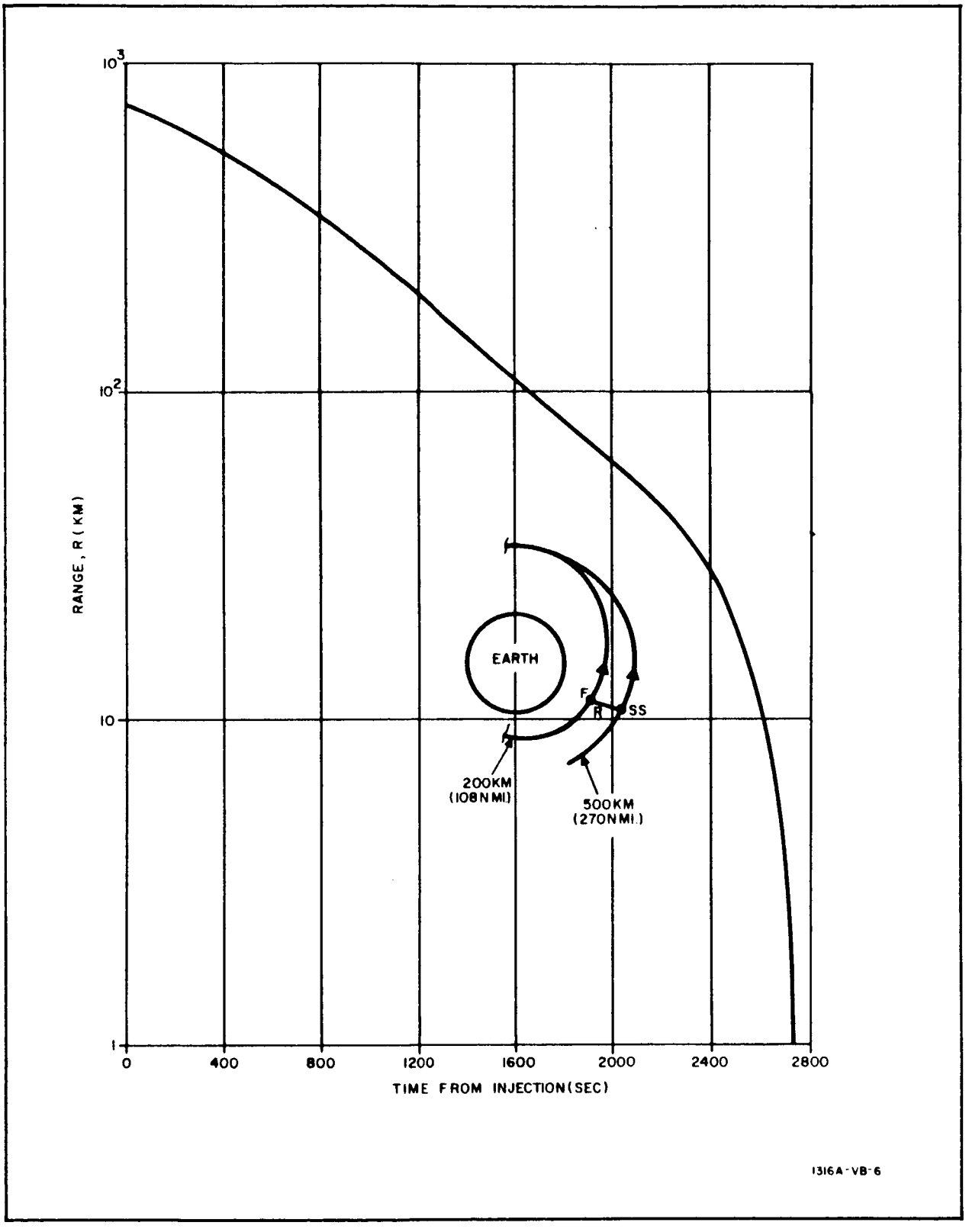


Figure 2-10. Range vs Transit Time

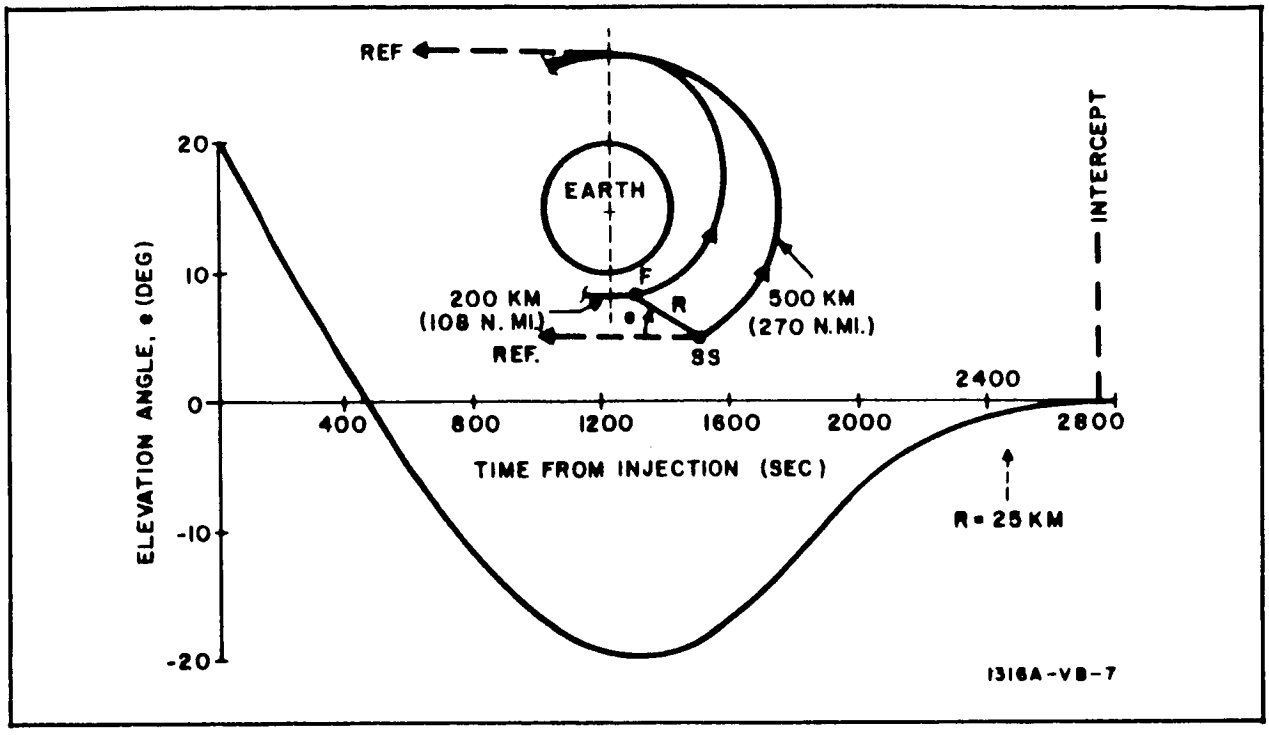


Figure 2-11. Elevation Angle vs Transit Time

threshold, $\epsilon$ = 0.3 mr/sec, for two consecutive seconds. Normal thrust of magnitude $a_N$ m/sec$^2$ is then applied for a given firing time as determined by the equation

$$t_F = \frac{C|R\dot{e}|}{|a_N|} \tag{2-22}$$

where $R$ = chaser-to-target range (m)

$\dot{e}$ = angular rate between the line-of-sight and the inertial reference (rad/sec)

$a_N$ = 1.0 m/sec$^2$

$C$ = 0.9 (This is a control constant included to prevent wasteful overshoot in the presence of noise.)

The direction of thrust application is such as to null the line-of-sight rate and is repeated whenever necessary. Two limitations are applied to firing the normal rockets to minimize nuisance firings and curtail firings resulting from noise modulations.

- Firing does not occur if $t_F < 2$ sec.

- A coasting period (dead time) of 5 sec minimum is required between firings.

(2) Longitudinal Control

Longitudinal control is effected when the chaser-to-target range decreases to 3.5 km, the range at which the phase plane trajectory enters the switching region defined by the parabolic curves in figure 2-12. Thrusting is executed so as to bring the range and range rate to the stipulated final values within the switching region. The nominal terminal conditions chosen are a range of 200 m with zero range rate.

The upper curve is defined by the equation:

$$\dot{R} = \sqrt{K_2 |R-R_f|} \tag{2-23}$$

and the lower curve by equation

$$\dot{R} = \sqrt{K_1 |R-R_f|} \tag{2-24}$$

where $R_f$ = final range = 200 m (2-25)

$K_1 = 1.5$ m/sec$^2$

$K_2 = 2.25$ m/sec$^2$

When the phase plane trajectory causes the upper boundary, a longitudinal thrust pulse is fired for a time duration:

$$t_F = \frac{2 \left| - \sqrt{K_1 |R-R_f|} - \dot{R} \right|}{|a_L|} \tag{2-26}$$

where $a_L = 1.5$ m/sec$^2$

This pulse is along the line of sight (longitudinal axis) and in such a direction so as to reduce the magnitude of the range rate between the chaser and target. To minimize nuisance firings and overshoots, the following control limitations are provided:

- The longitudinal rocket will not fire if $t_F < 2$ sec.

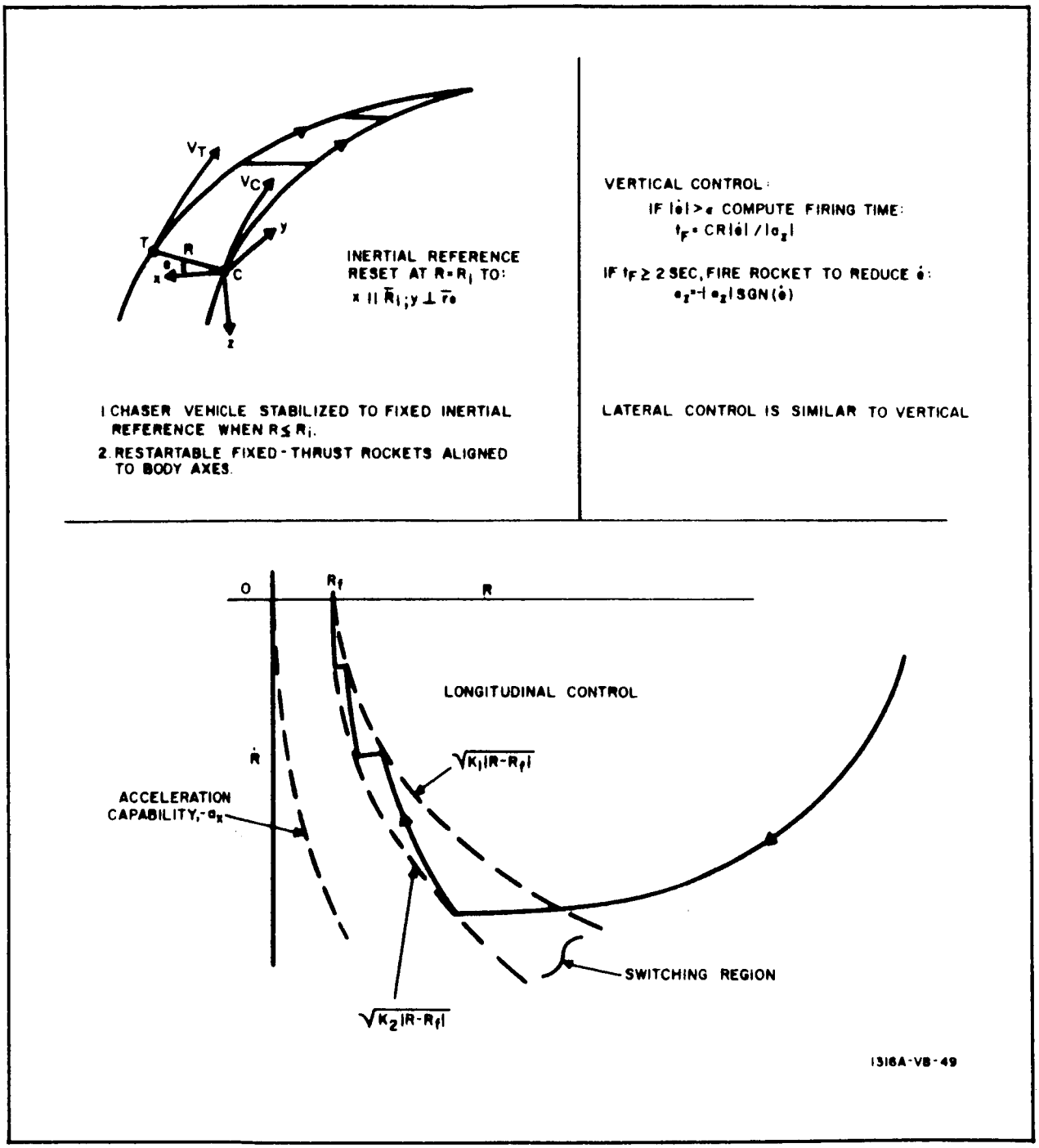


Figure 2-12. Rendezvous Guidance (Earth Space Station)

- A mandatory coast period of at least two seconds is stipulated between periods of rocket firing.

b. Onboard Data Processing

The inaccuracies of the rendezvous sensors are simulated in the computer

program by adding noise to the pure range and angle inputs. Noise values are generated by uncorrelated random number generating routines.

Because of the noise appearing on range and angle measurements, it is necessary to smooth the raw data before attempting to use these data for control purposes. A digital data smoother, illustrated in block form in figure 2-13, is included in the system to process and smooth the data for the control system, thereby permitting operation at higher noise levels.

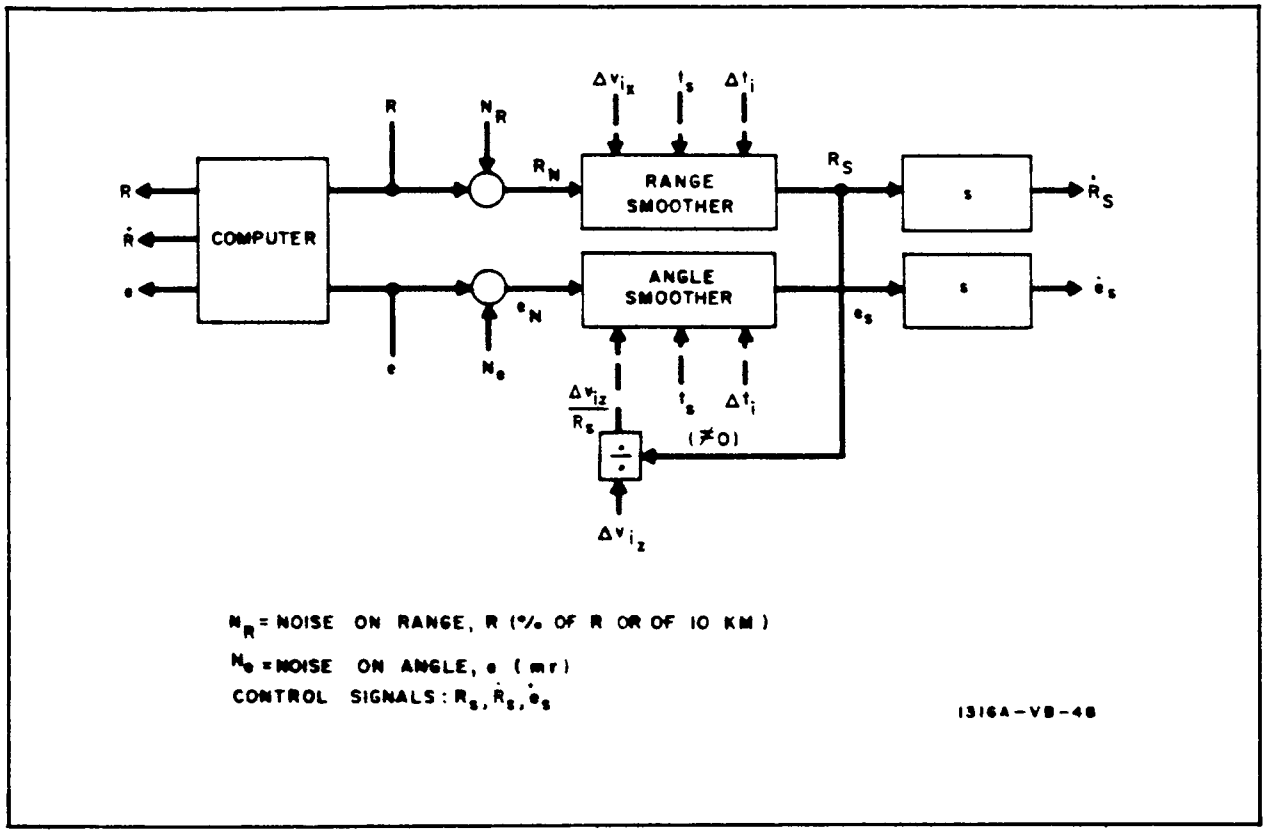


Figure 2-13. Digital Smoother (Range and Angle)

The onboard computer accepts components of the noisy range and angle inputs ($R_N$ and $e_n$) which are directly equivalent to actual sensor signals. These quantities are then fed to the appropriate digital data smoother at a rate of one sample, b, each data storage interval, $\Delta t_i$. The storage interval is taken as 1 second for this program. A smoothing time, $t_s$, of 15 seconds is stipulated during which n data samples of a given state variable are stored in the computer, where

$$n = \left( \frac{t_s}{\Delta t_i} + 1 \right) \qquad (2\text{-}27)$$

This produces 16 samples for the 15-second storage time utilized. These data samples are designated by $b_0$, $b_1$, $b_2 \ldots b_{15}$. with $b_0$ being the most recent. At a given sample time, $t_i$, these values may be plotted on a graph of the state variable vs time. A fit is then determined by the method of least squares and the curve is extrapolated over one storage interval, to obtain the smoothed value of the control variable. The slope of the curve yields the smoothed time derivative of the control variable. Smoothed values are used for all rendezvous control signals; i.e., $R_s$, $\dot{R}_s$, $\dot{e}_s$.

At each succeeding interval of $\Delta t_i$ the most recent data sample, $b_0$, is stored and the oldest, $b_{15}$, is discarded. Compensation is then included to permit smoothing to continue without appreciable error during actual thrusting periods. This procedure is illustrated using range as the state variable of interest. At time t', the sample values are $b'_0$, $b'_1$, $\ldots$ $b'_{15}$. A linear fit is determined and extrapolated by one storage interval. At time $t'' = t' + t_i$, new data samples are determined from the previous ones by adding a term to compensate for any thrusting during the sample time. The new sample points, $b''_i$, are expressed as

$$
\begin{aligned}
b''_0 &= \text{most recent value of R} \\
b''_1 &= b'_0 + 0.5\ \Delta v_i \\
b''_2 &= b'_1 + 1.5\ \Delta v_i \\
b''_3 &= b'_2 + 2.5\ \Delta v_i \\
b''_4 &= b'_3 + 3.5\ \Delta v_i \\
b''_5 &= \text{extrapolated (smoothed) value of R}
\end{aligned}
\qquad (2\text{-}28)
$$

where

$\Delta V_i = a_i \Delta t_F$ = velocity increment imparted along the range vector.

and

$\Delta t_F$ = amount of firing time within the storage interval.

The data points with the linear fit are shown in figure 2-14 for two successive time points.

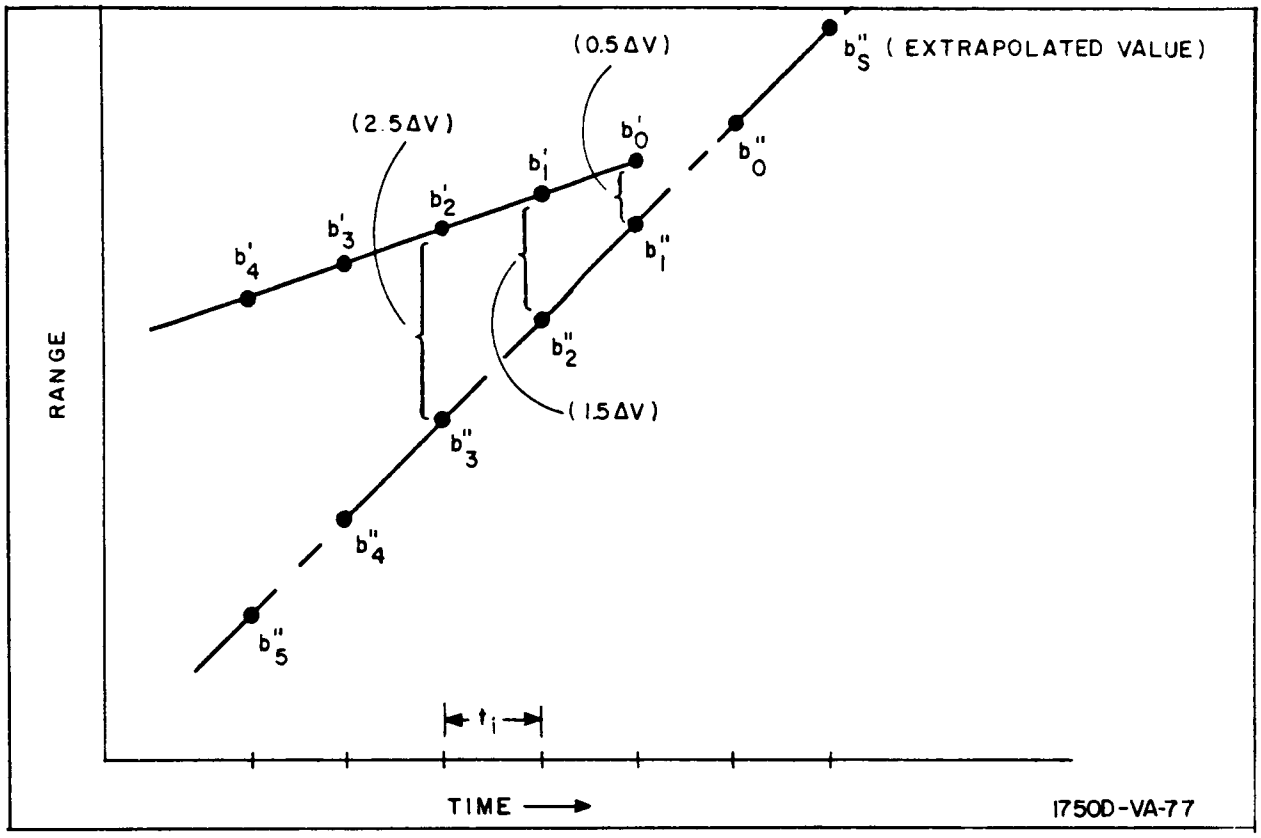


Figure 2-14. Graphical Illustration of Data Smoothing Technique

2.2.2.2 Analysis of the Injection Maneuver

When the transfer angle has been traversed with no active rendezvous, the errors at injection result in miss distances at the point of rendezvous. These miss distances are pessimistic in that they are not generally minimum; i.e., the minimum range may occur at some point prior to the chaser having traversed the full 180 degrees of the transfer trajectory.

Miss distance sensitivity coefficients are obtained by running the digital program with injection errors but no active rendezvous employed. Injection errors included are altitude ($\Delta h$), velocity ($\Delta V$), attitude (in plane) ($\Delta\gamma$), and timing ($\Delta t$).

The sensitivity coefficients obtained are presented in table 2-7. The final X- and Y- components of the range errors, $\Delta X_f$ and $\Delta Y_f$ are measured in the coordinate system centered at the chaser vehicle. The X-axis is along the nominal chaser-to-target line of sight and the Y-axis is along the earth interceptor radius vector at the nominal rendezvous point.

TABLE 2-7

MISS DISTANCE SENSITIVITY COEFFICIENTS

| Error | Horizontal Coef | | Vertical Coef | | Units |
|---|---|---|---|---|---|
| Altitude | $\frac{dx}{dh}$ | 4.83 | $\frac{dy}{dh}$ | 1.07 | $\frac{km}{km}$ |
| Velocity | $\frac{dx}{dV}$ | 8.32 | $\frac{dy}{dV}$ | 3.57 | $\frac{km}{m/sec}$ |
| Attitude | $\frac{dx}{d\gamma}$ | 5.21 | $\frac{dy}{d\gamma}$ | 0 | $\frac{km}{deg}$ |
| Timing | $\frac{dx}{dt}$ | 0.53 | $\frac{dy}{dt}$ | 0 | $\frac{km}{sec}$ |

The effects on fuel consumption of four types of injection errors are shown in figure 2-15. These are based on a series of runs made on the computer with the active rendezvous system in operation but no rendezvous sensor errors included. Comparison of the actual $\Delta V$ used in each case with that required for a Hohmann transfer, $\Delta V_H$, yields a non-dimensional indication of the incremental velocity requirements due to injection errors.

Additional quantities of interest, which are also obtained from the program are:

a. The deviation in range due to an error in central angle

$$\frac{dR}{d\phi} = 107 \ \frac{km}{deg}$$

b. The rate of change of the central angle between the target radius and chaser radius:

$$\frac{d\phi}{dt} = -0.0044 \ \frac{deg}{sec}$$

c. The chaser-to-target range at injection:

$$R_i = 749.8 \text{ km}$$

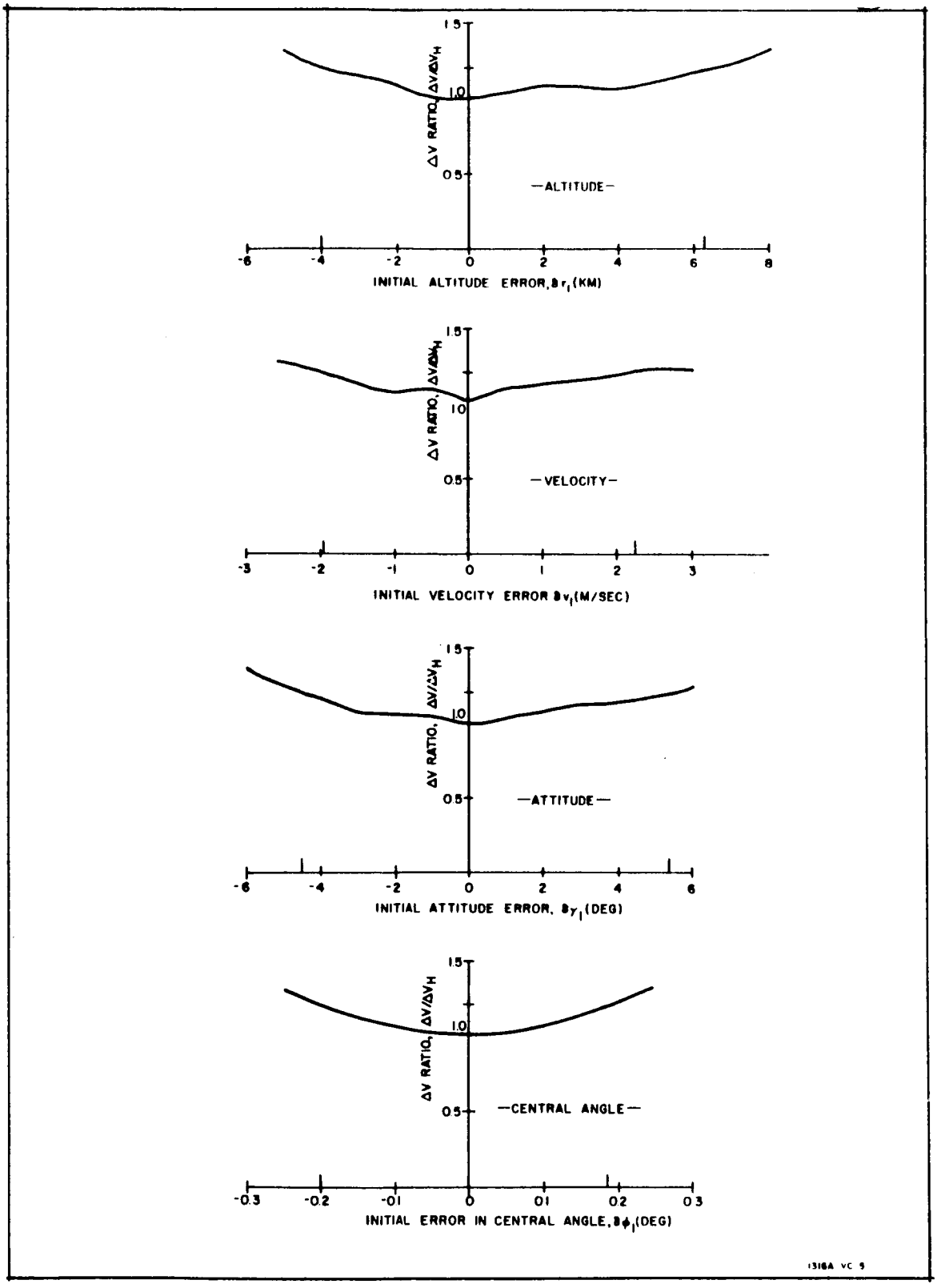


Figure 2-15. Effects of Initial Condition Deviations on Propellant Consumption

The lead angle error can be converted to an equivalent range error:

$$\Delta R_{(3\sigma)} = \frac{\partial R}{\partial \phi} \Delta\phi_{(3\sigma)} \tag{2-29}$$

The lead-angle error can be converted to an equivalent error in phasing time.

$$\Delta t_{(3\sigma)} = \frac{\Delta\phi(3\sigma)}{\frac{\partial \phi}{\partial t}} \tag{2-30}$$

In developing the acceptable error levels at injection, the four curves of figure 2-15 are employed. The criterion is made that a $3\sigma$ error in any one parameter at injection shall not result in more than a 20 percent increase in fuel consumption compared with the perfect Hohmann transfer. Consequently, the allowable errors in altitude, velocity, plane attitude (pitch), and central angle may be obtained directly from the curves. Allowable errors in range and timing are determined using equations 2-29 and 2-30:

$$\Delta R_{(3\sigma)} = (107)\,(0.19)$$

$$= 20.4 \text{ km}$$

where $\Delta\phi_{(3\sigma)}$ is obtained from figure 2-15.

This allowable range error can be expressed as a percent of initial range as

$$\Delta R_{(3\sigma)} = \frac{20.4}{749.8} = 2.72\% \text{ of } R_i$$

The $3\sigma$ timing error is:

$$\Delta t_{(3\sigma)} = \frac{0.19}{0.0044} = 43.2 \text{ sec}$$

An out-of-plane error in attitude ($\Delta\psi$) at injection imparts an out-of-plane velocity increment of magnitude:

$$\Delta V_N = \Delta V_p \sin \Delta\psi \tag{2-31}$$

where $\Delta v_p$ = velocity impulse necessary to inject into the Hohmann transfer. This out-of-plane velocity must be compensated for at apogee. Using the 20-percent criterion:

$$\Delta V_{N\,(3\sigma)} = 0.2\,\Delta V_H \tag{2-32}$$

Substituting equation 2-31 into equation 2-32 yields:

$$\Delta\psi_{(3\sigma)} = \sin^{-1}\left(\frac{0.2\,\Delta V_H}{\Delta V_p}\right) \tag{2-33}$$

$$= \sin^{-1}\left[\frac{(0.2)\,(171.9)}{(86.5)}\right]$$

$$= 26.6 \text{ deg}$$

A differential inclination between the target and chaser orbital planes also results in an out-of-plane velocity which must be corrected. Again if:

$$\Delta V_{N\,(3\sigma)} = 0.2\,\Delta V_H$$

then the $3\sigma$ value of differential inclination is:

$$\Delta i_{(3\sigma)} = \sin^{-1}\left(\frac{0.2\Delta V_H}{V_a}\right) \tag{2-34}$$

where $V_a$ = apogee velocity of Hohmann transfer ellipse

This is illustrated in figure 2-16 where both the normal and in-plane velocity impulses required to complete the transfer are shown.

Evaluating equation 2-34

$$\Delta i_{(3\sigma)} = \sin^{-1}\left[\frac{(0.2)\,(171.9)}{7616}\right]$$

$$= 0.26 \text{ deg}$$

The injection sensor requirements are summarized in table 2-8 along with reasonable state-of-the-art equivalents.

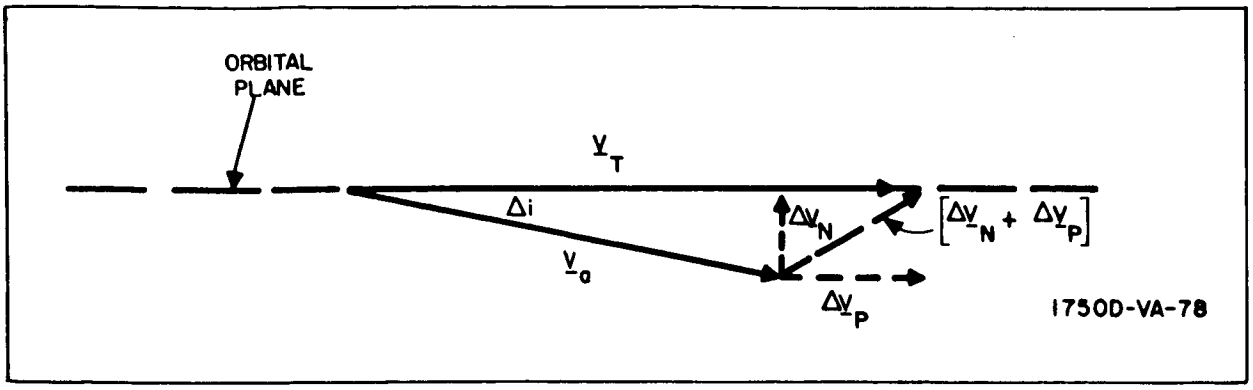


Figure 2-16. Velocity Errors at Injection

TABLE 2-8

INJECTION SENSOR ACCURACY REQUIREMENTS

| Symbol | Quantity | Sensor Accuracy ($3\sigma$) | State-of-the-art Accuracy ($3\sigma$) |
|---|---|---|---|
| $\Delta h$ | Altitude | 4.0 km (2% of R) | 200 m (0.1% of R)* |
| $\Delta V$ | Velocity | 2.0 m/sec | 0.3 m/sec |
| $\Delta \gamma$ | Pitch attitude | 4.5 deg | 0.3 deg |
| $\Delta \psi$ | Yaw attitude | 26.6 deg | 0.3 deg |
| $\Delta \phi$ | Central angle | 0.19 deg | - - - |
| $\Delta R$ | Range | 2.7% of R | 0.1% of R |
| $\Delta t$ | Timing | 43.2 sec | 3 sec |
| $\Delta i$ | Inclination | 0.26 deg | 0.1 deg |

*A radar altimeter can measure terrain altitude to this accuracy, but it cannot measure absolute altitude with this degree of precision.

2.2.2.3 Analysis of Active Rendezvous

a. Determination of Allowable Measurement Errors. - To determine the effects of sensor errors during the active phase of rendezvous the computer program is used to make a series of runs utilizing various noise levels on the sensor measurements. To provide a standard of comparison, all runs have a -0.3 m/sec velocity error at injection. Ten runs are made at each noise level each with a different random number routine. None of the noise levels degrades system performance sufficiently to prevent rendezvous. The ratio of angular noise to range noise is taken as:

$$\sigma_e \text{ (mr)} = 30\sigma_R \text{ (\% of Range)}$$

Comparison is made of the velocity expenditures for each run with the velocity required for the ideal Hohmann transfer. The results of this comparison are shown in figure 2-17 in the form of increased fuel required as a function of noise level on the sensor measurements. The rendezvous sensor requirements are based on an interpretation of these results. It is arbitrarily specified that where the 100-percent (maximum of the 10 samples) uses a velocity ratio $\frac{\Delta V}{\Delta V_H}$ of 1.5 constitutes a reasonable level of accuracy. Using this criterion, table 2-9 gives the results compared with a state of the art rendezvous radar system.

TABLE 2-9

REQUIRED SENSOR ACCURACY AND STATE OF THE ART ACCURACY

| Quantity | Required Sensor Accuracy ($3\sigma$) | State of the Art Accuracy** ($3\sigma$) |
|---|---|---|
| Range* | 0.3% of R or 30 m | 0.1% of R or 10 m |
| Angle | 9 mr | 3 mr |

* The required range accuracy is a percent of range or a fixed range whichever is larger.

** Gemini rendezvous radar

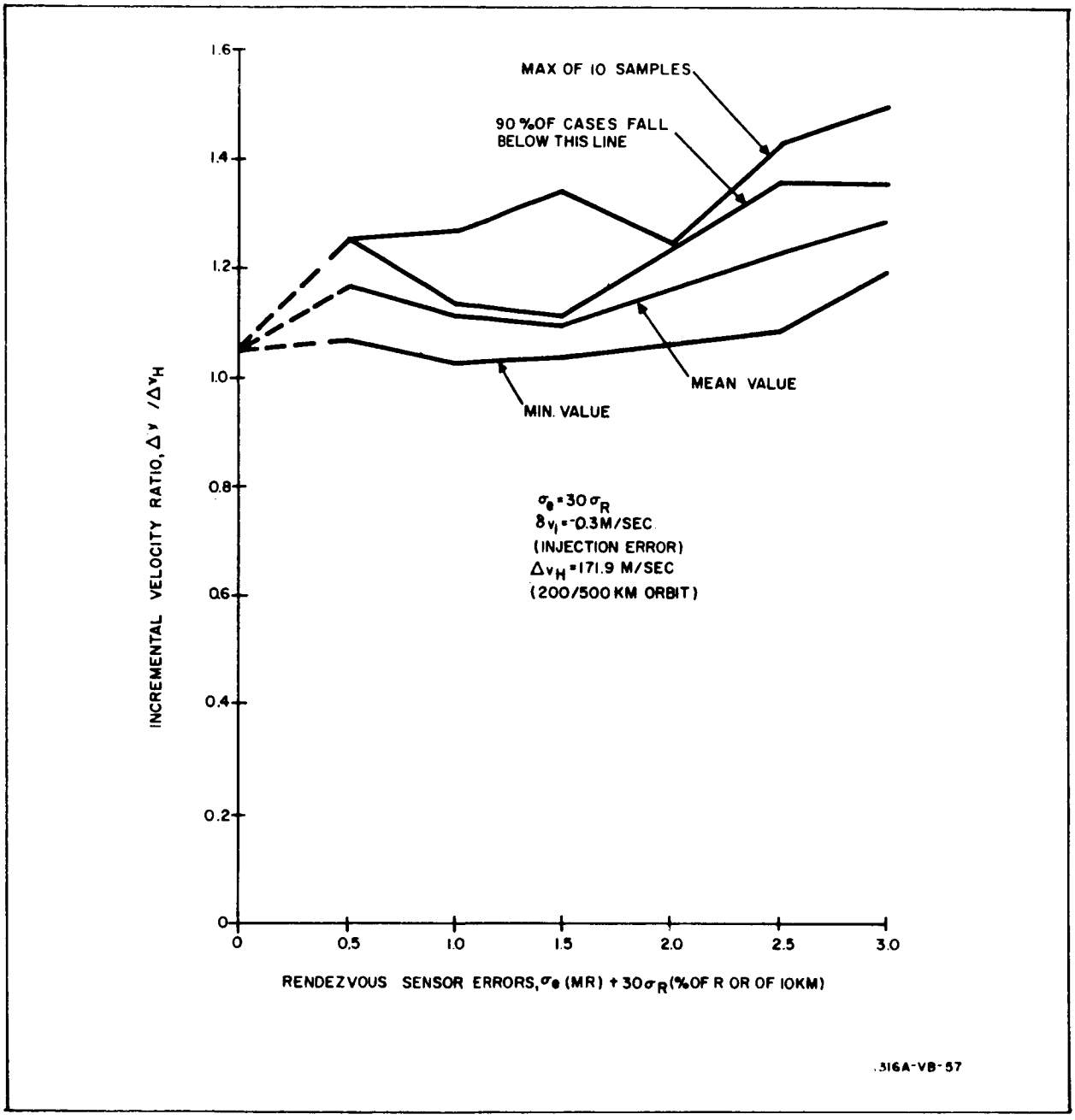


Figure 2-17. Effect of Rendezvous Sensor Errors on Propellant Consumption

It is seen that a state of the art rendezvous sensor is more than adequate for the rendezvous mission.

b. Determination of Dynamic Range Requirements. - Figure 2-18 gives the distribution of the line-of-sight angle due to $3\sigma$ injection errors. The rendezvous sensor must have an angular dynamic range at least as large as is indicated by this figure in order to acquire the target at the start of active rendezvous. Also, range capability must be sufficient to acquire the target at the nominal starting range (postulated as 25 km for this analysis).

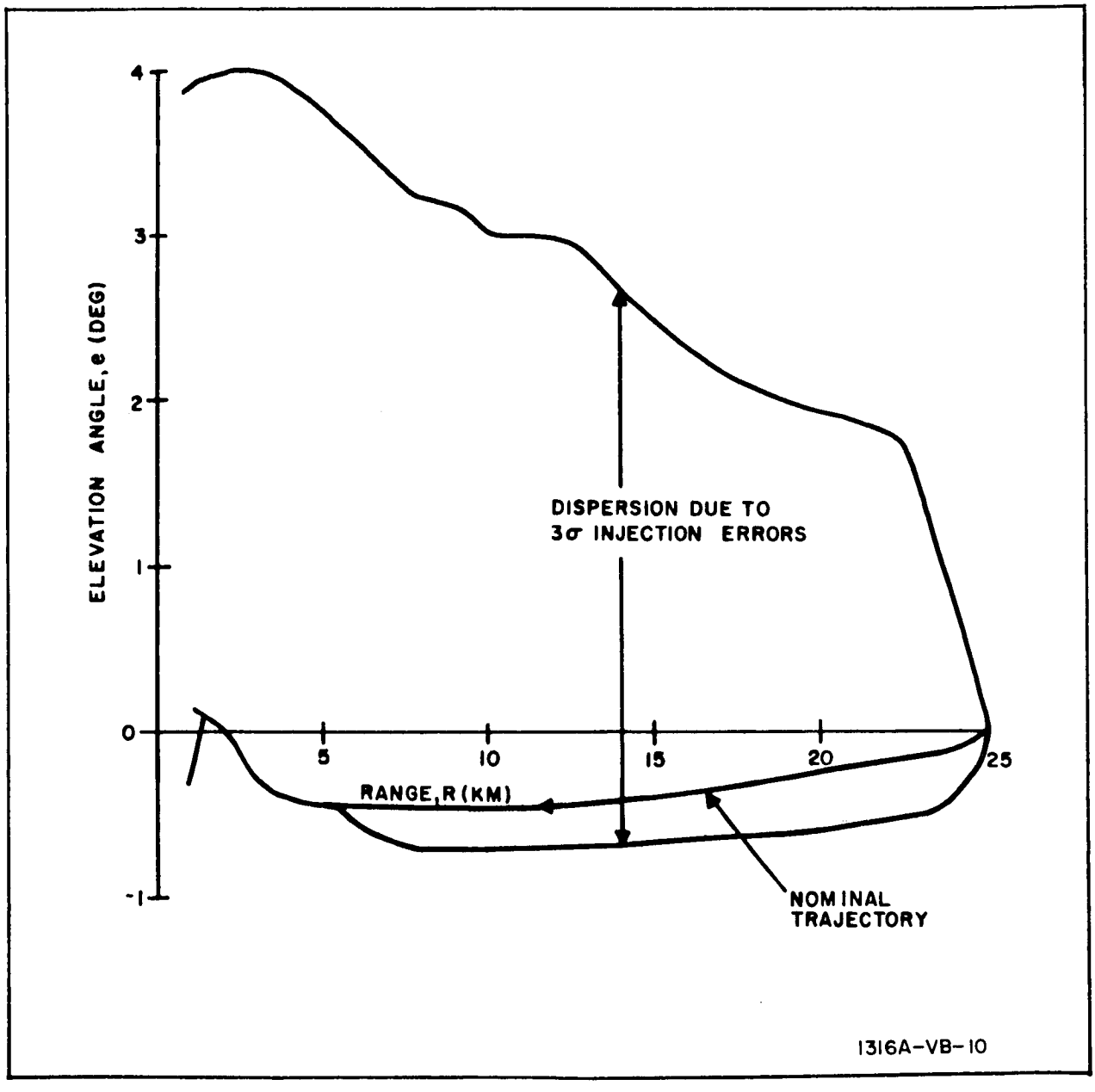


Figure 2-18. Variation in Elevation Angle With Range

c. Sensor Requirements. - The dynamic range and accuracy requirements of rendezvous sensors necessary to satisfactorily complete a rendezvous mission without an excessive expenditure of propellant is presented in the table 2-10

TABLE 2-10

RENDEZVOUS SENSOR REQUIREMENTS

| Quantity Measured | Dynamic Range | | Max Allowable RMS ($1\sigma$) Sensor Error |
|---|---|---|---|
| | Max | Min | |
| Range | 30 km* | 0 | 0.1% of R or 10 m |
| LOS angles (azimuth & elevation) | +20 deg | -20 deg | 3 mr |
| Vehicle attitude (pitch, roll, and yaw) | +90 deg - P and R<br>+180 deg - Y | -90 deg - P and R<br>-180 deg - Y | 0.2 deg during firing periods (to reduce cross coupling); 5 deg during tracking |

*The maximum range of the ranging device is that required solely for the active phase of rendezvous. If this device is the identical instrument that measured target range prior to injection and occasionally monitors the target during the coasting position of the ascent, its dynamic range should then be extended to 1000 km.

Although rendezvous sensors with the above accuracy will provide a satisfactory rendezvous, it should be emphasized that better accuracy will result in lower propellant consumption.

The sensor requirements given are based solely on fuel considerations since all sensors measurements were sufficiently accurate to permit the rendezvous to be completed.

### 2.2.3 Manual Guidance

This rendezvous model is similar in principle to the on-off system presented in paragraph 2.2.2. The primary difference is the lack of complete automatic control. A pilot is included in the control loop to

determine the effect on the rendezvous procedure. Because of the human element, the model, which is three dimensional, is set up on an analogue computer utilizing the equations of Appendix A. Appendix F presents assumptions made in mechanizing the program.

2.2.3.1 Model

Two target attitudes are utilized in this analysis, 555 km and 925 km with the chaser in a 185-km parking orbit. A nominal Hohmann transfer between the orbits is assumed as the reference trajectory.

Active rendezvous is postulated as starting when the chaser-to-target range has decreased to 30.5 km and the stipulated range and range rate at termination of the phase are 305 m and -3.05 m/sec respectively. The geometric and dynamic relationships are measured in a rotating local horizontal coordinate system centered at the target in which the x-axis is along the horizontal and the y-axis is along the earth-target radius vector. Neglecting gravity, the basic equations describing the motion of the chaser are

$$\ddot{X} = a_X + 2\omega_T \dot{Y} \qquad (2\text{-}35)$$

$$\ddot{Y} = a_Y - 2\omega_T \dot{X}$$

$$\ddot{Z} = a_Z$$

where $a_X$, $a_Y$ and $a_Z$ are the chaser accelerations due to thrusting referred to the rotating coordinate system, and $\omega_T$ is the rotation of the system which is equal to the angular orbital velocity of the target.

a. Control Philosophy. - Figure 2-19 illustrates the basic configuration postulated for the chaser. Shown also are the seeker angles, A and E. As in the automatic on-off system, the longitudinal engine is used to control the range rate and the normal engines are used to control the line-of-sight angular rate. The pilot is required to control the attitude of the vehicle so that the normal engines are in the plane of line-of-sight rotation.

Acceleration along the normal axis is applied whenever the magnitude of the line-of-sight angular rate exceeds 1.0 mr/sec and is maintained until the angular rate is reduced to a value below 0.1 mr/sec.

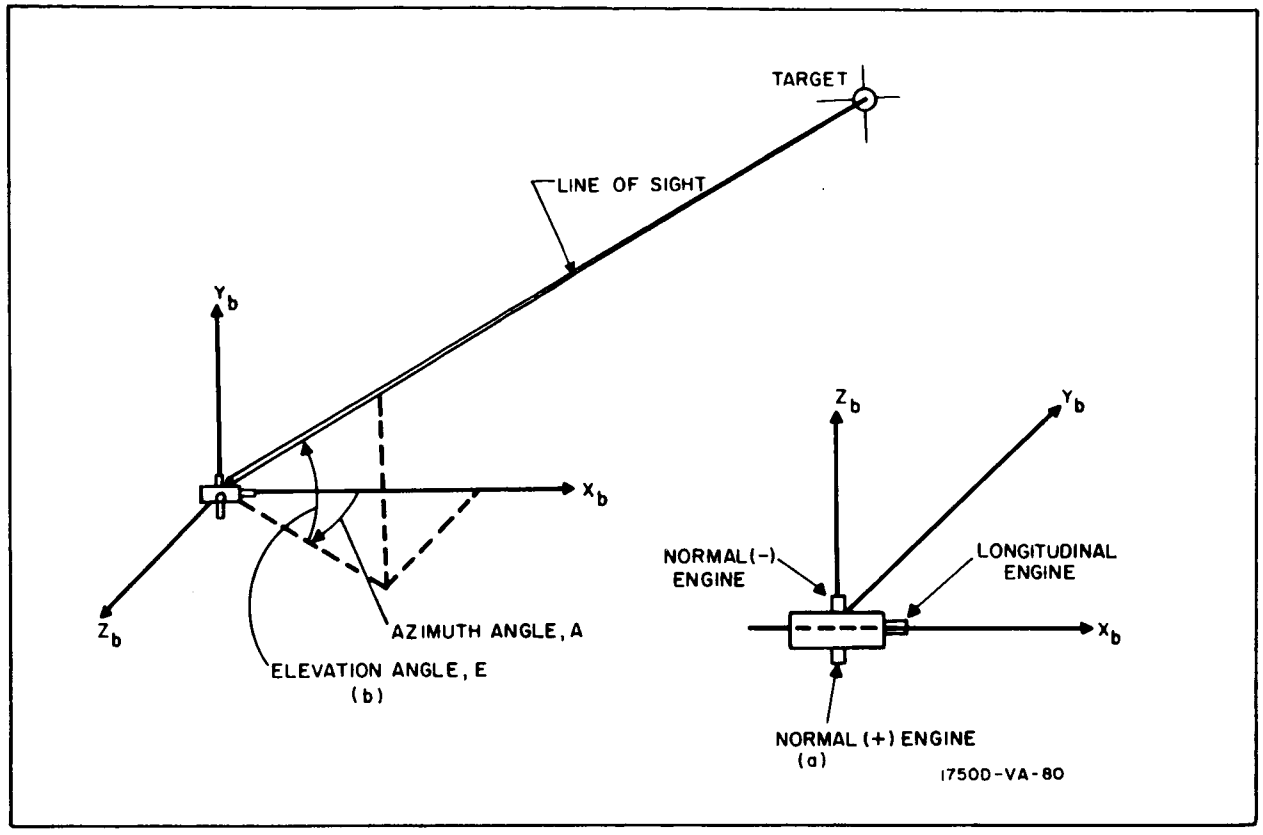


Figure 2-19. Chaser Configuration Showing Seeker Angles

The switching boundaries which determine when the longitudinal acceleration is to be applied; are shown in a phase plane plot in figure 2-20. The upper boundary is defined by

$$\dot{R} = \sqrt{\dot{R}_f^2 + 2\, a_\mu \left| R - R_f \right|} \tag{2-36}$$

and the lower boundary by

$$\dot{R} = \sqrt{\dot{R}_f^2 + 2\, a_\ell \left| R - R_f \right|} \quad \text{if } R \geq R_L$$

$$\dot{R} = \dot{R}_L \quad \text{if } R < R_L \tag{2-37}$$

where

$$a_\mu = 0.305 \text{ m/sec}^2$$

$$a_\ell = 0.22 \text{ m/sec}^2$$

$R_f$ = 305 m (terminal range)

$\dot{R}_f$ = -3.05 m/sec (terminal range rate)

Chaser accelerations assumed for both rendezvous cases considered are indicated in table 2-11

b. Display and Control. - Since a human pilot is included in the model, it is appropriate here to discuss the manner in which information is displayed and the method by which the vehicle is controlled.

A cockpit mockup, used in performing the simulations, is represented in figure 2-21. Quantities postulated as being measured by onboard sensors are the range, range rate, line-of-sight angular rate and the attitude rates of the chaser.

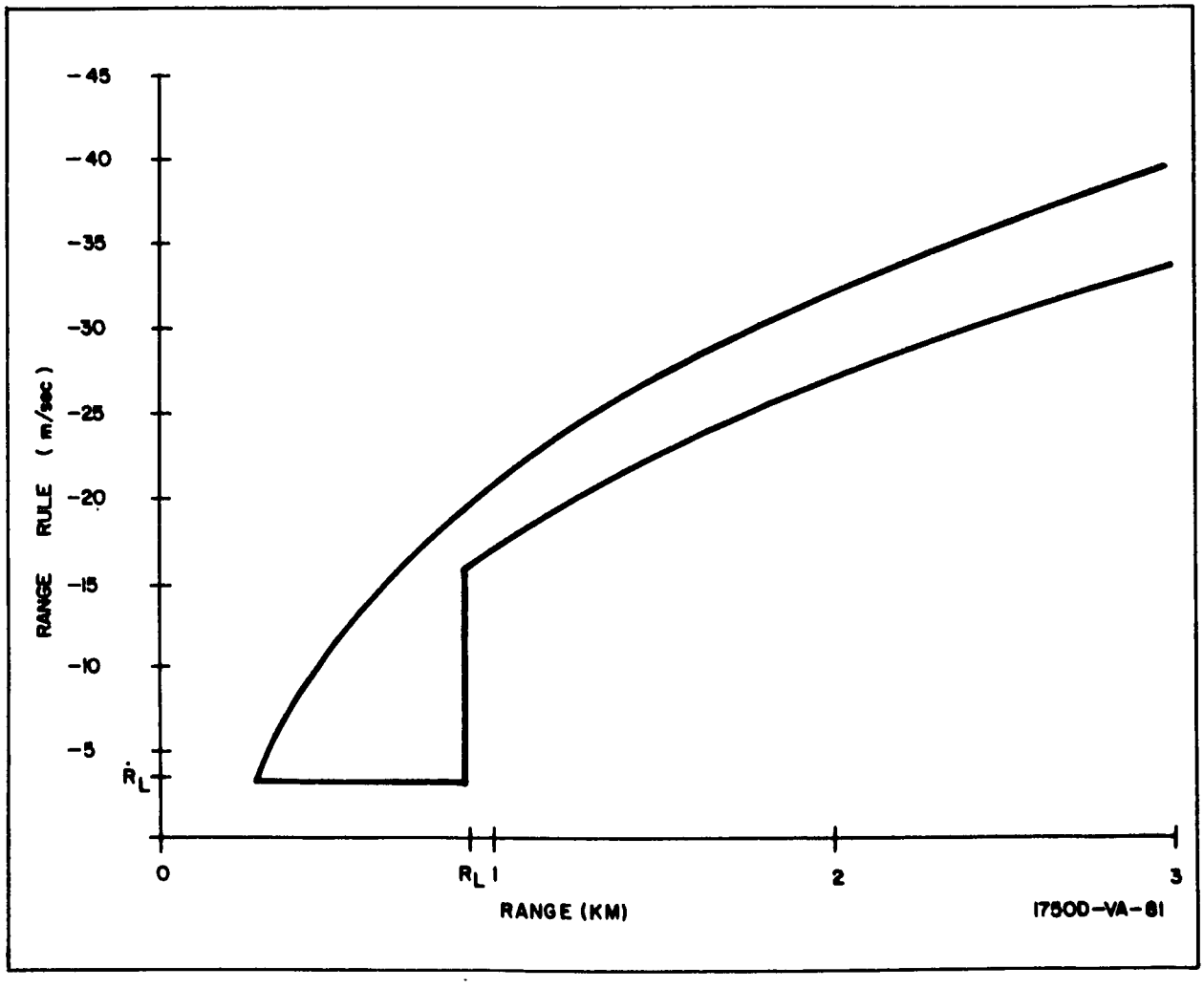


Figure 2-20. Phase-Plane Plot for Active Rendezvous Showing Switching Regions and Nonimal Trajectory

TABLE 2-11

CHASER ACCELERATIONS FOR ACTIVE PHASE OF MANNED RENDEZVOUS

| Target (km) Altitude | $a_L$ ($m/sec^2$) | $a_N$ ($m/sec^2$) |
|---|---|---|
| 555 | 0.97 (0.1g) | 0.295 (0.03g) |
| 925 | 1.94 (0.2g) | 0.59 (0.06g) |

A phase plane plot of range rate vs range is presented on an x-y plotter. Included are the boundaries which define the switching region. Logarithmic scales are used to provide greater sensitivity at lower values of range and range rate.

The pitch and yaw components of line-of-sight angular rates are referred to the body axes and displayed on an oscilloscope. The pitch component is displayed on the vertical axis; the yaw component on the horizontal axis. This arrangement is used to provide compatibility with the procedure used to control the line-of-sight rate as discussed subsequently. Vector addition of the components produces the total line-of-sight vector, the end of which is defined by the dot presented on the scope.

A two-pointer meter is used to display the seeker angles, A and E. The horizontal pointer indicates the elevation angle; that angle being zero when the pointer is aligned with the horizontal scale. Figure 2-22 illustrates pointer orientation for two different values of E. The azimuth angle A is indicated by the vertical pointer in a similar fashion.

Three separate meters are used to display the vehicle attitude rates in pitch, roll, and yaw. In general, these meters are seldom consulted except to occasionally verify that no attitude rates are inadvertently present.

Engine firing is controlled by the pushbuttons shown in figure 2-21. Pressing the center button activates the longitudinal engine which controls the range-range rate relationship displayed on the x-y plotter. The engine is fired whenever the phase plane trajectory crosses the upper boundary of the switching region and shut down when it crosses the lower boundary.

The outer buttons activate the normal engines to control the line-of-sight angular rate. Should the dot be to the left of the scope, the left button is

pressed thereby driving the dot to the right. Similarly, the right button is pressed when the dot is on the right hand side of the scope.

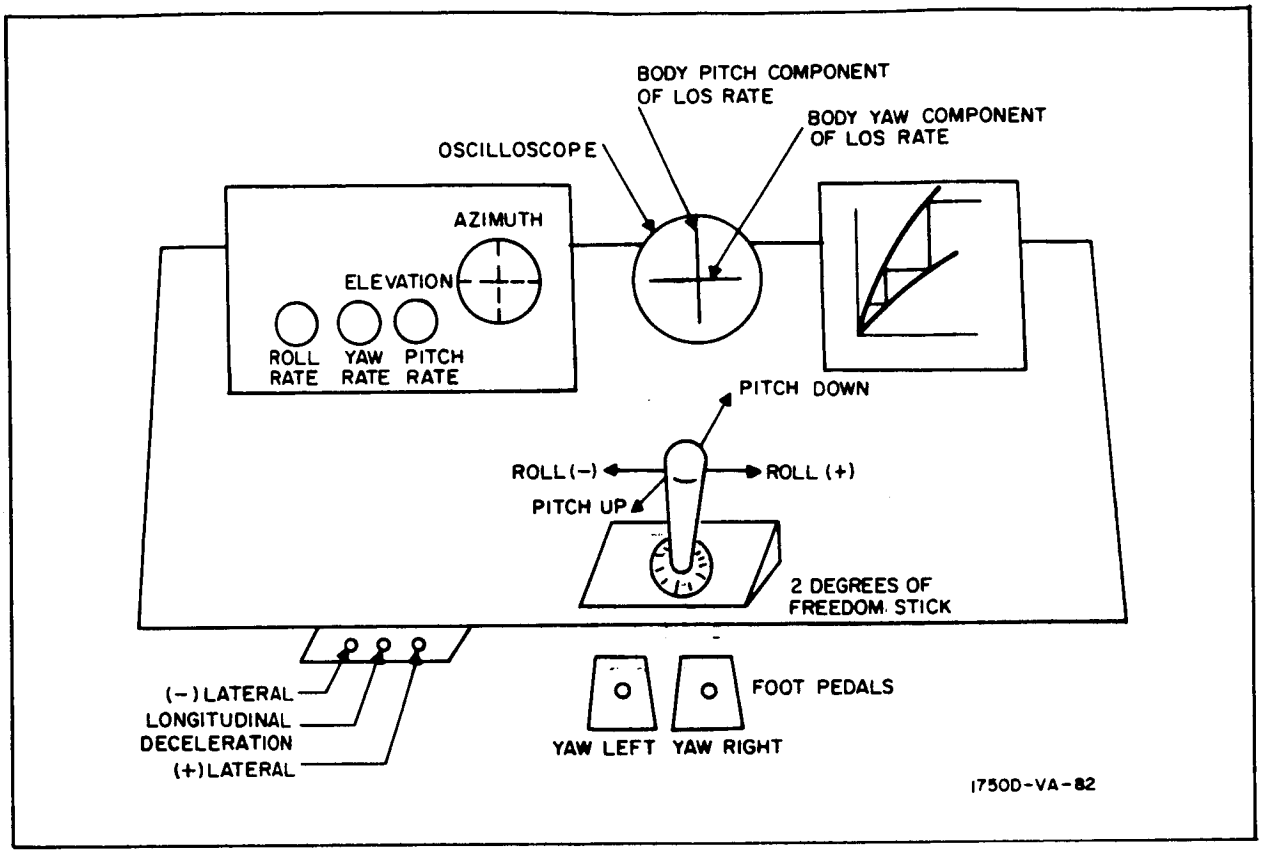


Figure 2-21. Sketch of Pilot Cockpit

Vertical control of the dot is exercised by keeping the axis of the lateral engines in the plane of line-of-sight rotation; i.e., by maintaining the proper roll attitude of the vehicle. This places the line-of-sight rotation vector entirely along the yaw axis, thereby permitting the lateral engines to null the line-of-sight rotation. Foot pedals are used to control the roll attitude to maintain the desired orientation.

It is necessary to place the longitudinal axis along the range vector to provide proper orientation of the engines. This is accomplished by controlling the vehicle attitude in pitch and yaw in such a manner as to drive the seeker angles to zero. Pitch and yaw attitude are controlled by a two-degrees-of-freedom stick. Fore-and-aft movement of the stick controls pitch (elevation), left and right movement controls yaw (azimuth). The stick is moved so as to follow the pointers; i.e., when a positive azimuth angle is indicated (pointer to the right of the vertical line) the stick is moved to the right, and when a positive elevation angle is indicated (pointer above

the horizontal line), the stick is moved forward. Opposite movement of the stick is required for negative angles. Figure 2-23 represents the vehicle attitude control system. The inputs from the stick or pushbuttons are in essence of an on-off nature and the maximum attitude rates are $\pm 2.5$ deg/sec.

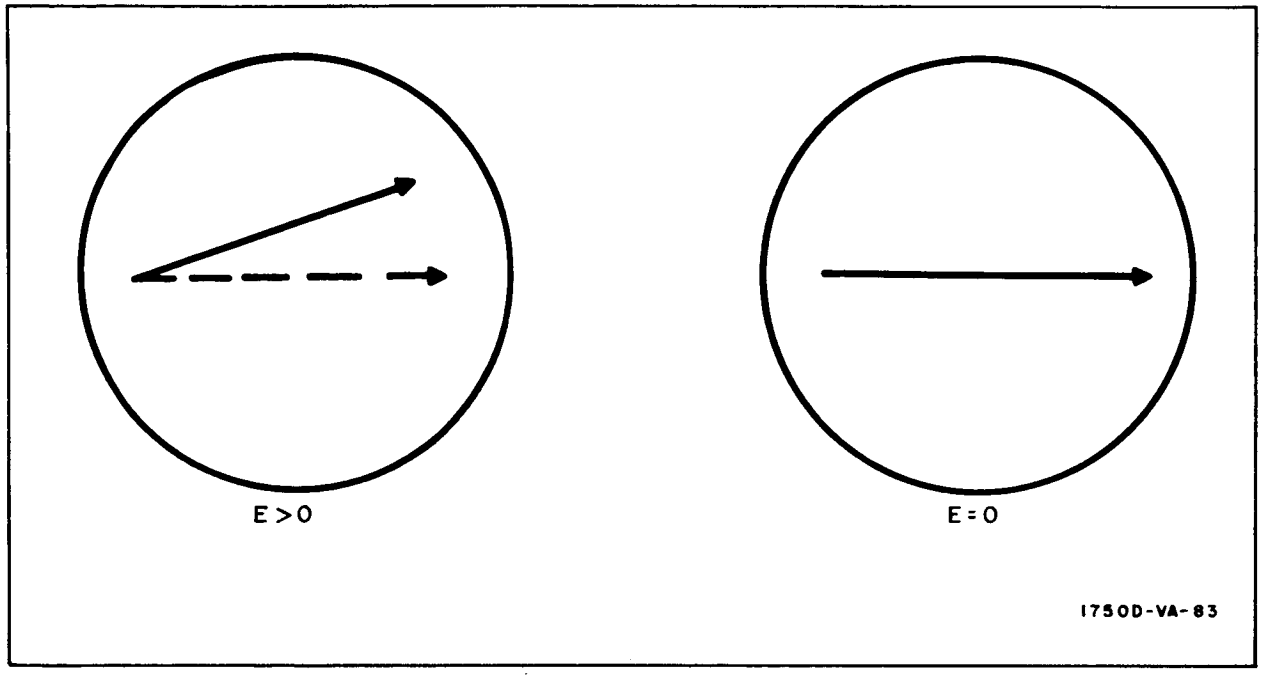


Figure 2-22. Line-of-Sight Elevation Angle Indicator

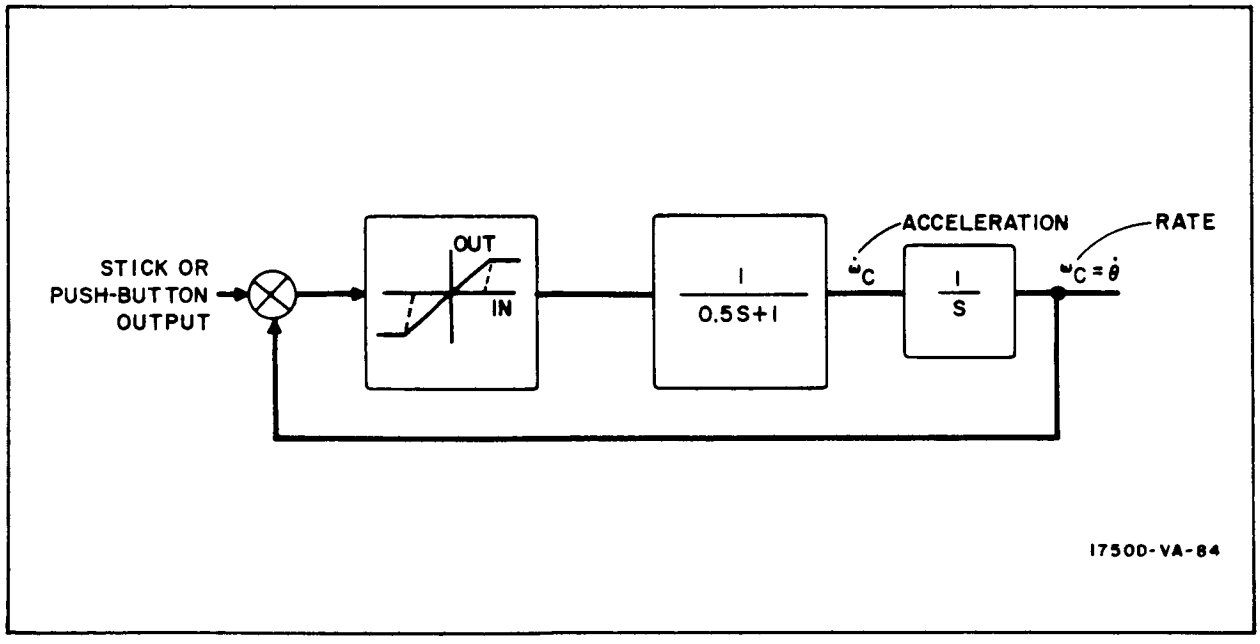


Figure 2-23. Attitude Rate Control System Used by Pilot in Analog Simulation of Orbital Rendezvous Maneuver

2.2.3.2 Analysis of Injection Maneuver

Effects of two injection errors on the rendezvous maneuver are investigated. One error occurs when the chaser injects into the transfer orbit prior to the proper time. The second is a position error in altitude. This error is given consideration over other position and velocity errors because it has the greatest effect on the propagation of errors along the reference trajectory.

Deviation at the start of the active rendezvous phase caused by the altitude injection error are determined using the Clohessey-Wiltshire matrix discussed in Ref. 1-1. These deviations are given in table 2-12 for both the 185-555 km and 155-925 km transfers.

TABLE 2-12

DEVIATIONS* IN STATE VARIABLES AT INITIATION OF ACTIVE RENDEZVOUS FOR MANNED GUIDANCE

| Reference Trajectory | $\Delta X$ (km) | $\Delta Y$ (km) | $\Delta \dot{X}$ (m/sec) | $\Delta \dot{Y}$ (m/sec) |
|---|---|---|---|---|
| 185-555 km | 13.8 | 5.1 | 0.99 | 0.18 |
| 185-925 km | 13.78 | 5.12 | 0.887 | 0 |

*These deviations result from an injection error in altitude equivalent to the ephemeris error ($3\sigma$) in altitude of the earth tracking network ( $\Delta Y$=732 meters).

Runs of the active rendezvous phase are made using initial conditions resulting from various combinations of the timing and altitude injection errors. These initial conditions are given in table 2-13. Initial conditions for a run with an A-deviation are obtained by subtracting the deviations in table 2-12 from the values of the state variables of the reference trajectory when the chaser-to-target range is 18.5 km. For a run with a B-deviation, the deviations are added to the state variables of the reference trajectory when the chaser-to-target range is 37 km. The active phase of rendezvous is then run with zero errors included on the sensor measurements, and the resulting end conditions and velocity expenditures are obtained.

TABLE 2-13

INITIAL CONDITIONS FOR PILOT CONTROLLED RENDEZVOUS

| Nominal Trajectory | Deviation | X (m) | Y (m) | $\dot{X}$ (m/sec) | $\dot{Y}$ (m/sec) |
|---|---|---|---|---|---|
| 100-300 n. mi transfer, 0-sec timing error | A | -30,500 | -8700 | +87 | +40 |
| | B | -20,000 | -9750 | +82.5 | +81 |
| 100-300 n. mi transfer, 1.5-sec timing error | A | -30,500 | -5800 | +100 | +15.5 |
| | B | -22,600 | -1525 | +92.5 | +57.4 |
| 100-500 n. mi transfer, 0-sec timing error | A | -30,500 | -6830 | +187 | +37 |
| | B | -22,600 | -1825 | +196 | +75.4 |
| 100-500 n. mi transfer, 1.5-sec timing error | A | -30,500 | -5800 | +196 | +15 |
| | B | -23,200 | +1670 | +196 | +53.4 |

The active rendezvous phase is postulated as terminated when the chaser-to-target range is 305 m. As an indication of the pilot's ability to achieve the desired terminal conditions, the final values of line-of-sight angular rate and range rate are observed at this point and the expended velocity increments are noted. The results are presented in table 2-14. Required incremental velocities (including injection into the ascent trajectory) are normalized with respect to the required velocity increment ( $\Delta V_H$ ) for the ideal Hohmann transfer. Because of the limited amount of data obtained, no attempt is made to establish injection sensor errors.

2.2.3.3 Analysis of Active Rendezvous

The effect of sensor measurement errors on the active rendezvous phase is investigated. Random noise of various levels and bandwidths is superimposed on the measurements of range, range rate, and the two components of line-of-sight angular rate. No data processing is performed on these measurements prior to their being displayed to the pilot.

TABLE 2-14

FINAL CONDITIONS ON PILOT CONTROLLED RENDEZVOUS

| Reference Trajectory | Deviation | $\dot{e}_f$ (mr/sec) | $\dot{R}_f$ (m/sec) | $\frac{\Delta V}{\Delta V_H}$ |
|---|---|---|---|---|
| 185-555 km transfer 0-sec timing error | None | 1.05 | 6.7 | 1.0 |
| | A | 1.1 | 5.25 | 1.12 |
| | B | 0.7 | 5.9 | 1.13 |
| 185-555 km transfer 1.5-sec timing error | None | 0.6 | 3.5 | 1.1 |
| | A | 0.92 | 4.4 | 1.3 |
| | B | (engines undersized) | | |
| 185-925 km transfer 0-sec timing error | None | 0.55 | 4.1 | 1.19 |
| | A | 0.35 | 4.7 | 1.26 |
| | B | 1.4 | 3.5 | 1.38 |
| 185-925 km transfer 1.5-sec timing error | None | 0.6 | 3.7 | 1.23 |
| | A | 0 | 2.6 | 1.45 |
| | B | 0.5 | 3.1 | 1.3 |

$R_f$ = 305 m; $\Delta V_H$ (185 km - 555 km) = 211 m/sec

$\Delta V_H$ (185 km - 925 km) = 301 m/sec

The 1σ noise values are of the following form:

$$R_N = \% R + R_e$$
$$\dot{R}_N = \dot{R}_e$$
$$\dot{e}_N = \dot{e}_e$$

where $R_e$, $\dot{R}_e$, and $\dot{e}_e$ signify bias errors

Runs are made of the active rendezvous phase, some with and some without the initial condition deviations of table 2-12; and the effect on the postulated terminal conditions and velocity requirements is noted.

Results of the computer runs using various noise values are shown in table 2-15. Each case represents an average of two to four individual runs: some with the same pilot, some with different pilots.

As in the investigation of the injection maneuver, the rendezvous is postulated as ending when the chaser to target range is 305 m, and the incremental velocities are normalized with respect to the required velocity increment for the ideal Hohmann transfer. It is noted that the ratio $\frac{\Delta V}{\Delta V_H}$ is nearly equal to, and in some cases less than, one. This is felt to be the result of not synchronizing the chaser with the target, i.e., not providing the final impulse to place the chaser co-orbital with the target.

As with the analysis of the navigation maneuver, the data is insufficient to establish any valid sensor requirements. Final values of the line-of-sight angular rate and range rate do not appear to have any direct relationship with the initial conditions or with the noise value(s) imposed on the measured quantities. Also, the ratio $\frac{\Delta V}{\Delta V_H}$ does not vary significantly when different noise levels are used.

### 2.2.4 Midcourse Reduction of Uncertainties in Determination of State Variables

Errors inherent in the injection maneuver are propagated along the transfer orbit thereby resulting in deviations of the actual state variables (position and velocity) of the chaser from those of the reference trajectory. In the following paragraphs, a procedure is presented by which the errors in the estimation of the actual state variables may be reduced utilizing one or two measurements of the relative dynamics between the chaser and target. These measurements are made during the midcourse portion of the rendezvous procedure.

The minimization procedure is as follows:

a. Uncertainties in the state variables at injection are propagated by means of the Clohessey Wiltshire Matrix (see Ref. 6) to the point where a measurement is to be made. Since no measurements have thus far been taken, these uncertainties are equal to the deviation of the state variables from the state variables of the reference trajectory.

TABLE 2-15

RESULTS OF ACTIVE PHASE OF MANNED RENDEZVOUS WITH RANDOM NOISE ERRORS

$R_f$ = terminal value of range = 305 m

$\dot{e}_N$ = LOS rate noise level (1σ), BW = 1.0 cps

$\dot{e}_f$ = terminal value of LOS rate

$\dot{R}_f$ = terminal value of range rate

| Results With LOS Rate Noise | | | | | |
|---|---|---|---|---|---|
| Reference Trajectory | Deviation | $\dot{e}_N$ (mr/sec) | $\dot{e}_f$ (mr/sec) | $\dot{R}_f$ (m/sec) | $\frac{\Delta V}{\Delta V_H}$ |
| 185-555 km transfer 1.5-sec timing error | None | 0 | 0.6 | 3.48 | 1.08 |
| | None | 0.1 | 0.5 | 3.18 | 1.11 |
| | None | 0.5 | 1.3 | 4.02 | 1.11 |
| | None | 1.0 | 1.2 | 3.66 | 1.10 |
| 185-555 km transfer 0-sec timing error | None | 0 | 1.05 | 6.68 | 0.99 |
| | None | 0.1 | 0.7 | 4.51 | 0.99 |
| | None | 0.5 | 0.8 | 4.73 | 1.01 |
| 185-925 km transfer 0-sec timing error | None | 0 | 0.55 | 4.09 | 1.19 |
| | None | 0.1 | 1.1 | 3.81 | 1.19 |
| | None | 0.5 | 2.0 | 4.09 | 1.19 |
| 185-925 km transfer 0-sec timing error | B | 0 | 1.4 | 3.48 | 1.38 |
| | B | 0.5 | 1.0 | 13.78 | 1.44 |

TABLE 2-15 (Continued)

| Results With Range and Range Rate Noise | | | | | | |
|---|---|---|---|---|---|---|
| Reference Trajectory | Deviation | $\dot{R}_N$ (m/sec) | $R_N$ (m) | $\dot{e}_f$ (mr/sec) | $\dot{R}_f$ (m/sec) | $\frac{\Delta V}{\Delta V_H}$ |
| 185-555 km transfer 1.5-sec timing error | None | 0 | 0 | 0.6 | 3.48 | 1.08 |
| | None | 0.061 | 0 | 0.85 | 2.29 | 1.04 |
| | None | 0.153 | 0 | 0.3 | 3.42 | 1.05 |
| | None | 0 | 0.001R + 3.05 | 1.6 | 3.87 | 1.06 |
| | None | 0 | 0.01 R + 7.64 | 1.0 | 3.50 | 1.03 |

b. At this point, measurement of certain relative dynamics between the chaser and target is made by an onboard sensor. These measurements are utilized in a correction matrix, $[C]$.

c. The uncertainties which have been propagated to the point of measurement are premultiplied by the correction matrix, yielding a new, reduced set of uncertainties. These updated uncertainties may then be propagated to a new correction point or to the terminal point of the rendezvous maneuver.

By reducing the uncertainties in the estimations of the state variables, the chaser vehicle is able to undertake more accurate and more efficient correction maneuvers.

The analysis presented in these paragraphs indicates the manner in which correction matrices are derived. Correction matrices are then presented for the following combinations of observables.

a. Range and range rate

b. LOS angle and angular rate

c. Range and LOS angle

d. Range rate and LOS angle

e. Range, LOS angle and range rate

f. Range, LOS angle and angular rate

A comparison of the results obtained when each correction matrix is utilized is presented to illustrate their relative effectiveness. The optimum point at which to make the correction is also indicated.

2.2.4.1 Relationship of Initial and Final Deviations

For purposes of the analysis only two dimensions are considered. The geometric and dynamic relationships are measured in a rotating local vertical coordinate system centered at the target as shown in figure 2-24. The angle $\theta$ is between the X-axis and the line-of-sight. The angle $\omega_T T_i$ is the angle between the instantaneous target position and the nominal rendezvous point and is defined by the target angular orbital velocity, $\omega_T$, (circular orbit assumed) and $T_i$, the time to go to the nominal point of rendezvous.

Matrix representation of the relationship between initial uncertainties and the final, updated uncertainties is as follows: Uncertainties at injection are expressed as $\left[\Delta_I\right]$ and are equal to the deviations of the actual state variables from these of the reference trajectory. The time to go from injection is $T_I$. Propagation of these uncertainties by means of the Clohessey-Wiltshire matrix yields the uncertainties, $\left[\Delta_1\right]$, at the point of the first measurement where the time to go is $T_1$.

$$\left[\Delta_1^-\right] = \left[M\,(T_I,\ T_1)\right]\left[\Delta_I\right] \tag{2-38}$$

The minus sign in the $\Delta_1^-$ matrix indicates the uncertainties prior to making the measurements.

Upon making the measurements, they are used in the correction matrix which is employed to obtain the updated uncertainties, $\left[\Delta_1^+\right]$, which exist at the measurement point.

$$\left[\Delta_1^+\right] = \left[C\right]\left[\Delta_1^-\right] \tag{2-39}$$

Substituting equation 2-38 into equation 2-39:

$$\left[\Delta_1^+\right] = \left[C\right]\left[M\,(T_I,\ T_1)\right]\left[\Delta_I\right] \tag{2-40}$$

Use of the Clohessey-Wiltshire matrix may then be made to propagate the updated uncertainties, $\left[\Delta_1^+\right]$, to the final point.

$$\left[\Delta_f\right] = \left[M\,(T_1,\ T_f)\right]\left[\Delta_1^-\right] \tag{2-41}$$

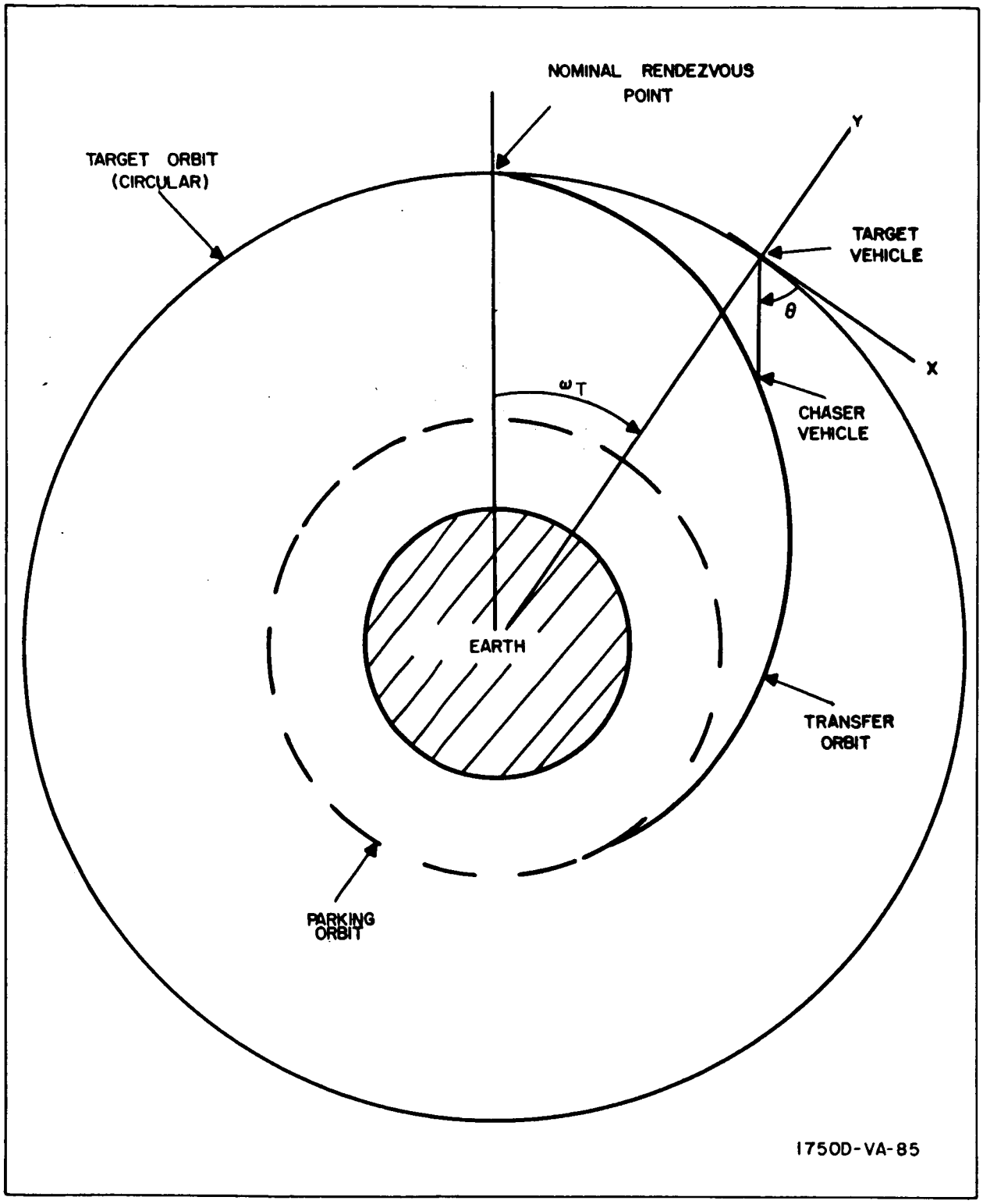


Figure 2-24. Geometry Ulitized for Midcourse Analysis

Combining equations 2-40 and 2-41:

$$\left[\Delta_f\right] = \left[M\,(T_1,\ T_f)\right]\left[C\right]\left[M\,(T_I,\ T_1)\right]\left[\Delta_I\right] \qquad (2\text{-}42)$$

In the case where a second measurement is to be made, the relationship between final and initial uncertainties is expressed as:

$$\left[\Delta_f\right] = \left[M\,(T_2,\ T_f)\right]\left[C_2\right]\left[M\,(T_1,\ T_2)\right]\left[C_1\right]\left[M\,(T_I,\ T_1)\right]\left[\Delta_I\right] \qquad (2\text{-}43)$$

where $C_1$ and $C_2$ are the correction matrices with the first and second measurements respectively.

2.2.4.2 Determination of Correction Matrices

The correction matrices relate the observables to the state variables and the uncertainties in the determination of the state variables. While derivation of each matrix is not included, a portion of the range, range rate matrix is derived in order to indicate the technique employed.

In deriving the matrices it is postulated that the error in the measurement of observables is negligible compared to the uncertainty in the determination of the state variables.

Uncertainties in the state variables at the measurement point, just prior to performing the measurement are represented by:

$$\begin{bmatrix} \Delta X_1^- \\ \Delta Y_1^- \\ \Delta \dot{X}_1^- \\ \Delta \dot{Y}_1^- \end{bmatrix}$$

And the uncertainties after the measurement are:

$$\begin{bmatrix} \Delta X_1^+ \\ \Delta Y_1^+ \\ \Delta \dot{X}_1^+ \\ \Delta \dot{Y}_1^+ \end{bmatrix}$$

From figure 2-21, it is seen that:

$$\theta = \tan^{-1}\left(-\frac{Y}{X}\right) \qquad (2\text{-}46)$$

Therefore, the uncertainty in $\theta$ prior to the measurement is:

$$\Delta\theta_1^- = \frac{Y\Delta X_1^- - X\Delta Y_1^-}{R^2} \tag{2-47}$$

The X- and Y-position coordinates are:

$$X = R\cos\theta \tag{2-48}$$

$$Y = -R\sin\theta$$

Differentiating produces the uncertainties in X and Y after the measurement:

$$\Delta X_1^+ = -R\sin\theta\,\Delta\theta_1^+ + \Delta R_1^+\cos\theta \tag{2-49}$$

$$\Delta Y_1^+ = -R\cos\theta\,\Delta\theta_1^+ - \Delta R_1^+\sin\theta \tag{2-50}$$

However, the error in the range measurement is assumed to be zero, i.e.,

$$\Delta R_1^+ = 0$$

Equations 2-49 and 2-50 thereby reduce to:

$$\Delta X_1^+ = -R\sin\theta\,\Delta\theta_1^+ \tag{2-51}$$

$$\Delta Y_1^+ = -R\cos\theta\,\Delta\theta_1^+ \tag{2-52}$$

The uncertainties in $\theta$ after the measurement is equal to that prior to the measurement.

$$\Delta\theta_1^+ = \Delta\theta_1^-$$

Using this relationship, equation 2-47 may be substituted in equations 2-51 and 2-52 to yield:

$$\Delta X_1^+ = \left(\frac{Y^2}{R^2}\right)\Delta X_1^- + \left(\frac{XY}{R^2}\right)\Delta Y_1^-$$

$$\Delta Y_1^+ = \left(\frac{XY}{R^2}\right)\Delta X_1^- + \left(-\frac{X^2}{R^2}\right)\Delta Y_1^-$$

The coefficients of the $\Delta X_1^-$ and $\Delta Y_1^-$ terms are the four upper left-hand elements of the range, range rate correction matrix.

Similar geometrical relationships are used to derive the remaining coefficients of the range, range rate matrix and the coefficients of the other correction matrices. The six correction matrices are presented in tables 2-16 through 2-18.

TABLE 2-16

CORRECTION MATRICES

$$\left[C(R, \dot{R})\right]$$

$$\left[\begin{array}{c|c|c|c}
\left(\frac{Y}{R}\right)^2 & -\frac{XY}{R^2} & 0 & 0 \\
\hline
-\frac{XY}{R^2} & \frac{X}{R}^2 & 0 & 0 \\
\hline
\frac{Y}{R^3}\left[\dot{R}Y - R\dot{Y} - 3XR\dot{\theta}\right] & \frac{1}{R^3}\left[Y(R\dot{X} - \dot{R}X) + (X^2 - 2Y^2)\, R\dot{\theta}\right] & \left(\frac{Y}{R}\right)^2 & -\frac{XY}{R^2} \\
\hline
\frac{1}{R^3}\left[X(R\dot{Y} - \dot{R}Y) - (Y^2 - 2X^2)\, R\dot{\theta}\right] & \frac{X}{R^3}\left[\dot{R}X - R\dot{X} + 3YR\dot{\theta}\right] & -\frac{XY}{R^2} & \left(\frac{X}{R}\right)^2
\end{array}\right]$$

$$\left[C(\theta, \dot{\theta})\right]$$

$$\left[\begin{array}{c|c|c|c}
\left(\frac{X}{R}\right)^2 & \frac{XY}{R^2} & 0 & 0 \\
\hline
\frac{XY}{R^2} & \left(\frac{Y}{R}\right)^2 & 0 & 0 \\
\hline
\frac{X}{R^3}\left[\dot{X}R - X\dot{R} + RY\dot{\theta}\right] & \frac{1}{R^3}\left[RX\dot{Y} - XY\dot{R} + RY^2\dot{\theta}\right] & \left(\frac{X}{R}\right)^2 & \frac{XY}{R^2} \\
\hline
\frac{1}{R^3}\left[RY\dot{X} - XY\dot{R} - RX^2\dot{\theta}\right] & \frac{Y}{R^3}\left[\dot{Y}R - Y\dot{R} - RX\dot{\theta}\right] & \frac{XY}{R^2} & \left(\frac{Y}{R}\right)^2
\end{array}\right]$$

TABLE 2-17

CORRECTION MATRICES

$$\left[C(R, \theta)\right]$$

$$\left[\begin{array}{cc|cc} 0 & 0 & 0 & 0 \\ 0 & 0 & 0 & 0 \\ \frac{1}{R^3}\left[R\dot{X}X - \dot{R}X^2 - R\dot{Y}Y - 2\dot{\theta}RXY\right] & \frac{1}{R^3}\left[R\dot{Y}X - \dot{R}XY + R\dot{X}Y - 2\dot{\theta}RY^2\right] & 1 & 0 \\ \frac{1}{R^3}\left[R\dot{X}Y - \dot{R}XY + R\dot{Y}X + 2\dot{\theta}RX^2\right] & \frac{1}{R^3}\left[R\dot{Y}Y - \dot{R}Y^2 - R\dot{X}X + 2\dot{\theta}RXY\right] & 0 & 1 \end{array}\right]$$

$$\left[C(\dot{R}, \theta)\right]$$

$$\left[\begin{array}{cc|cc} \left(\frac{X}{R}\right)^2 & \frac{XY}{R^2} & 0 & 0 \\ \frac{XY}{R^2} & \left(\frac{Y}{R}\right)^2 & 0 & 0 \\ -\frac{Y}{R^2}\left[\dot{Y} + X\dot{\theta}\right] & \frac{Y}{R^2}\left[\dot{X} - Y\dot{\theta}\right] & \left(\frac{Y}{R}\right)^2 & -\frac{XY}{R^2} \\ \frac{X}{R^2}\left[\dot{Y} + X\dot{\theta}\right] & -\frac{X}{R^2}\left[\dot{X} - Y\dot{\theta}\right] & -\frac{XY}{R^2} & \left(\frac{X}{R}\right)^2 \end{array}\right]$$

TABLE 2-18

CORRECTION MATRICES

$$\left[C(R, \theta, \dot{R})\right]$$

$$\begin{bmatrix} 0 & 0 & 0 & 0 \\ 0 & 0 & 0 & 0 \\ -\frac{Y}{R^2}\left[\dot{Y} + 2\dot{\theta}X\right] & \frac{Y}{R^2}\left[\dot{X} - 2\dot{\theta}Y\right] & \left(\frac{Y}{R}\right)^2 & -\frac{XY}{R^2} \\ \frac{X}{R^2}\left[\dot{Y} + 2\dot{\theta}X\right] & -\frac{X}{R^2}\left[\dot{X} - 2\dot{\theta}Y\right] & -\frac{XY}{R^2} & \left(\frac{X}{R}\right)^2 \end{bmatrix}$$

$$\left[(C(R, \theta, \dot{\theta})\right]$$

$$\begin{bmatrix} 0 & 0 & 0 & 0 \\ 0 & 0 & 0 & 0 \\ \frac{X}{R^2}\left(\dot{X} - \frac{\dot{R}}{R}X\right) & \frac{X}{R^2}\left(\dot{Y} - \frac{\dot{R}}{R}Y\right) & \frac{X^2}{R^2} & \frac{XY}{R^2} \\ \frac{Y}{R^2}\left(\dot{X} - \frac{\dot{R}}{R}X\right) & \frac{Y}{R^2}\left(\dot{Y} - \frac{\dot{R}}{R}Y\right) & \frac{XY}{R^2} & \frac{Y^2}{R^2} \end{bmatrix}$$

2.2.4.3 Results

To obtain an indication of the relative effectiveness of midcourse measurements, the six correction matrices listed in tables 2-16, 2-17, and 2-18 are employed on a trajectory. The resulting uncertainties in the estimated position coordinates at the nominal rendezvous point are then obtained.

As a basis for comparison, a specified reference trajectory is used and the deviations in the state variables at injection; i.e. the injection errors, are the same for each case. The reference trajectory is a Hohmann (180 degrees) transfer from a 185-km (100 n. mi) circular parking orbit to a 740-km (400 n. mi) circular target orbit. Injection errors are:

$$\Delta X_I = \Delta Y_I = 1.85 \text{ km (1 n. mi)}$$

$$\Delta \dot{X}_I = \Delta \dot{Y}_I = 3.05 \text{ m/sec (10 fps)}$$

a. Single Measurement. - The uncertainties ($\Delta X_f$, $\Delta Y_f$) in determining the final position when a single measurement is made are presented for each injection error in figures 2-25 through 2-30.

Each figure contains two graphs:

(1) $\Delta X_f$ vs $\omega_T T_1$

(2) $\Delta Y_f$ vs $\omega_T T_1$

which have errors for each injection error. The best point at which to perform the measurement is that value of $\omega_T T_1$ for which the position uncertainty is minimum.

The uncertainties which result when no measurement is performed, are presented in table 2-19 for each injection error. These figures may be compared with the data in figures 2-25 through 2-33 to determine the relative effectiveness of the measurement procedures.

Inspection of the curves shows that when two observables are measured, the combination of range and range rate gives the best combination and the point at which to perform the correction is 40 to 60 degrees prior to the nominal rendezvous point.

Of the two cases using measurements of three observables, the combination of range, range rate, and angle appears to provide the best combination (although only limited information is available). The uncertainties are less than for the case using range and range rate as would be

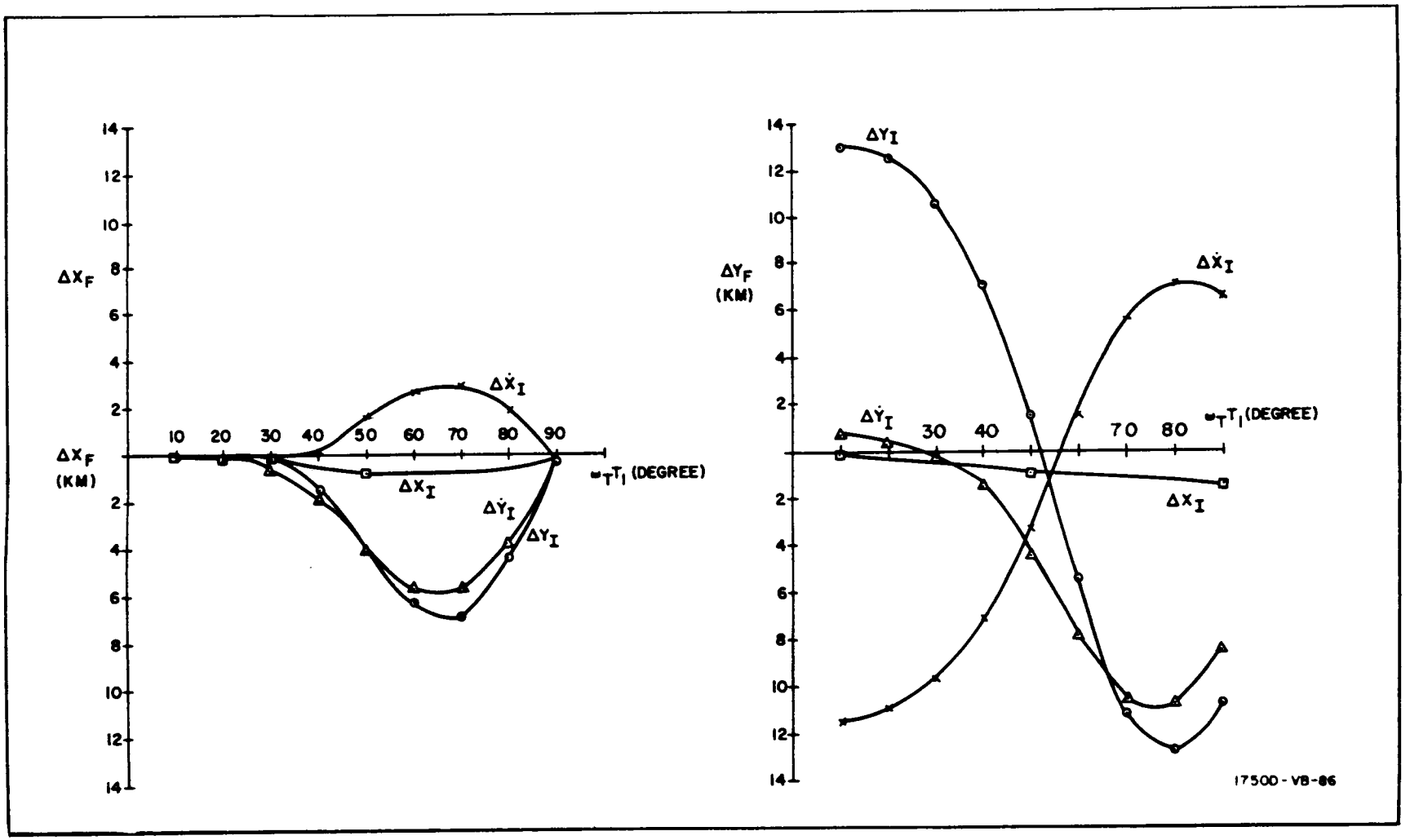


Figure 2-25. Uncertainties in Estimated Final Position vs Point of Measurement When Range, Range Rate Correction Matrix is Employed

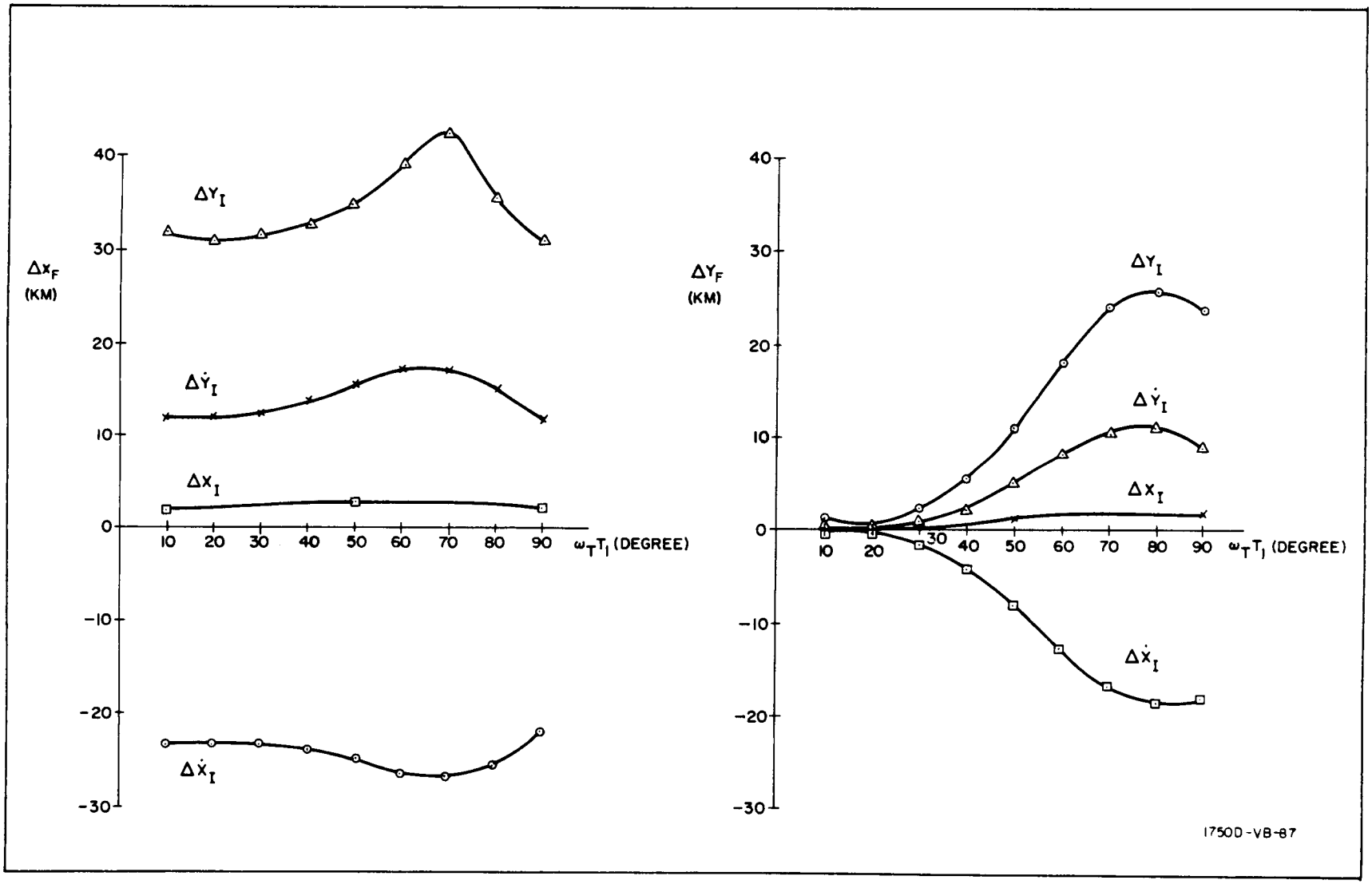


Figure 2-26. Uncertainties in Estimated Final Position vs Point of Measurement When Angle, Angular Rate Correction Matrix is Employed

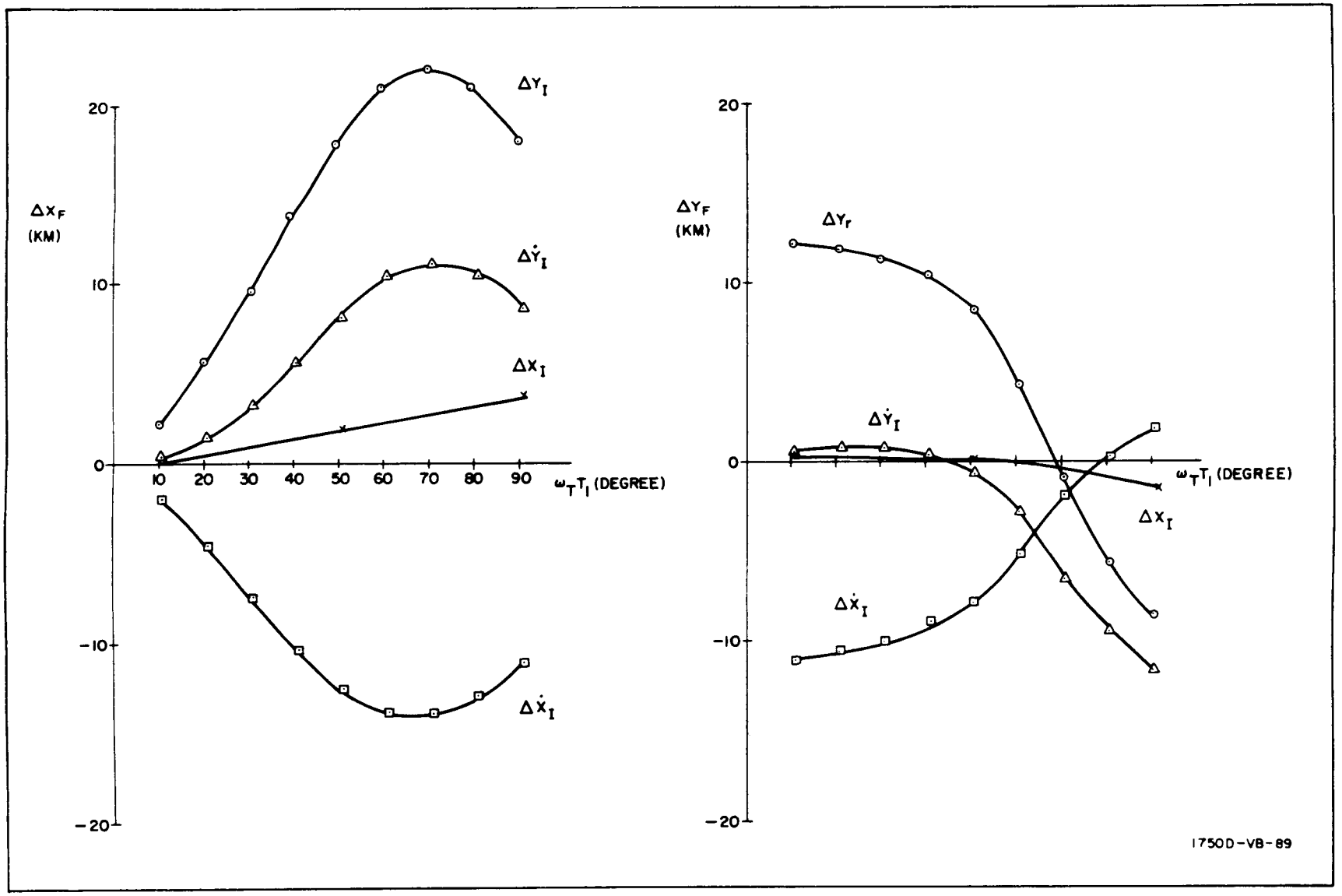


Figure 2-27. Uncertainties in Estimated Final Position vs Point of Measurement When Range, Angle Correction Matrix Is Employed

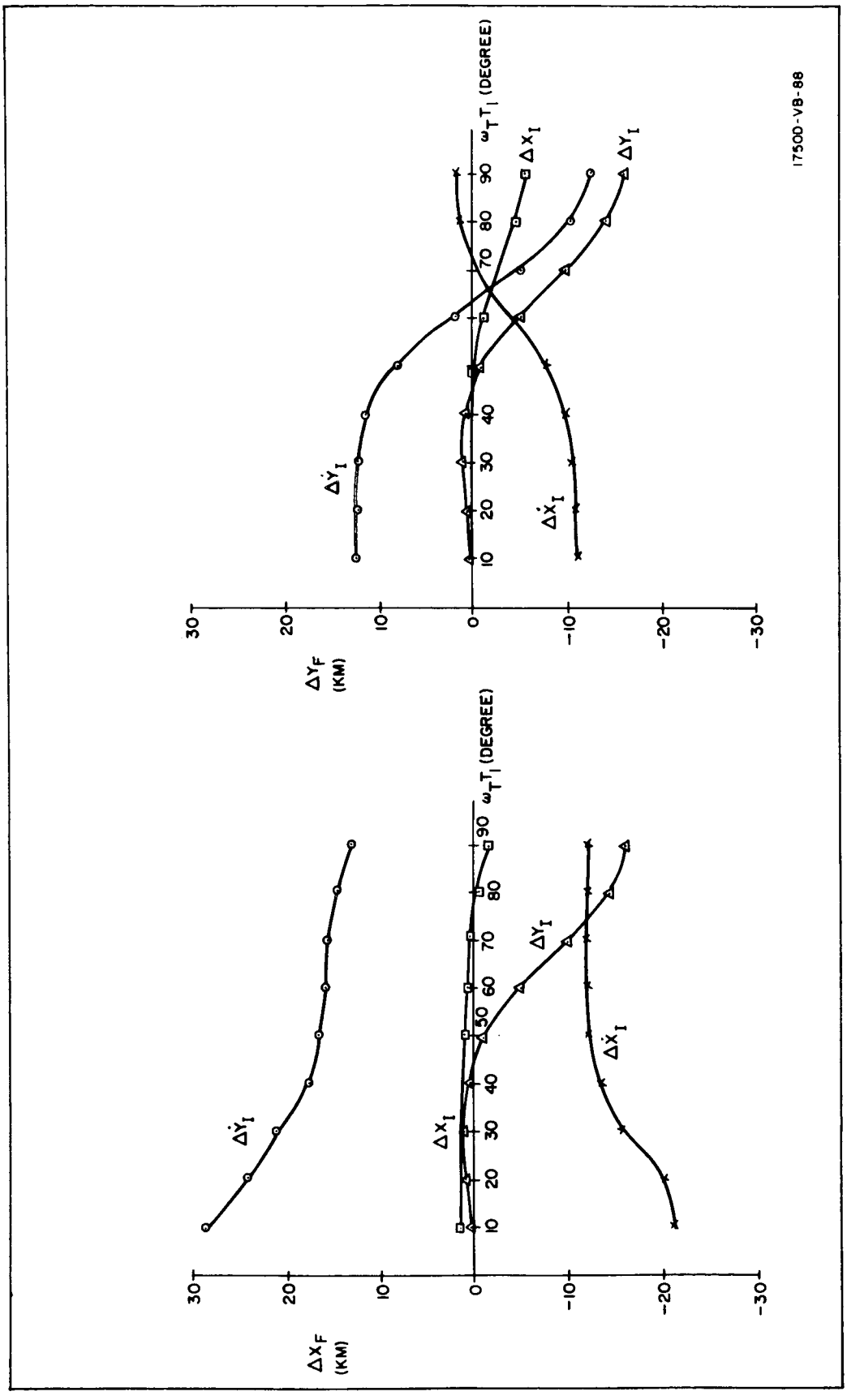


Figure 2-28. Uncertainties in Estimated Position vs Point of Measurement When Range Rate, Angle Correction Matrix Is Employed

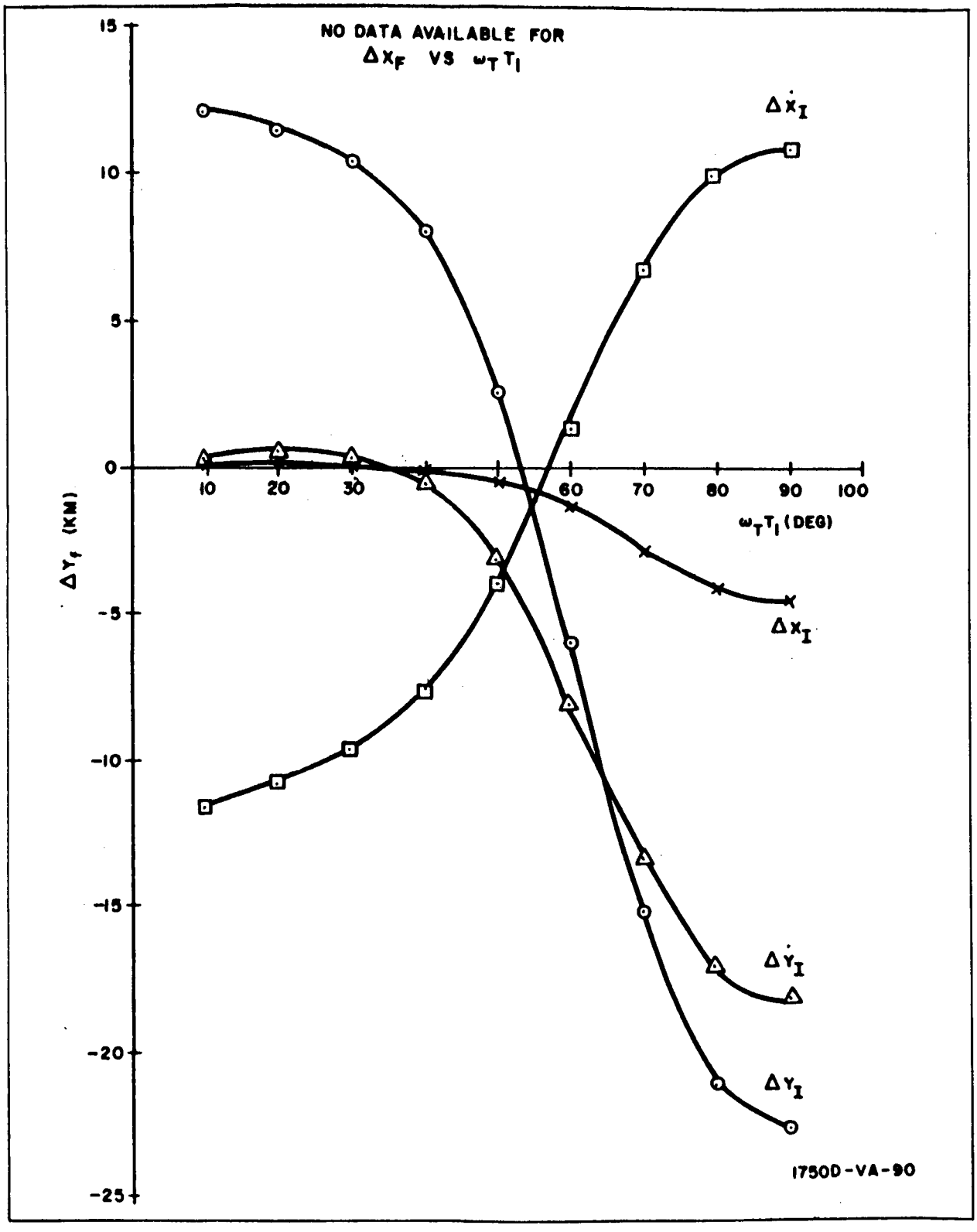


Figure 2-29. Uncertainties in Estimated Final Position vs Point of Measurement When Range, Range Rate - Angle Correction Is Employed

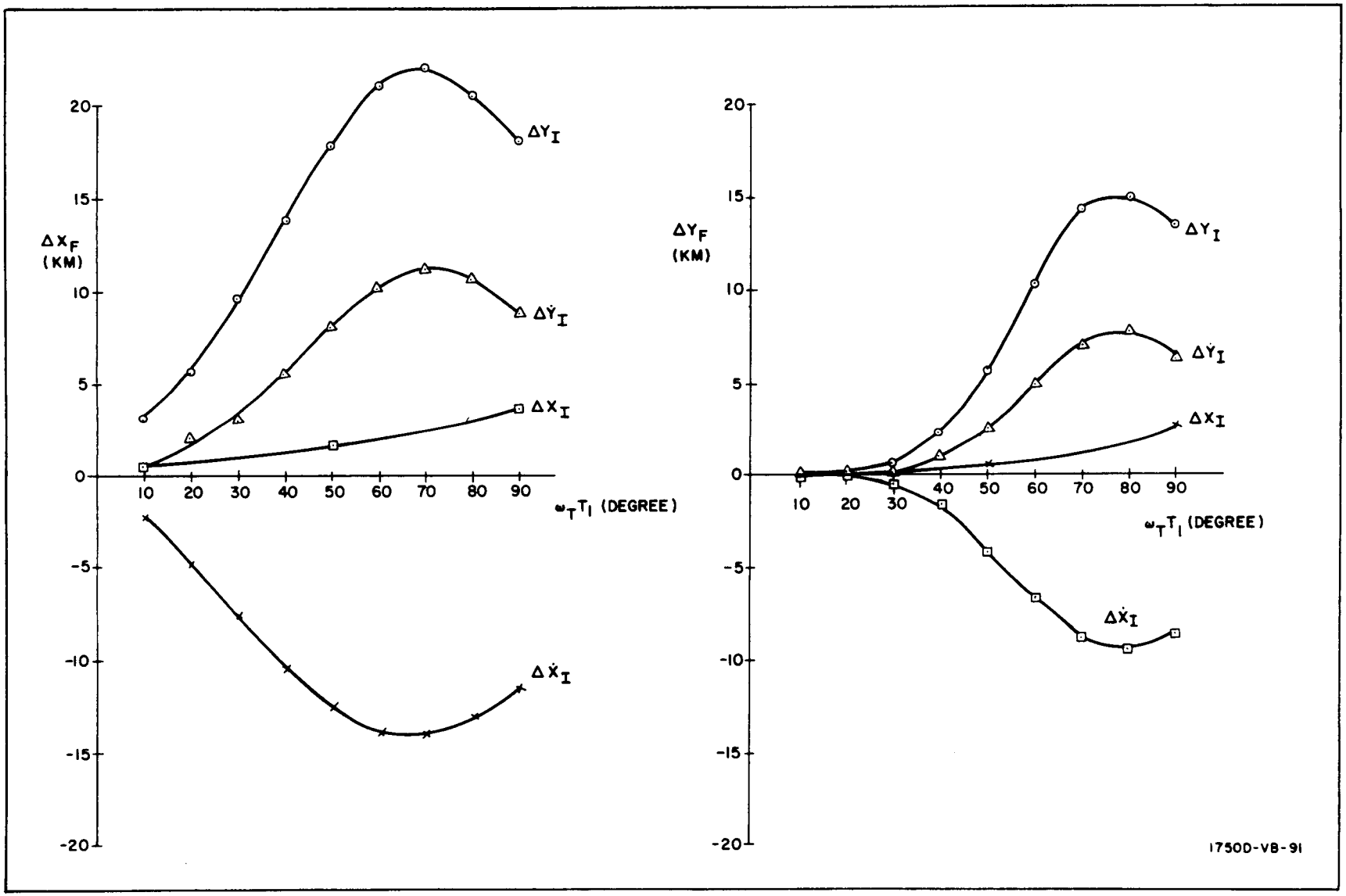


Figure 2-30. Uncertainties in Estimated Final Position vs Point of Measurement When Range, Angle, Angular Rate Correction Matrix Is Employed

expected because of the additional information used. As in the procedure using range and range rate, the best correction point is 40 to 50 degrees prior to rendezvous.

TABLE 2-19

FINAL POSITION UNCERTAINTIES WITH NO MIDCOURSE MEASUREMENT PERFORMED

| Injection Error / Position Uncertainties | $\Delta X_I$ (1.85 km) | $\Delta \dot{X}_I$ (5.4 m/sec) | $\Delta Y_I$ (1.85 km) | $\Delta \dot{Y}_I$ (5.4 m/sec) |
|---|---|---|---|---|
| $\Delta X_f$ (km) | 1.85 | -23.5 | 30.7 | 11.5 |
| $\Delta Y_f$ (km) | 0 | -11.5 | 12.7 | 5.5 |
| $\left[\Delta X_f^2 + \Delta Y_f^2\right]^{1/2}$ (km) | 1.85 | 26.2 | 33 | 11.7 |

b. Two Measurements. - Two sequential measurements utilizing the range, range rate correction matrix are also performed using the same 185-km to 740-km Hohmann transfer and the same fixed injection errors as for the single measurement cases. Performance of the first and second measurements are at $\omega_T T_1$ and $\omega_T T_2$ respectively. Combinations of these angles which are investigated are:

| | $\omega_T T_1$ | $\omega_T T_2$ |
|---|---|---|
| (1) | 80° | 70° |
| | 80° | 60° |
| | 80° | 50° |
| | 80° | 40° |
| | 80° | 30° |

| | | |
|---|---|---|
| | 80° | 20° |
| | 80° | 10° |
| (2) | 60° | 50° |
| | 60° | 40° |
| | 60° | 30° |
| | 60° | 20° |
| | 60° | 10° |
| (3) | 40° | 30° |
| | 40° | 20° |
| | 40° | 10° |

The resulting uncertainties, $\Delta X_f$ and $\Delta Y_f$, are presented in figures 2-31 through 2-33. Each figure represents a fixed value of $\omega_T T_1$ with $\omega_T T_2$ being plotted along the ordinate.

The curves indicate that of the various combinations of measurement points, the combination $\omega_T T_1$ = 40 degrees, $\omega_T T_2$ = 10 degrees appears to have the greatest effect in reducing the uncertainties. This assumes that all errors (i.e., $\Delta X_I$, $\Delta Y_I$, $\Delta \dot{X}_I$, $\Delta \dot{Y}_I$) are present at injection.

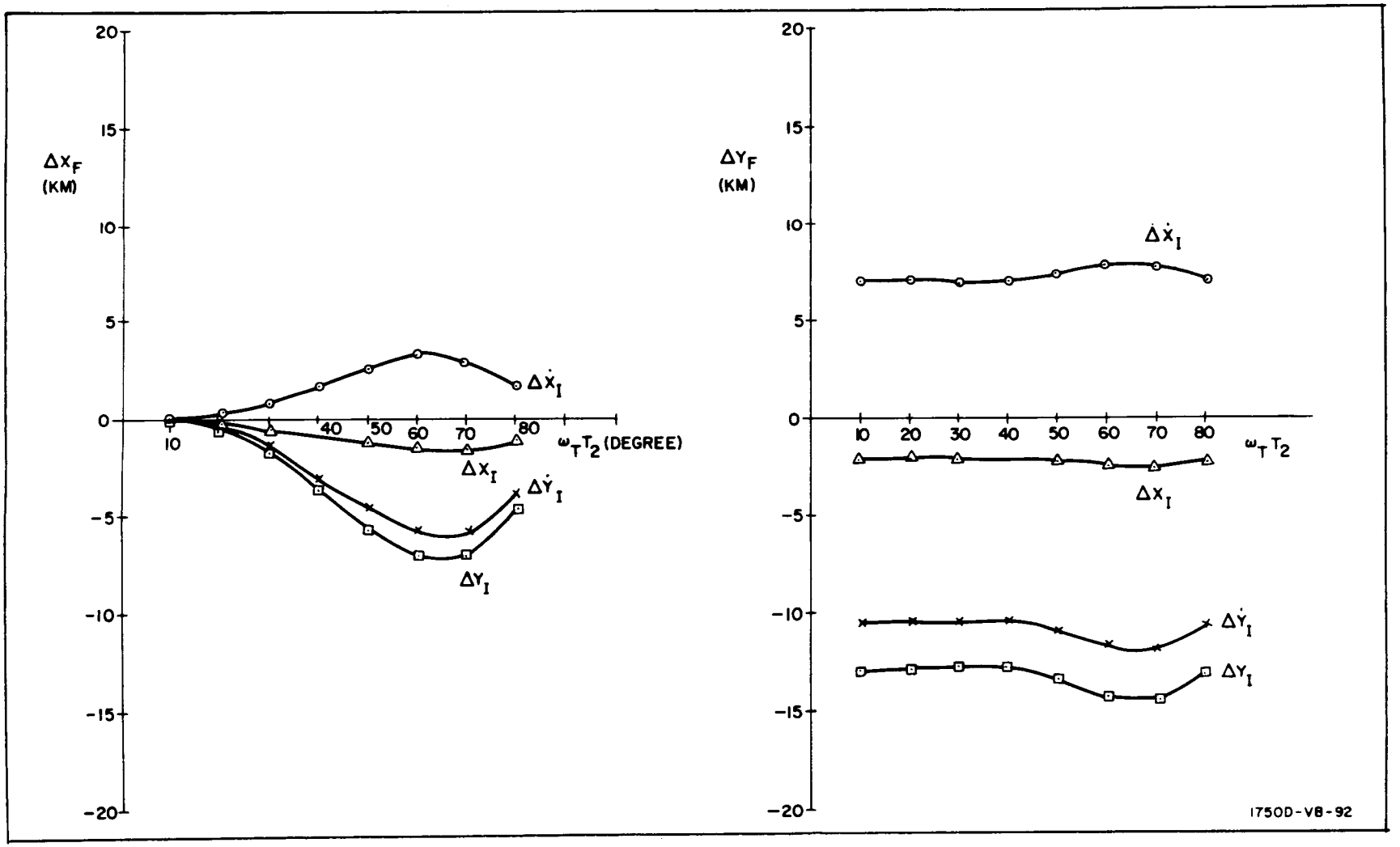


Figure 2-31. Uncertainties in Estimated Final Position vs Point of Second Measurement When Range, Range Rate Correction Matrix Is Employed; First Measurement Made at $\omega_T T_1 = 80°$

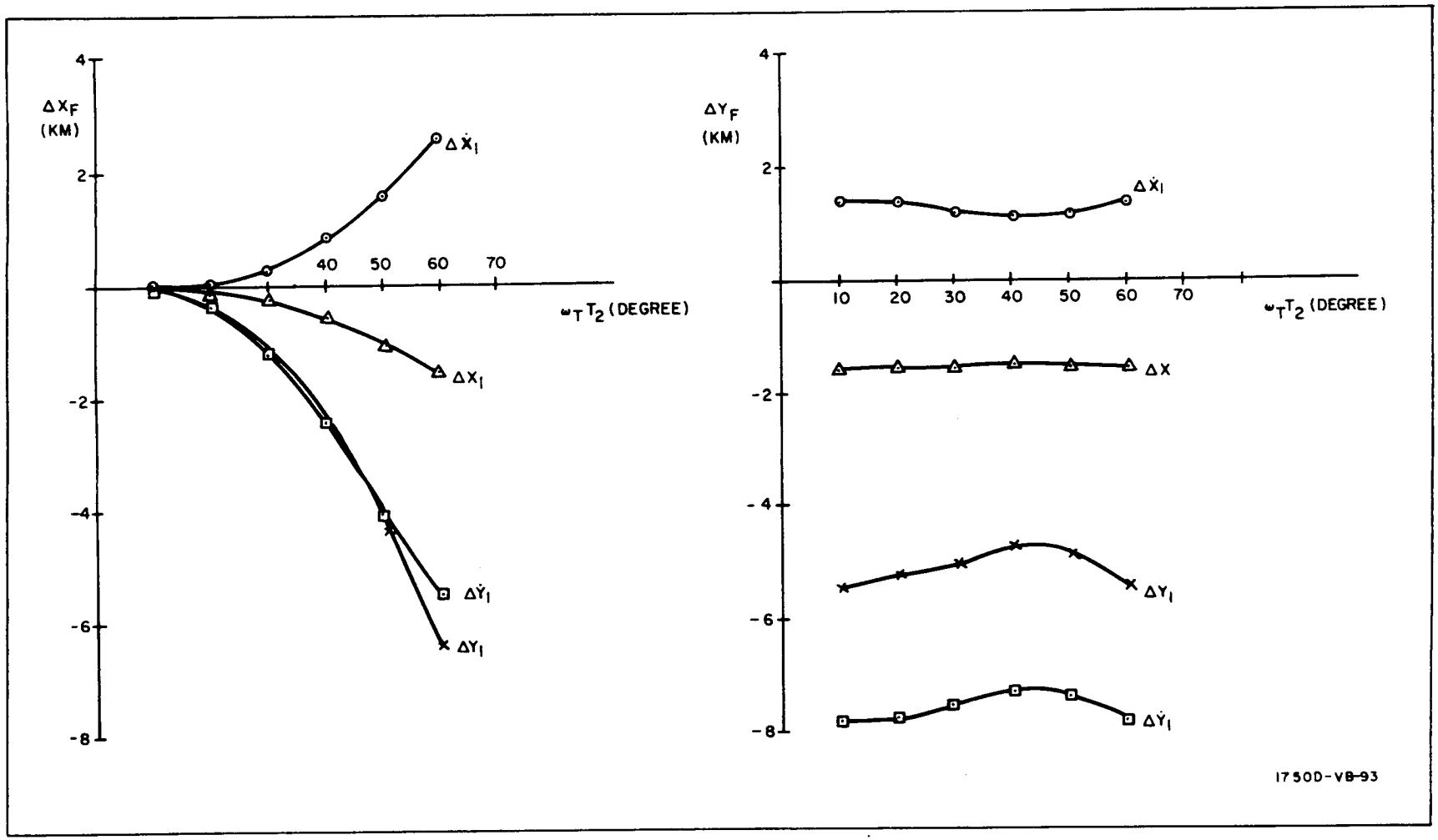


Figure 2-32. Uncertainties in Estimated Final Position vs Point of Second Measurement When Range, Range Rate Correction Matrix Is Employed; First Measurement Made at $\omega_T T_1 = 60°$

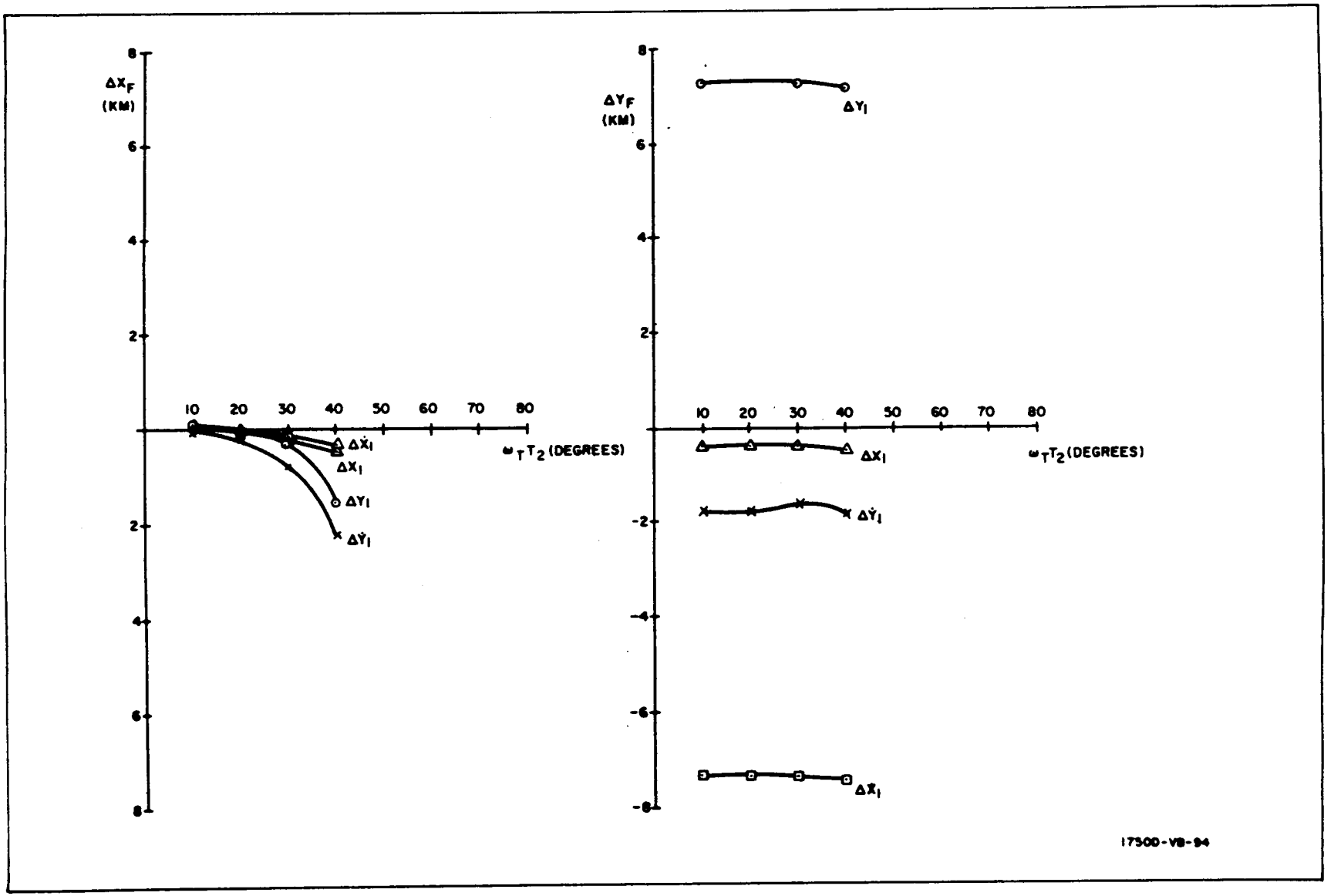


Figure 2-33. Uncertainties in Estimated Final Position vs Point of Second Measurement When Range, Range Rate Correction Matrix Is Employed; First Measurement Made at $\omega_T T_1 = 40°$

# 3. CONCLUSIONS

Comparison of the allowable errors obtained in paragraphs 2.2.1 and 2.2.2 indicates wide discrepancies. For example, the allowable $3\sigma$ error in altitude at injection is found to be 0.47 km in paragraph 2.2.1, and the same error is found to be 4 km in paragraph 2.2.2. Such discrepancies are felt to be the result of different assumptions and methods of analysis.

Injection errors for the modified proportional navigation model for instance are obtained using analytical methods while the errors for the on-off system are obtained by running the stochastic process on a computer. Further, the random sensor errors for active rendezvous are determined in conjunction with bias errors and dynamic errors in the modified proportional navigation model; whereas, sensor errors are considered individually in the on-off system. Also the criterion is not the same for each analysis.

Thus, the sensor requirements are seen to be sensitive to the dynamic characteristics of the system as would be expected, and also to the criteria utilized.

When a pilot is included in the control loop, it appears that sensor requirements may be relaxed somewhat because of the pilot's inherent ability to filter noisy signals. This filtering ability very likely increases with the pilot's "feel" for the dynamics and geometry of the rendezvous.

It may be stated, however, that state of the art sensor capabilities appear adequate for performance of rendezvous missions.

The midcourse reduction of uncertainties in the state variables has dubious value. The main reason for this contention is that it appears within the state of the art for the chaser to perform the injection maneuver with sufficient accuracy so that undue requirements are not placed on the performance of the active rendezvous phase.

If, however, a system were included for performing the indication process, it would be more expedient to take a greater number of successive measurements and so apply some type of data smoothing. This would reduce the vulnerability of the process to random errors.

## 4. BIBLIOGRAPHY


1 Cicolani, Luigi S., Trajectory Control in Rendezvous Problems Using Proportional Navigation, NASA TN D-772, April 1961

2 Irish, L. A., "A Basic Control Equation for Rendezvous Terminal Guidance, "IRE Transactions on Aerospace and Navigation Electronics, September 1961, pp 106-113

3 Green, W. G., "Logarithmic Navigation for Precise Guidance of Space Vehicles," IRE Transactions on Aerospace and Navigation Electronics, June 1961, pp 59-113

4 Bryson, Arthur E., Raytheon Internal Note entitled, "Statistically Optimizing Multivariable Terminal Control," dated 12 November 1962

5 Space Vehicle Navigation Systems Study, Raytheon Report, BR-1259A, 31 July 1961 (Unclassified)

6 Cohessy, W. H., R. S. Wiltshire, "Terminal Guidance System for Satellite Rendezvous," IAS Paper No. 59-93, June 1959

7 Hollister, W. M., "The Design of a Control System for the Terminal Phase of a Satellite Rendezvous," MIT, June 1959

8 Cramer, H., Mathematical Methods of Statistics, Princeton University Press, 1946

9 Hildebrand, F. B., Methods of Applied Mathematics, Prentice-Hall, 1952, Chapter 1

10 Steffan, Kenneth F., "A Satellite Rendezvous Terminal Guidance System," presented at the ARS 15th Annual Meeting, Shoreham Hotel, Washington, D. C., December 5-8, 1960; 1494-60

11 Erissenden, R. F., B. B. Burton, E. C. Foudriat, J. B. Whitten, Analog Simulation of a Pilot-Controlled Rendezvous, NASA TN-D-747 1961

12 Sears, N. E., P. G. Fellman, "Terminal Guidance for a Satellite Rendezvous," presented at the ARS Controllable Satellite Conference, MIT April and May 1959

13 Jensen J., G. Townsend, J. Kork and D. Kraft, Design Guide to Orbital Flight, McGraw-Hill Book Co, 1962

# APPENDIX A

## BASIC EQUATIONS FOR MECHANIZATION OF MPN AND PILOTED RENDEZVOUS PROGRAMS

This appendix presents the equations used in mechanizing the rendezvous models for the modified proportional navigation and manned simulations. These models are presented together, since they utilize the same equations to describe the relative geometry and dynamics.

In paragraph 1 the nomenclature and symbols used are presented. In paragraph 2 the coordinate systems are defined. The equations of motion used for the MPN and pilot controlled systems are discussed in paragraph 3.

### 1. NOTATION AND SYMBOLS

The vector notation that will be employed throughout the following discussions is:

$\underline{(\quad\quad)}$ = a vector quantity.

If the need arises where it is necessary to express a vector quantity in a particular coordinate system, a subscript designating the coordinate system will be attached to that vector. For example, $(\underline{R})_T$ is the range vector between target and chaser expressed in target local-vertical coordinates.

$\left.\frac{d}{dt}\right|_T (\underline{\quad})$ = time derivative of a vector quantity with respect to a coordinate frame designated by the subscript after the vertical line

$\left(\left.\frac{d}{dt}\right|_I \underline{R}\right)_T$ = time derivative of the range vector between target and chaser with respect to an inertial frame (I), this vector being expressed in target local-vertical coordinates (T)

In the discussions that follow, a vector will be represented in two different ways. First, if a vector, $\underline{A}$, can be represented by the components a, b, and c in a particular system, then $\underline{A}$ can be denoted by the column vector $[A]$; where,

$$[A] = \begin{bmatrix} a \\ b \\ c \end{bmatrix}$$

Secondly, $\underline{A}$ can be represented as $\underline{A} = a\underline{i} + b\underline{j} + c\underline{k}$.

The above notation will be used in the list of definitions that follow.

| | |
|---|---|
| $\omega_{T_l}$ | Angular velocity of target orbit; i.e., $\frac{d}{dt}\Big\|_I \theta_T$ |
| $a_{x_T}, a_{y_T}, a_{z_T}$ | Chaser thrust accelerations expressed in target coordinates |
| $a_{x_b}, a_{y_b}, a_{z_b}$ | Chaser thrust accelerations expressed in chaser body axes coordinates |
| $\theta_b, \psi_b, \phi_b$ | Pitch, yaw, and roll, respectively, of the chaser body axes with respect to the target coordinate system |
| $\omega_{b_{Tx}}, \omega_{b_{Ty}}, \omega_{b_{Tz}}$ | Components of the chaser body angular rate with respect to the target coordinate frame and expressed in chaser body axes coordinates with associated column vector $[\omega]$ |
| $e, \dot{e}$ | Line-of-sight angle and angular rate with respect to inertial space |
| $\dot{e}_x, \dot{e}_y, \dot{e}_z$ | Inertial line-of-sight rates expressed in target local-vertical coordinates |
| $\dot{e}_{y_b}, \dot{e}_{z_b}$ | Components of inertial line-of-sight rate in Y and Z directions of the chaser body coordinates |
| $\omega_{b_x}, \omega_{b_y}, \omega_{b_z}$ | Components of the inertial chaser body angular rate expressed in chaser body axes coordinates with its associated column vector being $[\omega]$ |
| A | Angle between $X_b$- axis and the projection of the range vector $(\underline{R}_{fs})_b$ on the $X_b$-$Z_b$ plane |
| E | Angle between the range vector $(\underline{R})_b$ and its projection on the $X_b$-$Z_b$ plane |
| T | Period of one complete orbit of the target |

| | |
|---|---|
| $a_o t_f$ | Initial phase shift of a target trajectory |
| $G_C$ | Gravitational acceleration acting on chaser |
| $F_C$ | Acceleration applied to chaser |
| $R_T$ | Distance from center of earth to target |
| $R_C$ | Distance from center of earth to chaser position |
| $e_T$ | Eccentricity of target orbit |
| $R_{TP}$ | Radius from center of earth to target position when target is at perigee |
| $V_{TP}$ | Velocity of target at perigee |
| $g_e$ | Gravitational acceleration at surface of the earth, 32.2 ft/sec$^2$ |
| $r_e$ | Radius of the earth |
| $[B]$ | Directional cosine matrix, target local-vertical axes to chaser body axes (the Eulerian transformation matrix) |
| $[\dot{e}_b]$ | Eulerian angular rates of the chaser body axes with respect to the target local-vertical frame |
| $[C]$ | Transformation matrix relating the chaser body rates to the Euler angle rates |
| $\underline{R}$ | Chaser-to-target range expressed in target coordinates |
| $\underline{R}_b$ | Chaser-to-target range expressed in chaser body coordinates |
| $R$ | Magnitude of $\underline{R}$ |
| $R_b$ | Magnitude of $\underline{R}_b$ |
| $G_T$ | Gravitational acceleration acting on target |
| $t$ | Time |

## 2. DEFINITIONS OF COORDINATE FRAMES

The main reference coordinate system to be used (as shown in figure 1) is a right-handed local-vertical coordinate frame centered at the target. The target moves in the plane defined by the $X_T$ - $Y_T$ axes with a rotational rate about the $Z_T$ axis of $\omega_T$ so that $Y_T$ is always aligned with the radius vector $R_T$ from the center of the earth (E). The chaser is defined relative to the target-centered, local-vertical coordinate frame by means of the coordinates X, Y, and Z. The chaser body axes, $X_b$, $Y_b$, and $Z_b$ ($X_b$ being along the logitudinal axis), are defined relative to the target local-vertical coordinate frame by means of Euler angles as shown in figure 2. The pitch angle, $\theta_b$, is the rotation in the $X_T$ - $Y_T$ plane about the $Z_T$ axis forming the $X_1$, $Y_1$, and $Z_1$ coordinate frame. The yaw angle, $\psi_b$ is the rotation in the $X_1$ - $Z_1$ plane about the $Y_1$ axis forming the $X_2$,

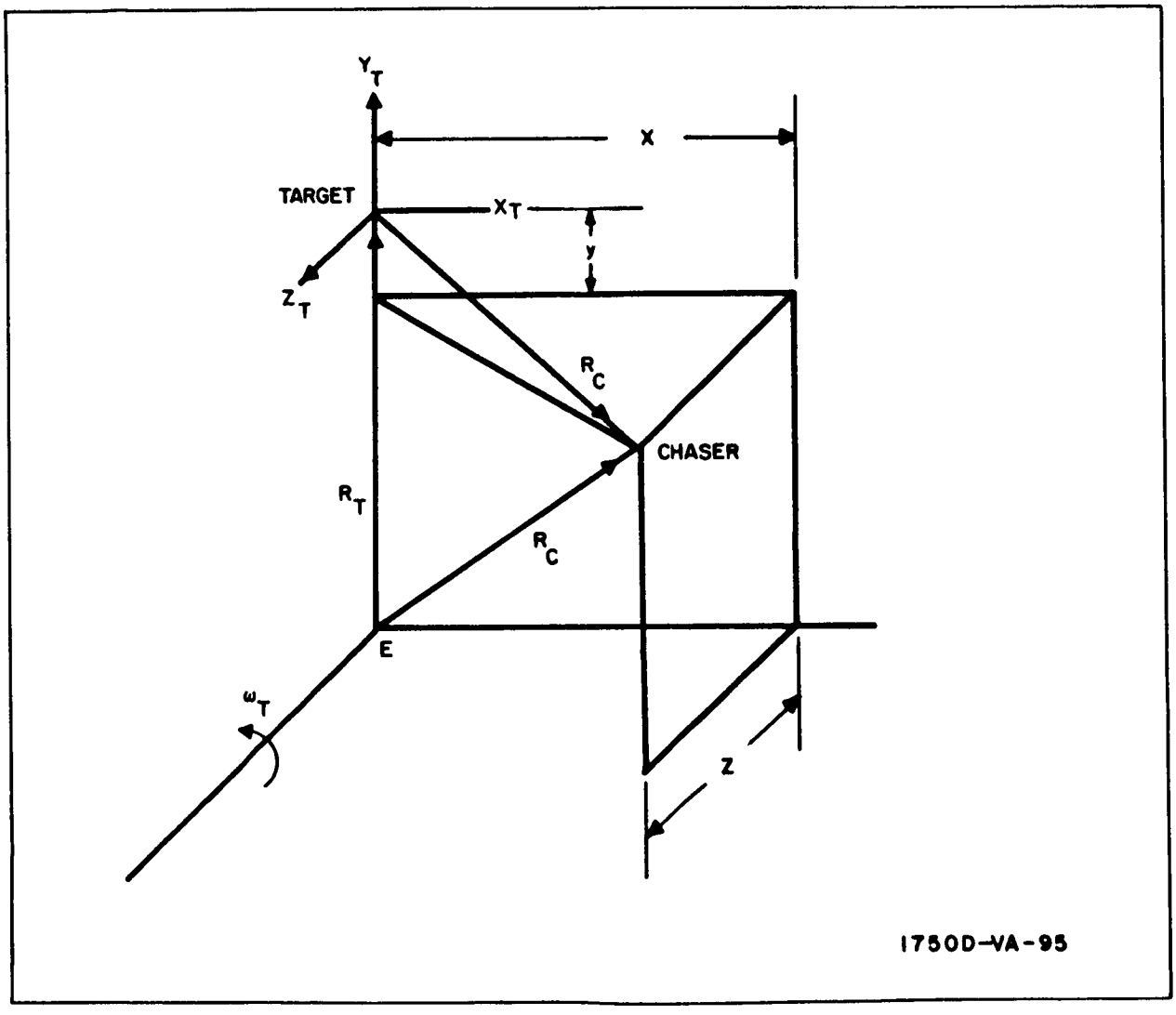


Figure 1. Vehicle Geometry

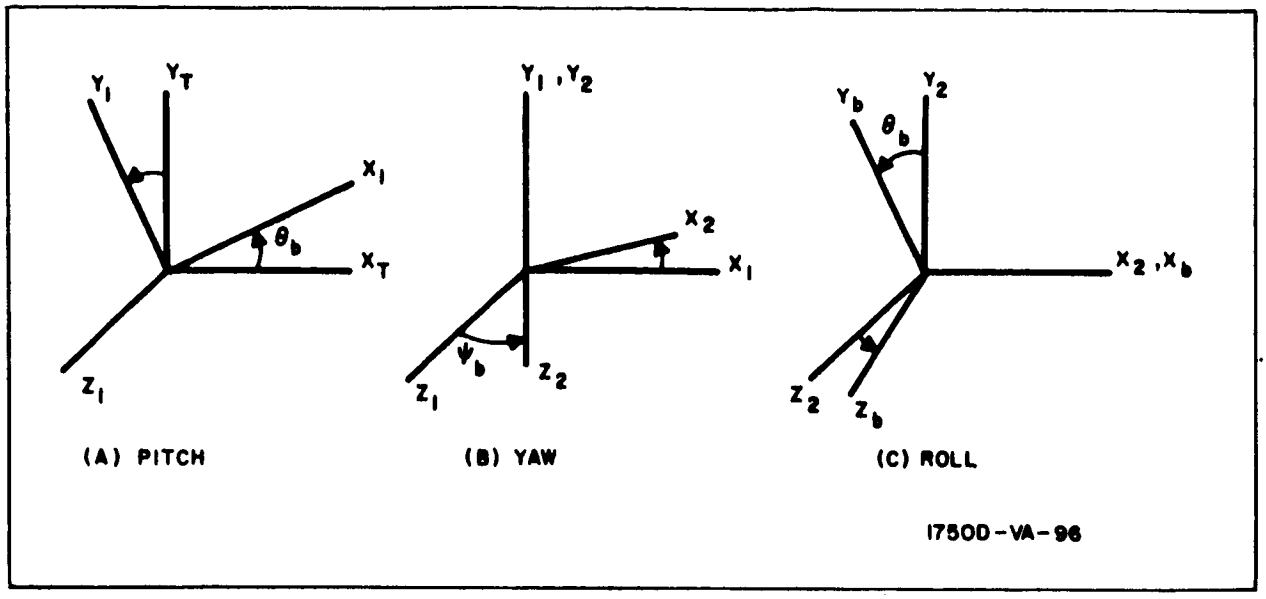


Figure 2. Euler Angles

$Y_2$, $Z_2$ coordinate frame. The roll angle, $\phi_b$ is the rotation in the $Y_2$ - $Z_2$ plane about the $X_2$ axis forming the ferry body axes coordinate system $X_b$, $Y_b$, $Z_b$. The sequence of rotation chosen here ($\theta_b$, $_b$, $\phi_b$) is somewhat arbitrary in that many other combinations of pitch, yaw, and roll will arrive at the same orientation of the chaser body axes with respect to the target location vertical axes. This particular sequence was chosen for reasons explained later. The accelerations of the chaser vehicle are applied along the body axes and the attitude control system moments about these same axes.

## 3. EQUATIONS OF MOTION AND MEASURED QUANTITIES COMMON TO BOTH MPN AND PILOTED GUIDANCE SYSTEMS

From figure 1, the chaser-to-target range is expressed vectorially as:

$$\underline{R} = \underline{R}_C - \underline{R}_T \tag{1}$$

Designating the gravitational acceleration on the target by $G_T$ and the gravitational and thrust accelerations on the chaser by $G_C$ and $F_C$, respectively, yields:

$$\left.\frac{d^2}{dt^2}\right|_I (\underline{R}_T) = \underline{G}_T \tag{2}$$

and

$$\frac{d^2}{dt^2}\Big|_I (\underline{R}_C) = \underline{F}_C + \underline{G}_C \tag{3}$$

Differentiating equation 1 twice with respect to an inertial reference system, I, produces:

$$\frac{d^2}{dt^2}\Big|_I (\underline{R}) = \frac{d^2}{dt^2}\Big|_I (\underline{R}_C) - \frac{d^2}{dt^2}\Big|_I (\underline{R}_T). \tag{4}$$

Substituting equations 2 and 3 into equation 4 yields:

$$\frac{d^2}{dt^2}\Big|_I (\underline{R}) = \underline{F}_C + (\underline{G}_C - \underline{G}_T) \tag{5}$$

By vector differentiation, $\frac{d^2}{dt^2}\Big|_I (\underline{R})$ is expressed as:

$$\frac{d^2}{dt^2}\Big|_I (\underline{R}) = \frac{d}{dt}\Big|_I \left(\frac{d}{dt}\Big|_I \underline{R}\right) = \frac{d}{dt}\Big|_T \left(\frac{d}{dt}\Big|_I \underline{R}\right) + \underline{\omega}_T \times \frac{d}{dt}\Big|_I \underline{R} \tag{6}$$

Performing the operations indicated on the right hand side of equation 6 and substituting the result into equation 5 yields the vector equation of motion of the chaser relative to the target:

$$\frac{d^2}{dt^2}\Big|_T R_{sf} + \frac{d}{dt}\Big|_T (\underline{\omega}_T) \times \underline{R} + 2\left[\underline{\omega}_T \times \frac{d}{dt}\Big|_T (\underline{R})\right] + \underline{\omega}_T \times (\underline{\omega}_T \times \underline{R}) \tag{7}$$

$$= \underline{F}_C + (\underline{G}_C - \underline{G}_T)$$

The above vector equation is expressed in scalar form in the target coordinate system as:

$$(\underline{R})_T = X\underline{i}_T + Y\underline{j}_T + Z\underline{k}_T \tag{8}$$

and similarly for $\left(\frac{d}{dt}\Big|_T \underline{R}\right)_T$ and $\left(\frac{d^2}{dt^2}\Big|_T \underline{R}\right)_T$

The gravitational acceleration acting on the target is:

$$(\underline{G}_T)_T = -\frac{g_e r_e^2}{R_T^2} \quad j_T \tag{9}$$

From figure 1 the gravitational acceleration acting on the chaser is along the vector $\underline{R}_C$. Expressing $\underline{G}_C$ in satellite coordinates by means of the directional cosines associated with $\underline{R}_C$, yields:

$$(\underline{G}_C)_T = -g_e r_e^2 \frac{X}{R_C^3} \underline{i}_T - g_e r_e^2 \frac{(R_T + y)}{R_C^3} \underline{j}_T - g_e r_e^2 \frac{Z}{R_C^3} \underline{k}_T \tag{10}$$

also

$$(\underline{F}_C)_T = a_{x_T} \underline{i}_T + a_{y_T} \underline{j}_T + a_{z_T} \underline{k}_T \tag{11}$$

Substituting equations 8, 9, 10, and 11 into 7 and performing the operations indicated in 7 in the target coordinate frame yields the following scalar equations of relative motion:

$$\ddot{X} = a_{x_T} + 2\omega_T \dot{y} + \dot{\omega}_T Y_T + \omega_T^2 X - g_e r_e^2 \frac{X}{R_C^3} \tag{12}$$

$$\ddot{Y} = a_{y_T} - 2\omega_T \dot{X} - \dot{\omega}_T X + \omega_T^2 Y + g_e r_e^2 \left( \frac{1}{R^2} - \frac{R_T + Y}{R_C^3} \right) \tag{13}$$

$$\ddot{Z} = a_{z_T} - g_e r_e^2 \frac{Z}{R_C^3} \tag{14}$$

also

$$R_C^2 = X^2 + (Y + R_T)^2 + Z^2$$

The dynamic equations of motion of a two-body system are (from any standard dynamics text):

$$R_T = \frac{R_{TP}(1 + e)}{1 + e \cos e_T} \tag{15}$$

$$\omega_T = \frac{R_{TP} V_{TP}}{R_T^2} \tag{16}$$

where $\omega_T = \dot{\theta}_T$

also,

$$R_T = \frac{R_{TP}^2 V_{TP}^2}{g_e r_e^2 (1 + e \cos \theta_T)} \tag{17}$$

Equation 17 may be rearranged to give:

$$g_e r_e^2 = \frac{R_{TP}^2 V_{TP}^2}{R_T (1 + e \cos \theta_T)} \tag{18}$$

From equation 16

$$R_{TP}^2 V_{TP}^2 = \omega_T^2 R_T^4 \tag{19}$$

Substituting equation 19 into equation 18

$$g_e r_e^2 = \frac{\omega_T^2 R_T^3}{1 + e \cos \theta_T} \tag{20}$$

Substitution of equation 20 into equations 12, 13, and 14 and combining yields:

$$\ddot{X} = a_{x_T} + 2 \omega_T \dot{Y} + \dot{\omega}_T Y + \omega_T^2 \left[ 1 - \left( \frac{R_T}{R_C} \right)^3 \frac{1}{1 + e \cos \theta_T} \right] X \tag{21}$$

$$\ddot{Y} = a_{y_T} - 2\omega_T \dot{X} - \dot{\omega}_T X + \omega_T^2 \left[ 1 - \left( \frac{R_T}{R_C} \right)^3 \frac{1}{1 + e \cos \theta_T} \right] Y + \frac{\omega_T^2 R_T}{1 + e \cos \theta_T} \left[ 1 - \left( \frac{R_T}{R_C} \right)^3 \right] \tag{22}$$

$$\ddot{Z} = a_{z_T} - \frac{\omega_T^2}{1 + e\cos\theta_T}\left(\frac{R_T}{R_C}\right)^3 Z \qquad (23)$$

The transformation relating the chaser body axes coordinates to the target local-vertical coordinate system must be determined since the accelerations, $a_{x_T}$, $a_{y_T}$, $a_{z_T}$, presented in equations 21, 22, and 23 are the chaser accelerations expressed in target coordinates whereas the chaser actually thrusts in its own body axes system.

The attitude of the chaser vehicle is measured with respect to the target local-vertical coordinates. The Euler transformation selected is $\theta_b$, $\psi_b$, and $\phi_b$ (pitch, yaw and roll, respectively). The result of the pitch rotation is from figure 2:

$$\begin{bmatrix} X_1 \\ Y_1 \\ Z_1 \end{bmatrix} = \begin{bmatrix} \cos\theta_b & \sin\theta_b & 0 \\ -\sin\theta_b & \cos\theta_b & 0 \\ 0 & 0 & 1 \end{bmatrix} \begin{bmatrix} X_T \\ Y_T \\ Z_T \end{bmatrix} \qquad (24)$$

or in shorter form

$$\left[X_1\right] = \left[B_1\right]\left[X_T\right] \qquad (25)$$

In a similar manner for yaw and roll, there results:

$$\left[X_2\right] = \left[B_2\right]\left[X_1\right] \qquad (26)$$

$$\left[X_b\right] = \left[B_3\right]\left[X_2\right] \qquad (27)$$

where,

$$\left[B_2\right] = \begin{bmatrix} \cos\psi_b & 0 & -\sin\psi_b \\ 0 & 1 & 0 \\ \sin\psi_b & 0 & \cos\psi_b \end{bmatrix} \qquad (28)$$

$$\left[B_3\right] = \begin{bmatrix} 1 & 0 & 0 \\ 0 & \cos\phi_b & \sin\phi_b \\ 0 & -\sin\phi_b & \cos\phi_b \end{bmatrix} \qquad (29)$$

Substitution of equations 25 and 26 into 27:

$$\left[X_b\right] = \left[B_3\right]\left[B_2\right]\left[B_1\right]\left[X_T\right] \tag{30}$$

Let

$$\left[B\right] = \left[B_3\right]\left[B_2\right]\left[B_1\right]$$

Thus, equation 30 becomes:

$$\left[X_b\right] = \left[B\right]\left[X_T\right] \tag{31}$$

where,

$$\left[B\right] = \begin{bmatrix} (\cos\theta_b \cos\psi_b) & (\sin\theta_b \cos\psi_b) & (-\sin\psi_b) \\ (\cos\theta_b \sin\psi_b \sin\phi_b - \sin\theta_b \cos\phi_b) & (\sin\theta_b \sin\psi_b \sin\phi_b + \cos\theta_b \cos\phi_b) & (\cos\psi_b \sin\phi_b) \\ (\cos\theta_b \sin\psi_b \cos\phi_b + \sin\theta_b \sin\phi_b) & (\sin\theta_b \sin\psi_b \cos\phi_b - \cos\theta_b \sin\phi_b) & (\cos\psi_b \cos\phi_b) \end{bmatrix} \tag{32}$$

Since B represents a coordinate transformation between orthogonal axis sets:

$$\left[B\right]^{-1} = \left[B\right]^T$$

$$\left[X_T\right] = \left[B\right]^T\left[X_b\right] \tag{33}$$

Thus, the chaser body accelerations can be written in terms of target coordinates by means of $\left[B\right]^T$ .

The angular rates of the chaser body axes with respect to the target local-vertical system may be related to the Eulerian rates $\dot{\theta}_b$, $\dot{\psi}_b$, and $\dot{\phi}_b$ by a matrix $\left[e\right]$ ; i. e.,

$$\left[\omega_{bT}\right]_b = \left[C\right]\left[\dot{\beta}\right] \tag{34}$$

where $\left[\dot{\beta}\right]$ represents the Euler rates:

$$\left[\dot{\beta}\right] = \begin{bmatrix} \dot{\phi}_b \\ \dot{\psi}_b \\ \dot{\theta}_b \end{bmatrix} \tag{35}$$

Each Euler rate may be referred to the body axis system, where the components when summed, form the components of the angular rotation $\left[\omega_{bT}\right]_b$, expressed in the body axes. This procedure is accomplished by the relationship expressed in equation 36 below.

$$\left[\omega_{bT}\right]_b = \left[\dot{\phi}_b\right] + \left[B_3\right]\left[\dot{\psi}_b\right] + \left[B_3\right]\left[B_2\right]\left[\dot{\theta}_b\right] \tag{36a}$$

$$\begin{bmatrix} \omega_{bT_x} \\ \omega_{bT_y} \\ \omega_{bT_z} \end{bmatrix} = \begin{bmatrix} \dot{\phi}_b \\ 0 \\ 0 \end{bmatrix} + \begin{bmatrix} 1 & 0 & 0 \\ 0 & \cos\phi_b & \sin\phi_b \\ 0 & -\sin\phi_b & \cos\phi_b \end{bmatrix} \begin{bmatrix} 0 \\ \dot{\psi}_b \\ 0 \end{bmatrix}$$

$$+ \begin{bmatrix} 1 & 0 & 0 \\ 0 & \cos\phi_b & \sin\phi_b \\ 0 & -\sin\phi_b & \cos\phi_b \end{bmatrix} \begin{bmatrix} \cos\psi_b & 0 & -\sin\psi_b \\ 0 & 1 & 0 \\ \sin\psi_b & 0 & \cos\psi_b \end{bmatrix} \begin{bmatrix} 0 \\ 0 \\ \dot{\theta}_b \end{bmatrix} \tag{36b}$$

Expanding and adding yields:

$$\begin{bmatrix} \omega_{bT_x} \\ \omega_{bT_y} \\ \omega_{bT_z} \end{bmatrix} = \begin{bmatrix} \dot{\phi}_b & -\dot{\theta}_b \sin\psi_b \\ \dot{\psi}_b \cos\phi_b + \dot{\theta}_b \cos\psi_b \sin\phi_b \\ -\dot{\psi}_b \sin\phi_b + \dot{\theta}_b \cos\psi_b \cos\phi_b \end{bmatrix} \tag{37a}$$

$$= \begin{bmatrix} 1 & 0 & -\sin\psi_b \\ 0 & \cos\phi_b & (\cos\psi_b \sin\phi_b) \\ 0 & -\sin\phi_b & (\cos\psi_b \cos\phi_b) \end{bmatrix} \begin{bmatrix} \dot{\phi}_b \\ \dot{\psi}_b \\ \dot{\theta}_b \end{bmatrix} \tag{37b}$$

Consequently:

$$[C] = \begin{bmatrix} 1 & 0 & -\sin\psi_b \\ 0 & \cos\phi_b & (\cos\psi_b \sin\phi_b) \\ 0 & -\sin\phi_b & (\cos\psi_b \cos\phi_b) \end{bmatrix} \tag{38}$$

The Eulerian rates in terms of the body angular rates are expressed as:

$$[\dot{\beta}] = [C]^{-1} [\omega_{bT}]_b \tag{39}$$

Since the axes about which the Euler rates are measured are not orthogonal:

$$[C]^{-1} \neq [C]^T \tag{40}$$

Taking the inverse of $[C]$ gives:

$$[C]^{-1} = \begin{bmatrix} 1 & (\tan\psi_b \sin\phi_b) & (\tan\psi_b \cos\phi_b) \\ 0 & \cos\phi_b & -\sin\phi_b \\ 0 & \left(\dfrac{\sin\phi_b}{\cos\psi_b}\right) & \left(\dfrac{\cos\phi_b}{\cos\psi_b}\right) \end{bmatrix} \tag{41}$$

One reason for the selection of the $\theta_b$, $\psi_b$, $\phi_b$ rotation is that in any order of rotation the middle angle of rotation will cause $[C]^{-1}$ to have a singular point when that angle passes through $\pm(2n+1)\,\pi/2$, where $n = 1, 2, 3, \ldots$. It was assumed that yaw would be the least likely attitude angle to go through $(2n+1)\,\pi/2$.

Determination of $[\omega_{bT}]_b$ is as follows:

$$[\omega_b]_b = [\omega_{bT}]_b + [\omega_T]_b$$

or

$$[\omega_{bT}]_b = [\omega_b]_b - [\omega_T]_b \tag{42}$$

The quantity $\left[\omega_T\right]_b$ is expressed as:

$$\left[\omega_T\right]_b = \left[B\right]\left[\omega_T\right]_T \tag{43}$$

where

$$\left[\omega_T\right]_T = \begin{bmatrix} 0 \\ 0 \\ \omega_T \end{bmatrix}$$

Substituting equation 43 into 41 gives:

$$\left[\omega_{bT}\right]_b = \left[\omega_b\right]_b - \left[B\right]\left[\omega_T\right]_T \tag{44}$$

$\left[\omega_b\right]_b$ is determined in terms of the attitude torques applied. These torques are expressed as:

$$\begin{aligned} \underline{M}_b &= \left.\frac{d}{dt}\right|_I \underline{I}_b\,\omega_b \\ &= \left.\frac{d}{dt}\right|_b \underline{I}_b\underline{\omega}_b + \underline{\omega}_b \times \underline{I}_b\underline{\omega}_b \end{aligned} \tag{45}$$

Performing the operations indicated in equations 45 gives:

$$\begin{bmatrix} M_{bx} \\ M_{by} \\ M_{bz} \end{bmatrix} = \begin{bmatrix} I_{bx}\,\dot{\omega}_{bx} + \omega_{by}\,\omega_{bz}\,(I_{bz} - I_{by}) \\ I_{by}\,\dot{\omega}_{by} + \omega_{bx}\,\omega_{bz}\,(I_{bx} - I_{bz}) \\ I_{bz}\,\dot{\omega}_{bz} + \omega_{bx}\,\omega_{by}\,(I_{by} - I_{bx}) \end{bmatrix} \tag{46}$$

Rearranging equation 46 produces the components of the angular acceleration of the chaser body axes:

$$\begin{aligned} \dot{\omega}_{bx} &= \frac{M_{bx}}{I_{bx}} - \omega_{by}\,\omega_{bz}\left(\frac{I_{bz} - I_{by}}{I_{bx}}\right) \\ \dot{\omega}_{by} &= \frac{M_{by}}{I_{by}} - \omega_{bx}\,\omega_{bz}\left(\frac{I_{bx} - I_{bz}}{I_{by}}\right) \\ \dot{\omega}_{bz} &= \frac{M_{bz}}{I_{bz}} - \omega_{bx}\,\omega_{by}\left(\frac{I_{by} - bx}{I_{bz}}\right) \end{aligned} \tag{47}$$

These equations may be integrated to obtain the components of which are used in equation 44.

Equations 15, 16, 21 through 23, 33, 39, 44, and 47 describe the relative motion of chaser and target in target local-vertical coordinates in terms of thrusts and attitude moments. These thrusts and attitude moments will be determined by the guidance scheme employed. The guidance schemes employed produce command signals which are dependent upon certain measurable quantities such as range and range rate.

## 3.1 MEASURED QUANTITIES

The measured quantities common to all guidance schemes considered are presented here in analytical form. The expression for range is:

$$R = \sqrt{X^2 + Y^2 + Z^2} \tag{48}$$

differentiating 2-35 yields the range rate, $\dot{R}$:

$$\dot{R} = \frac{dR}{dt} = \frac{1}{R}\left(X\dot{X} + Y\dot{Y} + Z\dot{Z}\right) \tag{49}$$

In some of the guidance schemes considered, the attitude control system requires information concerning the orientation of the range vector with respect to the chaser body axes. This information is represented by the angles A and E in figure 3.

From figure 3 it is evident that:

$$\frac{\underline{i}_b \times \underline{R}_b}{R_b} = \cos E \sin A \underline{j}_b + \sin E \underline{k}_b \tag{50}$$

Since it is postulated that A and E will be kept small by the attitude control system:

$$\sin A \approx A$$

$$\sin E \approx E$$

$$\cos E \approx 1$$

and also since

$$\underline{R}_b = -\underline{R}$$

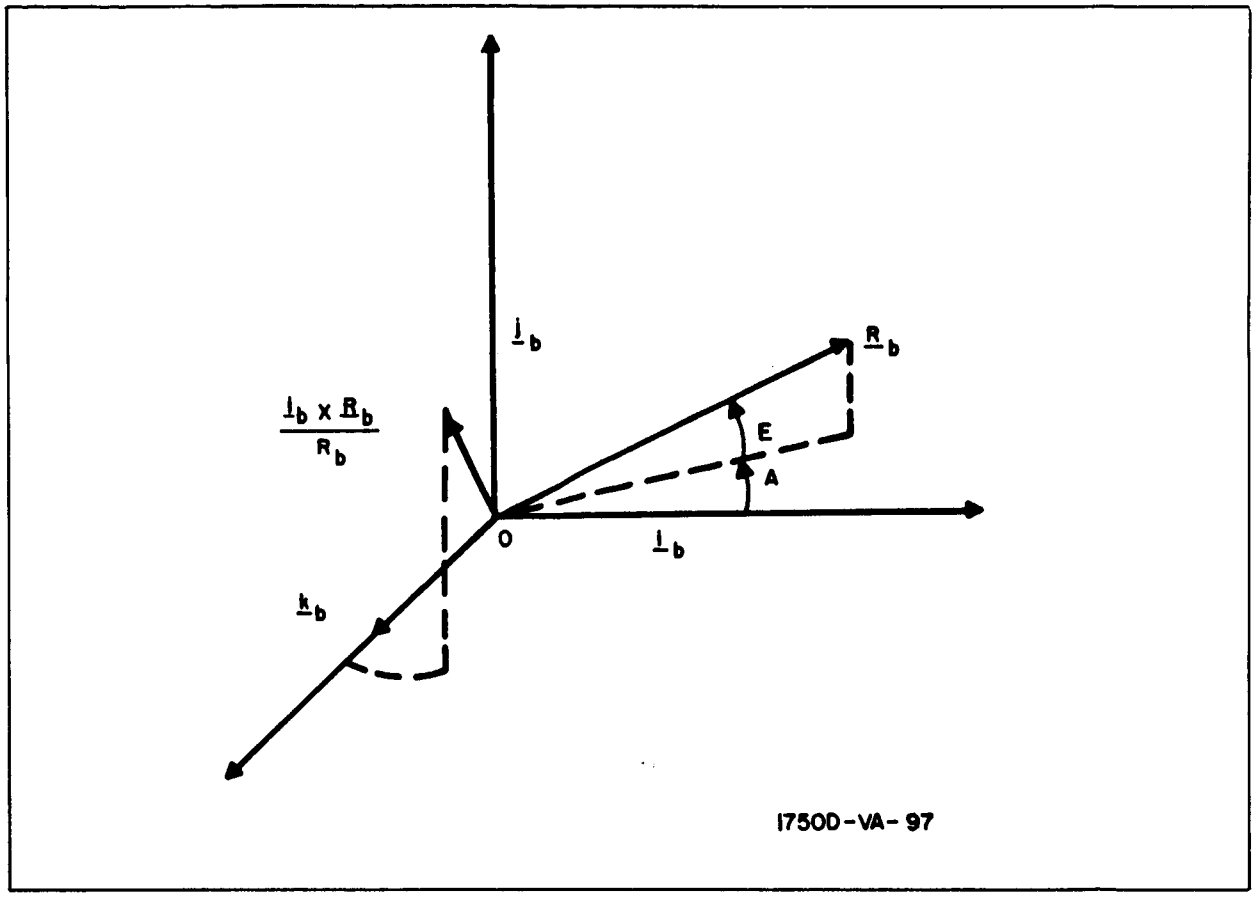


Figure 3. Relation Between A, E, and $R_b$

equation 50 becomes:

$$\frac{-\underline{i}_b \times \underline{R}}{R} \cong A\underline{j}_b + E\underline{k}_b \tag{51}$$

Taking the dot product of equation 51 with $\underline{j}_b$ yields:

$$A = \frac{-\underline{j}_b \cdot (\underline{i}_b \times \underline{R})}{R} \tag{52}$$

and similarly

$$E = \frac{-\underline{k}_b \cdot (\underline{i}_b \times \underline{R})}{R} \tag{53}$$

The inertial line-of-sight rate can be expressed as:

$$\left.\frac{d}{dt}\right|_I \underline{e} = \frac{1}{R^2} \left(\underline{R} \times \left.\frac{d}{dt}\right|_I \underline{R}\right) \tag{54}$$

where,

$$\left.\frac{d}{dt}\right|_I \underline{R} = \left.\frac{d}{dt}\right|_b \underline{R} + \underline{\omega}_T \times \underline{R}$$

If the line-of-sight rate in equation 54 is expressed in target local-vertical coordinates, then by using the transformation matrix $[B]$, it can be expressed in chaser body axes coordinates; i.e.,

$$\left[\dot{e}_I\right]_b = [B] \left[\dot{e}_I\right]_T \tag{55}$$

where,

$$\left[\dot{e}_I\right]_T = \begin{bmatrix} \dot{e}_x \\ \dot{e}_y \\ \dot{e}_z \end{bmatrix}$$

If it is assumed that the attitude of the vehicle can be controlled such that the $i_b$ axis is approximately colinear with $\underline{R}_b$ (by making A and E = 0), then $\dot{e}_{x_b} = 0$. Then:

$$\left[\dot{e}_I\right]_b = \begin{bmatrix} 0 \\ \dot{e}_{y_b} \\ \dot{e}_{z_b} \end{bmatrix}$$

Equations 48, 49, and 52 through 55 express the measurable quantities common to all schemes.

The complete set of orbital rendezvous equations which forms the basis of the MPN and manned rendezvous simulations is listed below.

## 3.2 BASIC EQUATIONS FOR SIMULATION

$$\ddot{X} = a_{x_T} + 2\omega_T \dot{Y} + \dot{\omega}_T Y + \omega_T^2 \left[1 + \left(\frac{R_T}{R_C}\right)^3 \frac{1}{1 + e\cos\theta_T}\right] X$$

$$\ddot{Y} = a_{y_T} + 2\omega_T \dot{X} + \dot{\omega}_T X + \omega_T^2 \left[1 - \left(\frac{R_T}{R_C}\right)^3 \frac{1}{1 + e\cos\theta_T}\right] Y \tag{56}$$

$$+ \frac{\omega_T^2 R_T}{1 + e\cos\theta_T} \left[1 - \left(\frac{R_T}{R_C}\right)^3\right] \tag{57}$$

$$\ddot{Z} = a_{z_T} - \frac{\omega_T^2}{1 + e \cos \theta_T} \left( \frac{R_T}{R_C} \right)^3 Z \tag{58}$$

$$\dot{\omega}_T = - \frac{2 \omega_T^2 \, e \sin \theta_T}{1 + e \cos \theta_T} \tag{59}$$

$$\omega_T = \frac{V_{TP} (1 + e \cos \theta_T)^2}{R_{TP} (1 + e)^2} \tag{60}$$

$$R_T = \frac{R_{TP} (1 + e)}{1 + e \cos \theta_T} \tag{61}$$

$$R_C = \left[ X^2 + (Y + R_T)^2 + Z^2 \right]^{1/2} \tag{62}$$

$$\dot{\theta}_b = \frac{\sin \phi_b}{\cos \psi_b} \omega_{bT_y} + \frac{\cos \phi_b}{\cos \psi_b} \omega_{bT_z} \tag{63}$$

$$\dot{\psi}_b = \cos \phi_b \, \omega_{bT_y} - \sin \phi_c \, \omega_{bT_z} \tag{64}$$

$$\phi_b = \omega_{bT_x} + \theta_b \sin \psi_b \tag{65}$$

$$\dot{\omega}_{bx} = \frac{M_{bx}}{I_{bx}} - \omega_{by} \, \omega_{bz} \left( \frac{I_{bz} - I_{by}}{I_{bx}} \right) \tag{66}$$

$$\dot{\omega}_{by} = \frac{M_{by}}{I_{by}} - \omega_{bz} \, \omega_{bx} \left( \frac{I_{bx} - I_{bz}}{I_{by}} \right) \tag{67}$$

$$\dot{\omega}_{bz} = \frac{M_{bz}}{I_{bz}} - \omega_{bx} \, \omega_{by} \left( \frac{I_{by} - I_{bx}}{I_{bz}} \right) \tag{68}$$

$$\omega_{bT_x} = \omega_{bx} + \omega_T \sin \psi_b \tag{69}$$

$$\omega_{bT_y} = \omega_{by} - \omega_T \cos \psi_b \sin \phi_b \tag{70}$$

$$\omega_{bT_z} = \omega_{bz} - \omega_T \cos \psi_b \cos \phi_b \tag{71}$$

$$a_{xT} = b_{11} a_{x_b} + b_{21} a_{y_b} + b_{31} a_{z_b} \tag{72}$$

$$a_{yT} = b_{12} a_{x_b} + b_{22} a_{y_b} + b_{32} a_{z_b} \tag{73}$$

$$a_{zT} = b_{13} a_{x_b} + b_{23} a_{y_b} + b_{33} a_{z_b} \tag{74}$$

$$b_{11} = \cos \theta_b \cos \psi_b \tag{75}$$

$$b_{12} = \sin \theta_b \cos \psi_b \tag{76}$$

$$b_{13} = - \sin \psi_b \tag{77}$$

$$b_{21} = \cos \theta_b \sin \psi_b \sin \phi_b - \sin \theta_b \cos \phi_b \tag{78}$$

$$b_{22} = \sin \theta_b \sin \psi_b \sin \phi_b + \cos \theta_b \cos \phi_b \tag{79}$$

$$b_{23} = \cos \psi_b \sin \phi_b \tag{80}$$

$$b_{31} = \cos \theta_b \sin \psi_b \cos \phi_b + \sin \theta_b \sin \phi_b \tag{81}$$

$$b_{32} = \sin \theta_b \sin \psi_b \cos \phi_b - \cos \theta_b \sin \phi_b \tag{82}$$

$$b_{33} = \cos \psi_b \cos \phi_b \tag{83}$$

$$R = (X^2 + Y^2 + Z^2)^{1/2} \tag{84}$$

$$\dot{R} = \frac{1}{R} (X\dot{X} + Y\dot{Y} + Z\dot{Z}) \tag{85}$$

$$\dot{e}_x = \frac{1}{R^2} (Y\dot{Z} - Z\dot{Y} - \omega_T XZ) \tag{86}$$

$$\dot{e}_y = \frac{1}{R^2} (Z\dot{X} - \dot{Z}X - \omega_T YZ) \tag{87}$$

$$\dot{e}_z = \frac{1}{R^2} \left( X\dot{Y} - Y\dot{X} + \omega_T \left[X^2 + Y^2\right] \right) \tag{88}$$

$$\dot{e}_{y_b} = b_{21}\dot{e}_x + b_{22}\dot{e}_y + b_{23}\dot{e}_z \tag{89}$$

$$\dot{e}_{z_b} = b_{31}\dot{e}_x + b_{32}\dot{e}_y + b_{33}\dot{e}_z \tag{90}$$

$$A = \frac{1}{R} (b_{31} X + b_{32} Y + b_{33} Z) \tag{91}$$

$$E = \frac{1}{R} (-b_{21} X - b_{22} Y - b_{23} Z) \tag{92}$$

# APPENDIX B

## EQUATIONS DEFINING MPN GUIDANCE

This appendix contains discussion of the equations used to mechanize the modified proportional navigation guidance scheme. Two control sections are presented which are incorporated in the program. Control section number 1 is used to determine the effects of dynamic errors such as engine time lags and thrust misalignments. Control section number 2 incorporates sensor measurements which have second-order frequency response characteristics and is used to determine the effect of measurement errors on the system.

The rotation, symbols, and coordinate systems described in Appendix A are applicable to this appendix.

### 1. DETERMINATION OF MPN EQUATIONS

The control equations used here are those derived in reference 1 by Cicolani. References 2 and 3 also present similar guidance relations.

From equation 23 of reference 1:

$$\left.\frac{d}{dt}\right|_I \underline{V} = \frac{V^2}{R}\left[(S-2)\cos L - \left(S - \frac{K+1}{K}\right)\frac{\sin L}{L}\right]\underline{l}_v + S\,\underline{\omega}_{Ls} \times \underline{V} \qquad (1)$$

where

$\underline{V}$ = velocity of the chaser with respect to the target

---

Ref. 1 Cicolani, Luigi S., Trajectory Control in Rendezvous Problems Using Proportional Navigation, NASA TN D-772, April 1961.

Ref. 2 Irish, L. A., A Basic Control Equation for Rendezvous Terminal Guidance, IRE Transactions on Aerospace and Navigation Electronics, September 1961, pp. 106-113.

Ref. 3 Green, W.G., Logarithmic Navigation for Precise Guidance of Space Vehicles, IRE Transactions on Aerospace and Navigation Electronics, June 1961, pp. 59-113.

$V$ = magnitude of $\underline{V}$

$\underline{1}_V$ = unit vector in the $\underline{V}$ direction

$L$ = lead angle, the angle between the relative range vector, $\underline{R}$, and the velocity vector $\underline{V}$

$\dot{\underline{e}}$ = angular velocity of the relative range vector, $\underline{R}$, in inertial space

$S, K$ = control parameters

These quantities are indicated in figure 1.

$\left.\frac{d}{dt}\right|_I \underline{V}$ = commanded acceleration vector to the ferry body axes system.

If $L \ll 1$, corresponding to a value of $R\dot{e}$ which is small relative to $R$, then equation 1 becomes:

$$\left.\frac{d}{dt}\right|_I \underline{V} = \frac{V^2}{R}\left(\frac{1-K}{K}\right)\underline{1}_V + S\dot{\underline{e}} \times \underline{V} \qquad (2)$$

It is desirable to view everything from the chaser body axes frame; i.e., to determine the inertial velocity of the target relative to the chaser:

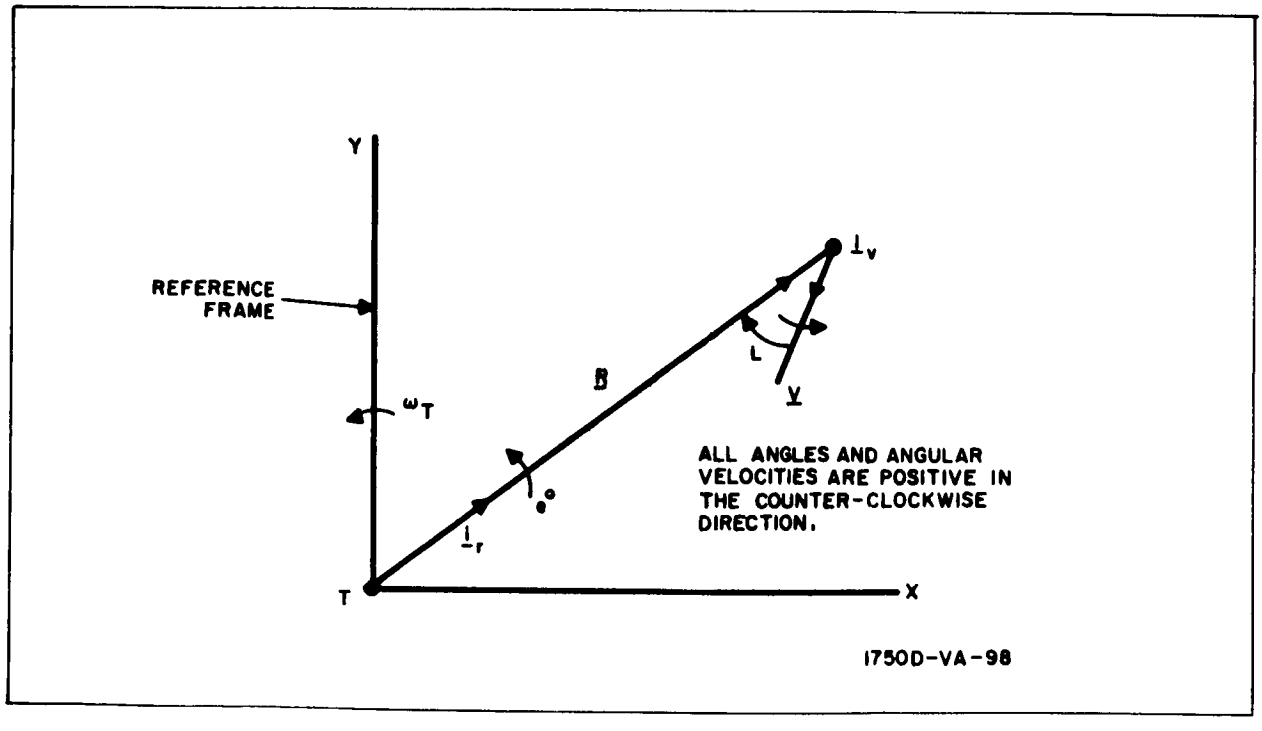


Figure 1. Geometry for Rendezvous

$$\underline{V} = -\underline{V}_f$$

$$\underline{1}_V = -\underline{1}_{V_f}$$

where,

$\underline{V}_f$ = velocity of the target relative to the chaser

$\underline{1}_{V_f}$ = unit vector in the $V_f$ direction

and since $\dot{\underline{e}}$ is the same in either frame equation 2 becomes:

$$\left.\frac{d}{dt}\right|_I \underline{V}_f = \frac{V_f^2}{R}\left(\frac{1-K}{K}\right)\left(-\underline{1}_{V_f}\right) + S\dot{\underline{e}} \times (-\underline{V}_f) \qquad (3)$$

Equation 3 is analogous to the expression for the derivative of a vector with respect to inertial space when it is expressed in a moving coordinate frame; i.e:

$$\left.\frac{d}{dt}\right|_I \underline{N} = \left.\frac{d}{dt}\right|_m \underline{N} + \underline{\omega} \times \underline{N}$$

where

$\underline{N}$ = the vector being differentiated

$\omega$ = rotation of the moving coordinate frame with respect to inertial space

In equation 3, $V_f$ is the vector being differentiated and $\dot{\underline{e}}$ is the rotation of the range vector $\underline{R}$ with respect to inertial space. Since $\underline{V}_f$ and $\underline{R}$ are essentially colinear ($L \ll 1$), $\dot{\underline{e}}$ is also the rotation of $\underline{V}_f$ with respect to inertial space. Hence the approximation expressed by equation 3 is, in essence, valid. In figure 2 the velocity vector is shown for positive values of $\dot{R}_{by}$ and it is evident that:

$$\underline{V}_f = \dot{R}\,\underline{i}_b + R\,\dot{e}_{bz}\,\underline{j}_b - R\,\dot{e}_{by}\,\underline{k}_b$$

$$\dot{\underline{e}} = \dot{e}_{by}\,\underline{j}_b + \dot{e}_{bz}\,\underline{k}_b \qquad (4)$$

$$l_{y_f} = \frac{\dot{R}}{V_f} \underline{i}_b + \frac{R\dot{e}_{bz}}{V_f} \underline{j}_b - \frac{R\dot{e}_{by}}{V_f} \underline{k}_b$$

also

$$\frac{d}{dt}_I \underline{V}_f = a_{x_b} \underline{i}_b + a_{y_b} \underline{j}_b + a_{z_b} \underline{k}_b$$

Substitution of equation 4 into equation 3 and performing the indicated operations results in:

$$a_{x_b} \underline{i}_b + a_{y_b} \underline{j}_b + a_{z_b} \underline{k}_b$$

$$= \frac{V_f^2}{R} \left( \frac{1 - K}{K} \right) \left( \frac{\dot{R}}{V_f} \underline{i}_b + \frac{R\dot{e}_{bz}}{V_f} \underline{j}_b - \frac{R\dot{e}_{by}}{V_f} \underline{k}_b \right)$$

$$+ RS\left( \dot{e}_{by}^2 + \dot{e}_{bz}^2 \right) \underline{i}_b - S\dot{R}\dot{e}_{bz} \underline{j}_b + S\dot{R}\dot{e}_{by} \underline{k}_b \qquad (5)$$

Assuming that:

$$\dot{e}_{by}^2 \ll 1$$

$$\dot{e}_{bz}^2 \ll 1$$

then

$$V_f \simeq \dot{R}$$

Equating like components of equation 5 yields the basic continuous modified proportional navigation law:

$$a_{x_b} = - \frac{(K - 1)}{K} \frac{\dot{R}^2}{R} \qquad (6)$$

$$a_{y_b} = - \left( S + \frac{K - 1}{K} \right) \dot{R} \dot{e}_{bz} \qquad (7)$$

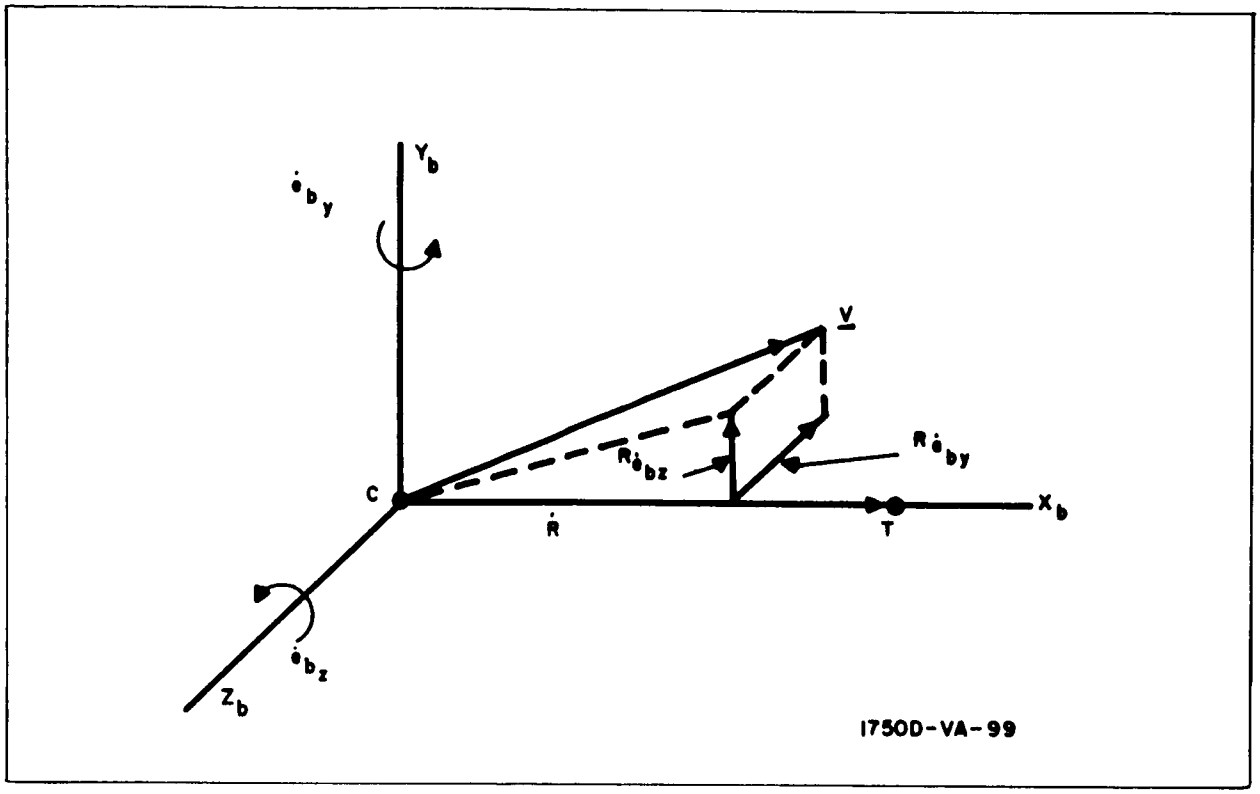


Figure 2. Relation Between $\underline{V}$ and Chaser Body Axes

$$a_{z_b} = \left(S + \frac{K - 1}{K}\right) \dot{R}\dot{e}_{bz} \tag{8}$$

## 2. MODIFICATION OF LONGITUDINAL CONTROL LAW FOR FINITE TERMINAL ACCELERATION

Equation 6 is the basic longitudinal control law used. Since it is not the intent of this study to analyze the docking phase of orbital rendezvous, the maneuver may be considered to be completed when nonzero terminal conditions have been reached. Accordingly, one-way equation 6 can be modified to achieve these terminal conditions is as follows:

$$a_{x_b} = -\frac{(K - 1)}{K} \frac{\dot{R}^2 - \dot{R}_f^2}{R - R_f} \tag{9}$$

where,

$\dot{R}_f$ = desired terminal range rate

$R_f$ = desired terminal range.

It is desirable in the case of a limited throttling range to employ a control law which not only requires a finite terminal velocity and range but also a finite terminal acceleration. To determine the expression that results in a finite terminal longitudinal acceleration, let:

$$a = \dot{R}\,\frac{d\dot{R}}{dR} = \frac{(K-1)}{K}\,\frac{\dot{R}^2 - R_f^2}{R - R_f} + C \tag{10}$$

where,

a = the acceleration along the range vector, $\underline{R}$.

Rearranging equation 10:

$$\frac{d\dot{R}}{dR} - \frac{K-1}{K}\,\frac{\dot{R}}{R - R_f} = \frac{1}{\dot{R}}\left(C - \frac{K-1}{K}\,\frac{R_f^2}{R - R_f}\right) \tag{11}$$

Equation 11 is Bernoulli's equation, where the substitution $n = \dot{R}^2$ converts equation 11 to:

$$\frac{dn}{dR} - 2\frac{(K-1)}{K}\,\frac{n}{R - R_f} = 2\left(C - \frac{K-1}{K}\,\frac{\dot{R}_f^2}{R - R_f}\right) \tag{12}$$

which is of the form:

$$\frac{dn}{dR} + P(R)Y(R) = Q(R)$$

where,

$$P(R) = \frac{-2(K-1)}{K}\,\frac{1}{R - R_f}$$

$$Q(R) = 2\left(C - \frac{K-1}{K}\,\frac{R_f^2}{R - R_f}\right)$$

Equation 12 has the solution

$$n = e^{-\int P(R)dR}\left[C_1 + \int Q(R)e^{\int P(R)dR}\,dR\right] \tag{13}$$

Substituting the expressions for P (R) and Q (R) into equation 13 and performing the operations indicated produces:

$$\dot{R}^2 - \dot{R}_f^2 = C_1 (R - R_f)^{\frac{2(K-1)}{K}} - \frac{2K}{K-2} C(R - R_f) \tag{14}$$

For $R = R_o$, $\dot{R} = \dot{R}_o$ we have:

$$C_1 = \frac{1}{(R_o - R_f)^{\frac{2(K-1)}{K}}} \left[ R_o^2 - R_f^2 + \frac{2K}{K-2} C (R_o - R_f) \right]$$

Thus equation 14 becomes:

$$\dot{R}^2 - \dot{R}_f^2 = \left[ \dot{R}_o^2 - \dot{R}_f^2 + \frac{2K}{K-2} C(R_o - R_f) \right] \left( \frac{R - R_f}{R_o - R_f} \right)^{\frac{2(K-1)}{K}} - \frac{2K}{K-2} C(R - R_f) \tag{15}$$

Substituting equation 15 into equation 10 yields:

$$a = \frac{K-1}{K} \left( \frac{\dot{R}_o^2 - \dot{R}_f^2}{R_o - R_f} + \frac{2K}{K-2} C \right) \left( \frac{R - R_f}{R_o - R_f} \right)^{\frac{K-2}{K}} - \frac{2(K-1)}{K-2} C + C \tag{16}$$

Imposing $a = a_f$ at $R = R_f$ on equation 16 yields:

$$a_f = C \left[ 1 - \frac{2(K-1)}{K-2} \right]; \quad C = - \frac{K-2}{K} a_f$$

Thus, equation 10 becomes:

$$a = \frac{K-1}{K} \frac{\dot{R}^2 - \dot{R}_f^2}{R - R_f} + \frac{2-K}{K} a_f \tag{17}$$

However the acceleration, $a_{x_b}$, of equation 9 or 6 and the one to be used in the computer model is the acceleration along the range vector, $\underline{R}$ (assuming A and E of figure 1 are held zero by the attitude control system) as viewed in the ferry body axes system. Therefore, $a_{x_b}$ is the negative of the "a" of equation 17.

Thus,

$$a_{x_b} = -\frac{K-1}{K}\left(R^2 - \frac{\dot{R}_f^2}{R-R_F}\right) - \frac{(2-K)}{K}\, a_f \qquad (18)$$

Equation 18 along with equations 7 and 8 are the modified proportional navigation equations that are used for translational control in the digital computer model.

The range rate as a function of R satisfying the terminal conditions is, using equation 15:

$$\dot{R}^2 = \dot{R}_f^2 + 2\, a_f (R-R_f) + \left[\dot{R}_o^2 - \dot{R}_f^2 - 2a_f (R_o - R_f)\right]\left(\frac{R-R_o}{R_o - R_f}\right)^{\frac{2(K-1)}{K}} \qquad (19)$$

The acceleration as a function of R is:

$$a_{x_b} = -a_f - \frac{(K-1)}{K}\left[\dot{R}_o^2 - \dot{R}_f^2 - 2\, a_f (R_o - R_f)\right]\frac{(R-R_f)^{\frac{(K-2)}{K}}}{(R_o - R_f)^{\frac{2(K-1)}{K}}} \qquad (20)$$

From equation 20 it is evident that when $R = R_f$:

$a_{x_b} = -a_f$ which is exactly the desired terminal acceleration.

## 2.1 Control Section Number 1

The control section represented by the equations in this section incorporates thrust misalignments and engine lags in the MPN guidance scheme in order that their effect on the overall system performance may be determined. Also included are attitude control equations for maintaining the proper orientation of the vehicle with respect to the line-of-sight. Hence, this control section certains six-degrees of freedom - three translational and three rotational.

### 2.1.1 Thrust Commands

Commanded accelerations along the chaser body axes are given as:

$$a_{x_{bc}} = -\frac{K-1}{K}\frac{\dot{R}^2 - \dot{R}_f^2}{R - R_f} - \frac{2-K}{K} a_f \tag{21}$$

$$a_{y_{bc}} = -\left(S + \frac{K-1}{K}\right)\dot{R}\,(\dot{e}_{z_b} + \dot{e}_b) \tag{22}$$

$$a_{z_{bc}} = \left(S + \frac{K-1}{K}\right)\dot{R}\,\dot{e}_{y_b} \tag{23}$$

where equation 22 is modified to include an LOS rate bias; $\dot{e}_b$.

The effects of thrust misalignments are defined by the thrust misalignments parameters $\rho_{xy}$, $\rho_{xz}$ etc (defined in figure 3 and the resulting acceleration along each axis are represented analytically by equations 24 through 26, below. In the equations, the $\rho$'s are in radians and the assumption is made that the $\rho$'s are small enough so that the small angle approximation is valid; i.e.,

$$\cos \rho \approx 1$$

$$\sin \rho \approx \rho$$

Let

$\rho_{xz}$ = the angle the projection of $a'_{x_b}$ on the $X_b - Z_b$ plane makes with the positive $X_b$ axis.

$\rho_{xy}$ angle $a'_{x_b}$ makes with the $X - Z_b$ plane

The remaining misalignments shown in figure 3 are defined similarly

$$a_{x_{bm}} = a_{x_b} + \rho_{yx}\, a_{y_b} + \rho_{zx}\, a_{z_b} \tag{24}$$

$$a_{y_{bm}} = \rho_{xy}\, a_{x_b} + a_{y_b} + \rho_{zy} \tag{25}$$

$$a_{z_{bm}} = \rho_{y_z}\, a'_{x_b} + \rho_{yz}\, a'_{y_b} + a'_{z_b} \tag{26}$$

In the above equations, the quantities $a'_{x_b}$, $a'_{y_b}$, and $a'_{z_b}$ are the accelerations which result when the engines are assumed to possess a single-order time lag.

These accelerations are related to the commanded accelerations by the following equations:

$$a'_{x_b} = \frac{1}{\tau_x s + 1} \; a_{x_{bc}} \tag{27}$$

$$a'_{y_b} = \frac{1}{\tau_y s + 1} \; a_{y_{bc}} \tag{28}$$

$$a'_{z_b} = \frac{1}{\tau_z s + 1} \; a_{z_{bc}}$$

2.1.2 Attitude Control

The main decelerating engine of the chaser, aligned with the $X_b$ axis, is used for range rate control, whereas the four engines mounted normal to the $X_b$ axis are used to control the line-of-sight rate. It is therefore, necessary to keep the $y_b$ axis aligned with the range vector. This is accomplished by means of the attitude control system.

The angles A and E (figure 1 of Appendix A) must be kept to zero in order to satisfy the requirement. In order to maintain A and E zero, attitude control torques might be produced about the $Y_b$ and $Z_b$ axes which are proportional to A and E, respectively. In addition, damping can be introduced by making the control torques proportional to the rates $e_{b_y}$ and $e_{b_z}$ If A and E are kept small, the inertial angular body rates, $\omega_{b_y}$ and $\omega_{b_z}$, will be approximately equal to the LOS rates $\dot{e}_{b_y}$ and $\dot{e}_{b_z}$ respectively. The torques $M_{b_y}$ and $M_{b_z}$ will thus be proportional to $\omega_{b_y}$ and $\omega_{b_z}$ as well as to A and E, respectively. Equations 30 and 31 result from these considerations. (It is possible to measure $\omega_{b_y}$ and $\omega_{b_z}$ by means of rate gyros.)

$$M'_{b_y} = K_y A - C_y \omega_{b_y} \tag{30}$$

$$M'_{b_p} = K_p E - C_p \omega_{b_z} \tag{31}$$

The roll rate is critical if it is sufficiently large to appreciably change the directions along which the normal translational engines thrust, in the time made available, because of delays in the actual initiations of the translational thrust commands. Therefore, a control torque about the $X_b$ axis proportional to the roll rate, $\omega_{b_x}$, was selected as indicated by equation 32.

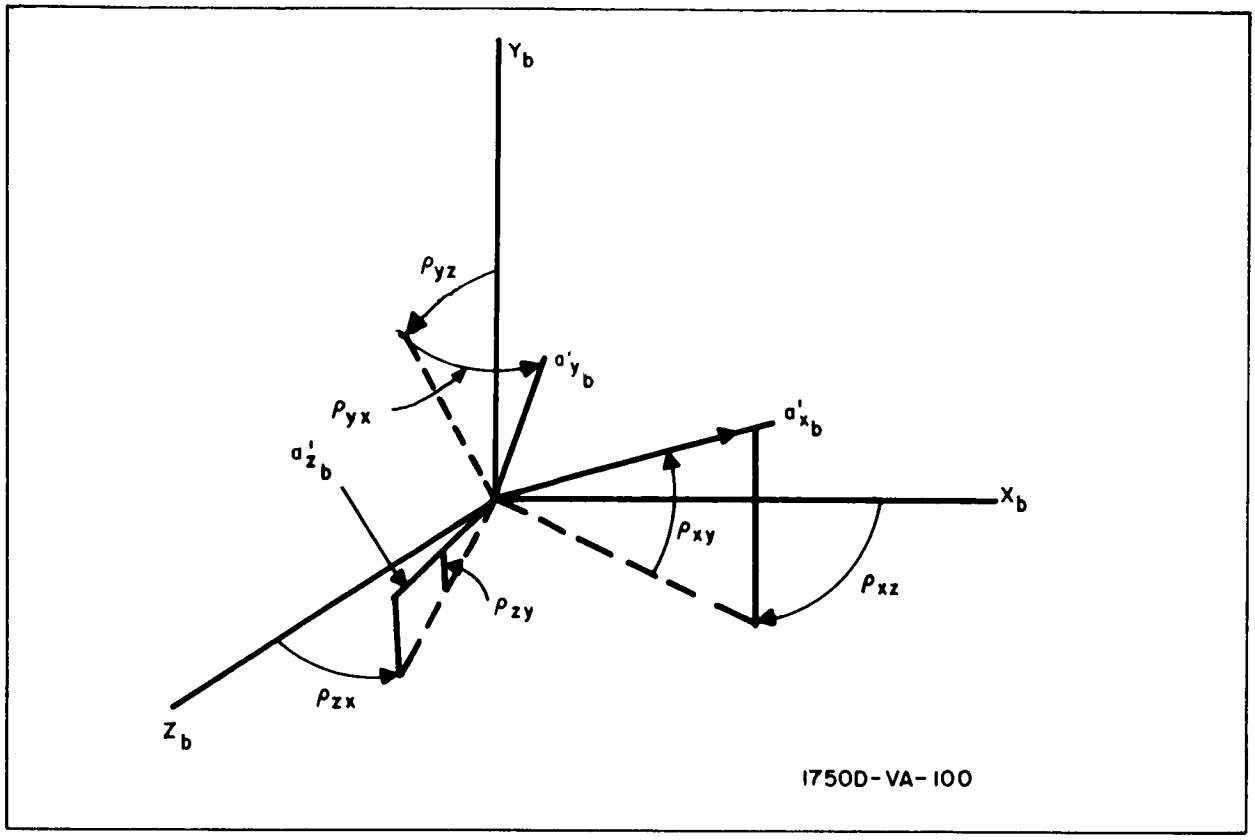


Figure 3. Thrust Misalignment

$$M'_{b_x} = - C_x \omega_{b_x} \tag{32}$$

If the thrust axes do not pass directly through the center of mass of the vehicle, moments are set up which can cause roll, pitch and for yaw rates. Combining these rate with equations 30 through 32 gives:

$$M_{bx} = M'_{bx} + I_{bx} \epsilon_{zy} a_{z_b} - I_{bx} \epsilon_{yz} a_{y_b} \tag{33}$$

$$M_{by} = M'_{by} + I_{by} \epsilon_{xz} a_{x_b} - I_{by} \epsilon_{zx} a_{z_b} \tag{34}$$

$$M_{bz} = M'_{bz} + I_{bz} \epsilon_{yx} + a_{y_b} - I_{bz} \epsilon_{xy} a_{x_b} \tag{35}$$

Each of the $\epsilon_{xy}$ etc, in the above equations is a ratio of a thrust offset to the square of a radius of gyration. For example, $\epsilon_{yz}$ is the ratio of the off-

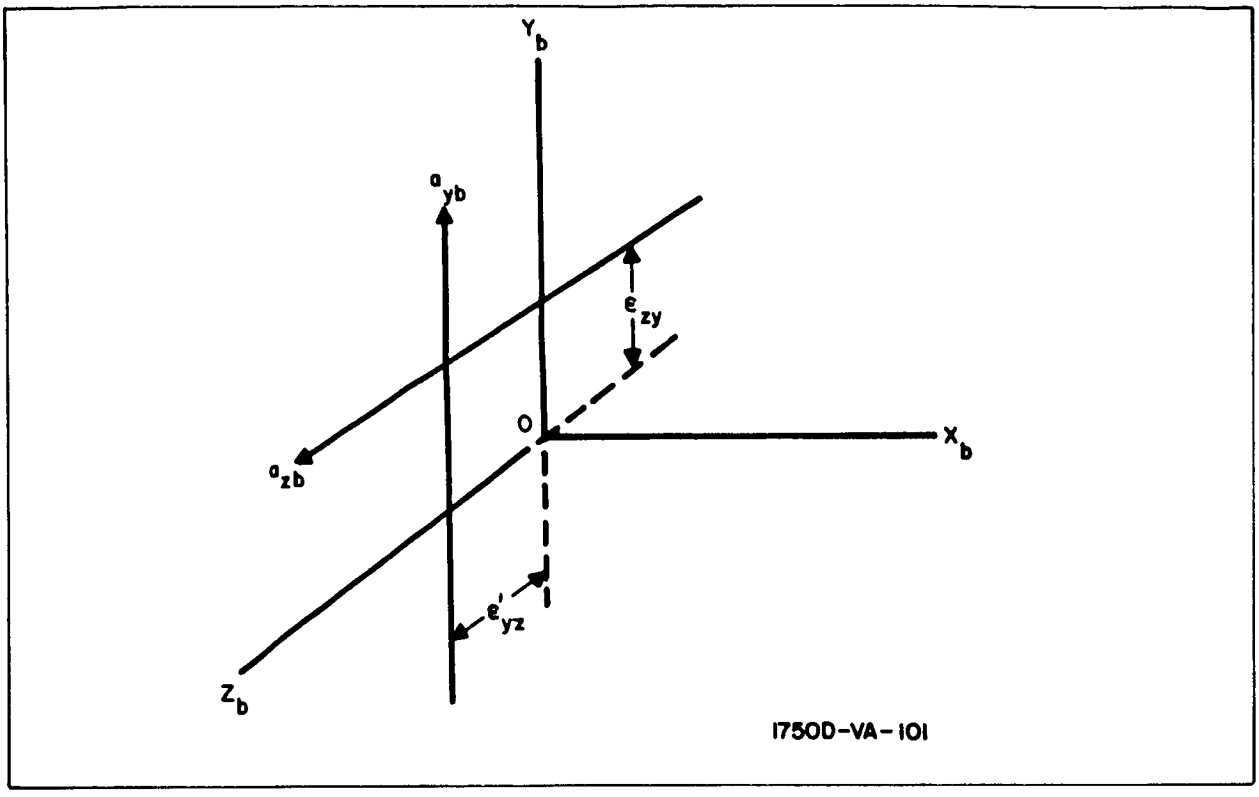


Figure 4. Thrust Offsets in the $Y_b$ - $Z_b$ Plane

set ($\epsilon'_{yz}$) of the $a_{y_b}$ thrust from the $Y_b$ axis in the $Y_b$ - $Z_b$ plane to the square of the radius of gyration, $r^2_{k_x}$, about the axis perpendicular to the $Y_b$ - $Z_b$ plane; i.e., along the $X_b$ axis. Then,

$$\epsilon_{yz} = \frac{\epsilon'_{yz}}{r^2_{k_x}} \tag{36}$$

and

$$\epsilon_{xz} = \frac{\epsilon'_{xz}}{r^2_{k_y}} \tag{37}$$

Figure 4 illustrates the $\epsilon'_{zy}$ and $\epsilon'_{yz}$ offset. Offsets in the $X_b$ - $Z_b$ and $X_b$ - $Y_b$ planes are defined similarly.

### 2.1.3 Velocity Determination

Velocity expenditures required to perform the rendezvous are obtained from equations 38 through 40.

$$\Delta V_x = \int \left| a_{x_b} \right| \, dt \tag{38}$$

$$\Delta V_y = \int \left| a_{y_b} \right| \, dt \tag{39}$$

$$\Delta V_z = \int \left| a_{z_b} \right| \, dt \tag{40}$$

Hence, the normal velocity expenditures is:

$$\Delta V_n = \int \left( a_{y_b}^2 + a_{z_b} \right)^{1/2} \, dt \tag{41}$$

and the total velocity is:

$$\Delta V_t = \int (a_{x_b}^2 + a_{y_b}^2 + a_{z_b}^2) \, dt \tag{42}$$

## 2.2 Control Section Number 2

When using the equations of this section, control of the chaser is limited to two dimensions, X and Y. Out-of-plane motion is not considered.

The quantities of range, range rate and angle rate, used to control the thrusting, are assumed to correspond to outputs from sensors which have quadiatic frequency response characteristics and are represented by $R_m$, $\dot{R}_m$ and $\dot{e}_m$. These quantities are determined using equations 43 through 51 below.

Range is determined as follows.

$$\ddot{R}_m = \omega_r^2 R - 2\zeta_r \omega_r R_m - \omega_r^2 R_m \tag{43}$$

$$\dot{R}_m = \int \ddot{R}_m \, dt \tag{44}$$

$$R_m = \int \dot{R}_m \, dt \tag{45}$$

Similarly for range rate:

$$\dddot{R}_m = \omega_{rd}^2 \dot{R} - 2\zeta_{rd}\omega_{rd}\ddot{R}_m - \omega_{rd}^2 \dot{R}_m \tag{46}$$

$$\ddot{R}_m = \int \dddot{R}_m \, dt \tag{47}$$

$$\dot{R}_m = \int \ddot{R}_m \, dt \tag{48}$$

Angular rate is found from:

$$\dddot{e}_{zm} = \omega_{ed}^2 \dot{e}_z - 2\zeta_{ed}\omega_{ed}\ddot{e}_{zm} - \omega_{ed}^2 \dot{e}_{zm} \tag{49}$$

$$\ddot{e}_{zm} = \int \dddot{e}_{zm} \, dt \tag{50}$$

$$\dot{e}_{zm} = \int \ddot{e}_{zm} \, dt \tag{51}$$

The fact that the above commands are actually analagous to those passed through a quadratic filter can be verified by considering equation 43. Using Laplace notation and rearranging yields:

$$(s^2 + \omega_r s 2\zeta_r + \omega_r^2) R_m(s) = \omega_r^2 R(s) \tag{52}$$

$$\frac{R_m(s)}{R(s)} = \frac{1}{\frac{s^2}{\omega_r^2} + \frac{2\zeta_r}{\omega_r} s + 1} \tag{53}$$

The commanded accelerations along the longitudinal and normal axis are given by equations 54 and 55 respectively:

$$a_{L_c} = \frac{(K-1)}{K} \quad \frac{\dot{R}_m^2 - \dot{R}_f^2}{R - R_f} + \frac{2-K}{K} a_f \tag{54}$$

$$a_{N_c} = (s + \frac{K-1}{K}) \dot{R}_m (\dot{e}_{zm} + \dot{e}_b) \tag{55}$$

The applied accelerations are analagous to the commanded accelerations after being passed through a quadratic filter. For the longitudinal accelerations:

$$\dddot{a}'_L = \omega_{aL}^2 \, a_{Lc} - 2\zeta_{aL}\omega_{aL}\ddot{a}'_L - \omega_{aL}^2 \dot{a}'_L \tag{56}$$

$$\ddot{a}'_L = \int \dddot{a}'_L \, dt \tag{57}$$

$$\dot{a}'_L = \int \ddot{a}'_L \, dt \tag{58}$$

Similarly, the normal acceleration is determined from:

$$\ddot{a}'_N = \omega_{aN}^2 \, a_{Nc} - 2\zeta_{aN}\omega_{aN}\dot{a}'_{aN} - \omega_{aN}^2 a'_N \tag{59}$$

$$\dot{a}'_N = \int \ddot{a}'_N \, dt \tag{60}$$

$$a'_N = \int \dot{a}'_N \, dt \tag{61}$$

Utilization of altitude control section assumes that the orientation of the vehicle is maintained such that the longitudinal axis is along the range vector and the normal axis is in the plane of rotation. Hence, no equations are used to represent the attitude control system.

# APPENDIX C

# LINEARIZED MODEL

The guidance system utilizing modified proportional navigation control was discussed in Appendix B of Volume IV. This system lends itself to a greater depth of hand analysis. Accordingly, the differential equations of motion developed in this section are based on MPN control. These equations are obtained by linearizing and idealizing the equations of Appendixes A and B of this volume.

The first portion of this section is devoted to obtaining the aforementioned differential equations. In the second portion solutions to the equations are obtained for a special case. These solutions serve as a check on the digital model.

## 1. LINEARIZATION

The first part of the linearization concerns itself with the equations used in paragraph 2.2 of Appendix B. In this development it is postulated that the guidance system brings the chaser to the target on a relatively straight-line course, such as the one in figure 1 which lies nearly in the plane of target motion. Further, it is presumed that the attitude control system keeps the longitudinal engine essentially aligned with the range vector, the $Y_b$ axis in plane and the $Z_b$ axis out of plane. These assumptions can be stated more explicitly as follows:

a. The pitch angle, $\theta_b$, is treated as a small variation, $\theta$, about a nominal pitch angle, $\theta_{bo}$. Similarly the yaw angle, $\psi_b$, is presumed to be a small perturbation, $\psi$, about 180 degrees.

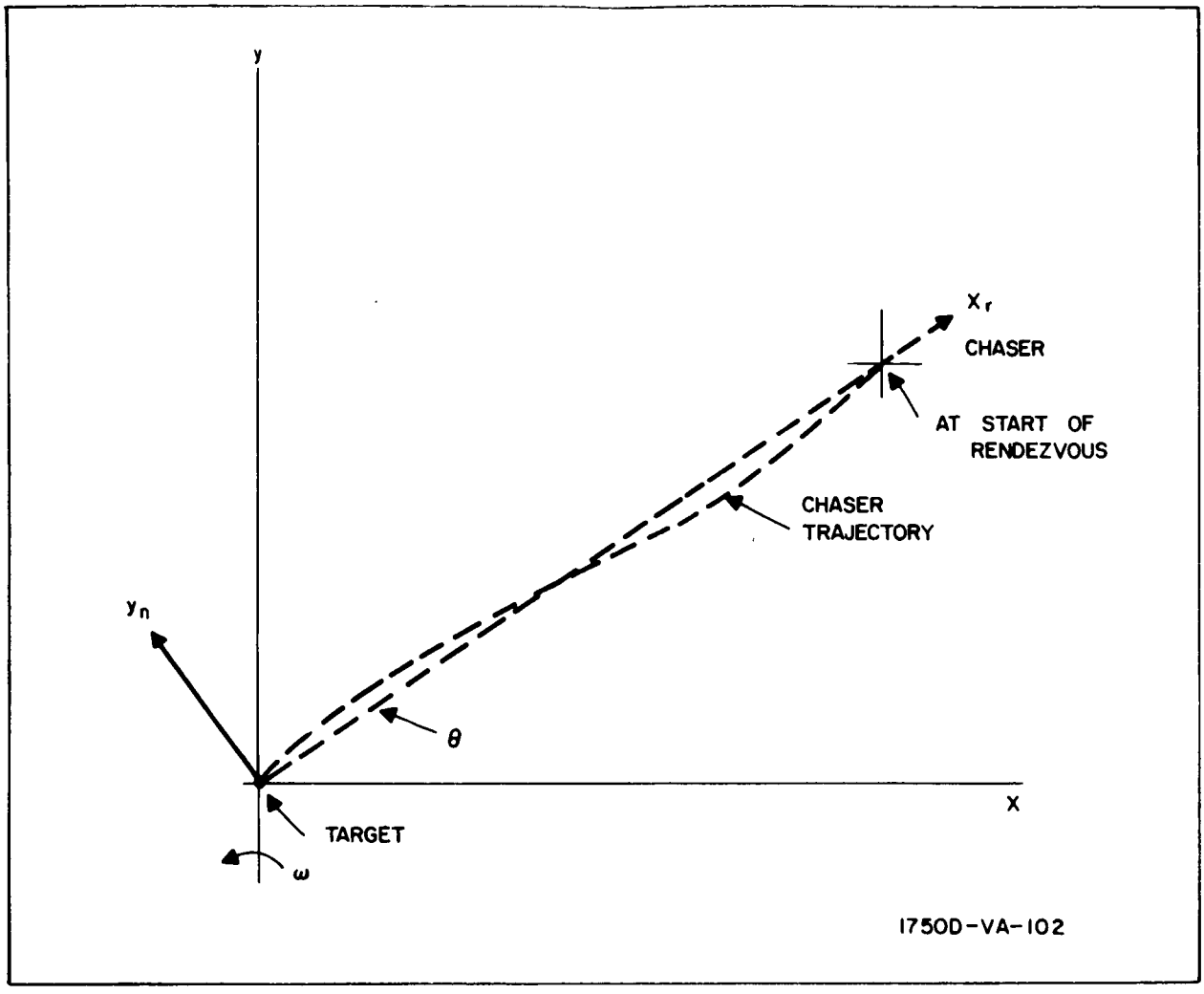


Figure 1. Chaser Trajectory and Modified Coordinate System

$$\theta_{bo} \triangleq \tan^{-1}\left(\frac{Y_o}{X_o}\right) \tag{1}$$

$$\sin \theta_b \cong \sin \theta_{bo} + \theta \cos \theta_{bo}$$

$$\cos \theta_b \cong \cos \theta_{bo} - \theta \sin \theta_{bo}$$

$$\sin \psi_b \cong -\psi \tag{2}$$

$$\cos \psi_b \cong -1$$

b. The roll angle approximations corresponding to the postulated attitude control are:

$$\sin \phi_b \cong \phi \tag{3}$$

$$\cos \phi_b \cong 1$$

c. The target is assumed to be in a circular orbit:

$$\therefore \text{Eccentricity} = 0 \tag{4}$$

d. Squares of small quantities are neglected when they occur as higher order terms. Small quantities, relative to unity, are:

$$\left.\begin{array}{l} \dfrac{X}{R_T} \\ \dfrac{Y}{R_T} \\ \dfrac{Z}{R_T} \\ \dfrac{Z}{R} \\ \theta \\ \phi \\ \psi \end{array}\right\} \ll 1 \tag{5}$$

e. It has been found convenient in the linearization to introduce the coordinate transformation shown in figure 1:

$$\begin{bmatrix} X_r \\ Y_n \\ Z \end{bmatrix} \triangleq \begin{bmatrix} \cos \theta_{bo} & \sin \theta_{bo} & 0 \\ -\sin \theta_{bo} & \cos \theta_{bo} & 0 \\ 0 & 0 & 1 \end{bmatrix} \begin{bmatrix} X \\ Y \\ Z \end{bmatrix} \tag{6}$$

$$Y_r/R \ll 1$$

Dividing both sides of equation 62 of Appendix A by $R_T$ and making use of equations 4 and 5:

$$\left[\frac{R_T}{R_C}\right] \cong \left[1 - \frac{^3Y}{R_T}\right] \tag{7}$$

Substituting 4 and 5 into equations 56 through 58 of Appendix A:

$$\ddot{X} = a_{x_T} + 2\omega_T \dot{Y} + 3\omega_T^2 \frac{Y}{R_T} X$$

$$\ddot{Y} = a_{y_T} - 2\omega_T \dot{X} + 3\omega_T^2 Y \left(1 + \frac{Y}{R_T}\right) \tag{8}$$

$$\ddot{Z} = a_{z_T} - \omega_T^2 Z \left(1 - \frac{3Y}{R_T}\right)$$

For a typical earth orbit, $\omega_T$ is about 1 milliradian/second whereas accelerations are of magnitude 1 ft/sec$^2$. Thus nonlinear terms of higher order than $\omega_T^2$ may be neglected. Equation 68 becomes:

$$\dot{X} = a_{x_T} + 2\omega_T \dot{Y} \tag{9}$$

$$Y = a_{y_T} - 2\omega_T X + 3\omega_T^2 Y$$

$$Z = a_{z_T} - \omega_T^2 Z$$

Substitution of 2 and 3 into equations 75 through 83 of Appendix A:

$$b_{11} = -\cos\theta_b \qquad b_{12} = -\sin\theta_b \qquad b_{13} = \psi \tag{10}$$

$$b_{21} = -\sin\theta_b \qquad b_{22} = \cos\theta_b \qquad b_{23} = \phi$$

$$b_{31} = -\psi\cos\theta_b \qquad b_{32} = -\psi\sin\theta_b \qquad b_{33} = -1$$

$$+\phi\sin\theta_b \qquad -\phi\cos\theta_b$$

Substituting equations 2 and 3 into equations 63, 64, 65, 69, 70, and 71 of Appendix A and solving simultaneously yields:

$$\omega_{b_x} = \dot{\phi} + \omega_T \psi \tag{11}$$

$$\omega_{b_y} = \dot{\psi} - \omega_T \phi$$

$$\omega_{b_z} = -\dot{\theta} - \omega_T$$

$$\ddot{\phi} = \frac{M_{bx}}{I_{bx}} - \omega_T \dot{\psi} \tag{12}$$

$$\ddot{\psi} = \frac{M_{by}}{I_{by}} - \omega_T \phi$$

$$\ddot{\theta} = -\frac{M_{bz}}{I_{bz}}$$

Substituting equations 5 and 6 into equations 84 and 88 of Appendix A:

$$R = X_r \tag{13}$$

$$\dot{R} = \dot{X}_r$$

Substituting equations 5, 6, and 13 into equations 85 through 92 of Appendix A giving:

$$\dot{e}_{y_b} = \frac{1}{X_r^2}\left[Z\dot{X}_r - \dot{Z}X_r\right] \tag{14}$$

$$\dot{e}_{z_b} = \frac{1}{X_r^2}\left[Y_n \dot{X}_r - \dot{Y}_n X_r\right] - H\omega_T$$

Note: The line-of-sight terms in 85, 87, 88, of Appendix A and thus in 14, arise from the fact that $\dot{e}_{z_b}$ is presumed to be measured with respect to inertial space. The term H = 1 then implies that $\dot{e}_{z_b}$ is with respect to inertial space whereas H = 0 implies $\dot{e}_{z_b}$ is with respect to the rotating frame.

Substituting equations 1, 5, 6 and 10 into equations 91 and 92 of Appendix A:

$$A = -Z/X_r - \psi \tag{15}$$

$$E = -Y_r/X_r + \theta$$

The purpose of the following substitutions is to re-express the differential equations, 9, in terms of the coordinates, $X_r$, $Y_n$ and Z, and the body axes accelerations, $a_{x_b}$, $a_{y_b}$, and $a_{z_b}$. Substituting equations 10 into 72, 73, and 74 of Appendix A

$$a_{x_T} = -a_{x_b} \cos\theta_b - a_{y_b} \sin\theta_b - a_{z_b} \left[\psi \cos\theta_b - \phi \sin\theta_b\right] \tag{16}$$

$$a_{y_T} = -a_{x_b} \sin\theta_b + a_{y_b} \cos\theta_b - a_{z_b} \left[\psi \sin\theta_b + \phi \cos\theta_b\right]$$

$$a_{z_T} = a_{x_b} \psi + a_{y_b} \phi - a_{z_b}$$

Differentiating equation 6:

$$\ddot{X}_r = \ddot{X} \cos\theta_{bo} + \ddot{Y} \sin\theta_{bo} \tag{17}$$

$$\ddot{Y}_n = -\ddot{X} \sin\theta_{bo} + \ddot{Y} \cos\theta_{bo}$$

From equation 9

$$\ddot{X} \cos\theta_{bo} = a_{x_T} \cos\theta_{bo} + 2\omega_T \dot{Y} \cos\theta_{bo} \tag{18}$$

$$-\ddot{X} \sin\theta_{bo} = -a_{x_T} \sin\theta_{bo} - 2\omega_T \dot{Y} \sin\theta_{bo}$$

$$\ddot{Y} \sin\theta_{bo} = a_{y_T} \sin\theta_{bo} - 2\omega_T \dot{X} \sin\theta_{bo} + 3\omega_T^2 Y \sin\theta_{bo}$$

$$\ddot{Y} \cos\theta_{bo} = a_{y_T} \cos\theta_{bo} - 2\omega_T \dot{X} \cos\theta_{bo} + 3\omega_T^2 Y \cos\theta_{bo}$$

Substituting 18 into 17:

$$\ddot{X}_r = a_{x_T} \cos \theta_{bo} + a_{y_T} \sin \theta_{bo} + 2\omega_T \left[ - \dot{X} \sin \theta_{bo} + \dot{Y} \cos \theta_{bo} \right] \qquad (19)$$

$$+ 3\omega_T^2 Y \sin \theta_{bo}$$

$$\ddot{Y}_n = - a_{x_T} \sin \theta_{bo} + a_{y_T} \cos \theta_{bo} - 2\omega_T \left[ \dot{X} \cos \theta_{bo} + \dot{Y} \sin \theta_{bo} \right]$$

$$+ 3\omega_T^2 Y \cos \theta_{bo}$$

Substituting 1 into 16 and dropping 2nd order terms:

$$a_{x_T} = - a_{x_b} \left[ \cos \theta_{bo} - \theta \sin \theta_{bo} \right] - a_{y_b} \left[ \theta \cos \theta_{bo} + \sin \theta_{bo} \right] \qquad (20)$$

$$- a_{z_b} \left[ \psi \cos \theta_{bo} - \phi \sin \theta_{bo} \right]$$

$$a_{y_T} = - a_{x_b} \left[ \sin \theta_{bo} + \theta \cos \theta_{bo} \right] + a_{y_b} \left[ \cos \theta_{bo} - \theta \sin \theta_{bo} \right]$$

$$- a_{z_b} \left[ \psi \sin \theta_{bo} + \cos \theta_{bo} \right]$$

$$a_{z_T} = a_{x_b} \psi + a_{y_b} \phi - a_{z_b}$$

Substituting 20 and 6 into 19:

$$\ddot{X}_r = a_{x_b} (-1) + a_{y_b} (-\theta) + a_{z_b} (-\psi) + 2\omega_T \dot{Y}_n \qquad (21)$$

$$+ 3\omega_T^2 \sin \theta_{bo} \left[ X_r \sin \theta_{bo} + Y_n \cos \theta_{bo} \right]$$

$$\ddot{Y}_n = a_{x_b} (-\theta) + a_{y_b} + a_{z_b} (-\phi) - 2\omega_T \dot{X}_r$$

$$+ 3\omega_T^2 \cos \theta_{bo} \left[ (X_r \sin \theta_{bo} + Y_n \cos \theta_{bo} \right]$$

$$Z = a_{x_b} (\psi) + a_{y_b} (\phi) + a_{z_b} (-1) - \omega_T^2 Z$$

The last equation of 21 was obtained by substituting the last equation of 20 into the last equation of 9.

In Appendix B, the idealized attitude and translational control equations are modified to account for time lags, engine offset, and misalignment, as well as a finite throttling range. The control equations will be treated in their original more idealized form here. The idealized control equations are given in equations 22 and 23:

$$M_{bx} = - C_r \omega_{b_x} \tag{22}$$

$$M_{by} = - C_y \omega_{b_y} + K_y A$$

$$M_{bz} = - C_p \omega_{b_z} + K_p E$$

$$a_{x_b} = - \frac{K - 1}{K} \frac{\dot{R}^2 - R_f^2}{R - R_f} + \frac{K - 2}{K} a_f \tag{23}$$

$$a_{y_b} = - \left[ S + \frac{K-1}{K} \right] \dot{R} \left( \dot{e}_{z_b} + \dot{e}_b \right)$$

$$a_{z_b} = + \left[ S + \frac{K - 1}{K} \right] \dot{R} \dot{e}_{y_b}$$

Substituting equation 22 into 12

$$\ddot{\phi} = - \frac{C_r}{I_{b_x}} \omega_{b_x} - \omega_T \dot{\psi} \tag{24}$$

$$\ddot{\psi} = - \frac{C_y}{I_{b_y}} \omega_{b_y} + \frac{K_y}{I_{b_y}} A + \omega_T \dot{\phi}$$

$$\ddot{\theta} = \frac{C_p}{I_{bz}} \omega_{b_z} - \frac{K_p}{I_{b_z}} E$$

Substituting equation 11 into 24:

$$\ddot{\phi} = - \frac{C_k}{I_{bx}} \dot{\phi} - \omega_T \left[ \dot{\psi} + \frac{C_r}{I_{bx}} \psi \right] \tag{25}$$

$$\ddot{\psi} = -\frac{C_y}{I_{by}}\dot{\psi} + \frac{K_y}{I_{by}} A + \omega_T\left[\dot{\phi} + \frac{C_y}{I_{by}}\phi\right]$$

$$\ddot{\theta} = -\frac{C_p}{I_{bz}}\dot{\theta} - \frac{K_p}{I_{bz}} E - \omega_T \frac{C_p}{I_{bz}}$$

Substituting equation 15 into 25:

$$\ddot{\phi} + \frac{C_r}{I_{bx}}\dot{\phi} = -\omega_T\left[\dot{\psi} + \frac{C_r}{I_{bx}}\psi\right] \tag{26}$$

$$\ddot{\psi} + \frac{C_y}{I_{by}}\dot{\psi} + \frac{K_y}{I_{by}} = -\frac{K_y}{I_{by}}\frac{Z}{X_r} + \omega_T\left[\dot{\phi} + \frac{C_y}{I_{by}}\phi\right]$$

$$\ddot{\theta} + \frac{C_p}{I_{bz}}\dot{\theta} + \frac{K_p}{I_{bz}}\theta = \frac{K_p}{I_{bz}}\frac{y_n}{x_r} - \frac{C_p}{I_{bz}}\omega_T$$

Defining the following quantities:

$$\tau_r \triangleq \frac{I_{bx}}{C_r} \qquad \omega_p^2 \triangleq \frac{K_p}{I_{bz}} \tag{27}$$

$$\omega_y^2 \triangleq \frac{K_y}{I_{by}} \qquad 2\zeta_p\omega_p \triangleq \frac{C_p}{I_{bz}}$$

$$2\zeta_y\omega_y \triangleq \frac{C_y}{I_{by}}$$

and substituting into equation 26 yields

$$\ddot{\phi} + (1/\tau_r)\dot{\phi} = -\omega_T\left[\dot{\psi} + \frac{1}{\tau}\psi\right] \tag{28}$$

$$\ddot{\psi} + 2\zeta_y\omega_y\dot{\psi} + \omega_y^2\psi = -\omega_y^2\frac{Z}{X_r} + \omega_T\left[\dot{\phi} + 2\zeta_y\omega_y\phi\right]$$

$$\ddot{\phi} + 2\zeta_r\omega_p\dot{\theta} + \omega_p^2\theta = \omega_p^2\frac{Y_n}{X_r} - 2\zeta_p\omega_p\omega_T$$

Equations 28 are the attitude control equations. Substituting equations 13 and 14 into 23:

$$a_{x_b} = -\frac{K-1}{K}\frac{\dot{X}_r^2 - R_f^2}{X_r - R_f} + \frac{K-2}{K}a_f$$

$$a_{y_b} = -\left[S + \frac{K-1}{K}\right]\frac{\dot{X}_r}{X_r^2}\left[Y_n\dot{X}_r - \dot{Y}_n X_r\right] + \left[S + \frac{K-1}{K}\right]\dot{X}_r\left[H\omega_T - \dot{e}_b\right] \qquad (29)$$

$$a_{z_b} = +\left[S + \frac{K-1}{K}\right]\frac{\dot{X}_r}{X_r^2}\left[Z\dot{X}_r - \dot{Z}X_r\right]$$

Substituting equations 29 into 21:

$$\ddot{X}_r = \frac{K-1}{K}\frac{\dot{X}_r^2 - \dot{R}_f^2}{X_r - R_f} - \frac{K-2}{K}a_f - \left[S + \frac{K-1}{K}\right]\left[H\omega_T - e_b\right]\theta\dot{X}_r + 2\omega_T\dot{Y}_n$$

$$+ 3\omega_T^2 X_r \sin^2\theta_{bo} + 3\omega_T^2 Y_n \sin\theta_{bo}\cos\theta_{bo}$$

$$\ddot{Y}_n = \frac{K-1}{K}\frac{\dot{X}_r^2 - \dot{R}_f^2}{X_r - R_f}\theta - \frac{K-2}{K}a_f\theta - \left[S + \frac{K-1}{K}\right]\frac{\dot{X}_r}{X_r^2}\left[Y_n\dot{X}_r - \dot{Y}_n X_r\right] \qquad (30)$$

$$+ \dot{X}_r\left[H\omega_T - \dot{e}_b\right]\left[S + \frac{K-1}{K}\right] - 2\omega_T\dot{X}_r + 3\omega_T^2 X_r\cos\theta_{bo}\sin\theta_{bo}$$

$$\ddot{Z} = -\frac{K-1}{K}\frac{\dot{X}_r^2 - \dot{R}_f^2}{X_r - R_f}\psi + \frac{K-2}{K}a_f\psi + \left[H\omega_T - \dot{e}_b\right]\dot{X}_r\left[S + \frac{K-1}{K}\right]\phi$$

$$- \left[S + \frac{K-1}{K}\right]\frac{\dot{X}_r}{X_b}\left[Z\dot{X}_r - \dot{Z}X_r\right] - \omega_T^2 Z$$

Equations 30 and 28 serve as the model for analytical studies.

## 2. PROGRAMMED MODEL CHECK SOLUTIONS

The usefulness of the equations derived in section 1 will be demonstrated in this section. Solutions to the rendezvous problem will be determined in six degrees of freedom for the case where:

$$\omega_T = a_f = R_f = \dot{R}_f = \dot{e}_b = 0 \tag{31}$$

and

$$\left.\begin{array}{l} \omega_y t_f \\ \omega_p t_f \\ t_f/\tau_r \end{array}\right\} \quad >> 1$$

where $t_f$ is the time duration of the rendezvous.

First consider the attitude control equations, 28. With $\omega_T = 0$, they become:

$$\ddot{\phi} + (1/\tau_r)\,\dot{\phi} = 0 \tag{32}$$

$$\ddot{\psi} + 2\zeta_y \omega_y \dot{\psi} + \omega_y^2 \psi = -\omega_y^2 Z/x_r$$

$$\ddot{\theta} + 2\zeta_p \omega_p \theta + \omega_p^2 \theta = \omega_r^2 Y_n/X_r$$

Inspection of Equations 31 and 32 implies the following concerning the attitude control system. After a short transient, relative to the time of flight, the roll angle settles out at a fixed value. In general, the natural frequency, $\omega_y$, must be greater than the frequency components of $Z/X_r$ if the yaw attitude control system is to do its job; i.e., keep A equal to zero. Assuming $\omega_y$ does meet this requirement, it is clear that $\psi$ undergoes a short transient and settles down at $-Z/X_r$. The same argument applies for the pitch angle control system. In short, except for a brief initial transient, the attitude control system may be summarized by:

$$\phi = \phi_e \quad \text{(a constant)} \tag{33a}$$

$$\psi = -Z/X_r \tag{33b}$$

$$\theta = Y_n/X_r \tag{33c}$$

In addition to the steady state solutions of equations 33, the transient solutions occurring at the beginning of the rendezvous are of some interest as check solutions. Since $Y_{n_o}$ is zero, by definition, and $Z_o$ is relatively small, the homogeneous solutions to equation 32 will serve to describe the history during the starting transient. These solutions are given by:

$$\phi = \tau_r \phi_o \left(1 - e^{-t/\tau_r}\right) + \phi_o \tag{34}$$

$$\psi = e^{-\zeta_y \omega_y t}\left[\psi_o \cos(\omega_{y_1} t) - \left(\frac{\psi_o}{\omega_{y_1}} + \frac{\zeta_y \psi_o}{\sqrt{1-\zeta_y^2}}\right) \sin(\omega_{y_1} t)\right]$$

$$\theta = e^{-\zeta_p \omega_p t}\left[\theta_o \cos(\omega_{p_1} t) - \left(\frac{\dot{\theta}_o}{\omega_{p_1}} + \frac{\zeta_b \theta_o}{\sqrt{1-\zeta_r^2}}\right) \sin(\omega_{p_1} t)\right]$$

where,

$$\omega_{y_1} = \omega_y \sqrt{1-\zeta_y^2}$$

$$\omega_{p_1} = \omega_p \sqrt{1-\zeta_p^2}$$

If equation 34 is differentiated and use is made of equation 11:

$$\omega_{b_x} = \omega_{b_{xo}} e^{-t/\tau_r}$$

$$\omega_{b_y} = e^{-\zeta_y \omega_y t}\left[\omega_{b_{yo}} \cos(\omega_y t) - \left(\frac{\zeta_y \omega_{b_{yo}}}{\sqrt{1-\zeta_y^2}} + \frac{\psi_o \omega_y}{\sqrt{1-\zeta_y^2}}\right)\sin(\omega_{y_1} t)\right] \tag{35}$$

$$\omega_{b_z} = e^{-\zeta_p \omega_p t}\left[\omega_{b_{zo}} \cos(\omega_{p_1} t) - \left(\frac{\zeta_p \omega_{b_{zo}}}{\sqrt{1-\zeta_p^2}} - \frac{\theta_o \omega_p}{\sqrt{1-\zeta_p^2}}\right)\sin(\omega_p t)\right]$$

Comparison of analytical and digital simulation results corresponding to equation 35 are shown in figures 2, 3, and 4.

Next the trajectory equations, 30, will be considered. Substituting in equation 31.

$$\ddot{X}_r = \frac{K-1}{K}\frac{\dot{X}_r^2}{X_r} \tag{36}$$

$$\ddot{Y}_n = \frac{K-1}{K}\frac{\dot{X}_r^2}{X_r}\theta - \left[S + \frac{K-1}{K}\right]\frac{\dot{X}_r^2}{X_r^2} Y_n + \left[S + \frac{K-1}{K}\right]\frac{\dot{X}_r}{X_r}\dot{Y}_n$$

$$Z = \frac{K-1}{K}\frac{\dot{X}_r^2}{X_r} - \left[S + \frac{K-1}{K}\right]\frac{\dot{X}_r^2}{X_r^2} Z + \left[S + \frac{K-1}{K}\right]\frac{\dot{X}_r}{X_r}\dot{Z}$$

Substituting the steady state attitude control equations, 33, into equation 36:

$$\ddot{X}_r = \frac{K-1}{K}\frac{\dot{X}_r^2}{X_r} \tag{37a}$$

$$\ddot{Y}_n = \left[S + \frac{K-1}{K}\right]\frac{\dot{X}_r}{X_r}\dot{Y}_n - S\frac{X_r^2}{X_r^2} Y_n \tag{37b}$$

$$\ddot{Z} = \left[S + \frac{K-1}{K}\right]\frac{\dot{X}_r}{X_r}\dot{Z} - S\frac{\dot{X}_r^2}{X_r} Z \tag{37c}$$

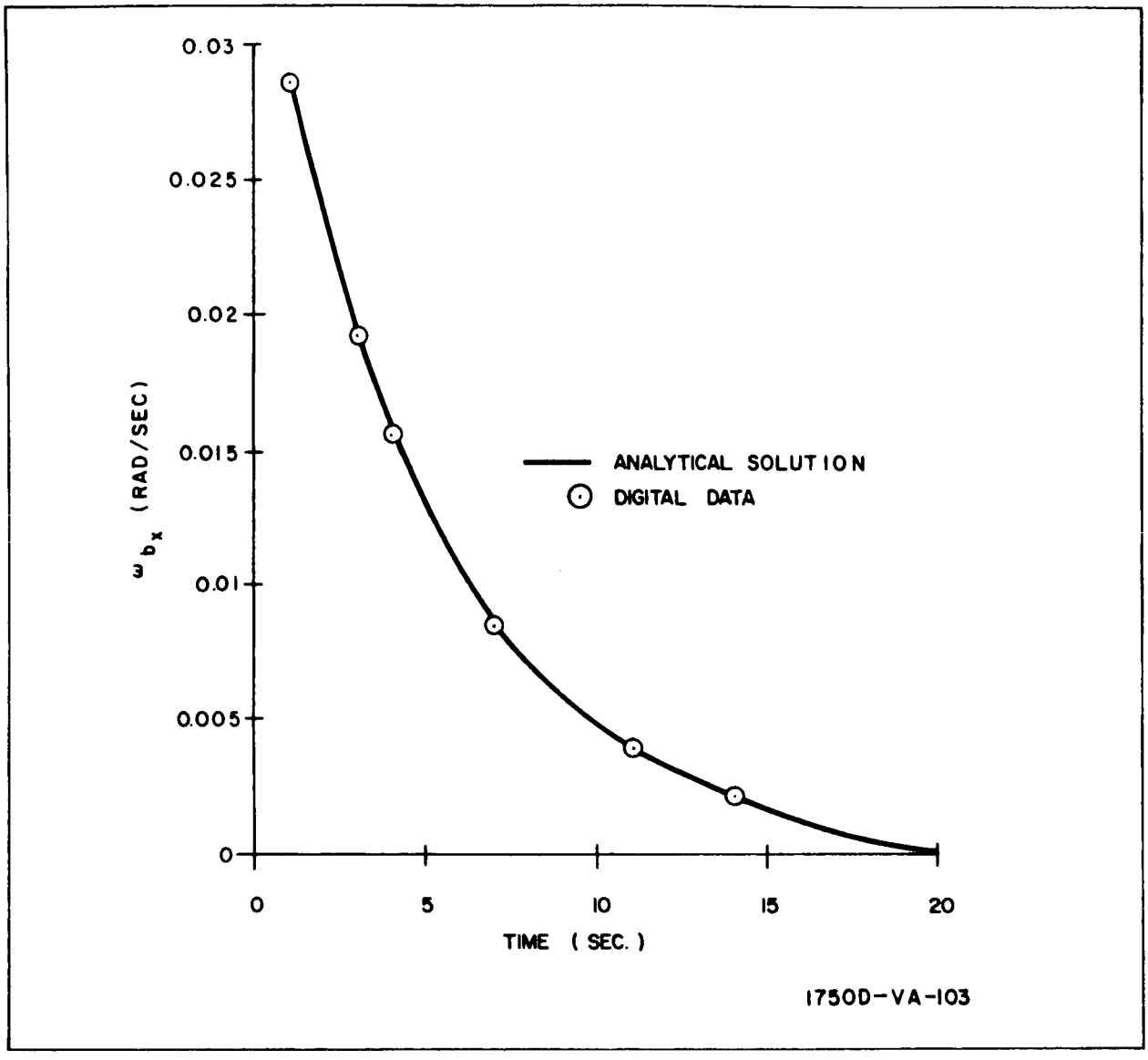


Figure 2. Comparison of Linearized Analytical Check Solution and Digital Computer Results

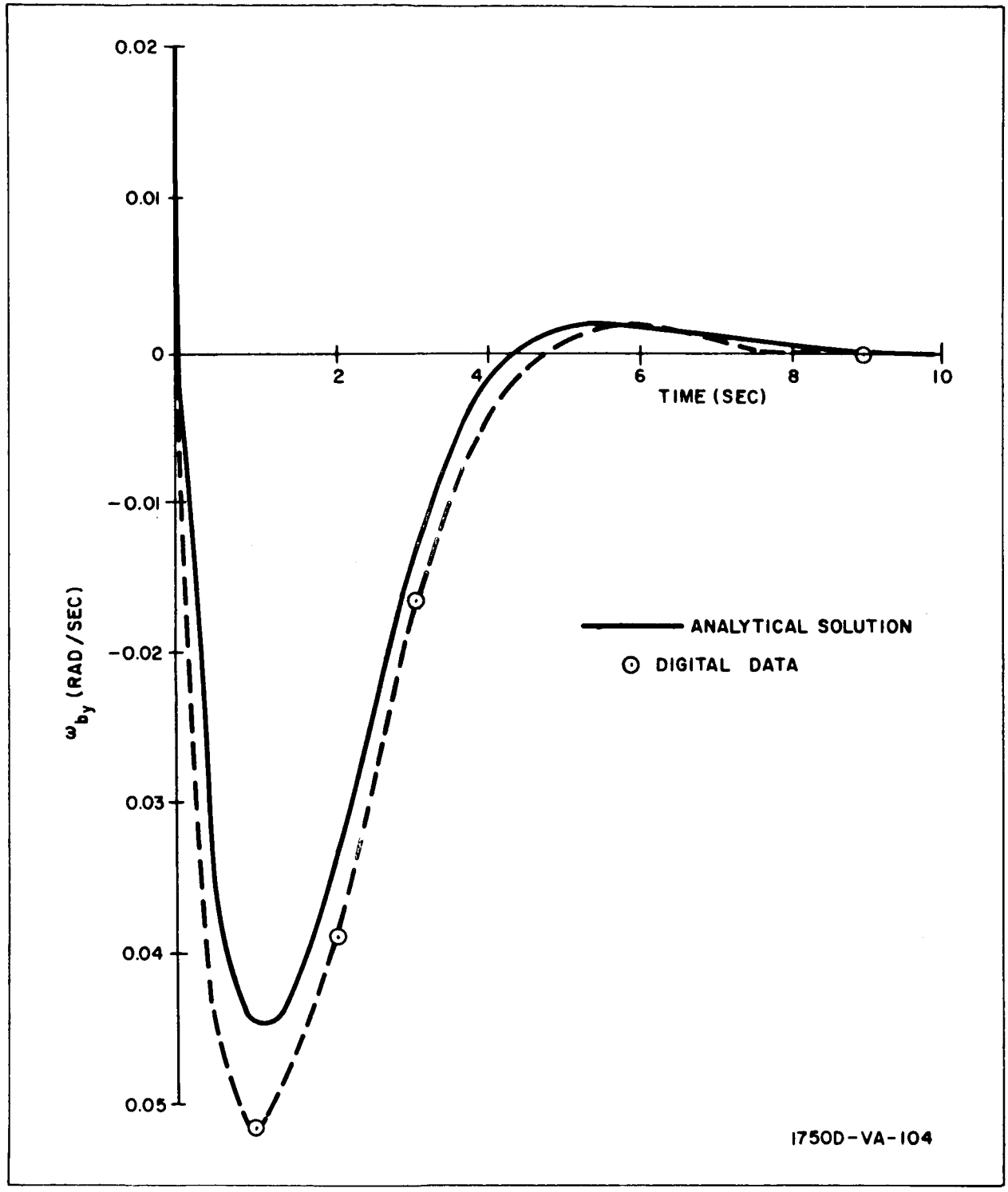


Figure 3. Comparison of Linearized Analytical Check and Digital Computer Results

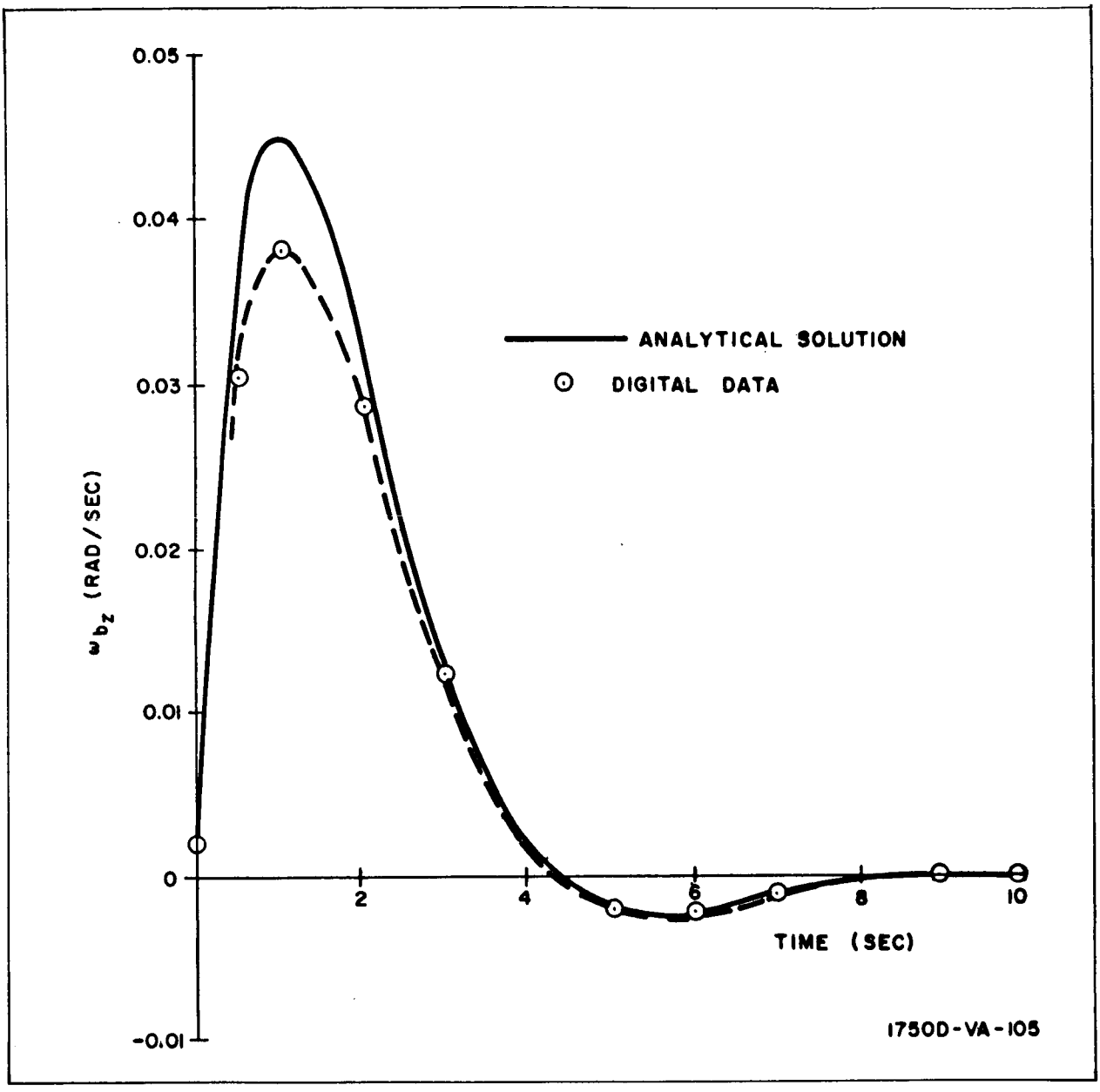


Figure 4. Comparison of Linearized Analytical Check Solution and Digital Computer Results

The solution to equation 37 is as follows. The nonlinear range equation is solved by separation of variables. Substituting the solution for $\dot{X}_r/X_r$ into the two identical lateral channels transforms them into equidimensional equations which are readily solved. Equation 37a may be expressed as:

$$\frac{\ddot{X}_r}{\dot{X}_r} = \frac{K-1}{K}\frac{\dot{X}_r}{X_r} \tag{38}$$

Integrating equation 38:

$$\frac{\dot{X}_r}{\dot{X}_{ro}} = \left[\frac{X_r}{X_{ro}}\right]^{\frac{K-1}{K}} \tag{39}$$

Integrating equation 39:

$$\frac{X_r}{X_{ro}} = \left[1 + \frac{\dot{X}_{ro}}{Kx_{ro}}t\right]^{K} \tag{40}$$

In equation 40, $X_r$ goes to zero when:

$$t = -\frac{KX_{ro}}{\dot{X}_{ro}} \triangleq t_f \tag{41}$$

Defining

$$\tau = 1 - t/t_f \tag{42}$$

Substituting equation 41 and 42 into 40:

$$X_r = X_{ro}\,\tau^{k} \tag{43}$$

Substituting equation 43 into 39:

$$\dot{X}_r = \dot{X}_{ro}\,\tau^{K-1} \tag{44}$$

Differentiating equation 43

$$\dot{X}_r = \frac{dX_r}{d\tau}\frac{d\tau}{dt} = -\frac{kX_{ro}\tau^{K-1}}{t_f} \tag{45}$$

Dividing 45 by 43

$$\frac{\dot{X}_r}{X_r} = -\frac{K}{t_f\tau} \tag{46}$$

Substituting 46 into 37b

$$\ddot{Y}_n + \left[S + \frac{K-1}{K}\right]\frac{K}{t_f\tau}\dot{Y}_n + S\left(\frac{K}{t_f\tau}\right)^2 Y_n = 0 \tag{47}$$

Equation 47 can be put in equidimensional form by the following procedure:

Let

$$\frac{d^2Y_\eta}{dt^2} = \frac{dY_n}{d\tau}\frac{d\tau}{dt} \tag{48}$$

and

$$\frac{d^2Y_n}{dt^2} = \frac{d}{d\tau}\left(\frac{dY_n}{d\tau}\quad\frac{d\tau}{d\tau}\right)\quad\frac{d\tau}{dt}$$

$$= \frac{d}{d\tau}\quad\left(\frac{dY_n}{d\tau}\right)\left(\frac{d\tau}{dt}\right)^2 = \quad\frac{d^2Y_n}{d\tau^2}\quad\left(\frac{d\tau}{dt}\right)^2 \tag{49}$$

From equation 42,

$$\frac{d\tau}{dt} = -\frac{1}{t_f} \tag{50}$$

Substituting equation (50) into equations (48) and (49):

$$\frac{dY_n}{dt} = -\frac{dY_n}{d\tau}\frac{1}{t_f} \tag{51}$$

$$\frac{d^2y_n}{dt^2} = \frac{d^2Y_n}{d\tau^2}\frac{1}{t_f^2} \tag{52}$$

Equations (51) and (52), when substituted into equation (47) yield:

$$\frac{d^2y_n}{d\tau^2}\frac{1}{t_f^2} - \left[S + \frac{K-1}{K}\right]\frac{K}{t_f^2\tau}\frac{dY_n}{d\tau} + S\left(\frac{K}{t_f\tau}\right)^2 Y_n = 0 \tag{53}$$

Multiplying by $\tau^2 t_f^2$:

$$\tau^2\frac{d^2Y_n}{d\tau^2} - \left[S + \frac{K-1}{K}\right]\tau K\frac{dY_n}{d\tau} + SK^2Y_n = 0 \tag{54}$$

Equation 54 has the form of Euler's differential equation, the solution to which is of the form:

$$Y_n = C_1\tau^k + C_2\tau^{SK} \tag{55}$$

The solution to equation 37c is obtained in a similar manner.

where,

$$Z = C_3\tau^K + C_4\tau^{SK} \tag{56}$$

where,

$$C_1 = Y_{no}\frac{S}{S-1} + \frac{\dot{Y}_{no}t_f}{K(S-1)}$$

$$C_2 = -\frac{Y_{no}}{S-1} - \frac{\dot{Y}_{no} t_f}{K(S-1)}$$

$$C_3 = \frac{Z_o S}{S-1} = \frac{\dot{Z}_{o_f} t_f}{K(S-1)}$$

$$C_4 = -\frac{Z_o}{S-1} - \frac{\dot{Z}_{o_f} t_f}{K(S-1)} \qquad (57)$$

Substituting equations 43, 55 and 56 into equations 33b and 33c yield:

$$\psi = -\left[\frac{Z_o S}{(S-1)} + \frac{\dot{Z}_{o_f} t_f}{K(S-1)}\right] \frac{\tau}{X_r} k + \left[\frac{Z_o}{(S-1)} + \frac{\dot{Z}_{o_f} t_f}{K(S-1)}\right] \frac{\tau}{X_r} SK \qquad (58)$$

$$\theta = \left[\frac{Y_{no} S}{(S-1)} + \frac{\dot{Y}_{no} t_f}{K(S-1)}\right] \frac{\tau K}{X_r} - \left[\frac{Z_o}{S-1} - \frac{\dot{Z}_{o_f} t_f}{K(S-1)}\right] \frac{\tau SK}{X_r} \qquad (59)$$

As stated on page C-1, the yaw and pitch angles, $\psi_b$ and $\theta_b$ are represented by

$$\psi_b = \psi_{bo} + \psi \qquad (60)$$

$$\theta_b = \theta_{bo} + \theta \qquad (61)$$

where $\psi$ and $\theta$ are given by equations 58 and 59 respectively.

Equations 60 and 61 are plotted in figures 5 and 6 respectively, along with digital program results, for the case where

$\psi_{bo} = 180°$

$\theta_{bo} = 0°$

Figure 7 presents analytical results of equation 43 along with digital program results and figure 8 presents similar data for equations 55 and 56.

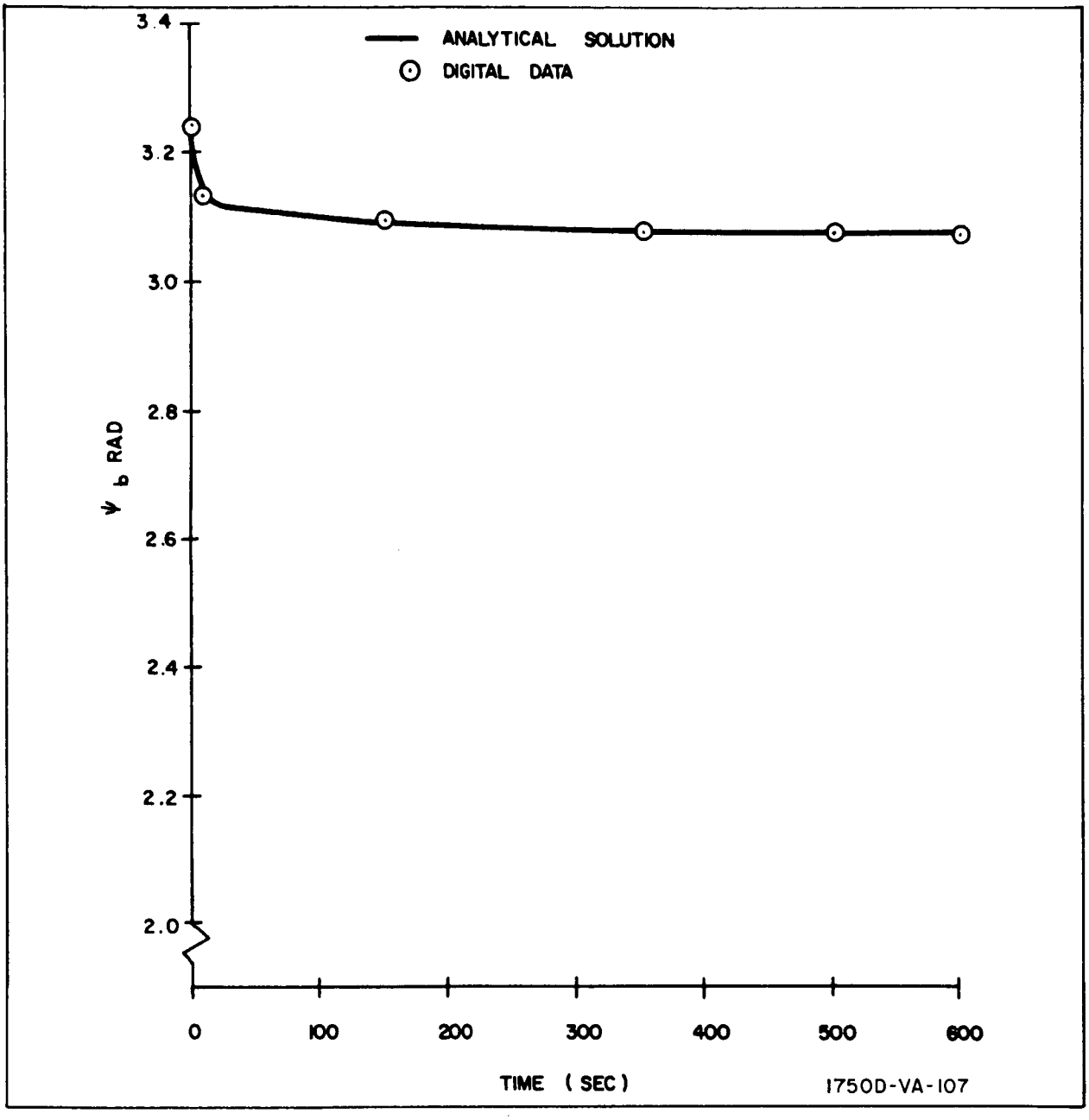


Figure 5. Comparison of Linearized Analytical Check Solution and Digital Computer Results

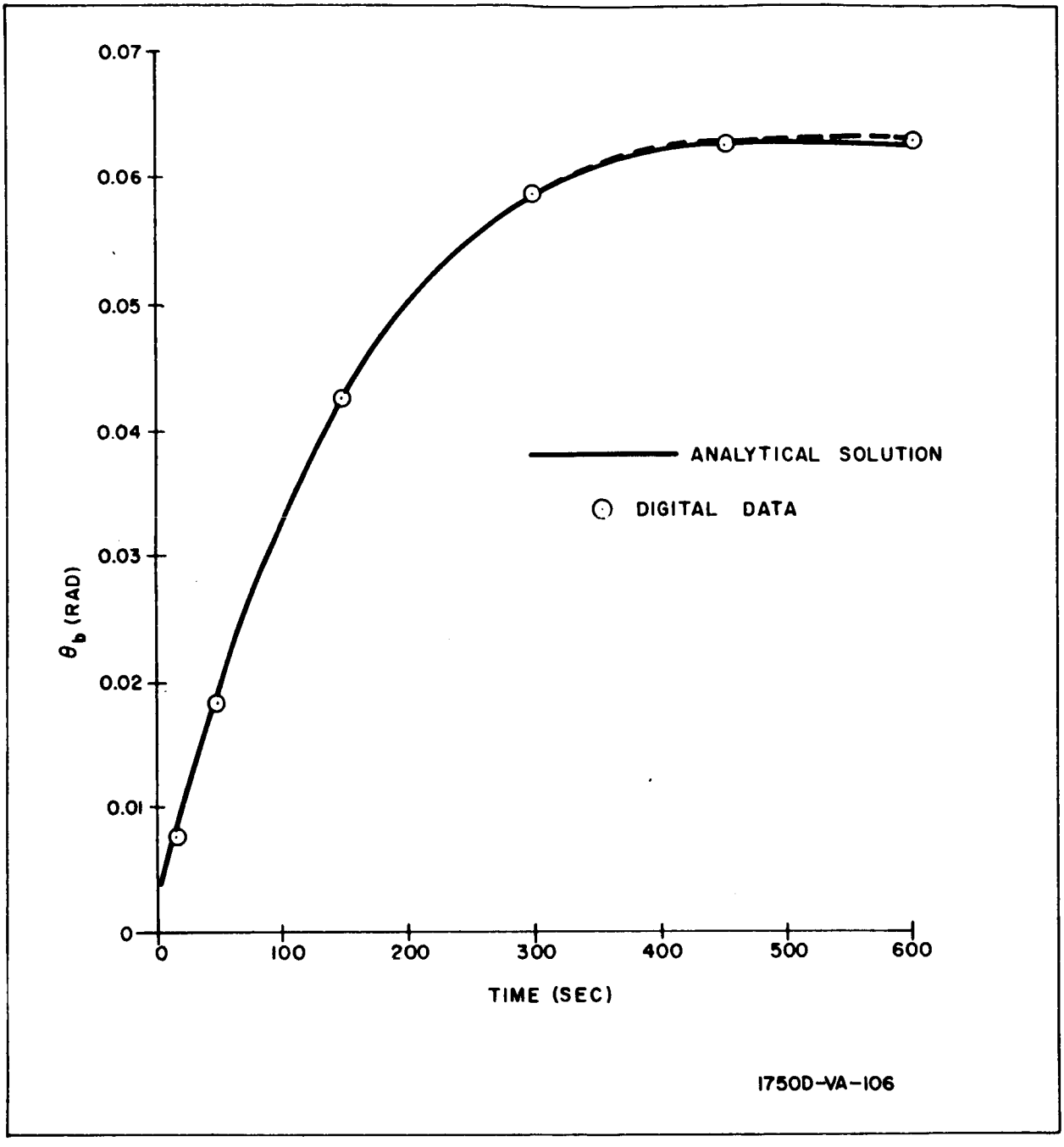


Figure 6. Comparison of Linearized Analytical Check Solution and Digital Computer Results

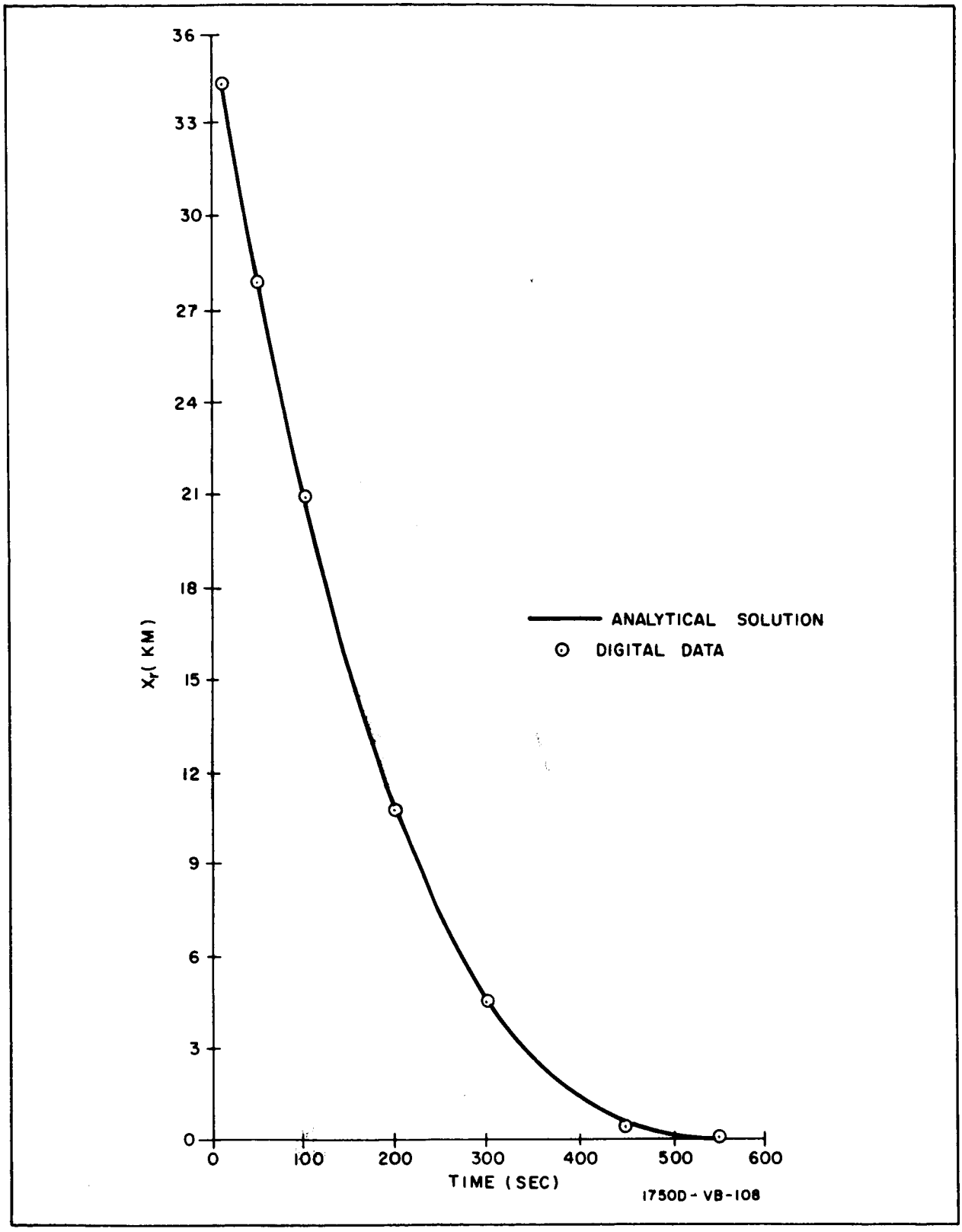


Figure 7. Comparison of Linearized Analytical Check Solution and Digital Computer Results

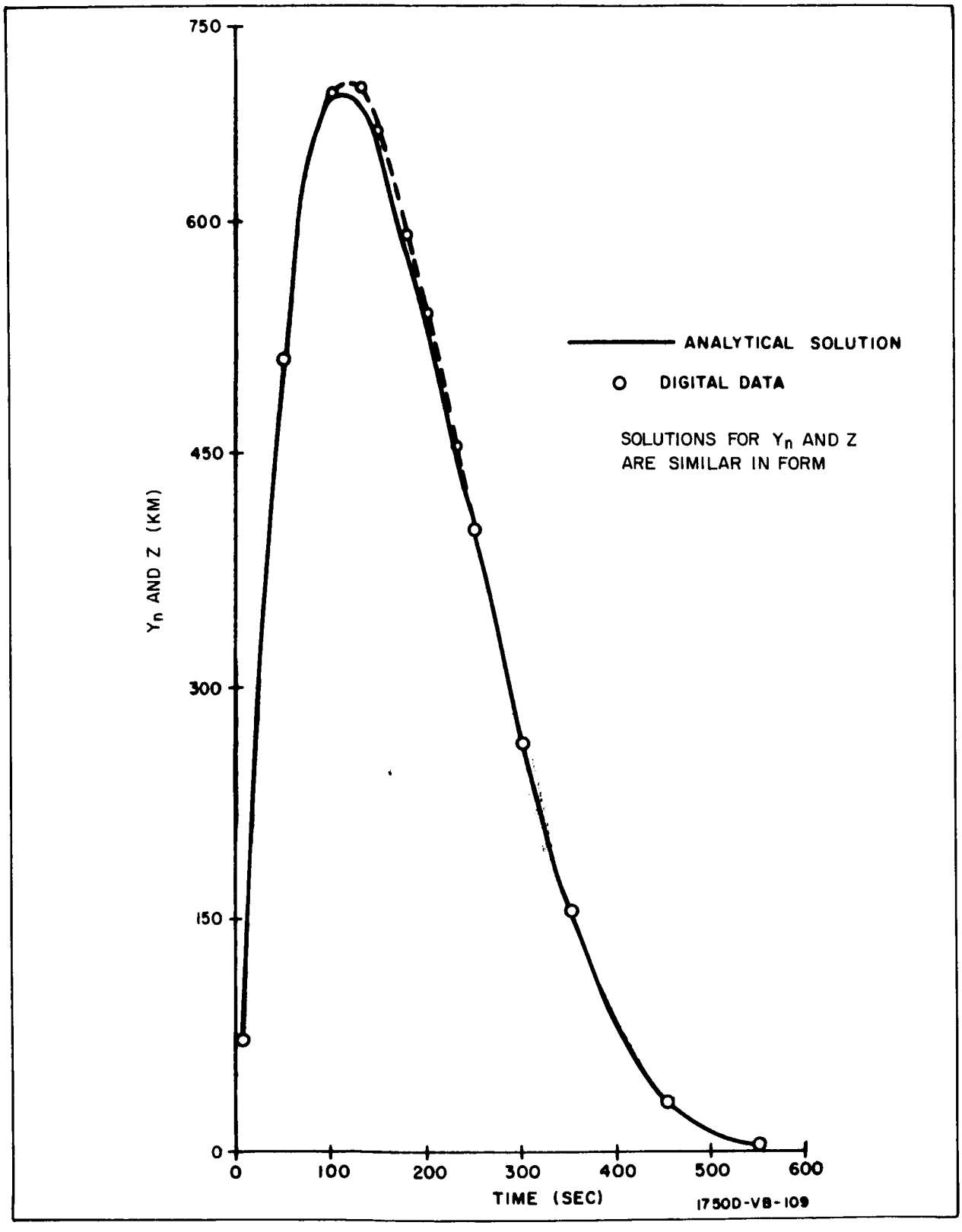


Figure 8. Comparison of Linearized Analytical Check Solution and Digital Computer Results

# APPENDIX D

## ADJOINT COMPUTER MODEL

This section develops the adjoint equations for rendezvous, employing the continuous modified proportional navigation guidance law. The general equations from Appendix C are linearized and restricted here to two dimensions and small angle approximations. The resultant adjoint equations are solved by the Satellite Rendezvous Sensor Error analysis digital computer program to yield the influence of bias and random (fluctuation) sensor errors on the terminal conditions of the rendezvous maneuver.

The first portion of this appendix develops the linearized forward differential equations, the second part is devoted to the derivation of the adjoint equations, the third section derives the nominal closed form time solutions of relative motion about which the linearization is done, and finally, the outputs generated are described.

### 1. LINEARIZATION

To utilize the adjoint method of analysis, the differential equations of relative motion and control must be linearized. From Appendix C, the following equations are obtained.

From equation 9 of Appendix C, the relative motion in the satellite local level frame is given by:

$$\ddot{X} = a_{x_T} + \omega_T \dot{Y}$$

$$\ddot{Y} = a_{y_T} - \omega_T \dot{X} + 3\omega_T^2 Y \qquad (1)$$

From equation 16 of Appendix C, the transformation from ferry body axes to satellite axes is:

$$a_{x_T} = - a_{x_b} - a_{y_b} \theta$$

$$a_{y_T} = - a_{x_b} \theta + a_{y_b} \qquad (2)$$

where,

$$\theta = \frac{Y_n}{X_r} << 1$$

$$\theta_b = \theta_{b_o} + \theta \; ; \theta_{b_o} = 0$$

The value of $\theta_{b_o}$ is arbitrarily set equal to zero.

From equations 29 of Appendix C, the MPN guidance laws, assuming $a_f = 0$, are

$$a_{x_b} = -\frac{K-1}{K} \frac{\dot{X}_r^2 - \dot{R}_b^2}{X_r - R_b}$$

$$a_{y_b} = -\left[S + \frac{K-1}{K}\right] \frac{\dot{X}_r}{X_r^2} \left[Y_n \dot{X}_r - \dot{Y}_n X_r\right] - \left[S + \frac{K-1}{K}\right] \dot{X}_r \dot{\lambda}_b \tag{3}$$

where $\dot{\lambda}_b$ denotes both random and bias sensor errors in line-of-sight measurement.

Combining equations 2 and 3 expresses the guidance law in satellite coordinates. Second order terms in the perturbations (i.e., $\theta Y_n$) are neglected, yielding,

$$a_{x_T} = \frac{K-1}{K} \frac{\dot{X}_r^2 - \dot{R}_b^2}{X_r - R_b}$$

$$a_{y_T} = \left[S + \frac{K-1}{K}\right] \frac{\dot{X}_r}{X_r} \dot{Y}_n - S\left(\frac{\dot{X}_r}{X_r}\right)^2 Y_n + \left[S + \frac{K-1}{K}\right] \dot{X}_r \dot{\theta} \tag{4}$$

where $\dot{\theta} = -\dot{\lambda}_b$ denotes line-of-sight rate errors.

Before proceeding to the adjoint set of equations it is necessary to linearize the above equations. The $a_{x_T}$ equation is linearized about the nominal trajectory as follows:

$$\delta a_{x_T} = \frac{\partial a_{x_T}}{\partial X_r}\bigg|_{\text{nominal}} \delta X_r + \frac{\partial a_{x_T}}{\partial \dot{X}_r}\bigg|_{\text{nominal}} \delta \dot{X}_r$$

or

$$\delta a_{x_T} = -\frac{K-1}{K}\left\{\frac{\dot{X}_r^2 - \dot{R}_b^2}{(X_r - R_b)^2}\right\}_{\text{nominal}} \delta X_r + \frac{K-1}{K}\left\{\frac{2\dot{X}_r}{X_r - R_b}\right\}_{\text{nominal}} \delta \dot{X}_r \qquad (5)$$

Similarly, the expression for $a_{y_T}$ is linearized.

$$\delta a_{y_T} = \left\{\frac{\partial a_{y_T}}{\partial X_r}\right\}_{\text{nominal}} \delta X_r + \left\{\frac{\partial a_{y_T}}{\partial \dot{X}_r}\right\}_{\text{nominal}} \delta \dot{X}_r + \left\{\frac{\partial a_{y_T}}{\partial Y_n}\right\}_{\text{nominal}} \delta Y_n + \left\{\frac{\partial a_{y_T}}{\partial \dot{Y}_n}\right\}_{\text{nominal}} \delta \dot{Y}_n + \left\{\frac{\partial a_{y_T}}{\partial \dot{\theta}}\right\}_{\text{nominal}} \delta \dot{\theta}$$

Performing the indicated operations and recalling that:

$$(Y_n)_{\text{nominal}} = (\dot{Y}_n)_{\text{nominal}} = (\dot{\theta})_{\text{nominal}} = 0$$

and therefore

$$\delta \dot{\theta} = \dot{\theta};\ \delta Y_n = Y_n,\ \delta \dot{Y}_n = \dot{Y}_n$$

yields the following expression:

$$a_{y_T} = \left[S + \frac{K-1}{K}\right]\left(\frac{\dot{X}_r}{X_r}\right)_{\text{nominal}} \dot{Y}_n - S\left(\frac{\dot{X}_r}{X_r}\right)^2_{\text{nominal}} Y_n + \left[S + \frac{K-1}{K}\right](\dot{X}_r)_{\text{nominal}} \dot{\theta} \qquad (6)$$

The complete set of linearized forward differential equations is composed of equations 1, 5, and 6.

## 2. ADJOINT EQUATIONS

A set of equations, adjoint to the above equations, is derived here. Essentially the adjoint set of equations provides the capability to determine the propagation of bias and random errors, occurring throughout the rendezvous maneuver, to the terminal point of the rendezvous without resorting to Monte Carlo techniques. Mathematically, a linear matrix first-order differential equation

$$\dot{\underline{X}}(t) = \left[A(t)\right] \underline{X}(t), \quad \underline{X}(o) = \underline{X}_o \tag{7}$$

has a corresponding first-order, matrix differential equation which is adjoint to the original set, given by:

$$\left[\dot{\Lambda}(t)\right] = -\left[A(t)\right]^T \left[\Lambda(t)\right], \left[\Lambda(o)\right] = \left[\Lambda_o\right] \tag{8}$$

where the initial conditions $[\lambda_o]$ are chosen dependent upon the output error quantities of interest. $[\ ]^T$ means transpose. Solution of this equation yields the influence of sensor errors on terminal conditions. (See Appendix A of Volume V for a detailed discussion of the adjoint error analysis technique.)

Rather than listing the resultant adjoint equations, figure 1 shows the equations in block diagram form. In addition to the equations of relative motion and the idealized guidance laws, second-order filters are included to represent lateral and longitudinal engine lags and sensor dynamics. The initial conditions on the adjoint equations are chosen so as to obtain errors in position (X, Y) and velocity ($\dot{X}$, $\dot{Y}$) about the nominal terminal point (range = $R_b$, range rate = $\dot{R}_b$, line-of-sight rate equals zero). (See reference 1 for discussion of adjoint system block diagrams.)

## 3. NOMINAL TRAJECTORY

The adjoint perturbation equations developed in the previous part of this section are viewed as describing small departures about a nominal trajectory determined by assuming no system dynamic lags and $\omega_T = 0$. In addition it is assumed that the nominal trajectory is initiated with:

---

Ref. 1 Laning and Battin, Random Processes in Automatic Control, New York: McGraw-Hill Book Co., 1956, pp. 239-247.

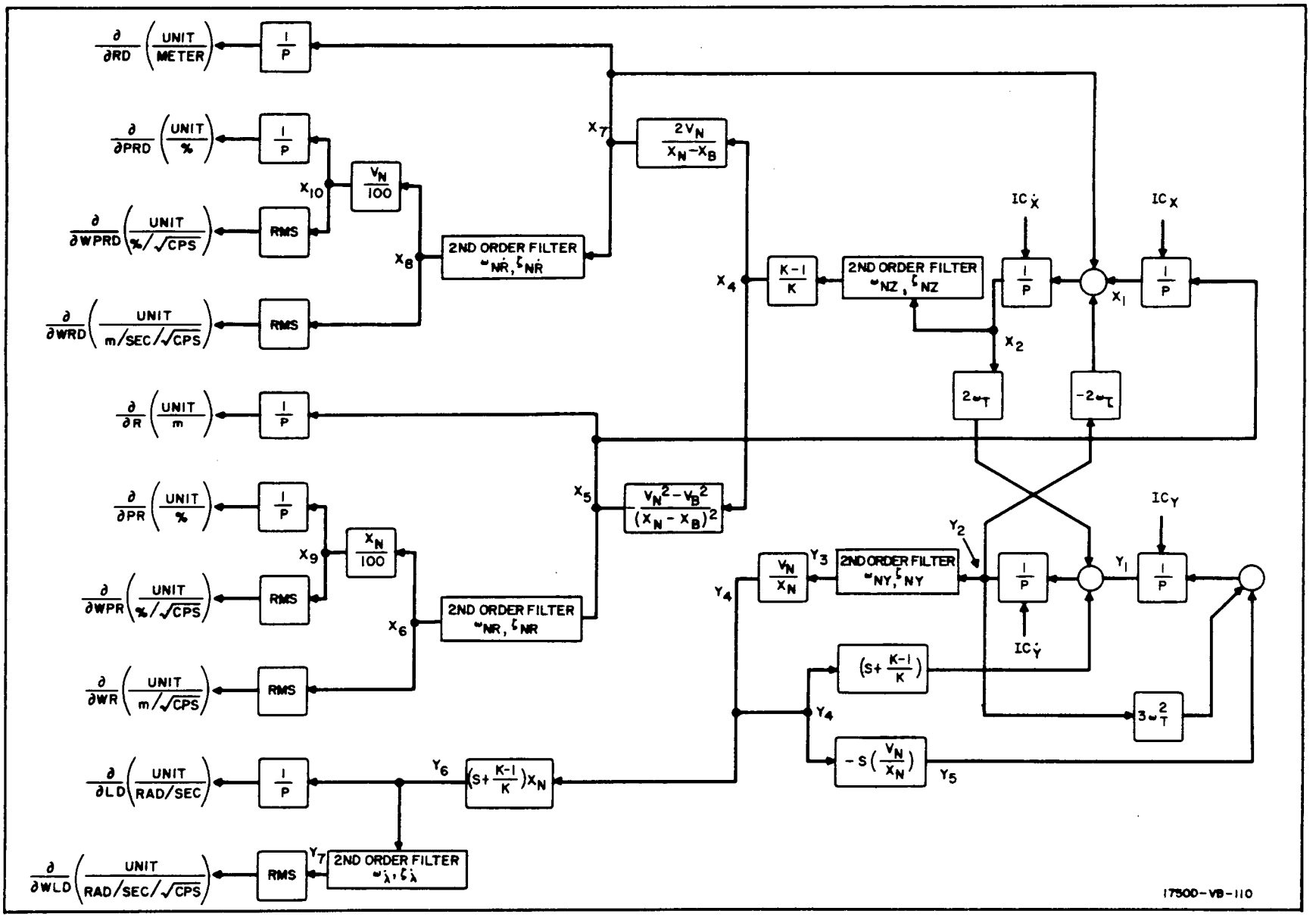


Figure 1. Adjoint Equations Block Diagram

$$X_{Tf} = X_o$$

$$\dot{X}_{Tf} = \dot{X}_o \tag{9}$$

$$Y_{Tf} = \dot{Y}_{Tf} = 0$$

In Appendix C the nominal solutions for relative position and velocity were derived assuming zero nominal terminal conditions ($R_b = \dot{R}_b = 0$) but including nonzero initial values of $Y_n$ and $\dot{Y}_n$. Here, starting from equation 37a of Appendix C but with $R_b \neq 0$, $\dot{R}_b \neq 0$ we have:

$$a = \frac{K-1}{K} \quad \frac{V^2 - V_b^2}{r - r_b} \tag{10}$$

where

$$a = \ddot{X}_r$$

$$V = \dot{X}_r$$

$$V_b = \dot{R}_b$$

$$r = X_r$$

$$r_b = R_b$$

It is desired to obtain solutions of equation 10 for $V = f(r)$, time histories of a, V, and r and the total rendezvous time, $t_f$.

$$a \equiv \frac{dV}{dt} = \frac{dV}{dr} \frac{dr}{dt} = V \frac{dV}{dr} \tag{11}$$

From equations 10 and 11:

$$\frac{VdV}{V^2 - V_b^2} = \frac{K-1}{K} \quad \frac{dr}{r - r_b} \tag{12}$$

Integrating equation 12 yields:

$$V^2 = V_b^2 + (V_o^2 - V_b^2)\left(\frac{r - r_b}{r_o - r_b}\right)^{\frac{2(K-1)}{K}} \tag{13}$$

where

$r_o = r(0)$, $V_o = V(0)$.

To obtain position, r, and velocity, V, as functions of time:

$$dt = \frac{dr}{V} \tag{14}$$

For $0 < t \leq t_1$, assume, from equation 13.

$$V^2 = V_o^2\left(\frac{r - r_b}{r_o - r_b}\right)^{\frac{2(K-1)}{K}} \tag{15}$$

Combining equations 14 and 15 and integrating:

$$t = \frac{K(r_o - r_b)}{V_o}\left[\left(\frac{r - r_b}{r_o - r_b}\right)^{\frac{1}{K}} - 1\right] \qquad 0 < t \leq t_1 \tag{16}$$

or solving for r,

$$r = r_b + (r_o - r_b)\left(1 + \frac{V_o t}{K(r_o - r_b)}\right)^K \quad \text{for } r_1 < r \leq r_o \tag{17}$$

For $t_1 < t \leq t_f$ assume, from equation 13

$$V = V_b \tag{18}$$

Combining equations 14 and 18 and integrating:

$$t = t_f + \frac{r - r_b}{V_b} \quad \text{for } t_1 < t \leq t_f \tag{19}$$

or

$$r = r_b - V_b (t_f - t) \quad \text{for } r_b \leq r \leq r_1 \tag{20}$$

Define $r_1$ as range where:

$$V_b^2 = (V_o^2 - V_b^2) \left(\frac{r_1 - r_b}{r_o - r_b}\right)^{\frac{2(K-1)}{K}} \tag{21}$$

or, making use of equation 13.

$$r_1 = r_b + (r_o - r_b) \left(\frac{V_b^2}{V_o^2 - V_b^2}\right)^{\frac{K}{2(K-1)}}$$

To determine, $t_f$:

$$\int_o^{t_f} dt = \int_o^{t_1} dt + \int_{t_1}^{t_f} dt \qquad \text{where } t = t_1, \text{ when } r = r_1$$

Hence,

$$t_f = \frac{K(r_o - r_b)}{V_o} \left[\left(\frac{V_b^2}{V_o^2 - V_b^2}\right)^{\frac{1}{2(K-1)}} - 1\right] - \frac{r_o - r_b}{V_b} \left(\frac{V_b^2}{V_o^2 - V_b^2}\right)^{\frac{K}{2(K-1)}} \tag{22}$$

In summary, the nominal, approximate closed form solutions for $X_r (= r)$ and $\dot{X}_r (= V)$ required in the adjoint perturbation equations are given by:

$$\left\{X_r(\tau)\right\}_{\text{nominal}} = \begin{cases} X_b + (X_o - X_b)\left[1 + \dfrac{V_o\,(t_f - \tau)}{K\,(X_o - X_b)}\right]^K & \tau > t_1 \\ X_b - V_b \tau & \tau \le t_1 \end{cases} \tag{23}$$

$$\left\{\dot{X}_r(\tau)\right\}_{\text{nominal}} = -\sqrt{V_b^2 + (V_o^2 - V_b^2)\left(\frac{X_r - X_b}{X_o - X_b}\right)^{\frac{2(K-1)}{K}}}_{\text{nominal}}$$

$$t_f = t_1 - \frac{X_o - X_b}{V_b}\left(\frac{V_b^2}{V_o^2 - V_b^2}\right)^{\frac{K}{2(K-1)}}$$

$$t_1 = \frac{K\,(X_o - X_b)}{-V_o}\left[1 - \left(\frac{V_b^2}{V_o^2 - V_b^2}\right)^{\frac{1}{2(K-1)}}\right]$$

and $\tau = t_f - t$, the adjoint independent variable, which, physically, is time to go to the terminal time, $t_f$.

## 4. ADJOINT PROGRAM OUTPUTS

Previous portions of this section have developed the adjoint set of equations, and the nominal trajectory solutions about which the adjoint equations are linearized. Here the initial conditions placed upon the adjoint equations and the outputs obtainable from the program are set forth.

Initial conditions for the adjoint equations are determined by the output errors of interest. In the rendezvous problem we are interested in the position and velocity errors at the nominal terminal point. In the satellite local level coordinate system utilized, the errors are specified by departures from the nominal end point in position (X, Y) and velocity ($\dot{X}$, $\dot{Y}$). Hence the initial conditions applied to the adjoint equations are unit initial conditions on

on the variables $X_1$, $X_2$, $Y_1$ and $Y_2$ shown in figure 1. The unit IC's are applied individually one at a time, the IC on $X_1$ generating X positional errors, $X_2(0) = 1$ giving $\dot{X}$ errors, $Y_1(0) = 1$ giving Y position errors and $Y_2(0) = 1$ giving $\dot{Y}$ errors.

The various output quantities shown in figure 1 are the result of postulating certain types of sensor output errors. For the range output of the sensor four types of error are assumed; constant range bias error, percentage of range bias error, a random range error of spectral density $W_R$ ($m^2$/cps) and a percentage of range random error of spectral density $W_{PR}$ ($\%^2$/cps).

Four similar types of error are assumed for the range rate output.

For line-of-sight rate errors, only two types are postulated; a constant bias error, line-of-sight (rad/sec) and a random line-of-sight rate error of spectral density $W_{LD}$ ($rad^2/sec^2$/cps).

Thus, the adjoint program provides forty influence coefficients (four output errors for ten types of input errors) which are utilized in determining the allowable magnitude of sensor errors to meet a certain tolerable set of output errors. An example employing these influence coefficients is given in paragraph 3.1.2.1 of this volume.

# APPENDIX E

## ADJOINT HAND ANALYSIS

This appendix develops analytical solutions for the adjoint impulse responses in the range channel. The solutions are determined for the special case in which orbiting effects may be neglected. The MPN range control law is given by:

$$\ddot{R}_c = \frac{K-1}{K} \frac{(\dot{R} + \dot{R}_n)^2}{(R + R_n)} \tag{1}$$

where

$\ddot{R}_c$ = command acceleration

$R$, $\dot{R}$ = range and range rate

$R_n$, $\dot{R}_n$ = range and range rate stochastic error inputs

$K$ = control variable

The engine response characteristics are treated as linear and time invariant. Thus the relation between R and $R_c$ is given by:

$$\frac{\ddot{R}}{\ddot{R}_c} = G(p) \tag{2}$$

where p represents the operator $\frac{d}{dt}$ .

Closed form solution for R(t) can be obtained from 1 and 2 if G(p) = 1 and $R_n = \dot{R}_n = 0$. This solution is derived in Appendix C and is given by:

$$R = R_o \left(1 - t/t_f\right)^K$$

Nominal Range Solution

$$t_f \triangleq -\frac{K R_o}{\dot{R}_o} \qquad = \text{duration of the rendezvous} \qquad (3)$$

$$\frac{\dot{R}}{R} = -\frac{K}{t_f - t}$$

Formal linearization of equation 1 about the nominal trajectory given by equation 3 results in:

Forward Equations

$$\ddot{R}_c = -\frac{2(K-1)}{t_f - t}\left(\dot{R} + \dot{R}_n\right) - \frac{K(K-1)}{(t_f - t)^2}\left(R + R_n\right) \qquad (4)$$

$$\frac{\ddot{R}}{\ddot{R}_c} = G(p)$$

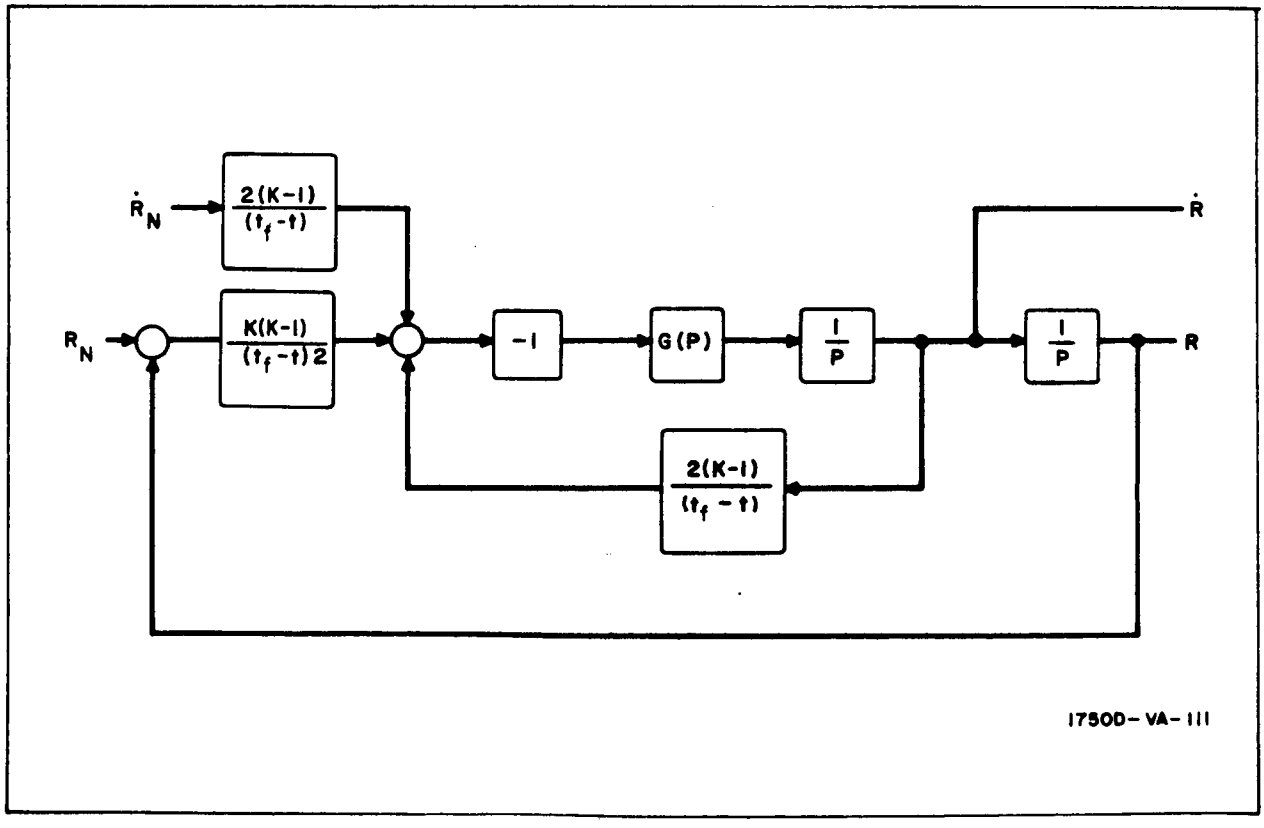


Figure 1. Forward Model

The block diagram corresponding to equation 4 is shown in figure 1. The corresponding adjoint of equation 4 is shown in figure 2. The adjoint time variable, $\tau_1$, is given by:

$$\tau_1 = t_f - t \tag{5}$$

The simplest linear time invariant controller which results in bounded impulse responses for the adjoint of equation 4 is given by equation 6.

$$G(p) = \frac{1}{1 + \frac{2\zeta}{\omega} p + p \frac{2}{\omega^2}} \tag{6}$$

Insertion of equation 6 into figure 2 and rearranging the block diagram leads to figure 3. The range and range rate impulse inputs are shown after they have been integrated once. Table 1 shows the initial conditions around the block diagram corresponding to the two-step inputs. The last column is the result of defining the signal at ① to be z and observing that the signal at ② is $1/\omega^2 z'$ etc. where the prime indicates differentiation with respect to $\tau_1$. Equating the signal at ⑧ to the forcing function and ① , ⑤ , ⑩ and ⑨ gives the adjoint differential equation:

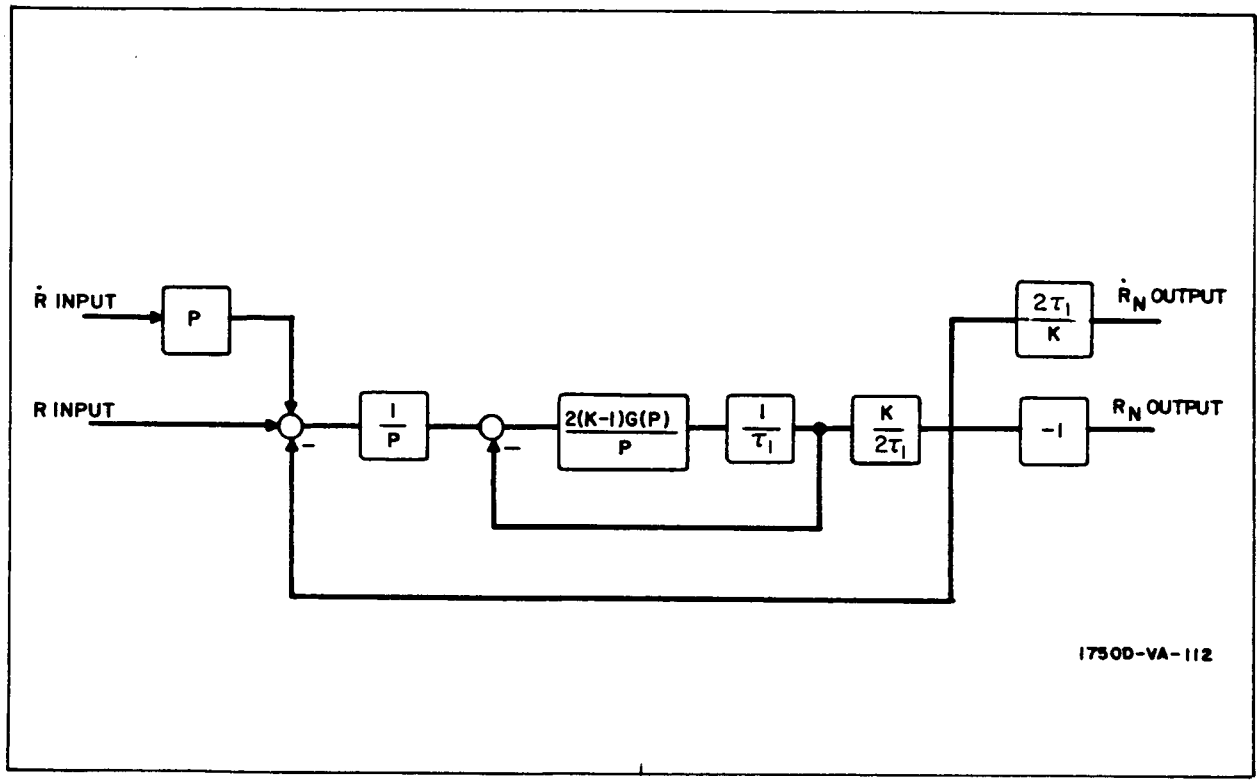


Figure 2. Adjoint Model

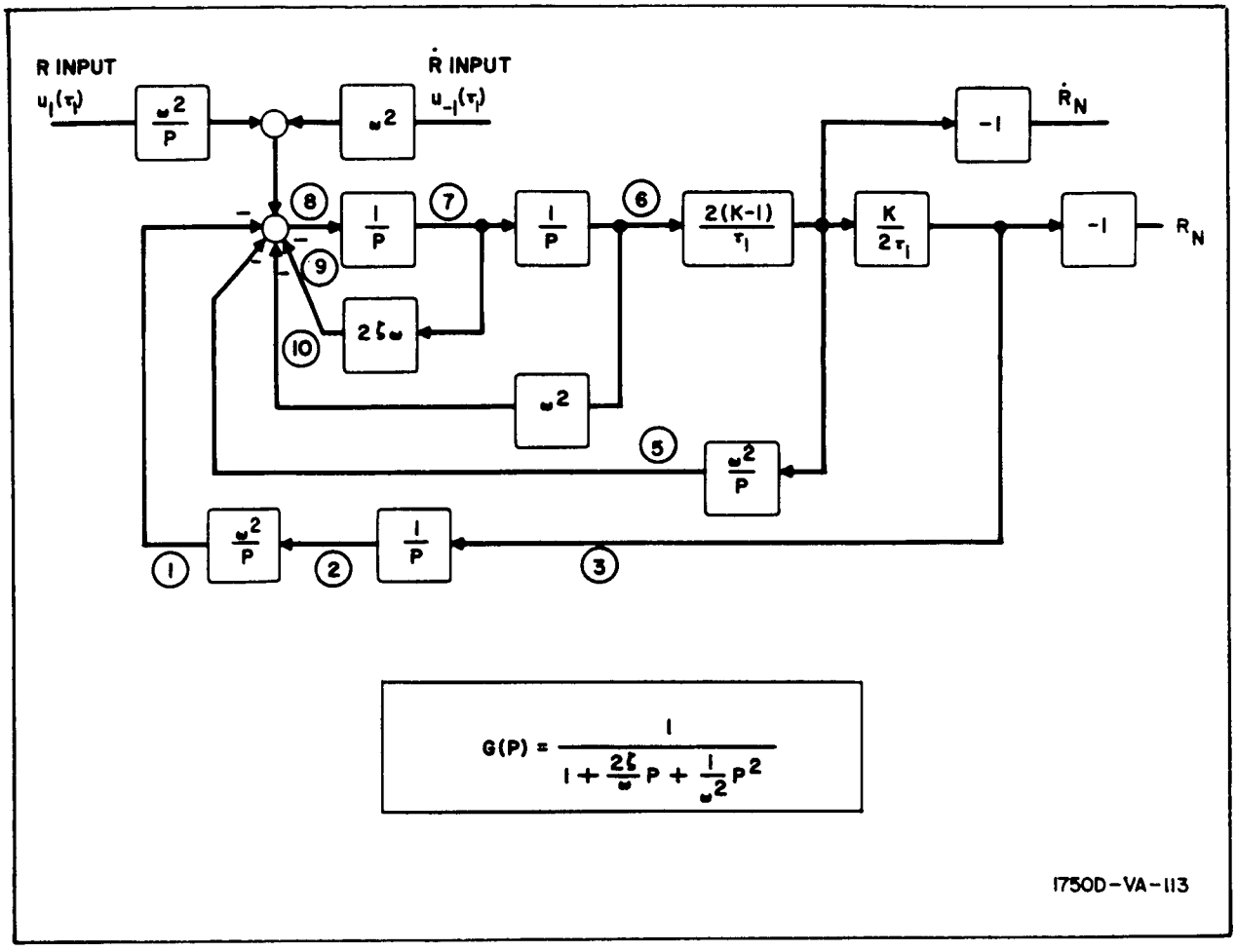


Figure 3. Rearranged Adjoint Model

$$z^{IV}\tau_1^2 + z^{III}(r\tau_1 + 2\zeta\omega\tau_1^2) + z^{II}(2 + 4\zeta\omega\tau_1 + \omega\tau_1^2) \tag{7}$$

$$+ z^{I}(2\left[K-1\right]\omega^2\tau_1) + z\,\omega^2(K-1)(K-2) = \begin{cases} \omega^4\tau_1 K(K-1) & \text{Range Forcing Function} \\ \omega^4 K(K-1) & \text{Range Rate Forcing Function} \end{cases}$$

Equation 7 is conveniently normalized by letting:

$$a = \omega\tau_1 \tag{8}$$

For convenience a new dependent variable is defined in conjunction with 8.

$$y^n(\alpha) \triangleq \left(\frac{1}{\omega}\right)^n z^n(\tau_1) \tag{9}$$

Substituting equation 9 into 7 results in:

$$\alpha^2 y^{IV} + \left[4\alpha + 2\zeta\alpha^2\right] y^{III} + \left[2 + 4\zeta\alpha + \alpha^2\right] y^{II} + \left[2(K-1)\alpha\right] y^1 + (K-1)(K-2)y = F(\alpha) \tag{10}$$

where

$$F(\alpha) = \begin{cases} \omega\alpha K(K-1) & \text{Range Input} \quad (11a) \\ \omega^2 K(K-1) & \text{Range Rate Input} \quad (11b) \end{cases}$$

The particular solutions of equation 10 are determined by inspection. These are given by:

$$y_F = \begin{cases} \omega\alpha & \text{Range Input} \quad (12a) \\ \omega^2 \dfrac{K}{K-2} & \text{Range Rate Input} \quad (12b) \end{cases}$$

The four homogeneous solutions to equation 10 are designated by subscripts 1 thru 4. Thus:

$$y = y_F + y_1 + y_2 + y_3 + y_4 \tag{13}$$

The next portion of this discussion is devoted to determining $y_1$, $y_2$, $y_3$ and $y_4$. The first step is to determine if series solutions of the form of equation 14 exist:

$$y_n = \sum_{r=0}^{\infty} A_r^{(h)}(p)\, \alpha^{r+p} \tag{14}$$

TABLE 1

INITIAL CONDITIONS AND SIGNALS FOR ADJOINT ANALYSIS

| Station | Initial Condition | | Signal |
|---|---|---|---|
| | R Input | R Input | |
| ① | $K(K-1)\omega^4\tau_1^3/36$ | $K(K-1)\frac{\omega^2\tau_1^2}{4}$ | $z$ |
| ② | $K(K-1)\omega^2\tau_1^2/12$ | $K(K-1)\omega^2\tau_1/2$ | $\frac{1}{\omega^2}z'$ |
| ③ | $K(K-1)\omega^2\tau_1/6$ | $K(K-1)\omega^2/2$ | $\frac{1}{\omega^2}z''$ |
| ④ | $(K-1)\omega^2\tau_1^2/3$ | $(K-1)\omega^2\tau_1$ | $\frac{R\tau_1}{K\omega^2}z''$ |
| ⑤ | $(K-1)\omega^4\tau_1^3/9$ | $(K-1)\omega^4\tau_1^2/2$ | $\frac{2}{K}(\tau_1 z'-z)$ |
| ⑥ | $\omega^2\tau_1^3/6$ | $\omega^2\tau_1^2/2$ | $\frac{1}{K(K-1)\omega^2}\tau_1^2 z''$ |
| ⑦ | $\omega^2\tau_1^2/2$ | $\omega^2\tau_1$ | $\frac{1}{\omega^2 K(K-1)}\left[\tau_1^2 z''' + 2\tau_1 z''\right]$ |
| ⑧ | $\omega^2\tau_1$ | $\omega^2$ | $\frac{1}{\omega^2 K(K-1)}\left[\tau_1^2 z'''' + \tau_1 z''' + 2z''\right]$ |
| ⑨ | $\zeta\omega^3\tau_1^2$ | $2\zeta\omega^3\tau_1$ | $\frac{2\zeta}{\omega}\frac{1}{K(K-1)}\left[\tau_1^2 z''' + 2\tau_1 z''\right]$ |
| ⑩ | $\omega^4\frac{\tau_1^3}{6}$ | $\omega^4\tau_1^2/2$ | $\frac{1}{K(K-1)}\tau_1^2 z''$ |

or for simplicity of notation the superscript, n, is dropped and h is substituted for r + p

$$y = \sum_{r=0}^{\infty} A_r(p)\,a^{r+p} = \sum_{r=0}^{\infty} A_r(p)\,a^{h} \tag{15}$$

$$h \triangleq r + p$$

Direct substitution of 15 into 10 results in the series of equation 18. For the reader's convenience, the term-by-term substitution is given in table 2:

$$L \triangleq a^2 \frac{d^4}{da^4} + \left[4a + 2\zeta a^2\right]\frac{d^3}{da^3} + \left[2 + 4\zeta a + a^2\right]\frac{d^2}{da^2} + \left[2(K-1)a\right]\frac{d}{da} + \left[(K-1)(K-2)\right] \tag{16}$$

$$L(y) = \sum_{r=0}^{\infty} \left\{h^2(h-1)^2 A_r a^{h-2} + 2\zeta h^2 (h-1) A_r a^{h-1} + \left[h(h-1) + 2h(K-1) + (K-1)(K-2)\right] A_r a^{h}\right\} \tag{17}$$

Next the summation is re-expressed in forms of like powers of a:

$$L(y) = \sum_{r=0}^{\infty} h^2(h-1)^2 A_r a^{h-2} + \sum_{r=1}^{\infty} 2\zeta(h-1)^2(h-2) A_{r-1} a^{h-2} + \sum_{r=2}^{\infty} \left[(h-2)(h-3) + 2(h-2)(K-1) + (K-1)(K-2)\right] A_{r-2} a^{h-2} \tag{18}$$

Separating those terms in 18 corresponding to r's less than two:

$$L(y) = p^2(p-1)^2 A_o a^{p-2} + p^2(p+1)^2 A_1 a^{p-1} + p^2(p-1) 2\zeta A_o a^{p-1} + \sum_{r=2}^{\infty} a^{h-2}\left\{h^2(h-1)^2 A_r + 2\zeta(h-1)^2(h-2) A_{r-1} + \left[(h-2)(h-3) + 2(K-1)(h-2) + (K-1)(K-2)\right] A_{r-2}\right\} \tag{19}$$

TABLE 2

TERM-BY-TERM SUBSTITUTION

| | |
|---|---|
| $a^2 y^{IV}$ | $h(h-1)(h-2)(h-3) A_r a^{h-2}$ |
| $4a y^{III}$ | $4h(h-1)(h-2) A_r a^{h-2}$ |
| $2 y^{II}$ | $2h(h-1) A_r a^{h-2}$ |
| $2\zeta a^2 y^{III}$ | $2\zeta h(h-1)(h-2) A_r a^{h-1}$ |
| $4\zeta a y^{II}$ | $4\zeta h(h-1) A_r a^{h-1}$ |
| $a^2 y^{II}$ | $h(h-1) A_r a^h$ |
| $2(K-1) a y^I$ | $2(K-1) h A_r a^h$ |
| $(K-1)(K-2) y$ | $(K-1)(K-2) A_r a^h$ |

Each member of the summation vanishes provided that:

$$A_r(p) = -2\zeta \frac{h-2}{h^2} A_{r-1}(p) - \frac{\left[(h-2)(h-3) + 2(K-1)(h-2) + (K-1)(K-2)\right] A_{r-2}(p)}{h^2 (h-1)^2} \tag{20}$$

where

$$r \geq 2$$

Of course, the series solutions are not of interest unless the coefficients, $A_r(p)$, are bounded and, in fact, converge. It is therefore necessary that equation 21 be satisfied for all r greater than or equal to two.

$$h = r + p \begin{cases} \neq 1 \\ \neq 0 \end{cases} \tag{21}$$

where

$$r \geq 2$$

If 20 is true, 19 becomes:

$$L(y) = p^2 (p-1)^2 A_o(p)\, a^{p-2} + p^2 (p+1)^2 A_1(p)\, a^{p-1} + p^2 (p-1)\, 2\zeta\, A_o(p)\, a^{p-1} \tag{22}$$

The coefficient of $a^{p-1}$ vanishes if either

$$p = 0 \tag{23a}$$

or

$$A_1(p) = -2\zeta \frac{(p-1)}{(p+1)^2} A_o(p)\,; \quad p \neq -1 \tag{23b}$$

in which case 22 becomes:

$$L(y) = p^2 (p-1)^2 A_o(p)\, a^{p-2} \tag{24}$$

Assuming nontrivial values of $A_o(p)$, only values of $p = 0$ and $p = 1$ cause the right hand side of equation 24 to be identically zero. Both roots satisfy equation 21 and 23b. In addition the root $p = 0$ satisfies equation 23a. Thus two of the homogeneous solutions to equation 10 have been determined. These solutions will next be presented explicitly.

Solution (1): $p = 0$

$$y_1 = \sum_{r=0}^{\infty} A_r^{(1)}\, a^r \tag{25}$$

$A_o^{(1)}$ arbitrary

$A_1^{(1)}$ arbitrary

Solution (1) (Continued):

$$A_r^{(1)} = -2\zeta \frac{(r-2)}{r^2} A_{r-1}^{(1)} - \frac{\left[(r-2)(r-3) + 2(K-1)(r-2) + (K-1)(K-2)\right] A_{r-2}^{(1)}}{r^2 (r-1)^2}$$

for $r \geq 2$

Solution (2): $p + 1$

$$y_2 = \sum_{r=0}^{\infty} A_r^{(2)} \alpha^{r+1} \tag{26}$$

$A_o^{(2)}$ arbitrary

$A_1^{(2)}$ = zero

$$A_r^{(2)} = -2\zeta \frac{(r-1)}{(r+1)^2} A_{r-1}^{(2)} - \frac{\left[(r-1)(r-2) + 2(K-1)(r-1) + (K-1)(K-2)\right] A_{r-2}^{(2)}}{r^2 (r+1)^2}$$

for $r \geq 2$

The next step is to show that equation 26 is linearly dependent with the portion of equation 25 corresponding to $A_1^{(1)}$. Thus equation 25 is sufficient to represent both $y_1$ and $y_2$ and equation 26 may be deleted.

Let:

$$B_r \triangleq A_{r-1}^{(2)} \tag{27}$$

Substituting equation 27 into 26

$$y_2 = \sum_{r=0}^{\infty} A_r^{(2)} \alpha^{r+1} = \sum_{r=1}^{\infty} A_{r-1}^{(2)} \alpha^{r} = \sum_{r=1}^{\infty} B_r \alpha^{r} \tag{28}$$

and

$$B_{r+1} = -2\zeta \frac{(r-1)}{(r+1)^2} B_r - \left[\frac{(r-1)(r-2) + 2(K-1)(r-1) + (K-1)(K-2)}{r^2 (r+1)^2}\right] B_{r-1} \tag{29}$$

Equation 29 can be rewritten as:

$$B_r = -2\zeta \frac{(r-2)}{r^2} B_{r-1} - \frac{\left[(r-2)(r-3) + 2(\bar{K}-1)(r-2) + (\bar{K}-1)(\bar{K}-2)\right] B_{r-2}}{r^2 (r-1)^2} \tag{30}$$

Examination of equations 30 and 28 shows that equation 26 is identical with the portion of 26 corresponding to $A_1^{(1)}$. Rewriting equation 25:

$$y_1 + y_2 = \sum_{r=0}^{\infty} A_r a^r \tag{31}$$

$A_o$ and $A_1$ arbitrary

$$A_r = -2\zeta \frac{(r-2)}{r^2} A_{r-1} - \left[\frac{(r-2)(r-3) + 2(K-1)(r-2) + (K-1)(K-2)}{r^2 (r-1)^2}\right] A_{r-2}$$

The indicial equation 24 shows that both roots are repeated. This indicates the following procedure for determining $y_3$ and $y_4$. Rewriting equation 26.

$$L(y) = p^2 (p-1)^2 A_o a^{p-2} \tag{32}$$

Differentiating both sides of equation 32 with respect to p:

$$\frac{\partial}{\partial p} L(y) = p^2 (p-1)^2 A_o a^{p-2} \ln_e a + 2p(p-1)(2p-1) A_o a^{p-2} \tag{33}$$

Thus equation 33 is also a solution to equation 10 for p = 0 and p = 1. Returning to equation 15 where $A_r(p)$ is defined by equation 20:

$$y_3 = \sum_{r-0}^{\infty} \left\{ \left[ \frac{\partial}{\partial p} A_r(0) \right] a^r + \left[ A_r(0) \right] a^r \ln_e a \right\} \tag{34a}$$

$$y_4 = \sum_{r=0}^{\infty} \left\{ \left[ \frac{\partial}{\partial p} A_r(1) \right] a^{r+1} + \left[ A_r(1) \ln_e a \right] a^{r+1} \right\} \tag{34b}$$

Inspection of equation 34a shows $y_3$ is unbounded at $a = 0$, whereas equation 34b shows $y_4$ has an unbounded first derivative at $a = 0$. Examination of the signal and initial conditions at stations ① and ② in table 1 shows that z and z' and thus y and y' are bounded initially. Therefore the arbitrary constants associated with $y_3$ and $y_4$ are zero in equation 34 and we may neglect this portion of the homogeneous solution in all further discussion.

The remainder of the solution is devoted to selection of the arbitrary constants in equation 31 corresponding to the forcing in equation 11a and 11b and compatible with the initial conditions in table 1.

a. Range Input

The leading terms of the solution corresponding to the range input are given by equations 12a and 31.

$$y = \omega a + A_0 + A_1 a + A_2 a^2 + A_3 a^3 \cdots \tag{35a}$$

or

$$z = \omega^2 \tau_1 + A_0 + A_1 \omega\tau_1 + A_2 (\omega\tau_1)^2 + A_3 (\omega\tau_1)^3 \cdots \tag{35b}$$

From table 1, the leading term of z is given by:

$$Z(0^+) = \frac{K(K-1)\omega^4 \tau_1^3}{36} \tag{36}$$

Thus:

$$A_0 = 0$$

$$A_1 = -\omega \tag{37}$$

$$A_2 = 0$$

$$A_3 = \frac{K\,(K-1)\,\omega}{36}$$

and from equation 31, given $A_0 = 0$, $A_1 = -\omega$:

$$A_2 = 0$$

$$A_3 = -\left[\frac{2\,(K-1) + (\bar{K}-1)\,(\bar{K}-2)}{36}\right](-\omega) = \frac{K\,(K-1)\,\omega}{36} \tag{38}$$

which checks with equation 37.

The block diagram of figure 3 shows that the negative of the signals at stations ③ and ④ are the impulse responses of interest in this problem. From table 1, the signal at ③ is $\frac{1}{\omega^2}\,z''$.

$$\frac{R}{R_n} = -\frac{1}{\omega^2}\,z'' = -\frac{1}{\omega^2}\,\frac{d^2}{d\tau_1^2}\left[\sum_{r=3}^{\infty} A_r\,(\omega\tau_1)^r\right] \tag{39}$$

$$\frac{R}{R_n} = -\sum_{r=3}^{\infty} r\,(r-1)\,A_r\,(\omega\tau_1)^{r-2} = -\sum_{r=2}^{\infty} r\,(r+1)\,A_{r+1}\,(\omega\tau_1)^{r-1} \tag{40}$$

Defining:

$$a_r \triangleq \frac{1}{\omega}\,r\,(r+1)\,A_{r+1} \tag{41}$$

$$a_{r-1} = \frac{1}{\omega}\,(r-1)\,(r)\,A_r$$

$$a_{r-2} = \frac{1}{\omega}\,(r-2)\,(r-1)\,A_{r-1}$$

$$a_{r-3} = \frac{1}{\omega}\,(r-3)\,(r-2)\,A_{r-2}$$

Substituting equation 41 into 40:

$$-\frac{1}{\omega}\frac{R}{R_n} = \sum_{r=2}^{\infty} a_r (\omega\tau_1)^{r-1} \tag{42}$$

Substituting equation 41 into 37:

$$a_1 = 0$$

$$a_2 = \frac{K(K-1)}{6} \tag{43}$$

Substituting equation 41 into 31:

$$\frac{\omega a_{r-1}}{r(r-1)} = -2\zeta \frac{(r-2)}{r^2} \frac{\omega a_{r-2}}{(r-1)(r-2)}$$

$$-\left[\frac{(r-2)(r-3) + 2(K-1)(r-2) + (K-1)(K-2)}{r^2 (r-1)^2}\right] \frac{\omega a_{r-3}}{(r-2)(r-3)}$$

or

$$a_r = \frac{-2\zeta}{r+1} a_{r-1} - \left[\frac{(r-1)(r-2) + 2(K-1)(r-1) + (K-1)(K-2)}{(r+1)(r)(r-1)(r-2)}\right] a_{r-2} \tag{44}$$

Equations 42, 43, and 44 constitute the adjoint impulse response of range due to range noise.

Similarly, the signal at (4) is given as $\frac{2\tau_1}{K\omega^2} z''$:

$$-\frac{R}{R_n} = \frac{2\tau_1}{K\omega^2} z'' = \frac{2}{K} \sum_{r-2}^{\infty} a_r (\omega\tau_1)^r \tag{45}$$

and 43, 44, and 45 represent the adjoint impulse response of range due to range rate noise.

b. Range Rate Solutions

The range rate solutions due to range noise and range rate noise are evaluated in the same manner as the range solutions. That is, the constants in equation 31 are adjusted using the initial condition data of table 1. These solutions are given by:

$$-\frac{1}{\omega^2}\frac{\dot{R}}{R_n} = \sum_{r=2}^{\infty} b_r a^{r-2} \tag{46}$$

$$-\frac{1}{\omega}\frac{\dot{R}}{\dot{R}_n} = \frac{2}{K}\sum_{r=2}^{\infty} b_r \alpha^{r-1}$$

$$b_2 = \frac{K(K-1)}{2}$$

$$b_3 = \frac{-2\zeta}{6} K(K-1)$$

$$b_r = \frac{-2\zeta}{r} b_{r-1} - \left[\frac{(r-2)(r-3) + 2(K-1)(r-2) + (K-1)K-2)}{r(r-1)(r-2)(r-3)}\right] b_{r-2}$$

The solutions of equations 42, 45, and 46 were evaluated by a computer program and are plotted in figures 4 and 5. Corresponding data outputs from the computer program of Appendix D are circled on the figures.

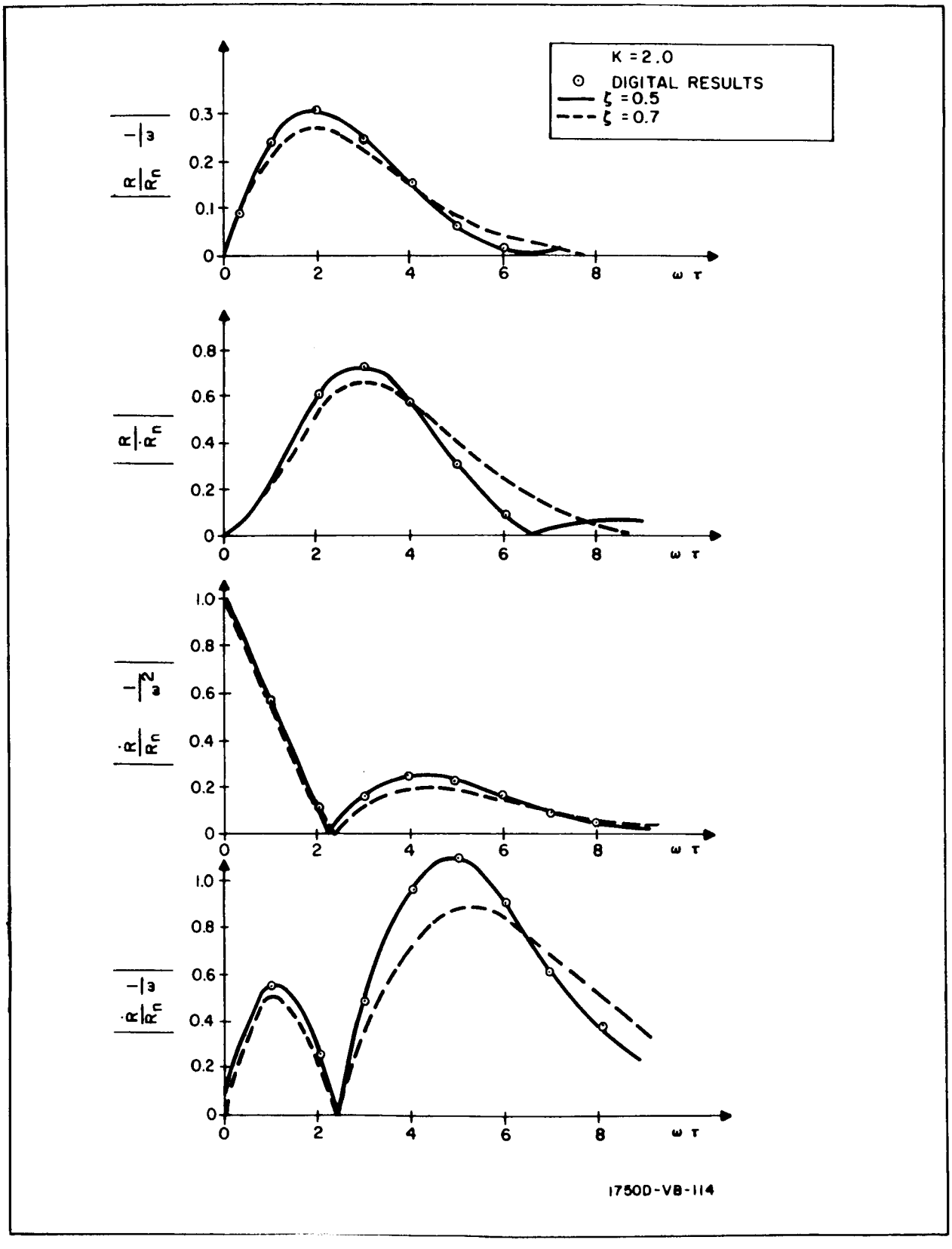


Figure 4. Adjoint Rendezvous Range Channel Impulse Response

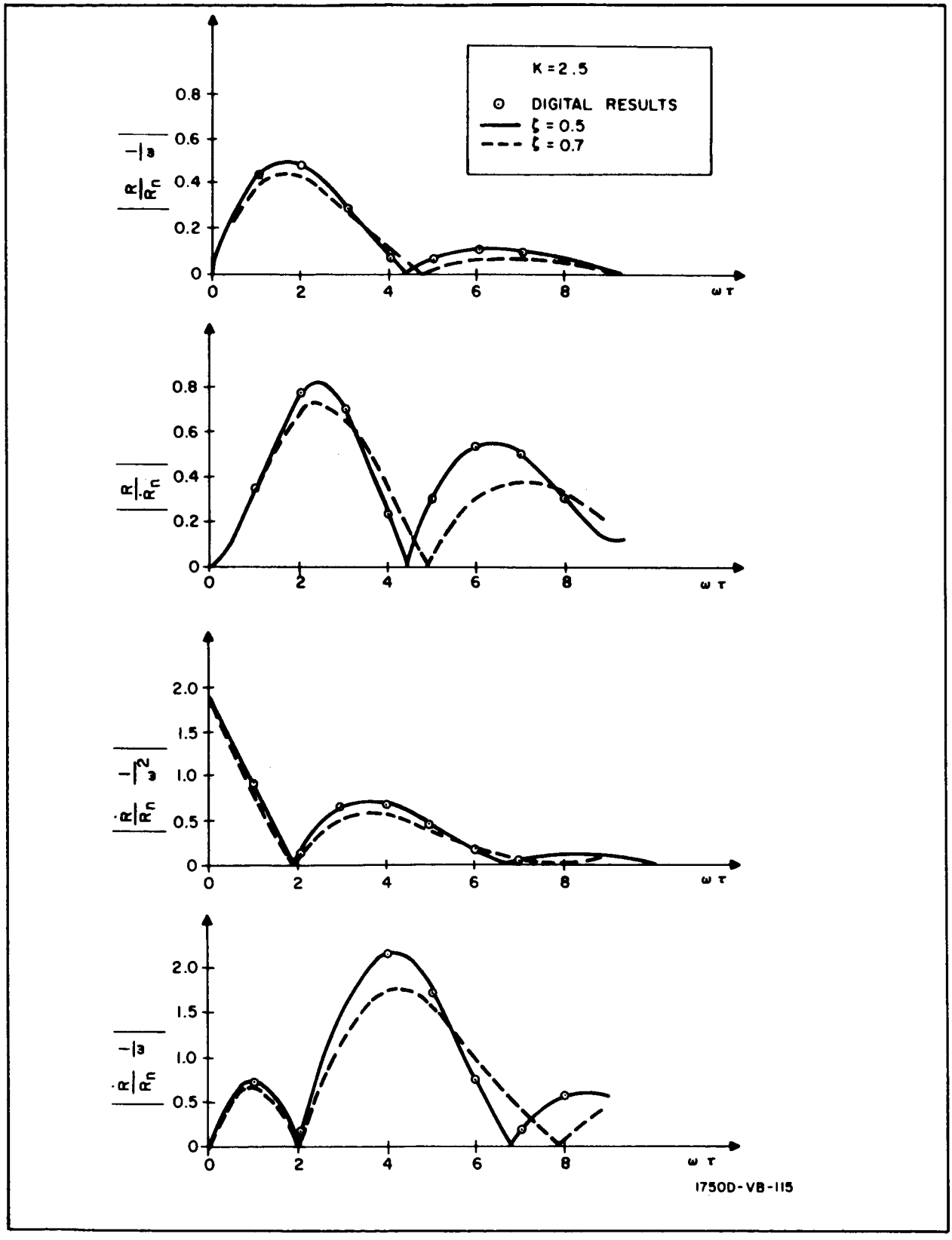


Figure 5. Adjoint Rendezvous Range Channel Impulse Response

# APPENDIX F

## ANALOG SIMULATION FOR PILOTED RENDEZVOUS

The analog simulation of manned rendezvous is three dimensional. The primary purpose for its initiation and use is to determine the effects of the operator in (or across) the rendezvous control loop. All data displayed to the pilot are representative of natural sensor outputs. No data processing is simulated. The pilot, using only the data displayed (no visual contact with the target is assumed), has full control in six degrees of freedom of the chaser attitude and translational movements - from the simulation initiation (at ranges up to 30.5 km) to the beginning of the docking phase (a range of about 305 meters and a relative closing velocity of less than 3.05 meters per second).

The simulation computations are performed in a local-vertical rotating coordinate system centered at the target as described in Appendix A. The method of obtaining the complete set of equations is indicated below. The basic equations of motion are (note, differential gravity is neglected):

$$\ddot{X} = a_{xT} - 2\omega_T \dot{Y}$$

$$\ddot{Y} = a_{yT} + 2\omega_T \dot{X}$$

$$\ddot{Z} = a_{zT}$$

Because of analog computer dynamic range limitations and drift characteristics over long time periods, the computer was scaled for a maximum range of 30,500 meters (100,000) feet. This scaling results in acceptable readout accuracy at the terminal point (a relative range of 305 meters and relative range rate of 3.05 meters per second). Another factor influencing the scaling chosen is the noise level inherent in the machine. The important noise levels are:

$\sigma_{\dot{R}} = 0.0061$ m/sec $(1\sigma)$

$\sigma_R = 0.488$ m $(1\sigma)$

$\sigma_{\dot{e}} = 1.6 \times 10^{-4}$ mr/sec $(1\sigma)$

Figure 1 is a flow diagram of the analog computer simulation. The computer simulates the kinematics of the problem and generates the quantities to be displayed namely, R, $\dot{R}$ and $\dot{e}$.

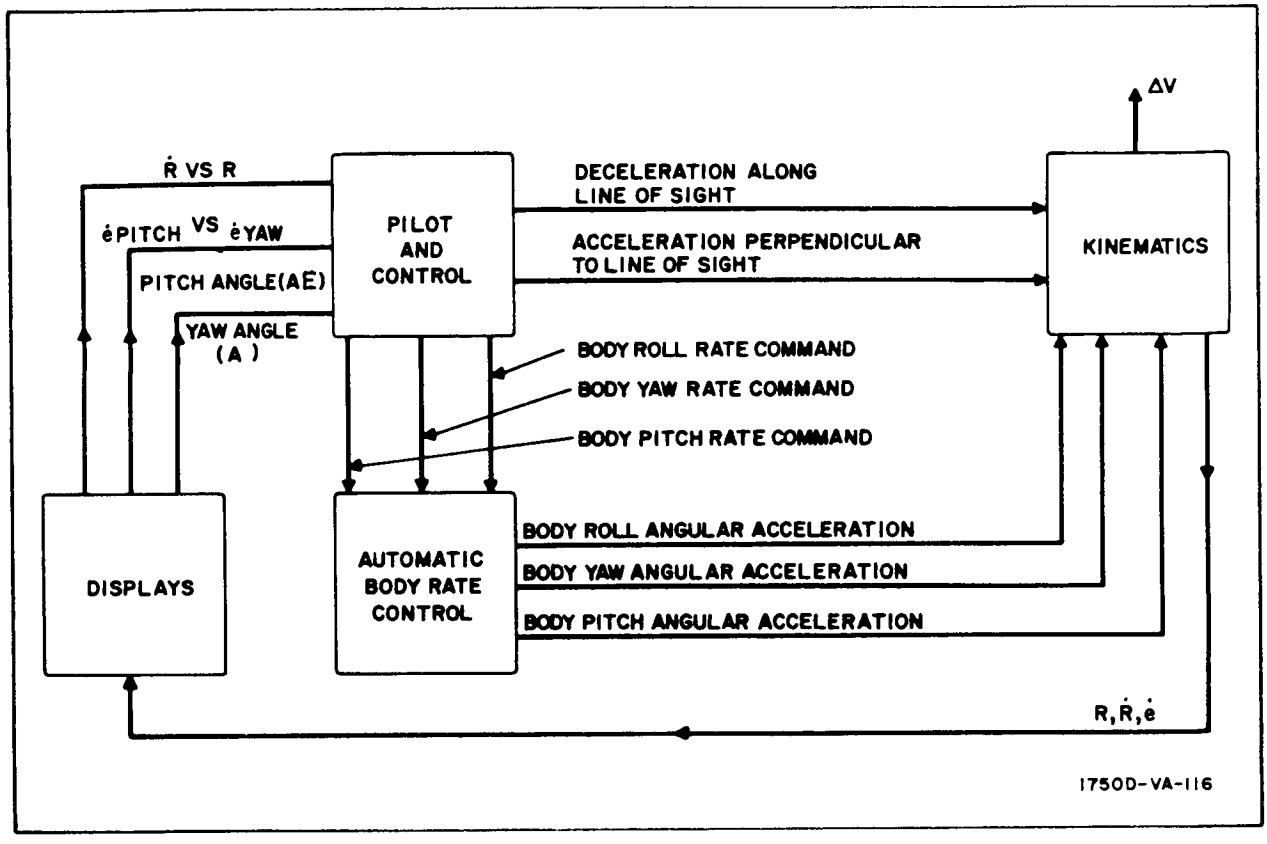


Figure 1. Flow Diagram on the Analog Computer Simulation

The analog computer equations correspond to the equation of Appendix A with the following assumptions:

a. Gravity terms are negligible

b. Higher powers of $\omega_T$ are negligible

c. $I_{by} = I_{bz}$

d. Orbital equation of motion of the target is linearized.

For an elliptical orbit, the motion of the target is described by

$$\omega_T = \frac{V_{TP}}{R_{TP}} \left( \frac{1 + e \cos \theta_T}{1 + e} \right)^2 \tag{1}$$

The quantity $\omega_T$ (which is a function of time and the eccentricity, e) can be expanded in a Taylor series for a circular orbit as follows:

$$\omega_T (t, e) = \omega_T (t, 0) + e \frac{\partial \omega_T}{\partial e} (t, 0) + \frac{e^2}{2} \frac{2\omega_T}{\partial e} (t, 0) + \cdots \tag{2}$$

Assuming e is small, equation 2 becomes:

$$\omega_T (t, e) = \omega_T (t, 0) + e \frac{\partial_{\omega t}}{\partial_e} (t, 0) \tag{3}$$

From equation 1:

$$\omega_T (t, 0) = \frac{V_{TP}}{R_{TP}} \tag{4}$$

$$\frac{\partial \omega_T}{\partial e} (t, 0) = \frac{2 V_{TP}}{R_{TP}} \qquad (\cos \theta_T - 1) \tag{5}$$

Substituting equations 4 and 5 into equation 3:

$$\omega_T = \frac{V_{TP}}{R_{TP}} - \frac{V_{TP}}{R_{TP}} 2e + 2e \frac{V_{TP}}{R_{TP}} \cos \theta_T$$

$$= \frac{V_{TP}}{R_{TP}} (1 - 2e) + 2e \frac{V_{TP}}{R_{TP}} \cos \theta_T \tag{6}$$

Hence, equation 6 is of the form:

$$\omega_T = a_o + a_1 \cos \theta_T \tag{7}$$

where,

$$a_o = \frac{V_{TP}}{R_{TP}} (1 - 2e)$$

$$a_1 = 2e \frac{V_{TP}}{R_{TP}}$$

$$\theta_T = a_o (t - t_f)$$

$a_o t_f$ = an initial phase shift

Equation 7 along with the approximations listed above and applied to the equations of Appendix A, results in the analog computer model equations.

The control equations for both longitudinal and normal control, as well as the displays and cockpit mockup used, are discussed in detail in paragraph 2. 2. 3. 1b of Volume IV.

# APPENDIX G

## COMPUTER SIMULATION OF ON-OFF RENDEZVOUS SYSTEM

In this appendix the digital computer program used to simulate the on-off system of paragraph 2.2.2 is discussed. Section 1 presents the symbols used, and Section 2 discusses the assumptions and equations used in the program mechanization.

### 1. SUMMARY OF NOTATION

| | |
|---|---|
| $a_L$ | Longitudinal acceleration of chaser |
| $a_N$ | Normal acceleration of chaser |
| $e$ | Orientation of LOS with respect to an inertial reference |
| $\dot{e}$ | LOS angular rate with respect to inertial space |
| $g$ | 9.81 $m/sec^2$ |
| $h$ | Chaser altitude |
| $I_{sp}$ | Propellant specific impulse |
| $K$, $K_1$, and $K_2$ | Control parameters |
| $M_o$ | Initial mass of chaser |
| $M_p$ | Propellant consumed by chaser because of thrusting |
| $R$ | Chaser-to-target range |
| $\dot{R}$ | Chaser-to-target range rate |
| $R_o$ | Chaser-to-target range at initiation of active rendezvous |
| $t$ | Time |
| $t_F$ | Firing time of chaser engines |

$t_s$ Data storage time for smoothing process

$t_i$ Time interval between data measurements

$\Delta V$ Velocity increment

$\Delta V_H$ Velocity increment required for nominal Hohmann transfer

X, Y, Z Position components (general)

$\dot{X}$, $\dot{Y}$, $\dot{Z}$ Velocity components (general)

$\psi$ Yaw (out of plane) attitude angle of chaser

$\gamma$ Pitch (in-plane) attitude angle of chaser

$\phi$ Central angle between chaser and target radius vectors during rendezvous

$\omega_T$ Angular orbital velocity of target

X, Y Inertial axis system

X', Y' Chaser centered coordinate system

Subscripts:

f Value of quantity at termination of active rendezvous

i Value of quantity at injection

o Value of quantity at start of active rendezvous

T Target

C Chaser

## 2. PROGRAM MECHANIZATION

The program is based on several assumptions about the orbits of the two vehicles. A nonmaneuvering target vehicle is assumed to be in a circular posigrade orbit about the earth. A maneuverable chaser vehicle is assumed to be initially in a lower altitude circular posigrade parking orbit. The orbits of the two vehicles are assumed to be coplanar and no out-of-plane deviations have been considered thereby reducing the problem to a two-dimensional model.

The nominal case has been defined to be the following. The altitudes of the target and chaser parking orbits are 500 and 200 km respectively. The initial angle $\phi_i$ (figure 1) between the two vehicles is defined to be such that a horizontal nominal thrust applied to the chaser at its initial position will cause the chaser to collide with the target exactly 180 degrees later. The program has been arranged so that deviations from this nominal case can be studied. The deviations which have been considered are a deviation in the altitude of the chaser parking orbit, a deviation from a nominal incremental velocity vector in both magnitude and direction, and a deviation from the nominal central angle between the two vehicles.

## 2.1 Initial Positioning of Target and Chaser

The initial relative positioning of the target and chaser vehicles depends upon a set of deviations from nominal which are inputs to the program. The chaser vehicle has arbitrarily been placed on the positive X-axis at the time when the injection into the ascent ellipse is made. The deviation from nominal thrust level is specified by an initial velocity increment $\Delta V_o$. Thus, the position and velocity vectors defining the ascent ellipse of the chaser are:

$$X_e = X_p$$

$$Y_e = 0$$

$$V_{xe} = \Delta V_i \sin \gamma$$

$$V_{ye} = V_{yp} + \Delta V_n + \Delta V_o \cos \gamma$$

where

$X_p$, $V_{yp}$ - position and velocity of chaser in parking orbit of specified altitude.

$\Delta V_n$ - velocity increment due to nominal thrust

$\gamma$ - deviation from nominal thrust angle (see figure 1)

A set of orbital elements for the chaser is calculated from this position and velocity vector by the method described in paragraph 2.7.2. The target vehicle is placed in a 200-km circular orbit and positioned initially with a specified deviation from the nominal angle $\phi_i$ (figure 1) between the two vehicles.

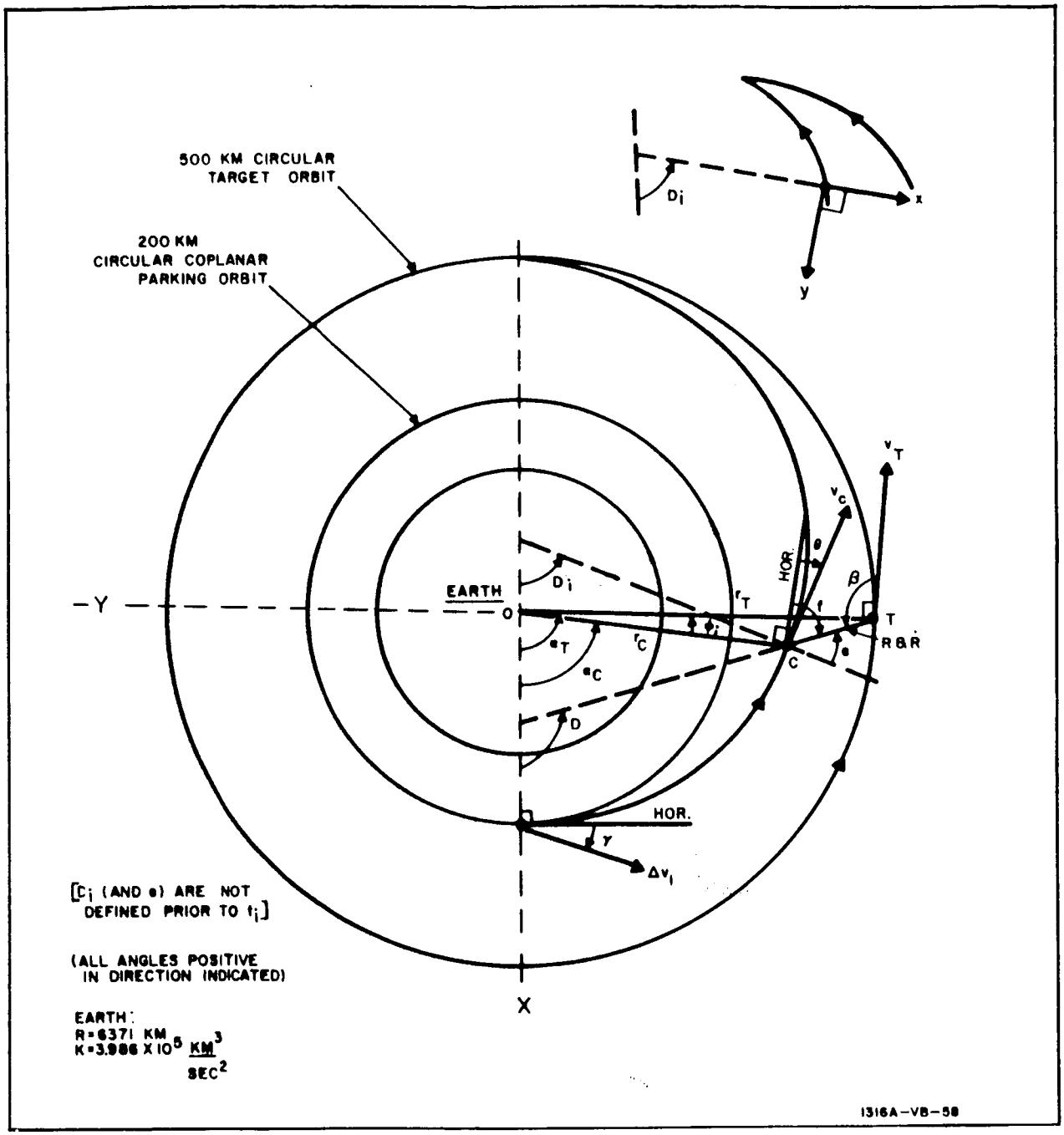


Figure 1. Rendezvous Geometry

## 2.2 General Flow of the Program

Time is incremented in the program at a specified interval and calculations are performed at each time point based on simulated sensor readings to determine when to make rendezvous achieving corrections to the orbit of the chaser vehicle. At each time point the geocentric coordinates of both

the target and chaser are determined by applying the method described in paragraph 2.7.1 to the orbital elements of each vehicle. These geocentric coordinates are then transformed into a local radar oriented $X' - Y'$ coordinate system with the origin located at the chaser. The positive $X'$-axis makes an angle D with the positive X-axis and the positive $Y'$-axis lies in the orbital plane in the direction opposite to the orbital motion. The angle D is expressed as

$$D = \tan^{-1}\left(\frac{Y_T - Y_C}{X_T - X_C}\right)$$

where $X_T$, $Y_T$, $X_C$, and $Y_C$ are the geocentric coordinates of the target and chaser.

When the chaser-to-target range decreases to 25 km, the angle $D_I$ is used as a reference for locking on the onboard coordinate system. The angle $D_I$ is set equal to D when R = 25 km, and the $X'$-axis is locked at an angle $D_I$ to the X-axis.

The coordinates of the target may be expressed in the chaser-centered system by means of the following rotation:

$$\begin{bmatrix} R_x & V_x \\ R_y & V_y \end{bmatrix} = \begin{bmatrix} \cos D & +\sin D \\ \sin D & -\cos D \end{bmatrix} \begin{bmatrix} (X_T - X_C) & (V_{xT} - V_{xC}) \\ (Y_T - Y_C) & (V_{yT} - V_{yC}) \end{bmatrix}$$

where

$R_x$, $R_y$, $V_x$, $V_y$ = position and velocity of target relative to chaser in $X' - Y'$ coordinate system

$X_T$, $Y_T$, $V_{xT}$, $V_{yT}$ = position and velocity of target in X-Y vertical coordinates

$X_C$, $Y_C$, $V_{xC}$, $V_{yC}$ = position and velocity of chaser in X-Y inertial coordinates

The quantities pertinent to sensor observations are range, range rate, and the line-of-sight angular rate. Inaccuracies in the sensor measurements are simulated by superimposing random members of zero mean and specified standard deviation upon the actual values. These observations are resolved into $X_\epsilon$ and $Y_\epsilon$ components and fed into a smoothing function. The smoothing function performs a least squares fit of a specified order on a given number of points and extrapolates the solution to the next observation point. The

extrapolated values of $R_x$, $R_y$, $\dot{R}_x$, $R_y$, and $\dot{e}$ are used as the control variables in the firing laws. The smoothing process is described in subsections 2.5 and 2.6.

## 2.3 Firing Laws

The firing laws used in the simulation are designed to hold the elevation angle close to zero by firing along the Y'-axis until the range and range rate can be driven to zero by firing along the X'-axis.

If the rate of change of elevation angle becomes greater in magnitude than 0.3 milliradians per second, a Y'-acceleration of the following direction and duration will be applied.

$$t_F = 0.9R \left| \frac{e}{a_y} \right|$$

$$a_y = -a_{yo} \frac{e}{\dot{e}}$$

$a_{yo} = 1$ m/sec$^2$ (acceleration due to thrust level of Y'-rockets)

The X'-axis firings are designed to drive $\dot{R}$ to zero between the two curves represented by the following inequality:

$$-\sqrt{K_2 \mid R - R_f \mid} \leq \dot{R} \leq -\sqrt{K_1 \mid R - R_f \mid}$$

where

$K_2 = 2.25$ m/sec$^2$

$K_1 = 1.5$ m/sec$^2$

$R_f$ = standoff range (has been set to 200 meters)

Firings on the X'-axis are triggered when

$$\dot{R} \geq -\sqrt{K_2 \mid R - R_f \mid}$$

Under these conditions a negative acceleration, $a_x$, of -1.5 m/sec$^2$ is applied for the following duration of time.

$$t_F = \frac{2\left| -\sqrt{K_1 \left| R - R_f \right|} - \dot{R} \right|}{\left| a_x \right|}$$

Several additional restrictions are superimposed on the firing laws to prevent firings due to spurious noise peaks. There must be at least a 5-second time delay between Y'-firings and at least a 2-second delay between X'-firings. All computed firings of less than 2 seconds duration are suppressed. When the range rate has been driven to less than 1 meter per second, the rendezvous maneuver is considered to be completed, and the program is stopped.

## 2.4 Corrections to Chaser Orbit for Firing

During periods of firing, corrections must be made to the orbit of the chaser vehicle. These corrections are made by superimposing the effects of firing over a short time period (1 second or less) on the position and velocity vectors of the chaser. The effects of firing must first be transformed back into the geocentric coordinate system before they can be added to the chaser position and velocity vectors. This operation can be represented by the following matric equation.

$$\begin{bmatrix} \hat{X}_C & \hat{V}_{xC} \\ \hat{Y}_C & \hat{V}_{yC} \end{bmatrix} = \begin{bmatrix} X_C & V_{xC} \\ Y_C & V_{yC} \end{bmatrix} + \begin{bmatrix} \cos D & \sin D \\ \sin D & -\cos D \end{bmatrix} \begin{bmatrix} 1/2\, a_x \Delta t^2 & a_x \Delta t \\ 1/2\, a_y \Delta t^2 & a_y \Delta t \end{bmatrix}$$

where

$\hat{X}_C$, $\hat{Y}_C$, $\hat{V}_{xC}$, $\hat{V}_{yC}$ - corrected position and velocity components of chaser

$\Delta t$ - time interval over which correction is made

The corrected position and velocity vectors of the chaser are used to calculate a new set of orbital elements by the method described in paragraph 2.7.2. The new orbital elements are used for subsequent positioning of the chaser.

## 2.5 Noise Generation and Smoothing

The program has been planned to provide a specified order N, of least squares smoothing for a specified number of points, M. The noisy values of $R_x$ and $R_y$ are saved for the previous M time points. At each new time point (intervals of 1 second are taken when program is in noise generating

mode) the blocks of noisy ranges are updated by adding the new values and dropping the values associated with the oldest time point.

It is desired to fit a function of the following form to the observed data.

$$a_o + a_1 t + a_2 t^2 + \ldots\ldots a_n t^n = R$$

If we express the observed data at each of the M-points in an equation of this form we obtain the matrix equation:

$$\begin{bmatrix} 1 & t_1 & t_1^2 & \ldots\ldots & t_1^n \\ 1 & t_2 & t_2^2 & \ldots\ldots & t_2^n \\ . & . & . & & . \\ . & . & . & & . \\ . & . & . & & . \\ 1 & t_m & t_m^2 & \ldots\ldots & t_m^n \end{bmatrix} \begin{bmatrix} a_0 \\ a_1 \\ . \\ . \\ . \\ a_n \end{bmatrix} = \begin{bmatrix} R_1 \\ R_2 \\ . \\ . \\ . \\ R_m \end{bmatrix}$$

or in the matrix form:

$$[T] \quad [A] = [R]$$

When the least squares technique is applied to this system of equations a solution for the coefficient matrix $[A]$ is obtained in the following form.

$$[A] = \left\{ [T]^T \quad [T] \right\}^{-1} \cdot [T]^T \cdot [R]$$

The smoothed value of range and range rate can now be found at the next time point by substituting the time of the next observation into the general equation.

$$R_n = a_0 + a_1 t_n + a_2 t_n^2 + \ldots a_n t_n^n$$

$$\dot{R}_n = a_1 + 2a_2 t_n + \ldots\ldots n a_n t_n^{n-1}$$

where

$t_n$ - time of the next observation

$R_n$ - smoothed value of range at time $t_n$

$\dot{R}_n$ - smoothed value of range rate at time $t_n$

Since the onboard computer system cannot instantaneously perform the smoothing operation the smoothed values have been projected ahead to the next time point so that they can be used as the control variables in the firing laws while the present observations are being smoothed.

## 2.6 Corrections to Smoother Input for Firing

During periods when the control rockets of the chaser are firing, the acceleration of the chaser due to the firing is much greater than the acceleration due to orbital motion. This extra acceleration would normally tend to cause the smoother output to lag behind the actual values. However, since the firing laws allow the anticipation of firing from one time point to the next, the smoother input can be corrected to offset the effects of the added acceleration.

The noisy ranges can be adjusted by adding to each of the stored values an increment equal to the effects of the added acceleration applied over a time period from the projected time point to the time point associated with each stored value. Thus, if the subscript 1 represented the oldest time point and the subscript M represented the most recent time point then the adjustment can be expressed as:

$$R_{ic} = R_i + (M - i + 1/2)\, a\, \Delta t \qquad 1 \leq i \leq M$$

where

$R_{ic}$ - adjusted value of noisy range

$R_i$ - uncorrected value of noisy range

$a$ - acceleration due to rockets being fired

$\Delta t$ - sample interval

These corrections are made to each of the components of range whenever there is firing on that axis. The adjusted values of range are inputs to the smoother and serve to keep the smoothed values in phase with the actual values.

The required adjustment to the noisy angle is as follows. If the subscript 1 represents the oldest time point and the subscript M represents the most recent time point then the adjustment can be expressed as

$$e_{ic} = e_i + (M - i + 1/2)\, \frac{a\Delta t^2}{R}$$

where

$e_{ic}$ - adjusted value of noisy elevation

$e_i$ - uncorrected value of noisy elevation

a - acceleration normal to the range vector

$\Delta t$ - sample interval

These corrections are made whenever there is a component of acceleration normal to the range vector. Corrections are made to the noisy range inputs whenever there is a component of acceleration parallel to the range vector.

## 2.7 Transformations Between Geocentric Coordinates and Orbital Elements[1/]

Under the following subheadings methods are discussed for transforming geocentric coordinates to orbital elements and vice versa. Throughout this section a system of units is used in which the mean equatorial radius is set equal to one. The product of Newton's constant of gravitation and the mass of the earth, $K^2M$ is also set equal to one. Symbols used in the following subheadings are defined as follows:

$Z_1$, $Z_2$, $Z_3$ - geocentric position components

$\dot{Z}_1$, $\dot{Z}_2$, $\dot{Z}_3$ - geocentric velocity components

The following six parameters are referred to as the orbital elements.

a - the length of the semimajor axis

e - the eccentricity of the ellipse

$\Omega$ - right ascension of ascending node (the ascending node is the point where the satellite crosses the $Z - Z_2$ plane, equator, from south to north)

i - inclination of the plane of the orbit to the $Z_1 - Z_2$ plane $0 \leq i \leq \pi$

w - argument of the perigee, the angle from the ascending node to the point of perigee $0 \leq w \leq 2\pi$

$T_o$ - epoch for the coordinate system and the time perigee occurred

---

[1/] Paragraphs 2.7.1, 2.7.2, and 2.7.3 are from Westinghouse Air Arm Report No. AA-2547-61 by Paul B. Davenport.

When e, r and w are set equal to zero, the $Z_1$ and $Z_2$ geocentric coordinates correspond to the previously mentioned X and Y coordinates respectively.

The following auxiliary parameters are also often used.

P - period of the orbit

n - mean angular motion of the satellite in the plane of the orbit

$T_n$ - time of ascending node

2.7.1 Geocentric Rectangular Coordinates From Orbital Elements

The geocentric position, Z, and velocity, $\dot{Z}$, are obtained from the elements a, e, $\Omega$, i, w, and $T_o$ (see figure 2) at time t by the following:

$$n = k^2 M_e a^{-3/2} *$$

$$M = n (t - T_o)$$

the quantity M is known as the mean anomaly.

$$E = M + e \sin E$$

The equation above is Kepler's equation and must be solved for the eccentric anomaly E (see paragraph 2.7.3). Once E has been obtained the sine and cosine of the true anomaly, u, (see figure 3) and the length of radius vector r are given by

$$\sin u = \frac{\sqrt{1 - e^2} \sin E}{1 - e \cos E}$$

$$\cos u = \frac{\cos E - e}{1 - e \cos E}$$

$$r = a (1 - e \cos E)$$

Let

$$C_1 = \cos \Omega \cos (w + u) - \sin \Omega \cos i \sin (w + u)$$

$$C_2 = \sin \Omega \cos (w + u) + \cos \Omega \cos i \sin (w + u)$$

$$C_3 = \sin i \sin (w + u)$$

(These are the direction cosines of the satellite.)

* As stated previously, the magnitude of the product $k^2 M_e$ is set equal to unity. It is included here to maintain the proper dimensions.

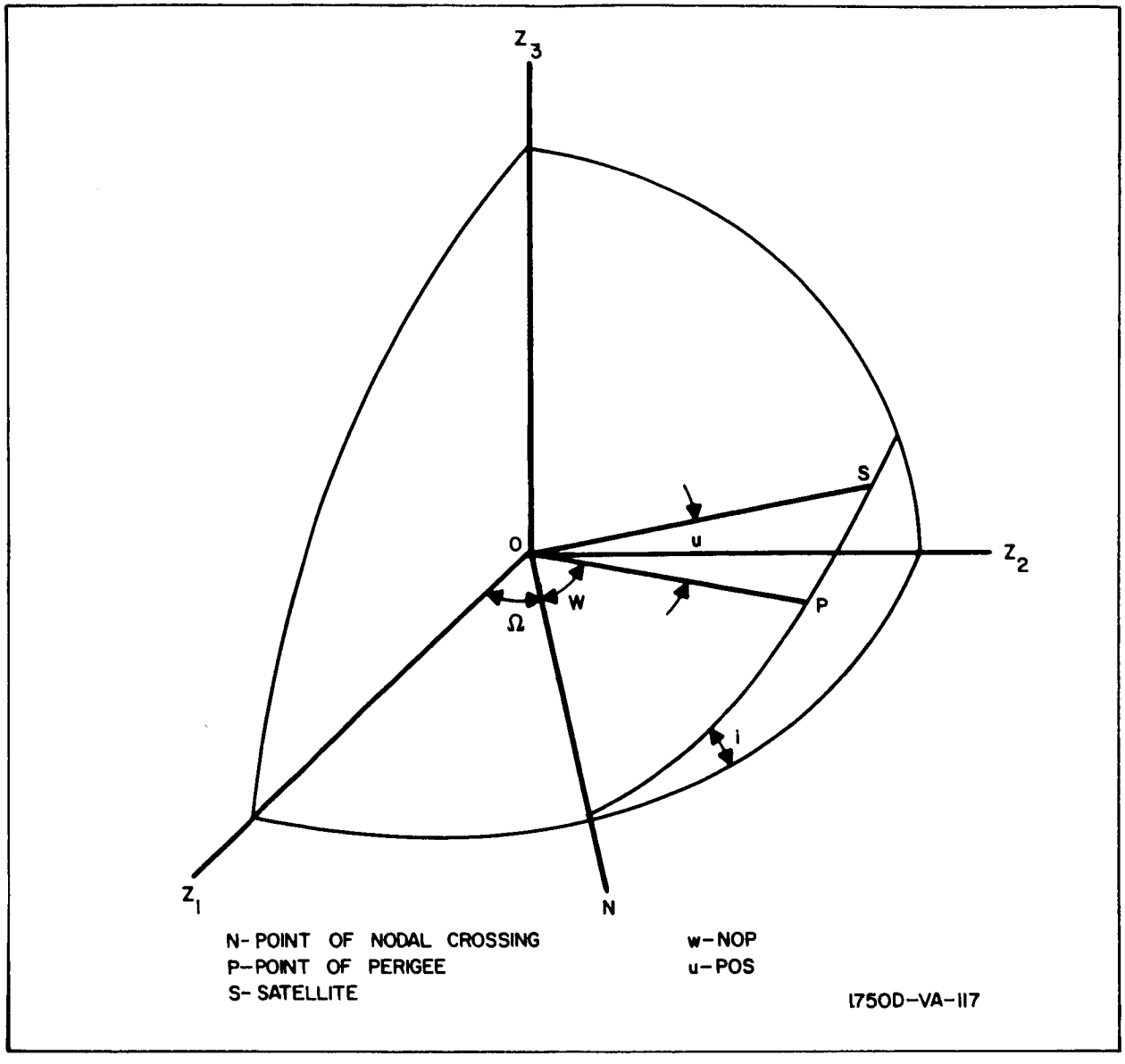


Figure 2. Geocentric Rectangular Coordinates from Orbital Elements

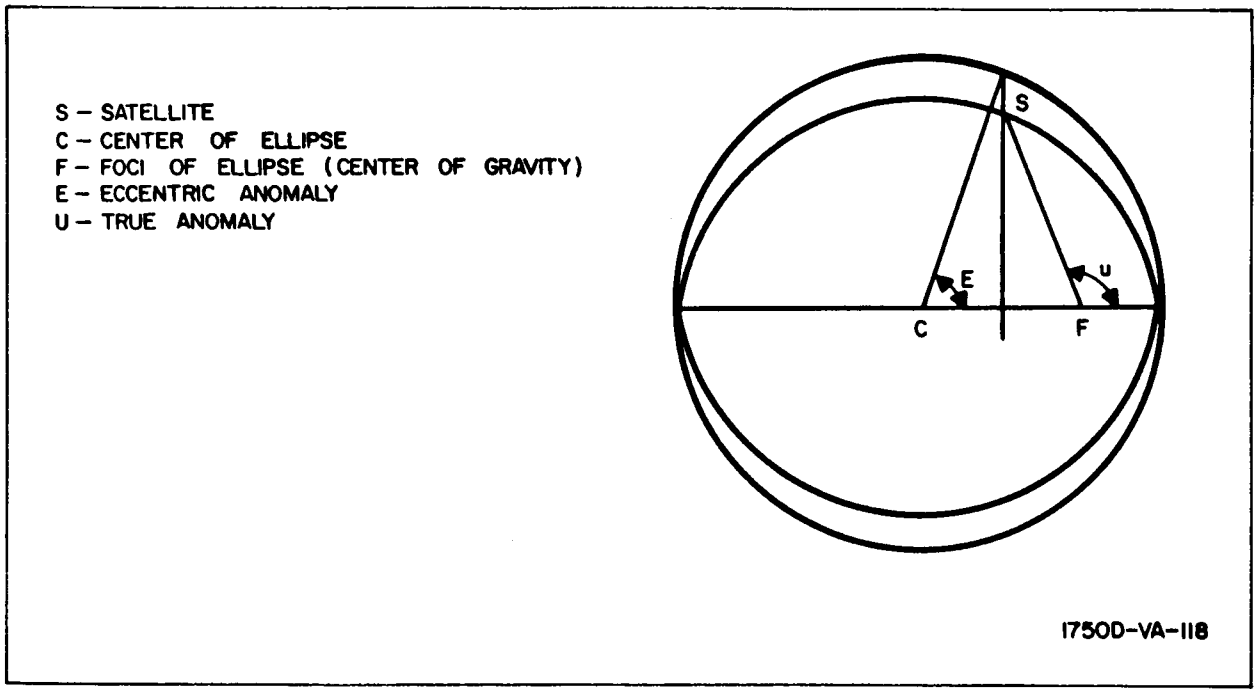


Figure 3. Geocentric Rectangular Coordinates from Orbital Elements

where

$$\sin (w + u) = \sin w \cos u + \cos w \sin u$$

$$\cos (w + u) = \cos w \cos u - \sin w \sin u$$

Then

$$Z_i = r\, C_i \quad (i = 1, 2, 3)$$

The geocentric velocity components, $\dot{Z}_i$, are obtained by differentiating the $Z_i$

$$\dot{Z}_i = k^2 M_e \frac{\sqrt{a}}{r} \quad b_i \quad (i = 1, 2, 3)$$

where

$$b_1 = C_1 e \sin E - \sqrt{1 - e^2} \cos \Omega \sin (w + u) + \sin \Omega \cos i \cos (w + u)$$

$$b_2 = C_2 e \sin E - \sqrt{1 - e^2} \sin \Omega \sin (w + u) - \cos \Omega \cos i \cos (w + u)$$

$$b_3 = C_3 e \sin E + \sqrt{1 - e^2} \sin i \cos (w + u)$$

Alternate expressions for the rates in terms of total velocity, V, but requiring further calculation are given below

$$V = \frac{\sqrt{a}}{r} \sqrt{1 - e^2 \cos^2 E}$$

$$s_i = \frac{b_i}{\sqrt{1 - e^2 \cos^2 E}} \qquad (i = 1, 2, 3)$$

(The $s_i$ are direction cosines of the velocity vector.)

$$\dot{Z}_i = V s_i \quad (i = 1, 2, 3)$$

In some instances the period, P, or mean motion, n, may be given as an element instead of length of the semimajor axis, a. In either case, a can be obtained by one or both of the following relationships:

$$n = \frac{2\pi}{p}$$

$$a = \left(\frac{n}{k^2 M_e}\right)^{-2/3}$$

The element $T_n$ (time or ascending node) is often given rather than $T_o$ (time of perigee). In this case $T_o$ is obtained by the following relations:

$$E_w = \tan^{-1}\left(\frac{-\sin w\sqrt{1-e^2}}{e+\cos w}\right)$$

$$\sin E_w = \frac{-\sin w\sqrt{1-e^2}}{1+e\cos w}$$

$$T_o = T_n - \left(\frac{E_w - e\sin E_w}{n}\right)$$

If $E_w$ is in the third or fourth quadrant then it should be changed to a negative angle to make the time between $T_n$ and $T_o$ a minimum.

2.7.2 Orbital Elements From Geocentric Rectangular Coordinates

$$r = \tan^{-1}\left[(Z_2\dot{Z}_3 - Z_3\dot{Z}_2)\Big/(Z_1\dot{Z}_3 - Z_3\dot{Z}_1)\right]$$

$$i = \tan^{-1}\left[Z_3\Big/(Z_2\cos\Omega - Z_1\sin\Omega)\right]$$

$$\epsilon = w + u = \tan^{-1}\left[Z_3\Big/\sin i\,(Z_1\cos\Omega + Z_2\sin\Omega)\right]$$

$$r\dot{r} = Z_1\dot{Z}_1 + Z_2\dot{Z}_2 + Z_3\dot{Z}_3$$

$$r^2 = Z_1^2 + Z_2^2 + Z_3^2$$

$$V^2 = \dot{Z}_1^2 + \dot{Z}_2^2 + \dot{Z}_3^2$$

$$a = \frac{1}{2/r - V^2}$$

$$e = 1/a\sqrt{a(r\dot{r})^2 + (a-r)^2}$$

If e = 0 then w = 0 and M = E = u = $\epsilon$

otherwise

$$E = \tan^{-1}\left[\sqrt{a}\;r\dot{r}/(a-r)\right]$$

$$u = \tan^{-1}\left[\sqrt{1-e^2}\;\sin E/(\cos E - e)\right]$$

$$M = E - e\sin E$$

$$w = \epsilon - u$$

In either case $T_o$ is found by the formulas

$$n = k^2 M_e a^{-3/2}$$

$$T_o = t - \frac{M}{n}$$

Additional Relations

$$p = a(1 - e^2) \quad \text{(known as orbit parameter)}$$

$$r = \frac{p}{1 + e \cos}$$

$$\dot{r} = \frac{\sqrt{a}\ e \sin E}{r} = \frac{a\, e\, n \sin E}{1 - e \cos E}$$

$$\sin u = \frac{\sqrt{a}\, \dot{r}\, (1 - e^2)^{3/2}}{e}$$

$$\cos u = \frac{p - r}{er}$$

$$\tan(u/2) = \sqrt{\frac{1 + e}{1 - e}} \quad \tan(E/2) = \sqrt{\frac{1 - \cos u}{1 + \cos u}}$$

$$u = \tan^{-1}\left[\sqrt{1 - e^2}\ \sin E\ /\ (\cos E - e)\right]$$

$$\dot{u} = \frac{\sqrt{a}\sqrt{1 - e^2}}{r^2} = \frac{n\sqrt{1 - e^2}}{(1 - e \cos E)^2}$$

$$\sin E = \frac{\sqrt{1 - e^2}\ \sin u}{1 + e \cos u} = \frac{r\, \dot{r}}{\sqrt{a}\, e}$$

$$\cos E = \frac{e + \cos u}{1 + e \cos u} = \frac{a - r}{a\, e}$$

$$\dot{E} = \frac{1}{r\sqrt{a}} = \frac{n}{1 - e \cos E}$$

$$\frac{dr}{du} = \frac{r\, e \sin E}{\sqrt{1 - e^2}}$$

$$V = \sqrt{r^2 \dot{u}^2 + \dot{r}^2} = \sqrt{2/r - 1/a}$$

$$Z_1 \dot{Z}_2 - Z_2 \dot{Z}_1 = \sqrt{a}\sqrt{1 - e^2} \cos i$$

$$Z_2 \dot{Z}_3 - Z_3 \dot{Z}_2 = \sqrt{a}\sqrt{1 - e^2} \sin \Omega \sin i$$

$$Z_1 \dot{Z}_3 - Z_3 \dot{Z}_1 = \sqrt{a}\sqrt{1 - e^2} \cos \Omega \sin i$$

$$e = \sqrt{\frac{a - p}{a}}$$

2.7.3 Solution of Kepler's Equation

$$E = M + e \sin E$$

Let

$$E_o = M + e \sin M (1 + e \cos M)$$

$$\Delta E = \frac{M - E_o + e \sin E_o}{1 - e \cos E_o}$$

$$E_1 = E_o + \Delta E$$

If $E_1$ and $E_o$ agree to the accuracy wanted then $E_1$ is the desired approximation to E. If they do not agree then replace $E_o$ by $E_1$ and compute a new $E_1$.

If the calculations are being done by hand the above process becomes more laborious as e approaches one. In this case a better value of $E_o$ can be obtained by plotting the two curves:

$$y = \sin E$$

and

$$y = 1/e (E - M)$$

as a function of E. The abscissa of their point of intersection is the value of E satisfying the equation.

Another iteration which is simpler than the one above, but requiring more iterations for the same accuracy is

$$E_{i+1} = M + e \sin E_i$$

# APPENDIX H

## EFFECT OF RANDOM NOISE ON ON-OFF SYSTEM

The effect of random noise on the switching boundaries of an on-off system may be regarded as a biasing of the boundaries, provided the rate of change of the noise time history is rapid compared to the time rate of change of the sensed variable. In other words, the bandwidth of the noise must be substantially wider than the harmonic content of the true value of the sensed variable.

Figure 1 indicates the manner in which line-of-sight angular rate noise will, in effect, give a net movement of the switching boundary. The amount by which the switching boundary is moved must be considered on an average basis and will depend upon the amplitude of the noise. The bandwidth of the noise (rate of fluctuation) will affect the consistency of the apparent bias effect. For instance, if the bandwidth is narrow with an attendant slowly varying noise waveform compared to the rate of change of the line-of-sight angular rate, the probability that switching will occur prior to the time at which the line-of-sight rate reaches the boundary value will decrease. For cases studied in which the noise bandwidth is 5 rad/sec, the line-of-sight rate switching boundary is, on the average, biased by twice the noise level standard deviation.

The effect of relative range upon line-of-sight angular rate control with fixed acceleration level lateral control is given by

$$\frac{\partial(\dot{e})}{\partial t} = \frac{a_N}{R}$$

This relationship indicates that line-of-sight angular rate sensitivity increases as range decreases. Consequently, the notion that superimposed noise may be treated as an equivalent average switching boundary bias becomes less valid for any one case as range decreases. On the other hand, the notion is valid if the switching boundary bias is averaged over a large ensemble of cases.

The range versus range rate switching boundary is similarly biased by noise superimposed on the sensed variables in a manner analogous to line-of-sight noise case. Figures 2 and 3 illustrate the effects of range and range rate noise.

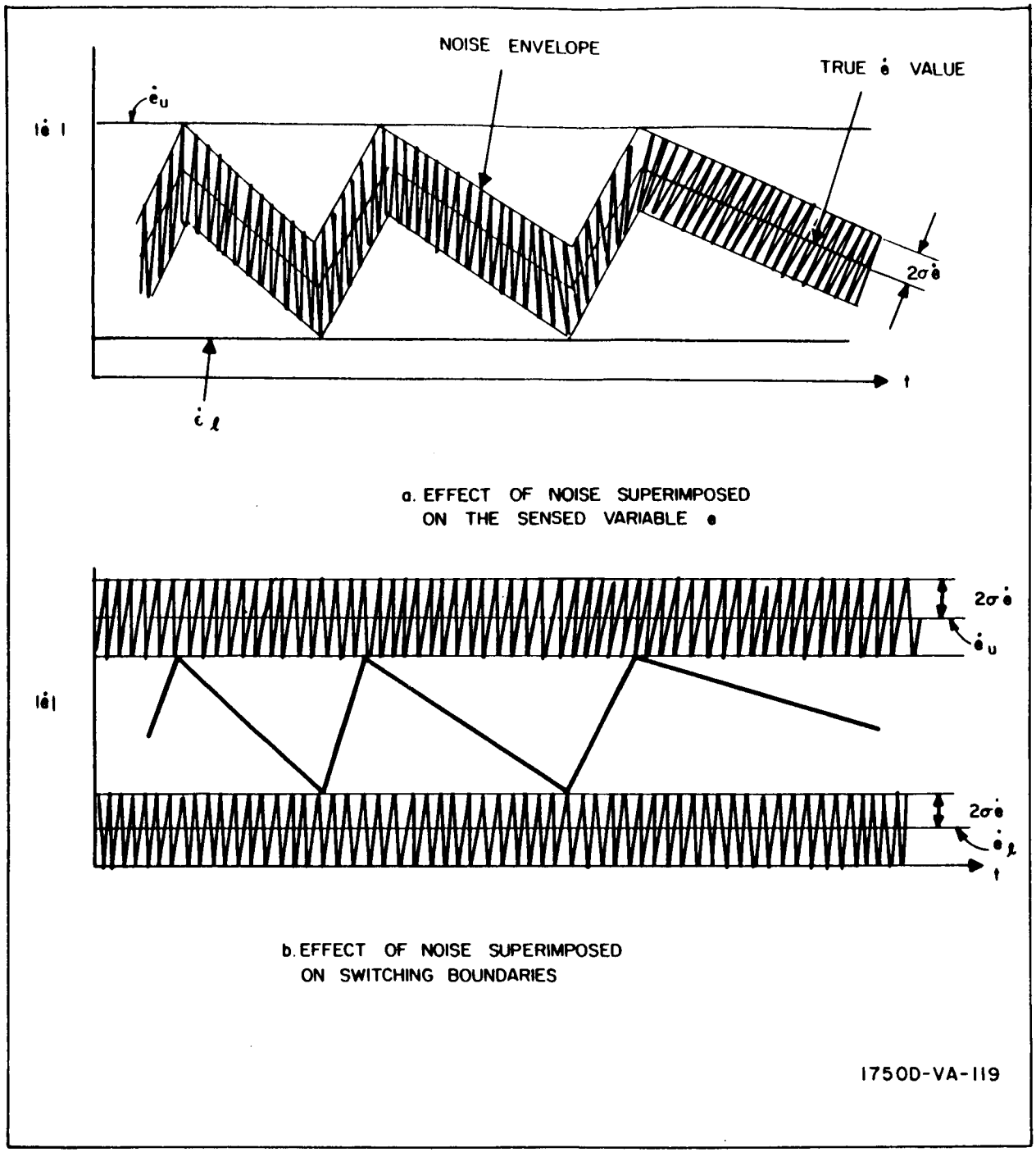


Figure 1. Effects of Line-of-Sight Angular-Rate Noise

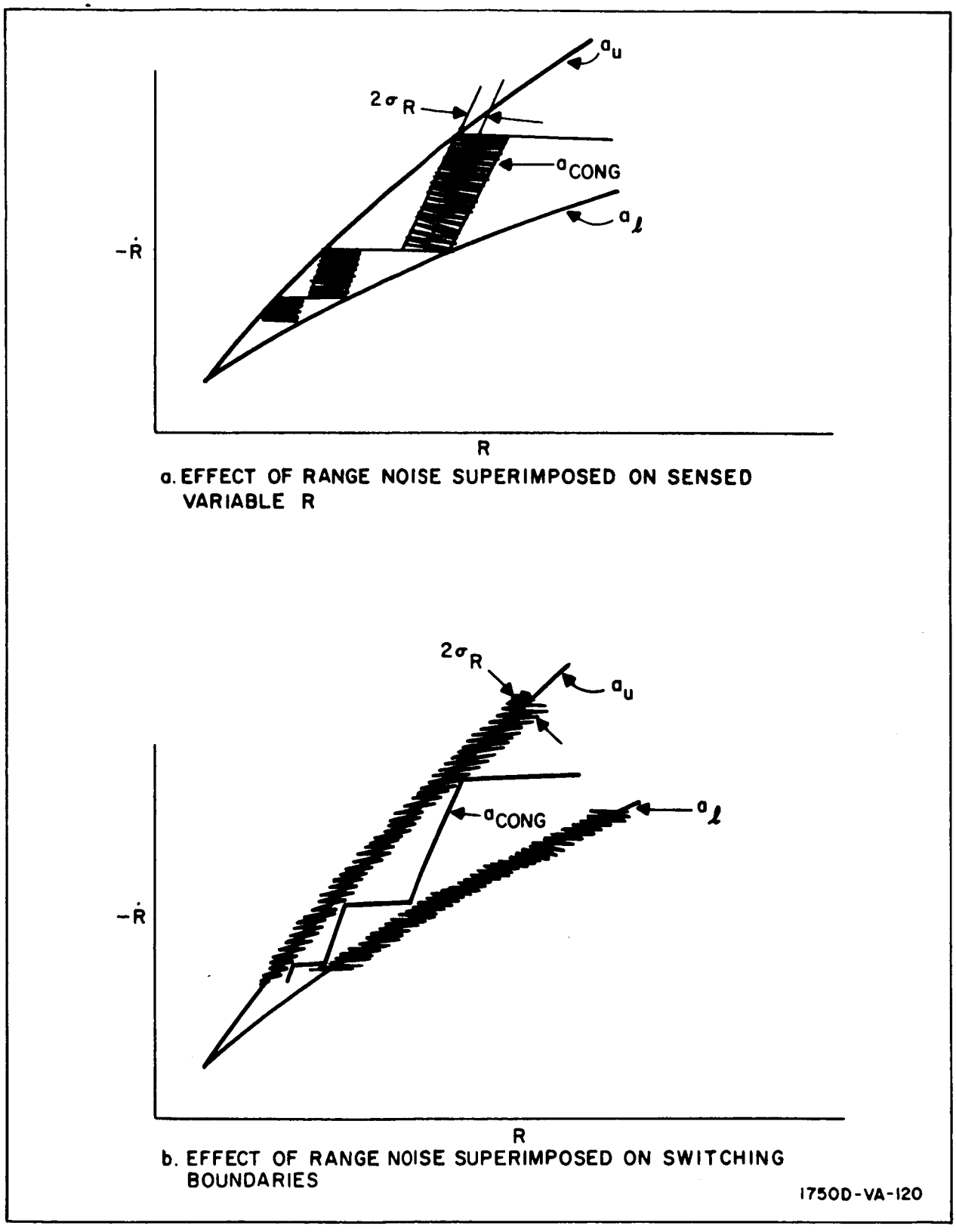


Figure 2. Effects of Line-of-Sight Range Noise

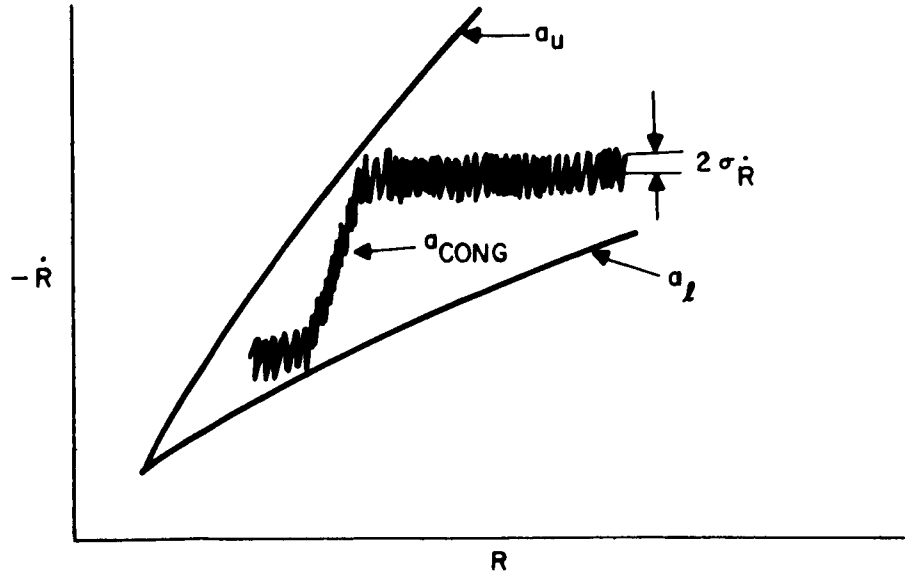


a. EFFECT OF RANGE RATE NOISE SUPERIMPOSED ON SENSED VARIABLE $\dot{R}$

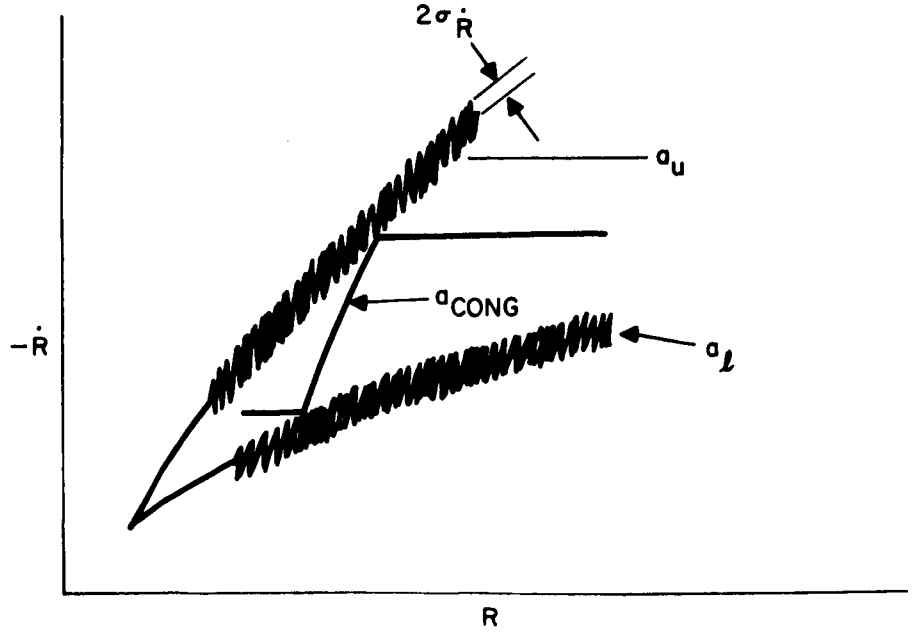


b. EFFECT OF RANGE RATE NOISE SUPERIMPOSED ON SWITCHING BOUNDARIES

17500-VB-121

Figure 3. Effects of Line-of-Sight Range-Rate Noise